frontiers | Research Topics

Growth and quality formation regulated by light in horticulture plants

Edited by
Houcheng Liu, Jung Eek Son, Genhua Niu and Qingming Li

Published in
Frontiers in Plant Science

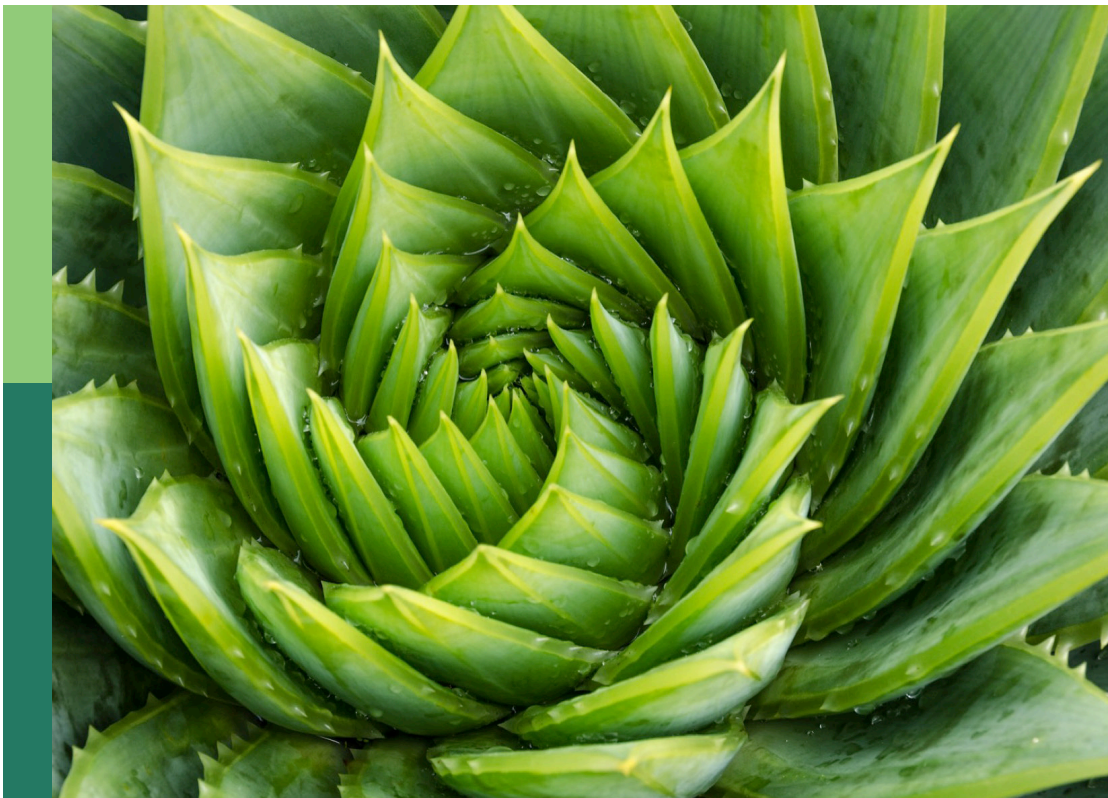

ISSN 1664-8714
ISBN 978-2-8325-4948-3
DOI 10.3389/978-2-8325-4948-3

About Frontiers

Frontiers is more than just an open access publisher of scholarly articles: it is a pioneering approach to the world of academia, radically improving the way scholarly research is managed. The grand vision of Frontiers is a world where all people have an equal opportunity to seek, share and generate knowledge. Frontiers provides immediate and permanent online open access to all its publications, but this alone is not enough to realize our grand goals.

Frontiers journal series

The Frontiers journal series is a multi-tier and interdisciplinary set of open-access, online journals, promising a paradigm shift from the current review, selection and dissemination processes in academic publishing. All Frontiers journals are driven by researchers for researchers; therefore, they constitute a service to the scholarly community. At the same time, the *Frontiers journal series* operates on a revolutionary invention, the tiered publishing system, initially addressing specific communities of scholars, and gradually climbing up to broader public understanding, thus serving the interests of the lay society, too.

Dedication to quality

Each Frontiers article is a landmark of the highest quality, thanks to genuinely collaborative interactions between authors and review editors, who include some of the world's best academicians. Research must be certified by peers before entering a stream of knowledge that may eventually reach the public - and shape society; therefore, Frontiers only applies the most rigorous and unbiased reviews. Frontiers revolutionizes research publishing by freely delivering the most outstanding research, evaluated with no bias from both the academic and social point of view. By applying the most advanced information technologies, Frontiers is catapulting scholarly publishing into a new generation.

What are Frontiers Research Topics?

Frontiers Research Topics are very popular trademarks of the *Frontiers journals series*: they are collections of at least ten articles, all centered on a particular subject. With their unique mix of varied contributions from Original Research to Review Articles, Frontiers Research Topics unify the most influential researchers, the latest key findings and historical advances in a hot research area.

Find out more on how to host your own Frontiers Research Topic or contribute to one as an author by contacting the Frontiers editorial office: frontiersin.org/about/contact

Growth and quality formation regulated by light in horticulture plants

Topic editors

Houcheng Liu — South China Agricultural University, China
Jung Eek Son — Seoul National University, Republic of Korea
Genhua Niu — Texas A&M AgriLife Research-Texas A and M University, United States
Qingming Li — Institute of Urban Agriculture, Chinese Academy of Agricultural Sciences, China

Citation

Liu, H., Son, J. E., Niu, G., Li, Q., eds. (2024). *Growth and quality formation regulated by light in horticulture plants*. Lausanne: Frontiers Media SA.
doi: 10.3389/978-2-8325-4948-3

Table of contents

frontiers | Frontiers in Plant Science

TYPE Editorial
PUBLISHED 16 May 2024
DOI 10.3389/fpls.2024.1414970

OPEN ACCESS

EDITED AND REVIEWED BY
Xinguang Zhu,
University of Chinese Academy of Sciences, China

*CORRESPONDENCE
Houcheng Liu
liuhch@scau.edu.cn

RECEIVED 09 April 2024
ACCEPTED 07 May 2024
PUBLISHED 16 May 2024

CITATION
Liu H, Son JE, Niu G and Li Q (2024) Editorial: Growth and quality formation regulated by light in horticulture plants. *Front. Plant Sci.* 15:1414970. doi: 10.3389/fpls.2024.1414970

Editorial: Growth and quality formation regulated by light in horticulture plants

Houcheng Liu[1]*, Jung Eek Son[2], Genhua Niu[3] and Qingming Li[4]

[1]College of Horticulture, South China Agricultural University, Guangzhou, China, [2]Department of Agriculture, Forestry and Bioresources, Seoul National University, Seoul, Republic of Korea, [3]Texas A&M AgriLife Research, Texas A&M University, Dallas, TX, United States, [4]Institute of Urban Agriculture, Chinese Academy of Agricultural Sciences, Chengdu, China

KEYWORDS

light environment, growth, quality, vegetable, fruit, herb

Editorial on the Research Topic
Growth and quality formation regulated by light in horticulture plants

Light plays a crucial role in the growth and metabolism of plants. It is one of the most important abiotic factors that regulate various physiological signals as well as primary and secondary metabolic responses in plants. Light intensity, spectrum, direction, photoperiod, and timing of lighting all play a role in regulating the physiological and molecular processes of plants. Light is also the most important environmental factor determining the yield and quality of horticultural crops. In this Research Topic 'Growth and Quality Formation Regulated by Light in Horticulture Plants', there are nine original research articles all focusing on the effects of different lighting environments on the growth and nutritional quality of fruits, vegetables, and herb.

Plants compete for sunlight and have evolved to perceive shade through both relative increases in the photon flux density of far-red (FR; 700 to 750 nm) and decreases in the flux of all photons (intensity). The FR photons and light intensity interact to control stem elongation and leaf expansion in plants. These interactions have important implications for horticultural crops. Kusuma and Bugbee studied this interaction between FR fraction and total light intensity with a range of 2 to 33% FR at 50/100, 200 and 500 μmol m^{-2} s^{-1} extended photosynthetic photon flux densities (ePPFD, 400 to 750 nm). Increasing FR light increased leaf expansion in three lettuce cultivars (rosette plant architecture) at the highest ePPFD, but not decreased expansion at the lowest ePPFD. The authors attributed this difference to biomass partitioning between leaves and stem. Increased FR favored stem elongation at low ePPFD and favored leaf expansion at high ePPFD. For cucumber seedlings (upright plant architecture), plants responded to FR differently: leaf expansion increased with increasing FR percent under all ePPFD levels showing minimal interaction. These results indicated that the interaction of FR and light intensity is species dependent.

The phytochrome photostationary state (PSS) sometimes called the phytochrome photo-equilibrium, is the ratio of active phytochrome to the total phytochrome (P_{fr}/P_{total}), and can be calculated from absorptivity data of isolated phytochromes (Sager et al., 1988). If the temporal PSS changes could be estimated, the effects of artificial lighting on plants could be estimated in more detail, and plant morphology and development could be controlled more efficiently and accurately. Jishi developed a model to estimate the time

course of a phytochrome photostationary state (PSS) under an arbitrary light environment. The model estimated that the 90% and 99% of the PSS changes were completed using approximately 3.4 and 6.9 mmol m^{-2} of integrated end-of-day FR, respectively. The rate at which the PSS changes reached equilibrium was maximized under a red light, followed by far-red, green, and blue light. This method could be used to control phytochrome responses for horticulture via artificial lighting.

Anthocyanins not only are an important factor in promoting fruit coloration but also have a rich nutritional and medicinal values. Anthocyanin accumulation is affected by light intensity and light spectrum, especially blue light. Anthocyanins are the main pigments affecting the color and quality of purple-fruited sweet pepper (*Capsicum annuum*). Gao et al. performed the anthocyanin content determination and transcriptome analysis on pepper fruits harvested from different light treatments. The levels of delphinidin (Dp) glycosides, including Dp-3-O-rhamnoside, Dp-3-O-rutinoside, and Dp-3-O-glucoside, were highly accumulated in blue-light–treated fruit, which are mainly responsible for the appearance color of purple pepper. There were 6 structural and 12 transcription factor (TF) genes involved in the anthocyanin biosynthetic pathway. Structural gene, such as, CaUFGT as well as TFs such as CaMYC2-like and CaERF113, which were highly expressed under blue light and presented similar expression patterns consistent with Dp glycoside accumulation. These might be candidate genes for anthocyanin synthesis in response to blue-light signal.

For greenhouse crop production, the spectral quality of supplemental lighting (SL) can not only directly influence crop yield but also nutritional quality. Manipulating the spectral quality of greenhouse SL enhanced the production of secondary metabolites, which can be used for culinary, medicinal, and commercial purposes (Holopainen et al., 2018). Hammock and Sams determined the impact of supplemental blue (B) and red (R) LED lighting ratios and discrete wavelengths on flavor volatiles in hydroponically grown basil (*Ocmum basilicum* var. Italian Large leaf). They found that SL spectral quality, changes in the spectra, and daily light integral (DLI) of ambient sunlight across growing seasons, directly affected basil aroma volatile concentrations. In addition, the specific ratios of narrowband B/R wavelengths, combinations of discrete narrowband wavelengths, and broadband wavelengths directly and differentially influence the overall aroma profile as well as specific compounds. They recommend SL using B and R light at a ratio of approximately 10B/90R at 100-200 μmol. m^{-2} s^{-1} for 12-24 h. d^{-1} for sweet basil standard greenhouse production.

Sweet potato (*Ipomoea batatas* (L.) Lam) is a staple and a critical food crop in developing countries. Sweet potato leaves have been demonstrated to be more nutritious than their stems, petioles, tubers, and other vegetables. Light conditions substantially impact sweet potato leaves, which differ in their shape and metabolic profiles. Tadda et al. determined the nutritional profile of sweet potato leaves were affected by red and blue LEDs. There were higher contents of soluble protein, total phenolic compounds, flavonoids, and total antioxidant activity under blue LEDs, while higher contents of chlorophyll, soluble sugar, protein, and vitamin C under red LEDs. A total of 615 genes were differentially expressed between sweet potato leaves exposed to red and blue LEDs. Among these, 510 differentially expressed genes were upregulated in leaves grown under blue light compared with those grown under red light, while the remaining 105 genes were expressed at higher levels in the latter than in the former. Blue light significantly induced anthocyanin and carotenoid biosynthesis structural genes.

Selecting suitable light conditions according to the plant growth characteristics is one of the important approaches to cultivating high-quality vegetable seedlings. Liu et al. investigated the growth characteristics of tomato and cucumber seedlings under LED light environments (CK, B, UV-A, FR, B+UV-A, UV-A+FR, and B+FR) in plant factories with artificial light (PFALS) and the development of these seedlings after transplanting into the plastic greenhouse. The seedling height and hypocotyl length increased in treatments with far-red light supplementation, but decreased in the B treatment, in both crops. The seedling index of tomato increased in the B+UV-A treatment, while that of cucumber increased in the FR treatment. After transplanting into the plastic greenhouse, tomato plants that radiated with UV-A had greater flower numbers on the 15th day after transplanting. In cucumber plants of the FR treatment, the flowering time was significantly delayed, and the female flower exhibited at a lower node position. The light environments with UV-A and FR were more beneficial for improving the overall quality of tomato and cucumber seedlings, respectively.

Improving the light environment and enhancing the utilization of light energy by plants have become critically important in greenhouse tomato production. Artificial supplemental lighting can improve the light conditions of plant canopies. Bifacial leaves can fix more carbon than leaves with one irradiation surface when exposed to the same irradiation amount (Zhang et al., 2016). Jiang et al. assessed the transcriptomic and proteomic changes in tomato leaves under abaxial (AB) and adaxial leafy supplemental lighting (AD). Under the two methods, a total of 7352 genes and 152 proteins were differentially expressed. Significant differences were observed in genes expression levels and proteins abundances across multiple pathways, mainly including cell process, metabolism process, biological regulation, environment information processing, genetic information processing, metabolism, and organismal systems. The effect of AB on plant growth and development might be due to the increasing expression of some key genes related to plant hormone signaling, light perception, photosynthesis, plant fitness, and promoting fruit ripening. AB mainly up-regulate a series of auxin-responsive genes or factors, auxin polarity transport genes, gibberellin synthesis genes, cell cycle regulator genes, sugar transporters, and fleshy fruit ripening genes. This study provides useful knowledge for improving both the light-use efficiency of plants and fruit yield by adjusting supplemental light approaches.

Tomato is the most economically important horticultural crop. Tomato plants can be cultivated as single- or two-shoot plants. In two-shoot plants, each shoot shares the roots capacity, necessitating double the root activity or transport efficiency to sustain the same solute flux per shoot as in one-shoot plants. The combination of supplemental top-lighting with high pressure sodium lamp (HPS)

and inter-lighting with LEDs increases the yield of tomato plants, with increased fruit weight being a commercially important component of this yield enhancement. The study by Paponov et al. investigated the combined effects of light and branching on fruit size and chemical fruit quality of greenhouse tomatoes. The two-shoot plants had lower yield mainly due to smaller fruit size, instead of source strength limitations, based on the evaluation of leaf weight ratio (LWR), chlorophyll index, specific leaf area (SLA), leaf dry matter percentage, and stem soluble carbohydrate accumulation. Enhanced lighting improved fruit weight and various fruit traits, such as dry matter content, total soluble carbohydrate content, and phenolic content, for both one- and two-shoot plant types. Despite lower mean fruit weight, two-shoot plants exhibited higher values for chemical fruit quality traits, indicating that the fruit growth of two-shoot plants is not limited by the available carbohydrates (source strength), but by the fruit sink strength. Overall, two-shoot branching primarily modified sink capacity, while lighting primarily affected source activity. Two-shoot cultivation reduced the xylem sap concentration of cytokinins that can inhibit the sink capacity of young fruits. Additionally, the increased hydraulic resistance associated with two-shoot plant architecture appears to improve fruit quality due to the higher solute flux from the phloem at the expense of the xylem. The stronger inhibition of sink than source activity, together with the increased hydraulic resistance in the stem, resulted in fruits that were smaller but showed higher accumulation of dry matter content and improved fruit quality traits. Notably, fruits from two-shoot plants had enhanced accumulations of dry matter and phenolic contents.

Coptis chinensis is a perennial, shade-tolerant, evergreen, understory medicinal plant. The rhizome (RO) of *C. chinensis*, which contains alkaloids, especially berberine, is the main effective component for its therapeutic effects. Light directly influences photosynthesis and the demand for metabolites by sinks, which indirectly regulates the redistribution of reserves (Iqbal et al., 2012). The early spring is a seasonal high-light "window" for new leaf growth and photosynthetic carbon capture by the shade-tolerant evergreen understory plants. Ke et al. conducted the study of *C. chinensis* under low and relatively high light intensities in a greenhouse. The plants grown under higher light intensity had higher starch in rhizome (RO) and higher RO biomass at the end of the year compared to those grown under lower light intensity. The photosystem II (PSII) operating efficiency [Y(II)], relative electron transport rate (rETR), and photochemical quenching (qP), as well as sucrose and glucose, in immature leaf (IL) and mature leaf (ML) under relatively higher light, was higher than those under lower light. The glucose and starch concentrations in ILs at 35 d was significantly higher than that at 15 d when plants were under 200 mmol m^{-2} s^{-1}, while they were not significantly changed and remained low at 50 mmol m^{-2} s^{-1}. The proportion of photosynthetic transport from ILs to MLs was significantly higher than that from MLs to ILs under the 50 mmol m^{-2} s^{-1} limit. Total P concentration in ILs was lower under relatively higher light, but there was no difference in nucleic acid P concentration in ILs under the two light intensity treatments. The alkaloid concentration in RO was lower under 200 mmol m^{-2} s^{-1} than that under 50 mmol m^{-2} s^{-1}. Relatively higher light reduces the need for carbohydrates and P stored in the RO to support IL growth by (1) accelerating the sink-to-source transition in ILs, which inhibits the use of reserves in the RO; (2) using energy from MLs to support IL growth, thereby reducing RO reserve consumption, and (3) reducing the demand for P by investing less in the development of photosynthetic machinery.

In summary, the articles in this Research Topic provide a broad overview of the key roles of light environment on growth and quality of horticultural crops. This will highlight innovative and emerging areas in light regulation of horticultural crops and will inspire researchers with a wide range of research interests.

Author contributions

HL: Writing – original draft, Writing – review & editing. JS: Writing – review & editing. GN: Writing – original draft, Writing – review & editing. QL: Writing – review & editing.

Conflict of interest

The authors declare that the research was conducted in the absence of any commercial or financial relationships that could be construed as a potential conflict of interest.

Publisher's note

References

Holopainen, J. K., Kivimaenpaa, M., and Julkunen-Tiitto, R. (2018). New light for phytochemicals. *Trends Biotechnol.* 36, 7–10. doi: 10.1016/j.tibtech.2017.08.009

Iqbal, N., Masood, A., and Khan, N. A. (2012). Analyzing the significance of defoliation in growth, photosynthetic compensation and source-sink relations. *Photosynthetica* 50, 161–170. doi: 10.1007/s11099-012-0029-3

Sager, J. C., Smith, W. O., Edwards, J. L., and Cyr, K. L. (1988). Photosynthetic efficiency and phytochrome photoequilibria determination using spectral data. *Trans. ASAE* 31, 1882–1889. doi: 10.13031/2013.30952

Zhang, Z. S., Li, Y. T., Gao, H. Y., Yang, C., and Meng, Q. W. (2016). Characterization of photosynthetic gas exchange in leaves under simulated adaxial and abaxial surfaces alternant irradiation. *Sci. Rep.* 6, 26963. doi: 10.1038/srep26963

frontiers | Frontiers in Plant Science

TYPE Original Research
PUBLISHED 05 April 2023
DOI 10.3389/fpls.2023.1118895

OPEN ACCESS

EDITED BY
Houcheng Liu,
South China Agricultural University, China

REVIEWED BY
Laszlo Balazs,
Óbuda University, Hungary
Na Lu,
Chiba University, Japan

*CORRESPONDENCE
Chengyao Jiang
catherinejiang@126.com
Jiaming Liu
liujiaming@cdxzy.cn
Yu Song
songyu150@163.com
Yangxia Zheng
zhengyangxia@163.com

†These authors have contributed equally to this work

SPECIALTY SECTION
This article was submitted to Photosynthesis and Photobiology, a section of the journal Frontiers in Plant Science

RECEIVED 08 December 2022
ACCEPTED 24 March 2023
PUBLISHED 05 April 2023

CITATION
Jiang C, Wu H, Zhang X, Liu J, Li Y, Song Y, Wang J and Zheng Y (2023) Integrating omics reveals insights into tomato abaxial/adaxial leafy supplemental lighting. *Front. Plant Sci.* 14:1118895. doi: 10.3389/fpls.2023.1118895

Integrating omics reveals insights into tomato abaxial/adaxial leafy supplemental lighting

Chengyao Jiang[1*†], Haolian Wu[1†], Xiaoying Zhang[2†], Jiaming Liu[2*], Yushan Li[3], Yu Song[3*], Jue Wang[1] and Yangxia Zheng[1*]

[1]College of Horticulture, Sichuan Agricultural University, Chengdu, China, [2]Laboratory of Crop Immune Gene Editing Technology, Chengdu NewSun Crop Science Co., Ltd., Chengdu, China, [3]Research Institute of Crop Germplasm Resources, Xinjiang Academy of Agricultural Sciences, Urumqi, China

Research revealed that the abaxial leafy supplemental lighting (AB) can significantly improve the net photosynthetic rate and stomatal conductance in the leaves of tomato plants compare to the adaxial leafy supplemental lighting (AD) method. However, the underlying regulatory mechanisms are still poorly understood. Here, we conducted AB and AD on tomato and assessed transcriptomic, and proteomic changes in leaves. The result showed that under the two supplemental lighting methods, a total of 7352 genes and 152 proteins were differentially expressed. Significant differences were observed in genes expression levels and proteins abundances across multiple pathways, mainly including cell process, metabolism process, biological regulation, environment information processing, genetic information processing, metabolism, and organismal systems. Additionally, we also found that some key genes that plant hormone signaling, light perception, photosynthesis, plant fitness, and promoting fruit ripening, have increased significantly, which can explain the effect of AB on plant growth and development. Finally, through the qPCR, we determined that AB mainly up-regulate a series of auxin-responsive genes or factors, auxin polarity transport genes, gibberellin synthesis genes, cell cycle regulator genes, sugar transporters, and fleshy fruit ripening genes. These results help us to understand plant light response mechanism and discover genes which contribute to efficient light energy utilization.

KEYWORDS

***Solanum lycopersicum*, irradiation orientation, photosynthesis, transcriptomic, proteomic**

1 Introduction

Photosynthesis plays a crucial role in determining plant yield, with 90% to 95% of the dry weight of the crop coming from this process (Murchie et al., 2009; Simkin et al., 2020). Improving photosynthetic efficiency can increase crop yield by over 50% (Covshoff and Hibberd, 2012). In tomato production, even a 1% increase in light irradiation can lead to a

20% increase in leaf photosynthesis, resulting in an over 1% increase in fruit yield and improved fruit quality (Jiang et al., 2017; Geelen, 2018). Therefore, enhancing photosynthesis has always been a research priority for improving tomato yield and quality.

Tomatoes (*Solanum lycopersicum*) are nutritious and widely cultivated in the world. In China, even one-third of greenhouses are used for tomato production. This plant prefers sunlight and warm climate. However, in Northern China, greenhouse tomato production faces a challenge of light insufficiency due to greenhouse shading, continuous rainy or snowy weather in winter and spring, and intensive cultivation schedules, greenhouse tomato production which can cause growth failure, decreased fruit yield and quality, and ultimately reduced profitability (Acock et al., 1978; Xu et al., 1997; Hogewoning et al., 2010; Lu et al., 2012; Terfa et al., 2013; Tewolde et al., 2016). Improving the light environment and enhancing the utilization of light energy by plants have become critically important in greenhouse tomato production.

Artificial supplemental lighting can improve the light conditions of plant canopies. Numerous studies have focused on the canopy layer (Hovi et al., 2004; Hovi and Tahvonen, 2008; Pettersen et al., 2010), light source (Lu et al., 2012; Song et al., 2016), light intensity (Dorais, 2003; Song, 2017), and light period (Matsuda et al., 2014; Tewolde et al., 2016). Recent studies have reported exciting results regarding the effective positioning of supplemental lighting (Zhang et al., 2015; Song et al., 2016; Zhang et al., 2016; Jiang et al., 2017; Li et al., 2017; Song, 2017; Jiang et al., 2019; Song et al., 2021; Jiang et al., 2022), including the use of abaxial leafy supplemental lighting (AB) and adaxial leafy supplemental lighting (AD) to greenhouse tomatoes. Leaves irradiated with AB demonstrated a 15.8% increase in the quantum yield of PSII electron transport (ΦPSII) compared to those treated with AD, resulting in a tomato fruit yield increase of at least 10.7% (Song et al., 2016; Jiang et al., 2017; Jiang et al., 2022). Similar results were observed in grapes (Li et al., 2017), and lettuce (Zhang et al., 2015). Blue light irradiation of grape leaf abaxial surfaces significantly increased CO_2 assimilation, while compound and red light both enhanced berry mass (Li et al., 2017), suggesting that light spectrum wavelength can have composite effects. Moreover, research on the characterization of photosynthetic gas exchange in leaves of trees (*Platanus orientalis* L. and *Melia azedarach* L.) and herbs (*Solanum lycopersicum* L.) demonstrated that bifacial leaves can fix more carbon than leaves with one irradiation surface when exposed to the same irradiation amount (Zhang et al., 2016). These exciting findings inspired us to consider efficient irradiated surfaces of the functional blade as a method to enhance the profitability of supplemental lighting in greenhouses. Additionally, these findings piqued our curiosity regarding the underlying mechanism which may present a new starting point for overcoming the damage of light insufficiency stress to greenhouse vegetable production and ensuring both high yield and quality of greenhouse-grown tomatoes.

The developmental mechanism that governs the functional behavior and formation of flat leaf lamina in relation to adaxial–abaxial fate has long been of interest to biologists. For several decades, researchers have recognized a functional relationship between photosynthesis activity and the differentiation of adaxial and abaxial leaf fate. According to some scholars the thicker cuticle of the leaf surface and smaller chloroplast volume lead to the highest internal photosynthesis rates in the middle and lower palisade layers, rather than near the adaxial leaf surface (Sun and Nishio, 2001; Evans and Vogelmann, 2003; Soares et al., 2008). Moreover, the adaxial/abaxial specification in the regulation of photosynthesis is influenced by the differential sensitivity of stomatal opening to light orientation and fixed gradients of enzyme activation across the leaf (Soares et al., 2008). Although several distinct regulators involved in leaf adaxial–abaxial photosynthetic response and lamina outgrowth have been identified (Yamaguchi et al., 2012), the underlying regulatory mechanisms, are still insufficiently understood, and the molecular basis of this interaction remains unclear.

In this study, we treated greenhouse-grown tomatoes with both AB and AD and assessed transcriptomic and proteomic changes in the leaves. By analyzing the significant differences in genes expression levels and proteins abundances, we hope to locate key genes and possible pathways involved, and create a regulatory map that we can use to investigate the underlying regulatory mechanisms of AB on tomatoes. This study provides useful knowledge for improving both the light-use efficiency of plants and fruit yield by adjusting artificial light sources.

2 Materials and methods

2.1 Materials and plant growth condition

Tomato (*S. lycopersicum*) '*Jinpeng* No.1'(Ding et al., 2019) was used in this research and experiments were conducted in Chengdu, Sichuan Province, China (104.06°E, 30.67°N) between December 2021 and March 2022. Seeds were sown in a plastic seedling tray (53 × 27.5 × 4.5 cm) filled with substrate (Pindstrup, Demark) and housed within an artificial climate chamber (RTOP-1000D, Top Yun Co. Ltd., Hanzhou, China) with climate settings held at 28 ± 1°C during the day and 18 ± 1°C during the night with 65 ± 5% relative humidity and a photoperiod of 14 h. Three replicated groups, each containing 100 seeds were established. Three weeks after sowing, 60 uniform seedlings from each group with two fully expanded leaves were transplanted into 7 × 7 × 8 cm black plastic pots filled with substrate (Pindstrup, Demark) in a Venlo-type arrangement, with double spans in a north–south orientation greenhouse (9.6×4×4.5m) at a set climate of 30°C/15° C temperatures (day/night) and 65% relative humidity with automatic air conditioning. The daily maximum natural indoor light intensity (PPFD) varied from 100 to 250 $\mu mol \cdot m^{-2} \cdot s^{-1}$ (measured at the same height of top canopy of tomato plants). Plants were set 10-13 cm apart from one another. After three weeks of irrigation with a half dose of Yamazaki nutrient solution (EC 1.0 ± 0.2 mS/cm), the dose of the solution was doubled (pH 6.5 ± 0.5, EC 2.0 ± 0.5 mS/cm) until the conclusion of the experiment.

2.2 Supplemental lighting treatment

120 tomato seedlings grown in the same environment were taken 2 weeks after transplanting and randomly divided into two groups. Light-emitting diodes (LED; Philips Netherlands Ltd.) were

used as light sources (Figure 1A). The lighting was processed in two orientations: abaxial leafy supplemental lighting (AB) and adaxial leafy supplemental lighting (AD) (Figure 1B), according to previous reports (Song et al., 2016; Jiang et al., 2017) with minor adjustments. The LED was fixed on a movable beam to ensure that illumination distance from the adaxial epidermis of the inner canopy truss or the abaxial epidermis of the lowest leaf truss was maintained at 10 cm. For this, the third leaf from both inner canopy truss or lowest truss was taken as a reference, and plant position was adjusted to ensure vertical growth and a consistent plane of stem axis within the same row when necessary. The supplemental lighting PPFD, measured at a distance of 10 cm from the LED module, was 200 μmol·m^{-2}·s^{-1} with a supplemental lighting photocycle of 16h (6:00-22:00), maintained by an integrated digital timer-dimmer-transformer (EEIO-600W-1000W, Shengyuan Electric Appliance Co., Ltd, Zhongshan, China). Each treatment consisted of three rows of

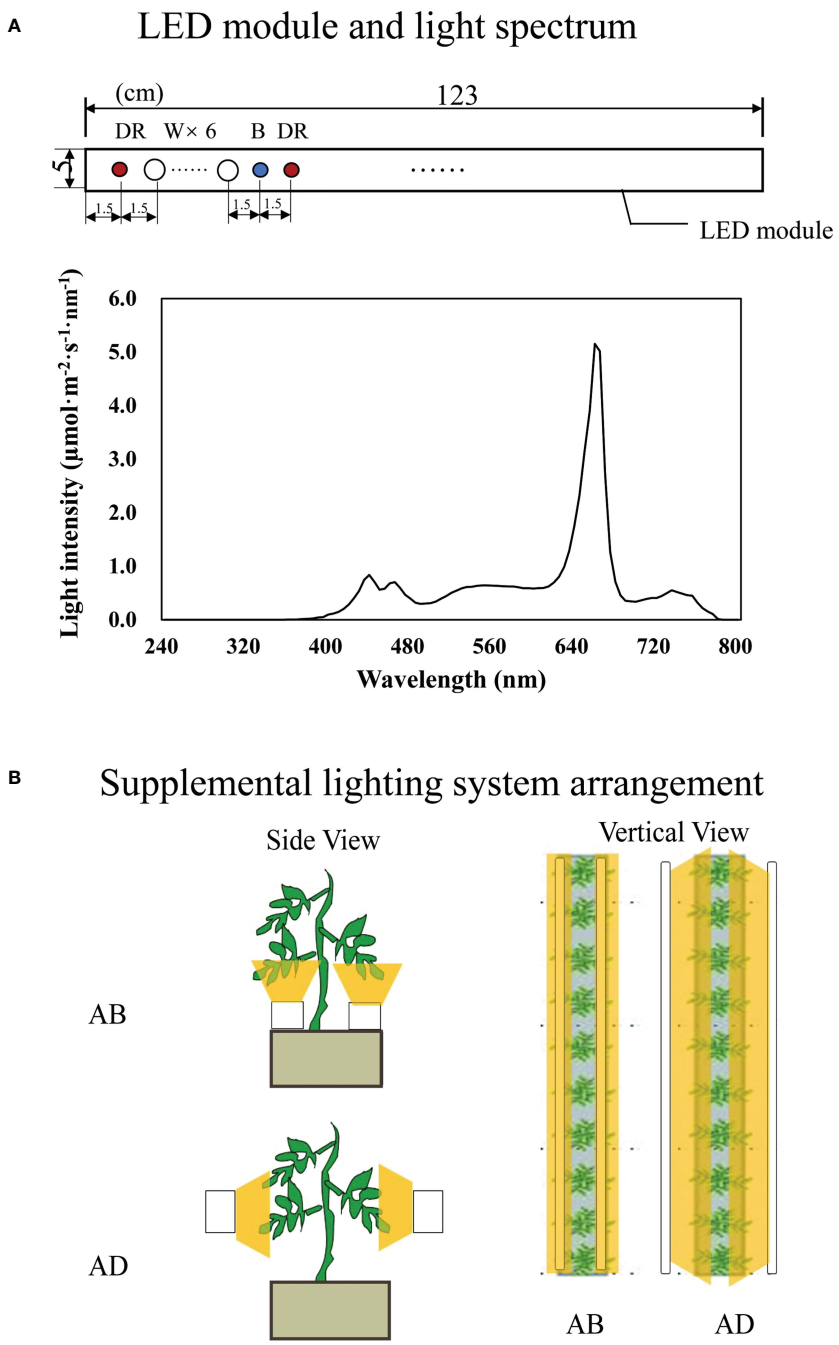

FIGURE 1
Schematic diagram of LED module characters **(A)** and the supplemental lighting arrangement **(B)**. Abaxial leafy supplemental lighting (AB) and the adaxial leafy supplemental lighting (AD) was applied to plants from the 14th day after transplanting. The supplemental lighting is powered by deep red, white and blue (DR/W/B) LEDs. Each LED module is at a size of 123×5cm and contains 9 groups of color chips (diameter of 7 mm with axis arrangement) at 1DR+6W+1B+1DR **(A)**. LEDs were provided 10 cm from the abaxial or adaxial epidermis of leaves **(B)**, with a PPFD of 200 μmol·m^{-2}·s^{-1}.

plant benches with each row containing 20 plants. After 16 hours of light treatment, the whole leaves of 5 plants from either AB or AD treatment which were randomly selected were mixed as a sample (Liu et al., 2020) for RNA-seq and proteomics analysis.

2.3 Gas-exchange parameter measurements

Gas-exchange measurements were conducted based on previous reports (Song et al., 2016). In brief, we selected the second terminal leaflets of leaves on the fifth youngest node with a portable photosynthesis system (Li-6400XT; Li-Cor Inc., Lincoln, NE, USA) during 11:00–16:00, GMT +8 (9:00–14:00, local time) on the 28th day after transplanting. The net photosynthetic rate (P_N), stomatal conductance (*Gs*), and transpiration rate (*Tr*) were measured. Measurements were conducted with PPFD, leaf temperature, CO_2 concentration, and relative humidity of 800 ± 5 μmol·m^{-2}·s^{-1}, 28 ± 1° C, 400 ± 2 μmol·m^{-2}, and 63 ± 2%, respectively.

2.4 RNA extraction and illumina sequencing

A total of 6 *S. lycopersicum* samples, including 3 AB samples and 3 AD samples, were analyzed by RNA-Seq. Total RNAs were extracted from frozen fresh tomato leaves using an EASYspin Plus Kit according to the manufacturer's instructions (Aidlab Biotechnologies Co. Ltd., Beijing, China). The quality and quantity of extracted RNAs were measured using agar gel electrophoresis and Nanodrop micro spectrophotometry in combination (Thermo Scientific, Wilmington, DE, USA). RNAs from three biological replicates (0.5 g per sample) across at least five plants with the same concentration and volume were combined for RNA-seq. The sequencing library was constructed using a NEBNext Ultra RNA library prep kit (NEB#E7530, New England Biolabs, Ipswich, MA, USA). The quality of the cDNA library was measured using a DNA 1000 assay Kit (5067-1504, Agilent Technologies, Santa Clara, CA, USA) prior to sequencing on an Illumina HiSeq TM 2500 by Gene *De novo* Biotechnology Co. (Guangzhou, China). RNA-seq data was downloaded from the SRA database (accession number: PRJNA895868). Clean reads were compared to the reference genome sequence using HISAT software (Kim et al., 2015).

2.5 Differentially expressed genes (DEGs) analysis

Differentially expressed genes (DEGs) between AB samples and AD samples were identified using the DEGseq software package (http://www.bioconductor.org/packages/2.6/bioc/html/DEGseq.html). Manually identified DEGs (log2 value≥1.5-fold difference, p-value less than 0.01) were then subjected to enrichment analysis using Gene Ontology (GO) functions and KEGG pathways. GO DEGs enrichment analysis provided all GO terms that were significantly enriched in DEGs compared to the genomic background. All DEGs were mapped to GO terms in the Gene Ontology database (http://www.geneontology.org/). Significantly enriched GO terms (FDR correction p-value ≤ 0.05) were identified by a hypergeometric test by comparing them to the genomic background. Pathway enrichment analysis was performed using the Kyoto Encyclopedia of Genes and Genomes (KEGG) database. Pathways with FDR-corrected p-values ≤ 0.05 were defined as significantly enriched DEG pathways.

2.6 Protein extraction, iTRAQ labeling, and proteomics analysis

At least 5 seedlings were mixed in each replicate. Total protein was extracted using the cold acetone method and labeled with iTRAQ tags. Shotgun proteomic analyses were performed using an EASYnLC^{TM}1200 UHPLC system (Thermo Fisher, Shanghai, China) with an Orbitrap Q Exactive HF-X mass spectrometer (Thermo Fisher, Shanghai, China). iTRAQ quantification was implemented using IQuant software (Wen et al., 2014). Proteins with a fold change of > 1.2 or < 0.8 and unadjusted significance level $p < 0.05$ were considered differentially expressed proteins.

The enrichment analysis of differentially expressed proteins (DEPs) was performed by GO and KEGG analysis. The iTRAQ proteomic data were deposited in the ProteomeXchange Consortium (http://proteomecentral.proteomexchange.org) *via* the iProX partner repository, using the iProX data license number is PXD038211.

2.7 Quantitative real time PCR (qPCR) analysis

A set of DEGs and DEPs identified in this research (30 total genes, 25 genes from RNA-seq and 5 from iTRAQ) were selected were selected for qPCR analysis and verification of transcriptional changes after AB treatments for 0, 1, 2, 4, 6, 8, 12, and 24 hours. AD plants were maintained as controls. Tomato *actin* was used as an internal reference. The primers used were designed using Primer Premier 5.0 (Premier) and are listed in Table S1.

2.8 Statistical analyses

Triplicate data were analyzed using SAS 9.0 software (SAS Institute Inc., North Carolina, USA) according to SAS Tutorials: Analyzing Data (https://libguides.library.kent.edu/SAS/AnalyzeData). The statistical significance of the difference was evaluated by a Student's t test and least square means analysis at the level <0.05.

3 Results

3.1 Phenotypic characterization and gas-exchange parameter

The morphology of tomato seedlings after 2 weeks of the abaxial leafy supplemental lighting (AB) and the adaxial leafy supplemental

lighting (AD) can be seen in Figure 2A. Compared with AD, AB significantly increased tomato plant height, while fresh weight increased slightly but not significantly (Figures 2B, C). In addition, AB significantly increased the P_N and *Gs* (Figures 2D, E), while *Tr* was increased slightly but not significantly (Figures 2F).

3.2 Transcriptome sequencing and *de novo* assembly

RNA-Seq analysis yielded an average of 11.23 Gb of data per sample. The average alignment rate of the sample comparison genome was 95.17%, and the average alignment rate of the compared gene set was 88.03%. The number of predicted new genes was 25,970 and the total number of detected expressed genes was 47,249, of which 22,279 were known, and 24,970 were predicted new genes. A total of 33,220 new transcripts were detected, of which 503 belonged to novel alternatively spliced isoforms of known protein-coding genes, and 25,970 belonged to new protein-coding gene transcripts. The remaining 6,747 belonged to long non-coding RNAs.

3.3 Gene expression difference analysis

The screening conditions for DEGs were FDR < 0.05 and | log2FC| > 1. A total of 10,998 genes were differentially expressed, with 5280 down-regulated and 5718 up-regulated genes (Tables S2). MA plot, Volcano plot, and Scatter-plot were used to display the distribution of DEGs, and an expression heat map was made for each group of DEGs, shown in Figure S1.

3.4 GO and KEGG enrichment analysis of DEGs

GO and pathway enrichment analyses were performed for all significantly DEGs (Figure 3). Different comparisons exhibited

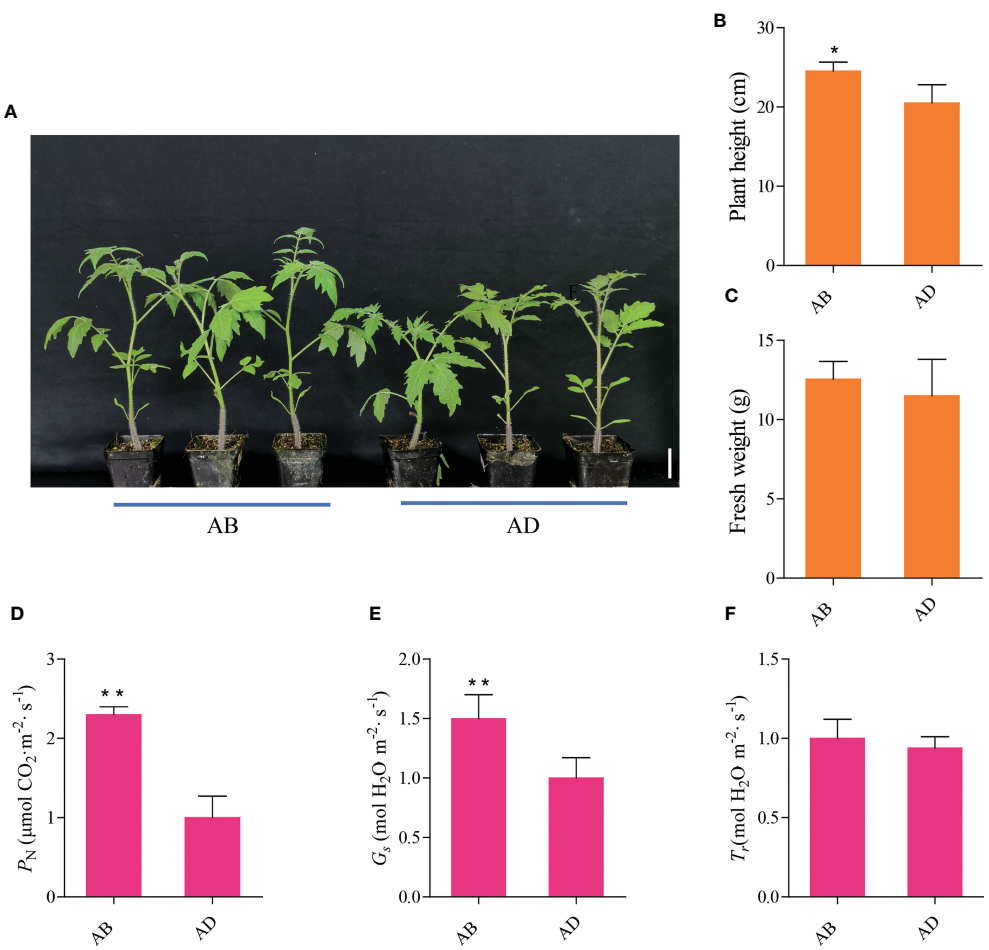

FIGURE 2
Phenotypic characterization and gas exchange parameters of the abaxial leafy supplemental lighting (AB) and the adaxial leafy supplemental lighting (AD). The ensemble morphology characteristics of plants **(A)**, the effects of AB and AD treatments on plant height **(B)**, fresh weight **(C)**, photosynthetic rate (P_N; **D**), stomatal conductance (*Gs*; **E**), and transpiration rates (T_r; **F**) in the leaves of tomato plants. Parameters were measured on the second terminal leaflet of the leaf and the fifth youngest node for each treatment. Measured using PPFD, leaf temperature, CO_2 concentration, and relative humidity at 800 ± 5 μmol m^{-2} s^{-1}, 28 ± 1°C, 400 ± 2 μmol m^{-2}, and 63 ± 2%, respectively. Mean ± SE (n = 8). Asterisk indicate significant differences at P < 0.05 according to Student's t test.

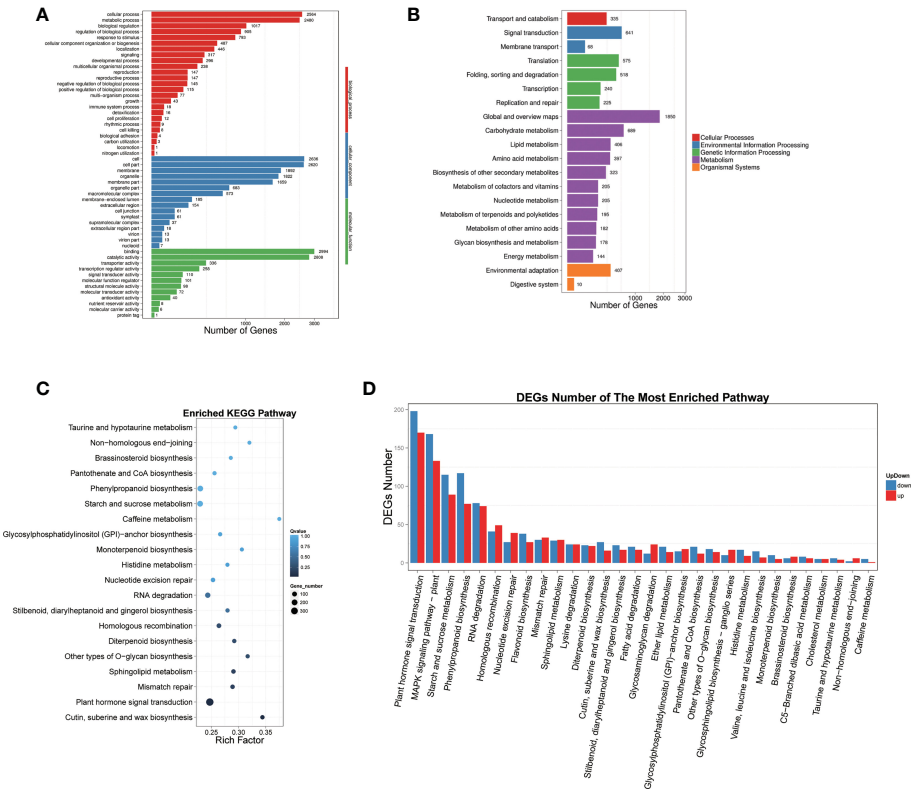

FIGURE 3
GO and pathway enrichment analyses were performed for all significant DEGs. **(A)** GO classification map of DEGs, the X-axis represents the number of genes, and the Y-axis represents the GO functional classification. **(B)** The X-axis represents the proportion of genes accounted for and the Y-axis represents the KEGG functional classification. **(C)** Pathway enrichment of DEGs, X-axis represents enrichment factor value, Y-axis represents pathway name. The color represents q-value (the whiter the color the larger the value, the bluer the smaller the value), the smaller the value means The smaller the value, the more significant the enrichment result. The size of the dot represents the number of DEGs. **(D)** Enrichment pathways of up- and down-regulated DEGs. The X-axis represents the Pathway entry, and the Y-axis represents the number of up- and down-regulated genes corresponding to the Pathway entry.

similar distribution patterns with regard to the numbers and types of enriched pathways, which may be divided into three main functional groups, including 25 biological processes, 16 molecular functions, and 12 cellular components (Figure 3A). Significant differences were observed at the level of gene expression in multiple pathways, chiefly including cell process (2564 genes), metabolism process (2480 genes), biological regulation (1017 genes), regulation of biological process (905 genes), response to stimulus (793 genes), and cellular component organization or biogenesis (487 genes).

According to the DEG results, we carried out KEGG biological pathway classification and enrichment analysis. The pathway classification findings illustrated that the functions of DEGs were mainly concentrated in five branches, including Cellular Processes, Environmental Information Processing, Genetic Information Processing, Metabolism, and Organic Systems (Figure 2B). The majority of gene functions were focused in metabolic pathways. Pathway enrichment results showed that the top five DEGs were predominantly concentrated in plant hormone signal transduction, cutin, suberine and wax biosynthesis, mismatch repair, sphingolipid metabolism, and other types of O-glycan biosynthesis (Figure 3C). Further analysis demonstrated that the DEGs could be classified into 30 categories, and the top five groups were plant hormone signal transduction, MAPK signaling pathway, starch and sucrose metabolism, and phenylpropanoid biosynthesis (Figure 3D).

3.5 Differentially expressed transcription factor (TFs) and specific regulated genes

We made predictions for DEGs with the ability to encode transcription factors (TFs), and, classified and counted transcription factor families to which the differently expressed genes belonged. Our findings showed that the six most abundant transcription factors were MYB, MYB-related, bHLH, AP2, MADS, and NAC which contained 486, 380, 274, 264, 169, and 155 transcription factors, respectively (Figure S2).

We also found that many plant hormone signal-regulated genes were significantly upregulated upon AB treatment, including three gibberellin biosynthesis genes *20ox-3*, *GA2ox5*, and *GAI*, four auxin transport genes *PIN4*, *PIN6*, *PIN7*, and *PIN9*, two auxin response genes *IAA13* and *IAA23*, five auxin response factors *ARF5*, *ARF8*, *ARF9*, *ARF12*, and *ARF18*. Special regulatory genes, such as three sugar transporters SWEET1, SWEET12, and SWEET14, four cell

cycle regulators cdkB2, CycA1, CycA2, and cycd3c3, were also significantly upregulated under AB treatment (Table S2).

3.6 iTRAQ analysis reveals AB responses of tomato leaf proteins

To investigate the effect of AB on protein expression, we performed iTRAQ analysis on tomato leaves under AB and AD treatments. Across all samples, a total of 338,790 secondary spectra were generated and downloaded. Using the filter standard of "1% FDR", a total of 21,668 peptides and 5,390 proteins were identified. The significantly different proteins (DEPs) were identified as having a fold change> 1.2 or <0.8 and a Q-value < 0.05, and 152 DEPs, including 65 upregulated proteins and 87 downregulated proteins, were identified (Table S3).

We further conducted functional classification and enrichment analyses of these identified DEPs. The biological processes of DEPs often included cellular process, metabolic process, biological regulation, response to stimulus, regulation of biological process, and cellular component organization or biogenesis (Figure 4A), which was consistent with GO analysis results of DEGs (Table S2). Pathway enrichment analysis of DEPs demonstrated that the altered biological pathways were mainly distributed in oxidative phosphorylation, AGE–RAGE signaling pathway in diabetic complications, arginine and proline metabolism, mRNA surveillance pathway, phagosome, and plant hormone signal transduction, et al. (Figure 4B).

3.7 Integration of transcriptomic and proteomic data

Integrating proteomic and comprehensive transcriptomic data analysis provided an important validation tool for the expression of key genes. However, it has been established that changes in gene expression do not imply a corresponding change in protein content. We integrated transcriptomic and proteomic data to analyze the regulation of gene expression changes in response to protein expression changes. Our findings indicated that 17 genes and proteins were upregulated together, including NADH dehydrogenase, aspartate aminotransferase 3 (ASP3), casein kinase II subunit alpha, stromal cell-derived factor 2-like protein (SDF), protein argonaute 5 (AGO5), xyloglucan endotransglucosylase/hydrolase 1(XTH1), putative ABC1 protein, metal transporter Nramp3 (NRAMP3), PLAT domain-containing protein 1 (PLAT1), lysophospholipase BODYGUARD 3 (BDG3), formate dehydrogenase (FDH1), thiamine pyrophosphokinase 1 (TPK1), inositol phosphorylceramide glucuronosyl transferase 1 (IPUT1), patatin-like protein 1(PLP1), LysM domain receptor-like kinase 3 (LYK3), Non-specific lipid-transfer protein 2 (LE16), and heat stress transcription factor A-1 (HSFA1) (Table S3).

Moreover, 18 genes and proteins were downregulated simultaneously, including phenylalanine ammonia-lyase (PAL5), pre-mRNA-splicing factor ATP-dependent RNA helicase (DEAH4), histone H2A.1, serine/threonine-protein kinase (SAPK3), DNA-directed RNA polymerases II, IV, and V subunit 9A (NRPB9A), KH domain-containing protein, protein SMAX1-LIKE 3 (SMXL3), 40S ribosomal protein S16 (RPS16), receptor-like protein kinase (HSL1), polyprenol reductase 2 (PPRD2), basic blue protein, nuclear pore complex protein (NUP1), eukaryotic translation initiation factor 3 subunit H (TIF3H1), histone H2A.1, Chlorophyllase-2 (CLH2), exocyst complex component (EXO70A1), and transcription termination factor (MTERF8).

3.8 Verification of RNA-seq using qPCR

We used qPCR to further determine gene expression levels in *S. lycopersicum* under AB treatment. The results were consistent with those from RNA-seq and proteomic analyses (Figure 5). It was shown that AB does promote upregulated expression of some key genes, such as *20ox-3*, *GA2ox5*, *GA2ox8*, *GA2ox10*, *GAI*, *IAA13*, *IAA23*, *PIN4*, *PIN6*, *PIN7*, *PIN9*, *SWEET12*, *SWEET14*, *CycA1*, *CycA2*, and *Cryptochrome DASH*. Our results ultimately contribute to the understanding of plant light response mechanisms and the discovery of efficient light utilization genes.

4 Discussion

Environmental factors can directly alter plant morphogenesis which is theoretically believed to be controlled solely by genetic factors (Wahidin et al., 2013; Song et al., 2016; Jiang et al., 2022). Supplemental lighting has been demonstrated to significantly improve plant photosynthetic performance, increase the biomass and yield of tomato plants, accelerate fruit ripening, improve later fruit quality, and make fruit size and color uniform (Seginer et al., 2006; Song et al., 2016; Jiang et al., 2017). In this study, we observed a significantly increased number of P_N, and G_s (Figures 2D, E), and a slightly but not significantly increased T_r in plants treated with AB (Figures 2F). This was largely consistent with previous research results (Song et al., 2016; Jiang et al., 2017). These results reconfirmed the feasibility of using AB to significantly improve photosynthetic efficiency of a plant to obtain higher economic benefits. From another perspective, this also demonstrated that in-depth analysis of the molecular regulation mechanism of AB treatment on plants bridges the gap between theory and practice for functional gene mining. Additionally, our approach has helped in overcoming or alleviating the damage of light insufficiency stress in greenhouse vegetable production, improving facility industry income, and realizing efficient photosynthetic breeding of crops.

In our study, phenotypic characterization was performed and gas exchange parameters were measured in tomato seedlings under AB and AD treatments, and the results were generally consistent with previous reports (Song et al., 2016; Jiang et al., 2017). However, there was a slight but not significant increase in *Tr*, which may have been related to the node of measurement. Subsequently, we assessed transcriptomic and proteomic changes in tomato leaves under two light supplementation methods by RNA-seq and iTRAQ,

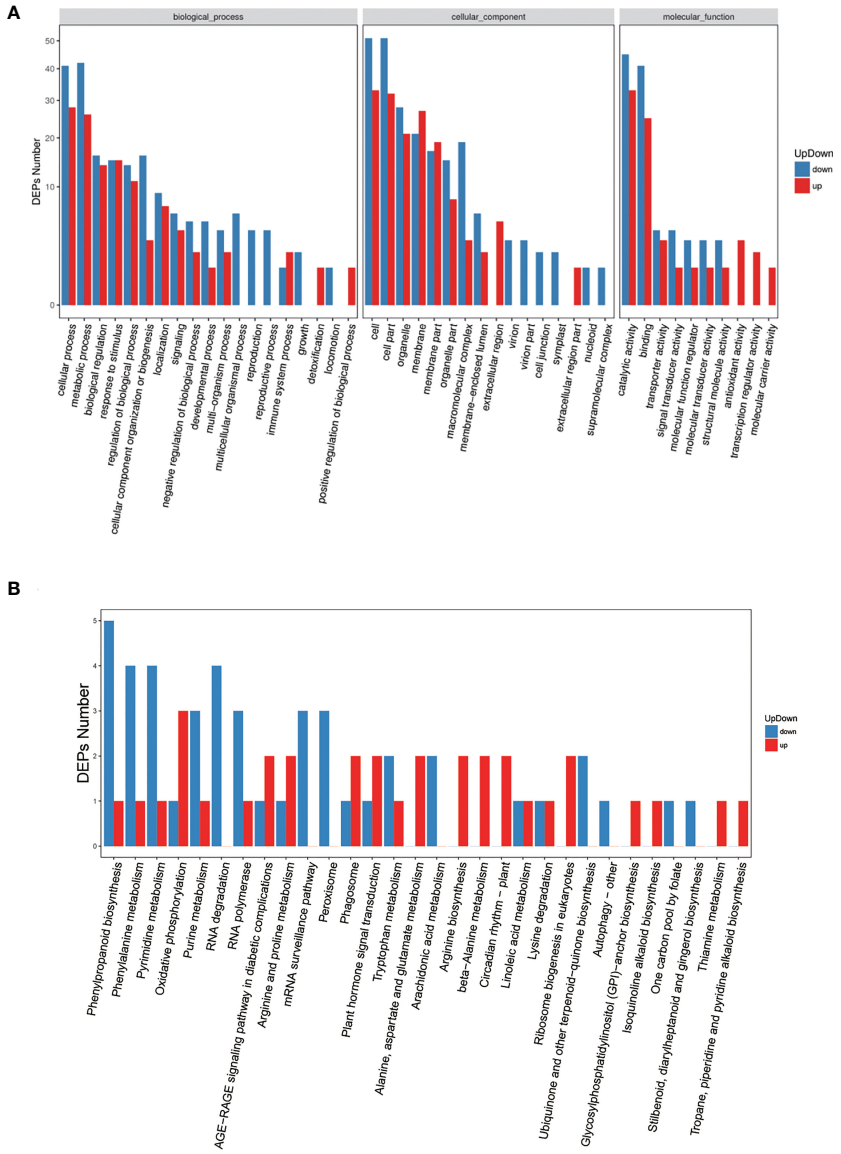

FIGURE 4
GO and pathway enrichment analyses for all significant DEPs. **(A)** Gene ontology analysis of DEPs, x-axis displays GO term, y-axis displays protein count。 **(B)** Pathway analysis of DEPs, x-axis displays pathway name, y-axis displays DEP count.

respectively. The results illustrated that there were 7,352 differentially expressed genes (DEGs) and 152 differentially expressed proteins (DEPs) between AB and AD treatments. The functions of these DEGs were mainly concentrated in five branches, including cellular processes, environmental information processing, genetic information processing, metabolism, and organic systems (Figures 3A, B). Pathway enrichment results demonstrated that the top five DEGs were mainly concentrated in keratin, folinic acid and wax biosynthesis, phytohormone signaling, mismatch repair, sphingolipid metabolism, and other types of O-glycan biosynthesis (Figure 3C). Further experiments revealed that DEGs can be divided into 30 categories, with the five most abundant being phytohormone signaling, MAPK signaling pathway, starch and sucrose metabolism, and phenylalanine biosynthesis (Figure 3D). Our previous study demonstrated that AB resulted in 15. 8% higher quantum yield of PSII electron transport (ΦPSII), 10.2% higher stomatal conductance (*Gs*), 8.5% higher CO_2 carboxylation efficiency (CE), 10.7% higher tomato fruit yield, and 13.5% higher fruit soluble solids content compared with AD (Song et al., 2016; Jiang et al., 2017). These findings suggest that the differential expression of these genes under AB treatment may be the main reason for the changes in physiological indicators of tomato plants.

Light is an important environmental signal responsible for regulating various growth and developmental processes in plants. Among these light-regulated processes, multiple hormone pathways are commonly regulated by light to mediate developmental changes, such as gibberellin (GA), abscisic acid (ABA), growth hormone, and cytokinin (Jiao et al., 2007; Lau and Deng, 2010). In our study, many phytohormone signaling regulatory genes were significantly upregulated under AB treatment, including three gibberellin

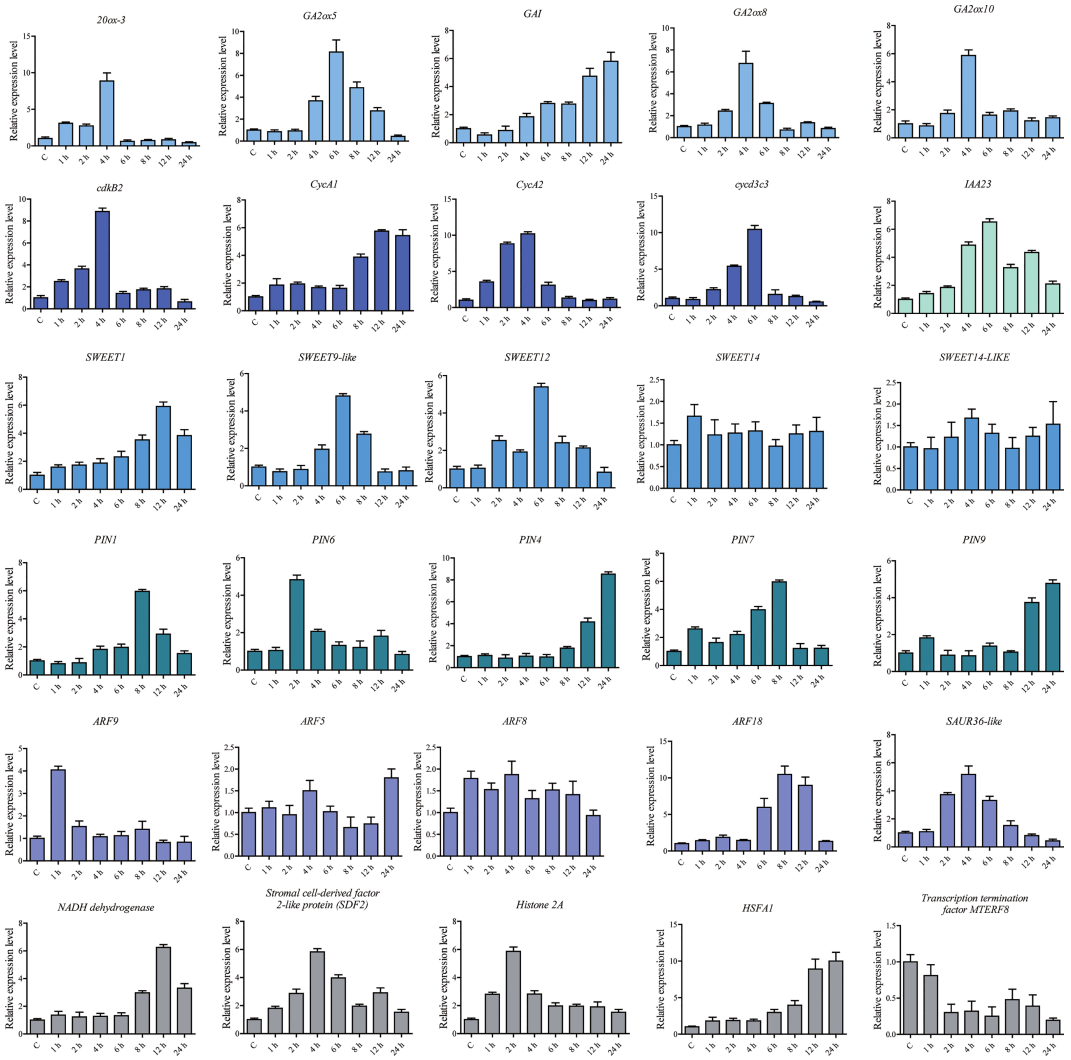

FIGURE 5
Relative expression levels of DEGs and DEPs analyzed using qPCR under the abaxial leafy supplemental lighting (AB) treatment. The relative expression level of each gene was calculated relative to the expression in the respective untreated control samples (0 h). *Solanum lycopersicum* Sly-*Actin* (*Solyc11g005330.2*) was used as an internal control to normalize the expression data. Different colors represent genes in different signaling pathways. The error bars represent the standard deviation calculated based on three biological replicates.

biosynthesis genes *20ox-3*, *GA2ox5*, and *GAI*, four auxin transporter genes *PIN4*, *PIN6*, *PIN7*, and *PIN9*, two auxin response genes *IAA13* and *IAA23*, and five auxin response factors *ARF5*, *ARF8*, *ARF9*, *ARF12*, and *ARF18*. In addition, we found specific regulatory genes, such as three sugar transporters *SWEET1*, *SWEET12*, and *SWEET14*, four cell cycle regulators *cdkB2*, *CycA1*, *CycA2*, and *cycd3c3* were significantly upregulated under AB treatment, suggesting that these genes may be related to plant light response.

Integrating proteomic and transcriptomic data revealed that 17 genes were upregulated and 18 were downregulated simultaneously with proteins. These include several key genes that promote plant photosensitivity, enhance photosynthesis, increase plant adaptability, and promote fruit ripening, suggesting that these genes possess potential light-regulated functionality which requires further validation. Notably, many key genes within the mTOR pathway were significantly upregulated (Figure S3). In mammals, mammalian target of rapamycin (mTOR), a highly conserved serine threonine protein kinase, is a component of the phosphatidylinositol 3-kinase (PI3K) cell survival pathway which monitors nutrient availability, mitogenic signals, as well as cellular energy and oxygen levels, and is therefore important in regulating cell growth and proliferation (Tsang et al., 2007; Zarogoulidis et al., 2014). mTOR primarily responds to growth factor stimulation and regulates cytoskeletal organization and metabolism. This protein achieves its regulatory effects on cell growth, cell cycle, and other physiological functions mainly through the PI3K/Akt/mTOR pathway, indicating that AB treatment may impact plant development by regulating key genes within the plant mTOR pathway.

To determine the expression levels of some genes under AB treatment, qPCR was performed, and it was determined that AB treatment did promote upregulated expression of some key genes,

including *20ox-3*, *GA2ox5*, *GA2ox8*, *GA2ox10*, *GAI*, *IAA13*, *IAA23*, *PIN4*, *PIN6*, *PIN7*, *PIN9*, *SWEET12*, *SWEET14*, *CycA1*, *CycA2*, and *Cryptochrome DASH*. Ultimately, our findings will contribute to a more complete understanding of plant light response mechanisms and to the discovery of genes which contribute to efficient light energy utilization.

Data availability statement

The datasets presented in this study can be found in online repositories. The names of the repository/repositories and accession number(s) can be found in the article/Supplementary Material.

Author contributions

CJ, JL, and YS conceived and coordinated the project; CJ and JL designed experiments, edited the manuscript, analyzed data, and wrote the first draft of the manuscript; HW analyzed data and performed experiments; XZ and YL provided analytical tools and managed reagents; JW and YZ contributed valuable discussions. All authors contributed to the article and approved the submitted version.

Funding

This research was financially supported by the National Natural Science Foundation of China (31960622 and 32202581), the China Postdoctoral Science Foundation (2021MD703889), the Natural Science Foundation of Sichuan Province (2022NSFSC1759) and Central Guidance on Local Science and Technology Development Fund of Shaanxi Province (2022ZY1-CGZY-07).

Conflict of interest

Authors XZ and JL were employed by Chengdu NewSun Crop Science Co., Ltd.

The remaining authors declare that the research was conducted in the absence of any commercial or financial relationships that could be construed as a potential conflict of interest.

Publisher's note

Supplementary material

The Supplementary Material for this article can be found online at: https://www.frontiersin.org/articles/10.3389/fpls.2023.1118895/full#supplementary-material

SUPPLEMENTARY FIGURE 1
Statistical results of differentially expressed genes (DEGs). **(A)** MA plot; **(B)** Volcano plot; **(C)** Scatter-plot; **(D)** The expression heat map was made for each group of DEGs. Red and blue points represent up- and down-regulated genes, respectively. Gray points represent no difference genes.

SUPPLEMENTARY FIGURE 2
Classification of transcription factor (TF) families to which DEGs belong.

SUPPLEMENTARY FIGURE 3
Differentially expressed genes (DEGs) in the mammalian target of rapamycin (mTOR) pathway.

References

Acock, B., Charles-Edwards, D. A., Fitter, D. J., Hand, D. W., Ludwig, L. J., Warren Wilson, J., et al. (1978). The contribution of leaves from different levels within a tomato crop to canopy net photosynthesis: An experimental examination of two canopy models. *J. Exp. Bot.* 29, 815–827. doi: 10.1093/jxb/29.4.815

Covshoff, S., and Hibberd, J. J. M. (2012). Integrating C4 photosynthesis into C3 crops to increase yield potential. *Curr. Opin. Biotechnol.* 23, 209–214. doi: 10.1016/j.copbio.2011.12.011

Ding, J. J., Zhao, J. T., Pan, T. H., Xi, L. J., Zhang, J., and Zou, Z. R. (2019). Comparative transcriptome analysis of gene expression patterns in tomato under dynamic light conditions. *Genes* 10, 662. doi: 10.3390/genes10090662

Dorais, M. (2003). "The use of supplemental lighting for vegetable crop production: Light intensity, crop response, nutrition, crop management, cultural practices," in *Proceedings of the Canadian Greenhouse Conference*, Toronto, QN, Canada, 1 August.

Evans, J. R., and Vogelmann, T. C. (2003). Profiles of 14C fixation through spinach leaves in relation to light absorption and photosynthetic capacity. *Plant Cell Environ.* 26, 547–560. doi: 10.1046/j.1365-3040.2003.00985.x

Geelen, P. A. M. (2018). "Monitoring plant load," in *Plant empowerment*. Eds. P. A. M. Geelen, J. O. Voogt and P. A. van Weel (Wallingford, UK: CABI Publishing), p 200–p 234.

Hogewoning, S. W., Douwstra, P., Trouwborst, G., Ieperen, W. V., and Harbinson, J. (2010). An artificial solar spectrum substantially alters plant development compared with usual climate room irradiance spectra. *J. Exp. Bot.* 61, 1267–1276. doi: 10.1093/jxb/erq005

Hovi, T., Nakkila, J., and Tahvonen, R. (2004). Intra-canopy lighting improves production of year-round cucumber. *Scientia Hortic.* 102, 283–294. doi: 10.1016/j.scienta.2004.04.003

Hovi, T., and Tahvonen, R. (2008). Effect of inter-lighting on yield and external fruit quality in year-round cultivated cucumber. *Scientia Hortic.* 116, 152–161. doi: 10.1016/j.scienta.2007.11.010

Jiang, C., Johkan, M., Hohjo, M., Tsukagoshi, S., Ebihara, M., Nakaminami, A., et al. (2017). Photosynthesis, plant growth, and fruit production of single-truss tomato improves with supplemental lighting provided from underneath or within the inner canopy. *Scientia Hortic.* 222, 221–229. doi: 10.1016/j.scienta.2017.04.026

Jiang, C., Rao, J., Rong, S., Ding, G., Liu, J., Li, Y., et al. (2022). Fruit quality response to different abaxial leafy supplemental lighting of greenhouse-produced cherry tomato (Solanum lycopersicum var. cerasiforme). *Horticulturae* 8, 423. doi: 10.3390/horticulturae8050423

Jiang, C., Song, Y., and Li, Y. (2019). Effects of different supplemental lightning modes on photosynthetic performance and carbon sequestration of tomato leaves in Gobi greenhouse. *China Vegetables* 10, 32–38. doi: 10.19928/j.cnki.1000-6346.2019.10.006

Jiao, Y., Lau, O. S., and Deng, X. W. (2007). Light-regulated transcriptional networks in higher plants. *Nat. Rev. Genet.* 8, 217–230. doi: 10.1038/nrg2049

Kim, D., Langmead, B., and Salzberg, S. L. (2015). HISAT: A fast spliced aligner with low memory requirements. *Nat. Methods* 12, 357–360. doi: 10.1038/nmeth.3317

Lau, O. S., and Deng, X. W. (2010). Plant hormone signaling lightens up: integrators of light and hormones. *Curr. Opin. Plant Biol.* 13, 571–577. doi: 10.1016/j.pbi.2010.07.001

Li, C. X., Chang, S. X., Khalil-Ur-Rehman, M., Xu, Z. G., and Tao, J. M. (2017). Effect of irradiating the leaf abaxial surface with supplemental light-emitting diode lights on grape photosynthesis. *Aust. J. Grape Wine Res.* 23, 58–65. doi: 10.1111/ajgw.12267

Liu, J., Jiang, C., Kang, L., Song, Y., Zou, Z., et al (2020). Over-expression of a 14-3-3 protein from foxtail millet improves plant tolerance to salinity stress in *Arabidopsis thaliana*. *Front. Plant Sci.* 11, 449. doi: 10.3389/fpls.2020.00449

Lu, N., Maruo, T., Johkan, M., Hohjo, M., Tsukagoshi, S., Ito, Y., et al. (2012). Effects of supplemental lighting with light-emitting diodes (LEDs) on tomato yield and quality of single-truss tomato plants grown at high planting density. *Environ. Control Biol.* 50, 63–74. doi: 10.2525/ecb.50.63

Matsuda, R., Ozawa, N., and Fujiwara, K. (2014). Leaf photosynthesis, plant growth, and carbohydrate accumulation of tomato under different photoperiods and diurnal temperature differences. *Scientia Hortic.* 170, 150–158. doi: 10.1016/j.scienta.2014.03.014

Murchie, E. H., Pinto, M., and Horton, P. (2009). Agriculture and the new challenges for photosynthesis research. *New Phytol.* 181, 532–552. doi: 10.1111/j.1469-8137.2008.02705.x

Pettersen, R. I., Torre, S., and Gislerod, H. R. (2010). Effects of intera-canopy lighting on photosynthesis characteristics in cucumber. *Scientia Hortic.* 125, 77–81. doi: 10.1016/j.scienta.2010.02.006

Seginer, I., Albright, L., and Ioslovich, I. (2006). Improved strategy for a constant daily light integral in greenhouses. *Biosyst. Eng.* 93, 69–80. doi: 10.1016/j.biosystemseng.2005.09.007

Simkin, A. J., Faralli, M., Ramamoorthy, S., and Lawson, T. (2020). Photosynthesis in non-foliar tissues: Implications for yield. *Plant J.* 101, 1001–1015. doi: 10.1111/tpj.14633

Soares, A. S., Driscoll, S. P., Olmos, E., Harbinson, J., Arrabaca, M. C., and Foyer, C. H. (2008). Adaxial/abaxial specification in the regulation of photosynthesis and stomatal opening with respect to light orientation and growth with CO2 enrichment in the c-4 species paspalum dilatatum. *New Phytol.* 177, 186–198. doi: 10.1111/j.1469-8137.2007.02218.x

Song, Y. (2017). *Study on the relationship between LED supplementary light and greenhouse tomato light utilization characteristics and growth and development* (Beijing, China: China Agricultural University). Ph.D. ThesisIn Chinese with English Abstract.

Song, Y., Jiang, C., and Gao, L. (2016). Polychromatic supplemental lighting from underneath canopy is more effective to enhance tomato plant development by improving leaf photosynthesis and stomatal regulation. *Front. Plant Sci.* 7, 1832. doi: 10.3389/fpls.2016.01832

Song, Y., Jiang, C., and Li, Y. (2021). Effects of different abaxial leaf supplemental lightning modes on fruit quality of tomato produced in Gobi greenhouses. *Xinjiang Agric. Sci.* 58, 294–303. doi: 10.6048 /j.issn.1001-4330.2021.02.011

Sun, J., and Nishio, J. (2001). Why abaxial illumination limits photosynthetic carbon fixation in spinach leaves. *Plant Cell Physiol.* 42, 1–8. doi: 10.1093/pcp/pce001

Terfa, M. T., Solhaug, K. A., GislerøD, H. R., Olsen, J. E., and Torre, S. (2013). A high proportion of blue light increases the photosynthesis capacity and leaf formation rate of Rosa × hybrida but does not affect time to flower opening. *Physiologia Plantarum* 148, 146–159. doi: 10.1111/j.1399-3054.2012.01698.x

Tewolde, F. T., Lu, N., Shiina, K., Maruo, T., Takagaki, M., Kozai, T., et al. (2016). Nighttime supplemental LED inter-lighting improves growth and yield of single-truss tomatoes by enhancing photosynthesis in both winter and summer. *Front. Plant Sci.* 7, 448. doi: 10.3389/fpls.2016.00448

Tsang, C. K., Qi, H., Liu, L. F., and Zheng, X. S. (2007). Targeting mammalian target of rapamycin (mTOR) for health and diseases. *Drug Discovery Today* 12, 112–124. doi: 10.1016/j.drudis.2006.12.008

Wahidin, S., Idris, A., and Shaleh, S. R. M. (2013). The influence of light intensity and photoperiod on the growth and lipid content of microalgae nannochloropsis sp. *Bioresource Technol.* 129, 7–11. doi: 10.1016/j.biortech.2012.11.032

Wen, B., Zhou, R., Feng, Q., Wang, Q., Wang, J., and Liu, S. (2014). IQuant: an automated pipeline for quantitative proteomics based upon isobaric tags. *Proteomics* 14, 2280–2285. doi: 10.1002/pmic.201300361

Xu, H.-L., Gauthier, L., Desjardins, Y., and Gosselin, A. (1997). Photosynthesis in leaves, fruits, stem and petioles of greenhouse-grown tomato plants. *Photosynthetica* 33, 113–123. doi: 10.1023/A:1022135507700

Yamaguchi, T., Nukazuka, A., and Tsukaya, H. (2012). Leaf adaxial–abaxial polarity specification and lamina outgrowth: evolution and development. *Plant Cell Physiol.* 53 (7), 1180–1194. doi: 10.1093/pcp/pcs074

Zarogoulidis, P., Lampaki, S., Turner, J. F., Huang, H., Kakolyris, S., Syrigos, K., et al. (2014). mTOR pathway: A current, up-to-date mini-review. *Oncol. Lett.* 8, 2367–2370. doi: 10.3892/ol.2014.2608

Zhang, Z. S., Li, Y. T., Gao HY. Yang, C., and Meng, Q. W. (2016). Characterization of photosynthetic gas exchange in leaves under simulated adaxial and abaxial surfaces alternant irradiation. *Sci. Rep.* 6, 26963. doi: 10.1038/srep26963

Zhang, G., Shen, S., Takagaki, M., Kozai, T., and Yamori, W. (2015). Supplemental upward lighting from underneath to obtain higher marketable lettuce (Lactuca sativa) leaf fresh weight by retarding senescence of outer leaves. *Front. Plant Sci.* 6, 1110. doi: 10.3389/fpls.2015.01110

frontiers | Frontiers in Plant Science

TYPE Original Research
PUBLISHED 30 May 2023
DOI 10.3389/fpls.2023.1181680

OPEN ACCESS

EDITED BY
Jung Eek Son,
Seoul National University, Republic of Korea

REVIEWED BY
Qi Yang,
Zhejiang Agriculture & Forestry University, China
Sofia D. Carvalho,
Independent Researcher, Laramie, United States

*CORRESPONDENCE
Xuanyang Chen
cxy@fafu.edu.cn
Dongliang Qiu
qiudl1970@fafu.edu.cn

RECEIVED 07 March 2023
ACCEPTED 02 May 2023
PUBLISHED 30 May 2023

CITATION
Tadda SA, Li C, Ding J, Li J, Wang J, Huang H, Fan Q, Chen L, He P, Ahiakpa JK, Karikari B, Chen X and Qiu D (2023) Integrated metabolome and transcriptome analyses provide insight into the effect of red and blue LEDs on the quality of sweet potato leaves.
Front. Plant Sci. 14:1181680.
doi: 10.3389/fpls.2023.1181680

Integrated metabolome and transcriptome analyses provide insight into the effect of red and blue LEDs on the quality of sweet potato leaves

Shehu A. Tadda[1,2,3], Chengyue Li[1], Jintao Ding[1], Jian'an Li[1], Jingjing Wang[1], Huaxing Huang[1], Quan Fan[1], Lifang Chen[1], Pengfei He[1], John K. Ahiakpa[3], Benjamin Karikari[3,4], Xuanyang Chen[5,6]* and Dongliang Qiu[1]*

[1]College of Horticulture, Fujian Agriculture and Forestry University, Fuzhou, China, [2]Department of Agronomy, Federal University Dutsin-Ma, Katsina, Nigeria, [3]Agriculture Research Group, Organization of African Academic Doctors (OAAD), Nairobi, Kenya, [4]Department of Agricultural Biotechnology, University for Development Studies, Tamale, Ghana, [5]College of Agriculture, Fujian Agriculture, and Forestry University, Fuzhou, China, [6]Key Laboratory of Crop Biotechnology, Fujian Agriculture and Forestry University, Fujian Province Universities, Fuzhou, China

Red and blue light-emitting diodes (LEDs) affect the quality of sweet potato leaves and their nutritional profile. Vines cultivated under blue LEDs had higher soluble protein contents, total phenolic compounds, flavonoids, and total antioxidant activity. Conversely, chlorophyll, soluble sugar, protein, and vitamin C contents were higher in leaves grown under red LEDs. Red and blue light increased the accumulation of 77 and 18 metabolites, respectively. Alpha-linoleic and linolenic acid metabolism were the most significantly enriched pathways based on Kyoto Encyclopedia of Genes and Genomes (KEGG) pathway analyses. A total of 615 genes were differentially expressed between sweet potato leaves exposed to red and blue LEDs. Among these, 510 differentially expressed genes were upregulated in leaves grown under blue light compared with those grown under red light, while the remaining 105 genes were expressed at higher levels in the latter than in the former. Among the KEGG enrichment pathways, blue light significantly induced anthocyanin and carotenoid biosynthesis structural genes. This study provides a scientific reference basis for using light to alter metabolites to improve the quality of edible sweet potato leaves.

KEYWORDS

leafy vegetable, illumination, metabolome profiling, nutrition, anthocyanin

1 Introduction

Sweet potato (*Ipomoea batatas* (L.) Lam) is a crop mainly cultivated for its enlarged edible roots and stems. Sweet potato shoots, conversely, have been neglected or restricted to animal feed and are rarely used as vegetables (Cui et al., 2011). Sweet potato leaves have been demonstrated to be more nutritious than their stems, petioles, tubers, and other vegetables (Wang et al., 2016a). Sweet potato is grown all year in China and other tropical regions, which allows for multiple leaf harvests in a single growing season, giving it an advantage over other vegetables (Li et al., 2017). The crop could tolerate extreme weather conditions, which makes it an interesting crop for combating food insecurity (Motsa et al., 2015; Iese et al., 2018). Due to its tenderness, lack of pubescence, and excellent eating quality, the young leaves of recently introduced leafy sweet potato cultivars are in higher demand than leaves from the common tuberous cultivars (Tang et al., 2020). To produce high-quality sweet potato shoots all year, an alternative production system to field conditions is needed.

Light quality and intensity are critical environmental factors affecting photomorphogenesis, plant development, and metabolism. In addition, the ability of plant photosynthetic systems and metabolism to adapt to light fluctuation correlates with their reproductive success and survival rate (Chen et al., 2021). Studies have shown that an increase in light intensity (100-250 μmol m^{-2} s^{-1}) enhance the accumulation of chlorophyll and β-carotene in *Dunaliella salina* (Lamers et al., 2010). Red light increases the phenolic and anthocyanin contents of lettuce leaves and pea seedlings (Wu et al., 2007; Li and Kubota, 2009) and the anthocyanin content of basil (Nadeem et al., 2019). Red and green basil exhibited differential responses to blue and red light intensities, where a higher proportion of blue light significantly increased the phytochemical content of the green cultivar (Lobiuc et al., 2017).

Approximately 200,000 metabolites can be produced in several plant cultivars, ecotypes, and species (Lisec et al., 2006; Kusano et al., 2011; Wang et al., 2019). These metabolites are usually measured *via* mass spectrometry (MS) analyses, which usually yield sensitive high-throughput data. MS analysis has been integrated with other analytical systems, including liquid chromatography (LC), capillary electrophoresis (CE), and gas chromatography (GC), to measure various metabolites (Gowda and Djukovic, 2014). In addition, the liquid chromatography –mass spectrometry (LC–MS) metabolomics separation technique has been employed in measuring secondary metabolites in foods and plants (Ma et al., 2013). Other separation techniques employed in metabolomic studies of plants exposed to environmental stress provide high-quality metabolomics data. As such, metabolome profiling is a promising analytical method for evaluating agricultural products, providing a variety of information on various metabolites. Comprehensive metabolome profiling reveals quantitative changes in the metabolite profiles of plants grown under certain environmental conditions (Ghatak et al., 2018).

As a protective mechanism, plants respond to light by regulating genes involved in energy and metabolism. As an important field of biology, transcriptome studies enable scientists to study gene expression at the cellular level to assess transcript-level changes with high precision (Chen et al., 2021). Transcriptome profiling has been used to investigate the effect of blue and red light on the development and growth of several plants, including Norway spruce seedlings (Ouyang et al., 2015), potato (Chen et al., 2021), and synthesis of various metabolites in plants in response to light stress (Xie et al., 2020). Previous studies have focused on understanding genetic, nutritional, metabolic, and transcriptional regulation of sweet potato tuber (He et al., 2020; Suematsu et al., 2020; Bennett et al., 2021). However, little is known about the effect of LEDs on the physicochemical quality of sweet potato leaves and their metabolic and transcriptome changes. We performed metabolome and transcriptome profiling on sweet potato leaves grown under monochromatic red or blue lights to identify differentially expressed genes and biosynthetic pathways affecting metabolite biosynthesis and their differential accumulation.

2 Materials and methods

2.1 Growth environment and plant materials

The experiment was conducted in a controlled chamber (Talos Technology, Fujian, China) illuminated with monochromatic red [100%, 632 (nm)] or blue [100% 462 (nm)] LEDs (Figure 1). Low intensity LEDs with photosynthetic photon flux density [PPFD (50 μmol m^{-2} s^{-1})] were used to induce sweet potato leaf development. The photoperiod (16/8 hrs), temperature (25 ± 2°C), and relative humidity (70 ± 5%) were kept constant. The sweet potato ('Fushu-18') vines were harvested from the Key Laboratory of Crop Biotechnology, Fujian Agriculture and Forestry University, China. The lower leaves were removed with disinfected scissors, leaving the fully opened leaves (18/22) to achieve uniformity before transplanting to pots (16 cm width x 14 cm height) filled with a mixture of 750 ± 10 g of organic soil (70% organic matter content, 40% humic acid, 3% NPK, and a pH of 6.5) and clean river sand (1:2). Three pots planted with three vines were assigned to each treatment and replicated three times. The vines were grown for two weeks under ambient conditions (open field with full sunlight exposure) before being transferred to the growth chamber and exposed to red or blue LEDs for three weeks. A nutrient solution (Sara Hyponica, Japan) containing (A%) nitrogen (1.0), phosphoric acid (3.80), alkali (5.50), magnesium oxide (1.0), manganese (0.03), boron (0.05), and nitric acid (3.0) was added to the irrigation water every three days.

2.2 Measurement of growth indices

The morphological and growth data were collected from three leaf samples in each replication in the third week after the vines were exposed to blue or red light regimes. The membrane stability index (MSI) was measured using a conductivity meter (Pancellent Inc., China) according to the method described by Dwivedi et al. (2018). The leaf water content (LWC) was estimated following the

FIGURE 1
Sweet potato (*I. batatas* (L.) Lam) vines growing under 100% red **(A)** and 100% blue **(B)** LEDs at three weeks after exposure, indicating the degree of leaf senescence and intumescence in both conditions.

procedure reported by He and Qin (2020). The leaf area (LA) was estimated with the method earlier reported by Yeshitila and Taye (2016). The length and width of the sixth leaves were marked and measured before and after transfer to the growth chamber. The number of abscised leaves (NAL) and the percentage of leaves with intumescence were calculated using the following equations:

$$NAL = TNAL/TNL*100$$

$$Intumescense(\%) = NAL/TNL*100$$

NAL, TNL, and TNAL are the number of affected leaves, number of whole leaves and total number of abscised leaves, respectively.

2.3 Determination of chlorophyll pigments, total soluble sugar, protein, and vitamin C

Chlorophyll pigments were measured spectrophotometrically (T6 series, Persee Analytics, Inc. Auburn, CA 95603) according to Lichtenthaler and Babani (2022). The biochemical contents were measured at three weeks after exposure to light regimes. Three middle leaves from each replication were removed, ground, and frozen in liquid nitrogen until use. The total soluble sugar, protein, and vitamin C were measured from the frozen leaf samples (0.2 and 1.0 g). The anthrone colorimetric method was employed to determine soluble sugar (Ahsen et al., 2019). Coomassie blue G250 was used to estimate the total soluble protein content (Ahsen et al., 2019). The titration method was used to estimate the vitamin C content (Kui et al., 2020). The absorbance of the samples (sucrose 620 nm and protein 595 nm) was measured with a UV–VIS spectrometer (T6 series., Persee Analytics, Inc. Auburn, CA 95603).

2.4 Total flavonoids, phenolics, and antioxidant scavenging activity

The total flavonoid content (TFC) was determined according to a method by Wei et al. (2019). Three middle leaves were collected from each replication and rutin standard solution was used for the calibration curve. The total phenolic content (TPC) was estimated using the Folin-Ciocalteu method of Alara et al. (2020), and garlic acid (0.1 mg ml^{-1}) was used in the standard curve. The total antioxidant activity was estimated using the 2,2-diphenyl-1-picrylhydrazyl (DPPH) assay (Guo et al., 2017).

2.5 Metabolome analyses of sweet potato leaves

Freshly opened leaves (fully opened) were harvested and used for metabolome profiling. A 0.5 g sample from each replicate was weighed, frozen in liquid nitrogen and subsequently stored in a -80° C refrigerator. The frozen samples were crushed with a mixer mill (MM 400, Retsch) and zirconia beads for 1.5 minutes at 30 Hz. The lyophilized powder (100 mg) was dissolved in 1.2 mL of methanol (70%) solution, vortexed six times for 30 secs every 30 mins, and placed in a 4°C refrigerator overnight. The samples were then centrifuged for ten minutes at 12,000 rpm, and the extracts were filtered (SCAA-104, 0.22 μm pore size; ANPEL, Shanghai, China; http://anpel.com.cn/) before ultra-performance liquid chromatography-Mass spectroscopy (UPLC–MS/MS) analysis. All reagents used in the metabolic analyses were sourced from Merck (Merck, China), except the standard (BioBio/Sigma –Aldrich, China).

Metabolite extraction, detection, and quantification were performed by the Wuhan MetWare Biotechnology Co., Ltd., China (https://metware.cn) according to the method described by Fraga et al. (2010). The sample extracts were analyzed using a UPLC –ESI–MS/MS system (UPLC, SHIMADZU Nexera X2, https://shimadzu.com.cn/; MS, Applied Biosystems 6500 Q TRAP). The analytical conditions were as follows: UPLC column, Agilent SB-C18 (1.8 μm, 100 mm * 2.1 mm). The mobile phase consisted of distilled water with 0.1% formic acid, solvents A and B, and 0.1% formic acid with acetonitrile. The sample analyses were performed with a gradient program that used 95% A and 5% B as starting conditions. Within the first nine minutes, a linear gradient of 5% A and 95% B was programmed, and a composition of 5% A and 95% B was maintained for 1 minute. Then, a composition of 95% A and 5.0% B was adjusted for 1.1 minutes and held for 2.9 minutes. The flow velocity was kept at 0.35 mL per minute, and the column temperature was maintained at 40°C. An injection volume of 2 μL was used, and the effluent was connected to the ESI-triple quadrupole-linear ion trap (QTRAP)-MS. Three biological replicates (young fresh leaves) were collected and analyzed for each sample, and the sample extract mixture was used for quality checks.

2.5.1 Differentially accumulated metabolites and KEGG annotation/enrichment analyses

The metabolites detected were screened with stringent threshold: absolute $\log_2$FC (fold change) ≥ 1 and variable importance in projection (VIP) ≥ 1 to identify differentially accumulated metabolites (DAMs). The VIP values were obtained from the Orthogonal Projections to Latent Structures-Discriminant Analysis (OPLS-DA) result with score and permutation plots. The data were generated using the R package *MetaboAnalyst*, log2-transformed ($\log_2$), and mean-centered before OPLS-DA. To avoid overfitting, a permutation test (200 permutations) was performed on the data (Hua et al., 2021; Xu et al., 2022). For the Kyoto Encyclopedia of Genes and Genomes (KEGG) annotation, the detected metabolites were annotated using the KEGG compound database (http://kegg.jp/kegg/compound/) and subsequently mapped to the KEGG pathway database (http://kegg.jp/kegg/pathway.html). The pathways with significantly regulated metabolites mapped were then subjected to metabolite set enrichment analysis (MSEA), and their significance was evaluated by the hypergeometric test using p-values ($p< 0.05$).

2.6 Transcriptome (RNA-Seq) analysis

Freshly opened leaves (0.5 g) were harvested from each replicate, immediately stored at -80°C and sent to the Biomarker Technologies Laboratory (http://en.biomarker.com.cn/) for analysis. The ribonucleic acid (RNA) concentration and purity were measured using a NanoDrop 2000 (Thermo Fisher Scientific, Wilmington, DE). The RNA integrity was assessed using the RNA Nano 6000 Assay Kit of the Agilent Bioanalyzer 2100 system (Agilent Technologies, CA, USA). A total of 1 μg of RNA per sample was used as input material for the RNA sample preparations. According to the manufacturer's recommendations, sequencing libraries were generated using the NEBNext UltraTM RNA Library Prep Kit for Illumina (NEB, USA). Then, PCR was performed with Phusion High-Fidelity DNA polymerase, Universal PCR primers, and Index (X) Primer. Finally, the PCR products were purified (AMPure XP system), and library quality was assessed on the Agilent Bioanalyzer 2100 system. The clustering of the index-coded samples was performed on a cBot Cluster Generation System using TruSeq PE Cluster Kit v4-cBot-HS (Illumina). Raw FASTQ format data were first processed through in-house Perl scripts to obtain clean data by removing reads containing adapter, poly-N, and low-quality reads. All downstream analyses were based on clean, high-quality data. After data processing, raw sequences were transformed into clean reads and mapped to the reference genome. Only reads with a perfect match or one mismatch were further analyzed and annotated based on the reference genome using HISAT2 software.

2.6.1 Gene functional annotation, quantification, and enrichment

The gene functions were annotated based on the National Center for Bioinformatic Information (NCBI) nonredundant protein sequences (Nr), NCBI nonredundant nucleotide sequences (Nt), protein family (Pfam), clusters of orthologous groups of proteins (KOG/COG), Swiss-Prot; KEGG ortholog database (KO), and gene ontology (GO) databases. Differential expression analysis of two conditions/groups (blue vs red lights) was performed using *DESeq2*. The resulting P values were adjusted using Benjamini and Hochberg's approach (Benjamini and Hochberg, 1995). False discovery rate (FDR)< 0.01 and fold change ≥ 2 were set as the thresholds for significant differential expression. Gene Ontology (GO) enrichment analysis of the differentially expressed genes (DEGs) was performed by the *GOseq* R package based on Wallenius noncentral hypergeometric distribution (Young et al., 2010). We used the KEGG (Kanehisa et al., 2008) database to understand the functions and utilities of the

biological and molecular datasets generated by genome sequencing (http://www.genome.jp/kegg/). The KOBAS software (Mao et al., 2005) was used to generate the statistical enrichment of DEGs in the KEGG pathways. The sequences of the DEGs were blasted (blastx) to the genome of related species (the protein–protein interaction (PPI) in the STRING database: http://string-db.org/) to obtain the predicted PPI of these DEGs. Then, the PPIs of these DEGs were visualized in Cytoscape (Shannon et al., 2003).

To validate the reliability of the transcriptome data, quantitative real-time polymerase chain reaction (qRT–PCR) was performed with nine randomly selected genes. The qRT–PCR gene-specific primers (Table S1) were designed using Primer Express software (v3.0, Applied Biosystems). The *ACTIN* gene (EU250003.1) was used as the internal reference gene to normalize the gene expression values. The $2^{-\Delta CT}$ method (Livak and Schmittgen, 2001) was used to calculate the relative gene expression levels.

2.7 Statistical analyses

The physiological and biochemical data obtained were analyzed in Microsoft Excel for the means and standard errors. Student's *t* test was used to evaluate the effect of red and blue lights on sweet potato leaves. Unsupervised principal component analysis (PCA) was performed using the statistical function *prcomp* in R (www.r-project.org). The data were unit variance scaled before the unsupervised PCA. Hierarchical cluster analysis (HCA) was performed by *pheatmap* (Kolde, 2012), and Pearson correlation coefficients (r) between the samples were calculated by the *corrplot* package in R (Wei et al., 2017).

3 Results

3.1 Effect of red and blue LEDs on physiological attributes and bioactive compounds in sweet potato leaves grown in a controlled environment

This study evaluated the effects of light on the physicochemical and growth parameters (Table 1) of sweet potato leaves grown under low intensity monochromatic red or blue LEDs. The Light quality significantly affected the quality of the sweet potato leaves (Figure 1) after three weeks of exposure to the red and blue LEDs. Growing sweet potato under blue light resulted in higher physiological indices (increased membrane stability (93 ± 0.33% vs 90 ± 1.06%), fresh leaf (0.50 ± 0.04g vs 0.32 ± 0.01g), dry weights (0.05 ± 0.01g vs 0.02 ± 0.00g), leaf area (165.1 cm^2 ± 1.84 vs 162.4 ± 0.10 cm^2), number of abscised leaves (25 ± 2.4% vs 47 ± 2.7%) and intumescence (13 ± 1.6% vs 25 ± 1.8%), in the leaves of the sweet potatoes, except for the leaf water content (89 ± 0.53% vs 95 ± 1.06%) relative to the red LEDs (Table 1; Figure S1). The vines grown under red LEDs showed an increase in biochemical activity; thus, they produced more chlorophyll *a*, *b*, and total carotenoid contents than those grown under blue LEDs. Conversely, the vines grown under blue LEDs recorded higher soluble protein contents, total phenols, flavonoids, and 2,2-diphenyl-1-picrylhydrazyl antioxidant activity (Table 1).

3.2 Metabolome profiles and analysis of differentially accumulated metabolites in sweet potato leaves grown under red and blue LEDs

The sweet potato vines were produced from a controlled growth chamber to investigate the effect of blue and red LEDs on the sweet potato leaves. Representative photographs of vine growth conditions and appearance after three weeks of light treatments are presented in Figure 1; S1. UPLC–ESI–MS/MS was used to analyze the key metabolites in sweet potato leaves produced under red or blue LEDs. In all, 744 compounds were detected, comprising 194 phenolic acids, 159 lipids (glycerol ester, free fatty acids, PC, sphingolipids, LPC and LPE), 114 organic acids, 111 amino acids

TABLE 1 Influence of red and blue LEDs on physiological attributes and bioactive compounds of sweet potato (*I. batatas* (L.) Lam) leaves.

Parameter	Treatments		
	Blue light (100%)	Red light (100%)	*P-value*
Physiological attributes			
Membrane stability index (%)	93 ± 0.33	90 ± 1.06	*
Leaf water content (%)	89 ± 0.53	95 ± 1.06	*
Leaf fresh weight (g)	0.50 ± 0.04	0.32 ± 0.01	*
Leaf dry weight (g)	0.05 ± 0.01	0.02 ± 0.00	**
Leaf area (cm^2)	165.1 ± 1.84	162.4 ± 0.10	NS
Number of abscise leaves (%)	25 ± 2.4	47 ± 2.7	**
Intumescence (%)	13 ± 1.6	25 ± 1.8	**
Bioactive compounds			
Chlorophyll (mg g^{-1})	16.47 ± 0.60	18.41 ± 0.66	NS
Chlorophyll (mg g^{-1})	5.33 ± 0.29	7.26 ± 0.37	**
Total Chlorophyl (mg g^{-1})	21.80 ± 0.89	25.67 ± 1.03	**
Carotenoids (mg g^{-1})	3.46 ± 0.12	4.07 ± 0.15	**
Total soluble sugar (%)	0.5 ± 0.02	0.7 ± 0.02	**
Total soluble protein (%)	1.3 ± 0.09	0.7 ± 0.01	**
Vitamin C (mg g^{-1})	10.4 ± 0.38	19.83 ± 0.77	***
Total Phenolics (mg g^{-1})	259.3 ± 8.61	199.8 ± 1.61	**
Total flavonoids (mg g^{-1})	54.7 ± 0.95	40.1 ± 0.64	***
Antioxidant scavenging activity	94.9 ± 0.14	91.1 ± 0.58	**

Means were separated by student t-test. The mean ± standard error with *, **, and *** indicates significance at P<0.05, P<0.01 and P<0.001, respectively. NS indicates no significant difference.

and derivatives, 73 nucleotides and derivatives, and 93 other compounds (saccharides, alcohols, and vitamins) (Table S2; Figure 2A). The data similarity and dissimilarity were evaluated using principal component analysis (PCA), hierarchical clustering (HCA) and correlation analyses using the ion intensities of the measured metabolites. The PCA revealed that the first two PCA axes could explain 54.91% of the variability between samples from the red and blue LED treatments. The clustering showed relatively distinct variation between the treatments alone and mixtures (Figure 2B). The PCA, together with HCA and high correlation coefficients (Figures 2B–D) suggest a high reproducibility and repeatability of the samples from the same light treatment in this study, lending credence to our dataset's reliability for downstream analyses.

To identify differentially accumulated metabolites, we applied stringent screening criteria (VIP ≥ 1 and absolute $\log_2$FC ≥ 1) were applied and detected 95 DAMs, comprising 77 and 18 down- and up-regulated metabolites, respectively (Figure 3A; Table S3), implying that red LED treatment induced increased accumulation of metabolites compared with blue LEDs. The DAMs consisted of 35 lipids, 23 amino acids and derivatives, 15 phenolic acids, 9 nucleotides and derivatives, 6 organic acids and 7 other compounds (Figure 3B). Only phenolic acids and other compounds were accumulated higher under blue light than red light conditions. All six classes of compounds showed contrasting accumulation levels between sweet potato vines evaluated under red and blue LEDs (Figure 4A).

3.2.1 Comparative analysis of changes in metabolites in the sweet potato leaves under red and blue LED treatment

The light quality caused significant variations in the DAMs (Figure 5). Red light significantly increased the accumulation of 23 amino acids and derivatives including eight essential amino acids (Figure 5A). The essential amino acids consist of L-allo-isoleucine, L-histidine, N6-acetyl-L-lysine, L-tryptophan, γ-glutamyl-L-valine, L-γ-glutamyl-L-leucine, γ-glutamylmethionine and γ-glutamylphenylalanine. The remaining 15 compounds comprise non-essential amino acids. In addition to amino acids and derivatives, six nucleotides and derivatives accumulated differentially in potato leaves treated with red and blue LEDs. Of these, only 2'-deoxyadenosine-5'-monophosphate accumulated higher in blue light than in red light, while the remaining five all accumulated highly under red LEDs (Figure 5B).

Light quality significantly altered lipid composition and abundance in the sweet potato leaves (Figure 5C). Red light sharply increased the abundance of 25 free fatty acids including stearidonic acid (SDA) and arachidic acid as well as two lysophosphatidylcholine (lysoPC) (lysoPC 15:1 and lysoPC 19:0) and two lysophosphatidylethanolamine (lysoPE) (lysoPE 15:1(2n isomer) and lysoPE 15:1) relative to blue light. Interestingly, three other lipids (lysoPE 16:0, lysoPE 18:0 and PC(oxo-11:0/18:2)) and three glycerol ester (1-linoleoylglycerol, 2-linoleoylglycerol and lysoPG 16:1) accumulated higher under blue LEDs than in red LEDs (Figure 5C). Red light increased the abundance of nine organic acids, including suberic acid, 2-hydroxyhexadecanoic acid and 6-aminocaproic acid compared to sweet potato leaves cultivated under blue LEDs (Figure 5D). In addition, phenolic acid composition in the sweet potato leaves varied significantly under the two light treatments. Among the phenolic acid compounds, eight compounds (such as 4-aminobenzoic acid, p-coumaryl alcohol and isovanillin) increased highly under red LEDs, while seven others including caffeic acid increased highly under blue light (Figure 5E).

Also, the light quality altered saccharide and alcohol, and vitamin composition in the sweet potato leaves (Figure 5F). Three saccharide and alcohol; 2-decanol, 1-decanol and D-glucosamine 1-phosphate accumulated higher under red light than blue light (Figure 5F). While four vitamins mainly vitamin B6 (pyridoxal, pyridoxine, pyridoxine-5'-O-glucoside and pyridoxine-5'-O-diglucoside) accumulated highly under blue LEDs (Figure 5F). Altogether, the above results indicate that the light quality altered the composition of metabolites in the sweet potato leaves including essential amino acids and other compounds of nutritional importance to humans.

3.2.2 KEGG pathway enrichment analyses among the DAMs

The DAMs detected were subjected to KEGG pathway enrichment analyses (P value< 0.05). We observed that alpha-linoleic acid metabolism (ko00592) and linolenic acid metabolism (ko00591) were the two most significantly enriched pathways, with 9 and 5 DAMs, respectively (Table S4; Figure 4B), indicating that the light quality caused differential accumulation of metabolites in these two metabolic pathways. The metabolites involved in linolenic acid metabolism (ko00591) increased by 59.45% for 9S-hydroperoxy-10E,12Z-octadecadienoic acid and 76% for 9,10-dihydroxy-12,13-epoxyoctadecanoic acid in sweet potato leaves grown under red LEDs compared to blue LEDs (Figure 4C). Similarly, red light treatment increased stearidonic acid, 9-hydroxy-12-oxo-15(Z)-octadecenoic acid, 9-hydroxy-10,12,15-octadecatrienoic acid, 9-hydroperoxy-10E,12,15Z-octadecatrienoic acid and 12-oxo-phytodienoic acid by 62.54, 61.94, 60.89, 53.53 and 51.36%, respectively, compared with blue LED treatment (Figure 4D). These results suggest that red light treatment could be exploited to increase the metabolome profile in sweet potato leaves for food and nutritional purposes.

3.3 Transcriptome profiling of sweet potato leaves

The transcriptome analysis generated 40.08 Gb of clean data Table S5). At least 5.97 Gb clean data were generated for each sample, with a minimum of 94.27% clean data based on the Q30 quality score Table S5). Clean reads of each sample were mapped to the sweet potato reference genome database (http://public-genomes-ngs.molgen.mpg.de/sweetpotato/). The mapping ratio ranged from 75.49% to 76.50% (Table S5). Then, all expressed transcripts were analyzed using pairwise comparisons of the two

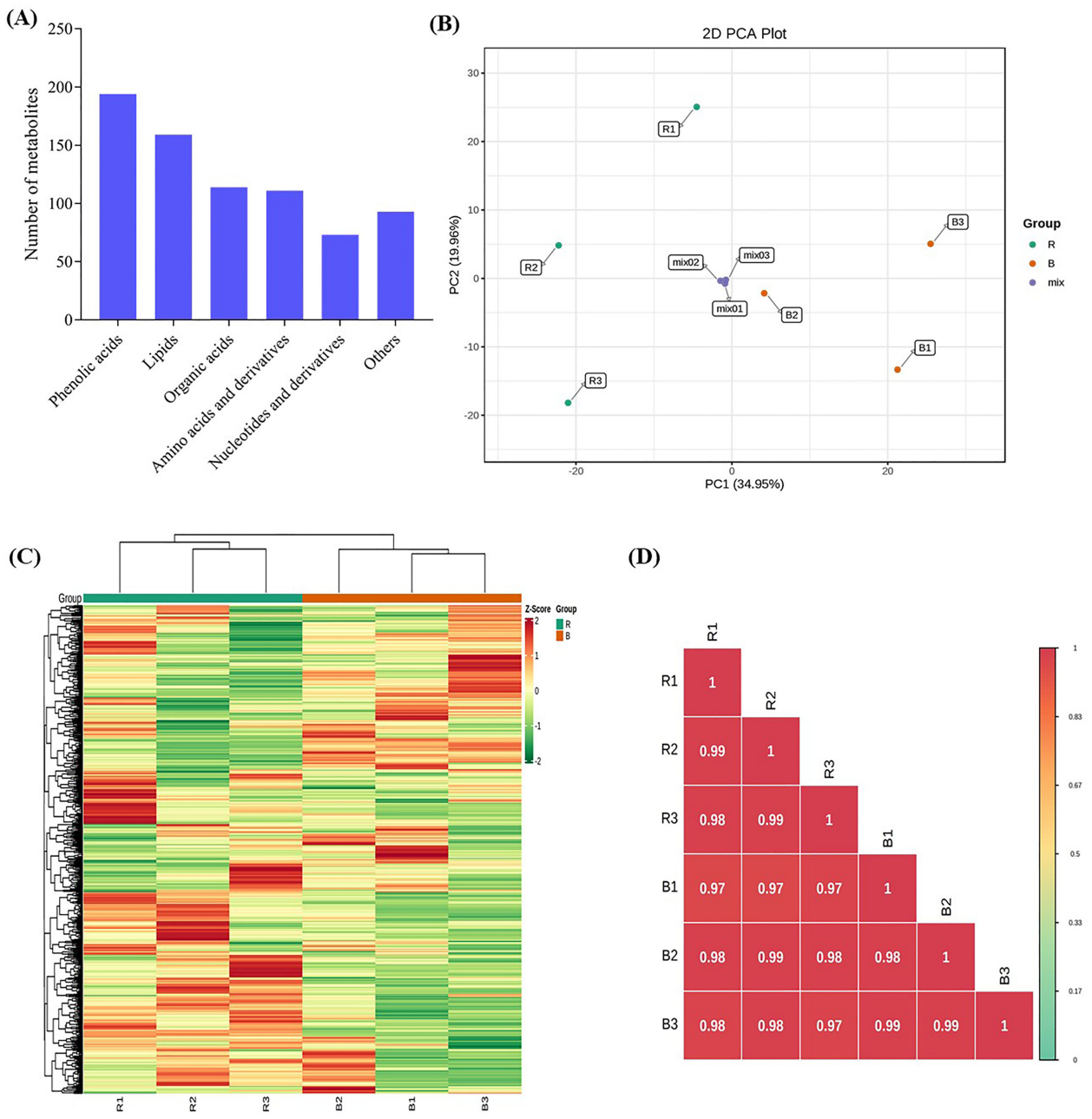

FIGURE 2
Metabolites detected in the sweet potato (*I. batatas* (L.) Lam) leaves growing under red (R) and blue **(B)** LEDs. L1-100% is blue (100%), and L2-100% is red (100%) LEDs. All analyses were done in triplicates, thus R (R1-R3) and B (B1-B3). **(A)** Classes of compounds detected. **(B)** Principal component analysis plot based on two principal components axes. **(C)** Hierarchical heatmap clustering. **(D)** Pearson correlation coefficients plot of differentially accumulated metabolites.

samples. However, prediction of alternative splicing, gene structure optimization, and novel gene discovery were made from the mapping results. A total of 17,995 genes were discovered, and 14,039 novel genes were annotated with putative functions.

3.3.1 Analysis of differentially expressed genes and functional annotation

We further subjected the expressed genes to differential analysis with a stringent threshold of FDR< 0.01 and FC ≥ 2. From this analysis, a total of 615 DEGs were detected, with 510 down-regulated (higher expression in blue LED-treated sweet potato than red LED) and 105 up-regulated (higher expression in red LED-treated sweet potato than blue LED) DEGs (Figure S2). These results indicate that LED treatment of sweet potato leaves causes transcriptional alterations.

With the nutritional importance of sweet potato leaves to human nutrition, we mined DEGs enriched in the nutritionally-rich anthocyanin and carotenoid biosynthetic pathways from the KEGG analyses (Figure S3). The blue light treatment resulted in higher expression of anthocyanin biosynthetic (ko00942)

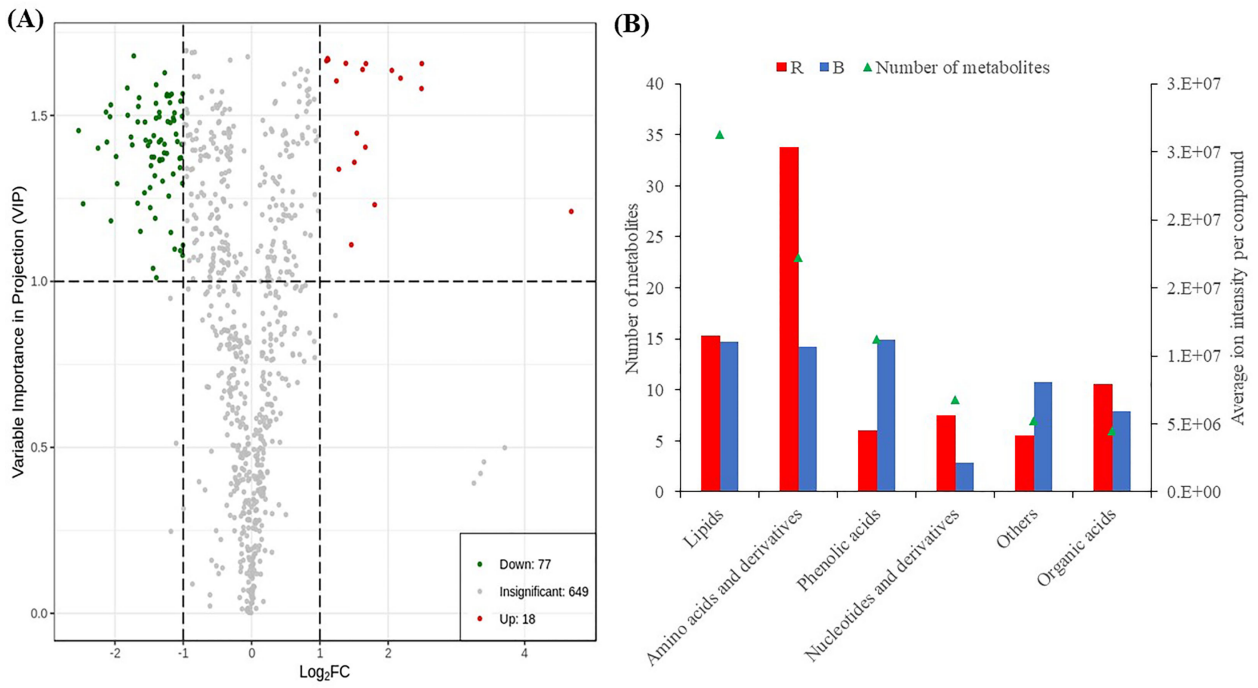

FIGURE 3
Differentially accumulated metabolites detected between sweet potato leaves under red (R) and blue **(B)** LEDs. **(A)** Volcano plot of metabolites. The red and blue points indicate the up-regulated and down-regulated metabolites, respectively, and the gray area represents metabolites detected but not significant. **(B)** Classes of compounds detected as DAMs. The primary Y-axis represents the number of metabolites, while secondary Y-axis represents the classes of compounds.

genes (*Ipomoea_batatas_newGene_14427*, *Ipomoea_batatas_newGene_29385* and *Ipomoea_batatas_newGene_7186*) than the red light treatment (Figure 6A). These three genes encode anthocyanidin 3-O-glucosyltransferase [EC:2.4.1.115] (Figure S4). These genes could be targeted for functional validation and verification to unravel their regulatory role in improving the nutritional composition of sweet potato leaves.

Additionally, seven carotenoid biosynthetic (ko00906) genes (*Ipomoea_batatas_newGene_14029*, *Tai6.24200, Ipomoea_batatas_newGene_26163*, *Tai6.33677, Tai6.4118, Ipomoea_batatas_newGene_7887* and *Tai6.39633*) were expressed at higher levels in blue LED-treated leaves than in red LED-treated leaves (Figure 6B). These genes encode different enzymes (carotenoid isomerase (crtH, crtISO) [EC:5.2.1.13], beta-carotene 9-cis-all-trans isomerase [EC:5.2.1.14], zeaxanthin [EC:1.14.1521], antheraxanthin [EC:1.23.5.1] and abscisate [EC:1.14.14137]) on the carotenoid biosynthetic pathways (Figure S5). These results suggest that blue LED treatment could be used to improve the nutritional value of sweet potato leaves for human and animal consumption.

To validate the transcriptome data, total RNA from the same two samples used for RNA sequencing was used as a template for qPCR. The qRT–PCR validation results revealed high similarity to the RNA sequences identified with the fragments per kilobase of exon per million mapped fragments (FPKM) values from the sequencing results under the red and blue light treatments (Figure 7).

4 Discussion

Light conditions substantially impact sweet potato leaves, which differ in their shape and metabolic profiles (Lv et al., 2021). Commercial horticultural producers have been experimenting with red and blue LEDs in their production systems, as these lights are utilized to produce high-quality horticultural products (Bantis et al., 2018). Leaves are the principal light collectors during photosynthesis, which impacts their quality and metabolite accumulation (Yue et al., 2021). There was less abscission and intumescence in the sweet potato leaves grown under blue LEDs than in those produced under red LEDs. Ornamental sweet potatoes and tomatoes have been found to have a lower frequency of anatomical disorders when exposed to blue light (Craver et al., 2014; Eguchi et al., 2016). Intumescence formation is genetically controlled in various plant species and significantly affects photosynthesis. It also negatively impacts plant tissues by inducing chlorosis, senescence, abscission and downward curling of leaves (Williams et al., 2016). However, red light has long been thought to delay leaf senescence (Sakuraba, 2021). Senescence in grapes has also been shown to be delayed under red light exposure (Wang et al., 2016b). In this study, harvested leaves were more robust under blue light and had higher fresh and dry weights. Zheng and Van Labeke (2017) reported that light intensity and quality affect biomass accumulation in ornamental plants. In sweet potato leaves grown under red LEDs, we found significant concentrations of chlorophyll *a* and *b*, total chlorophyll, and carotenoid pigments

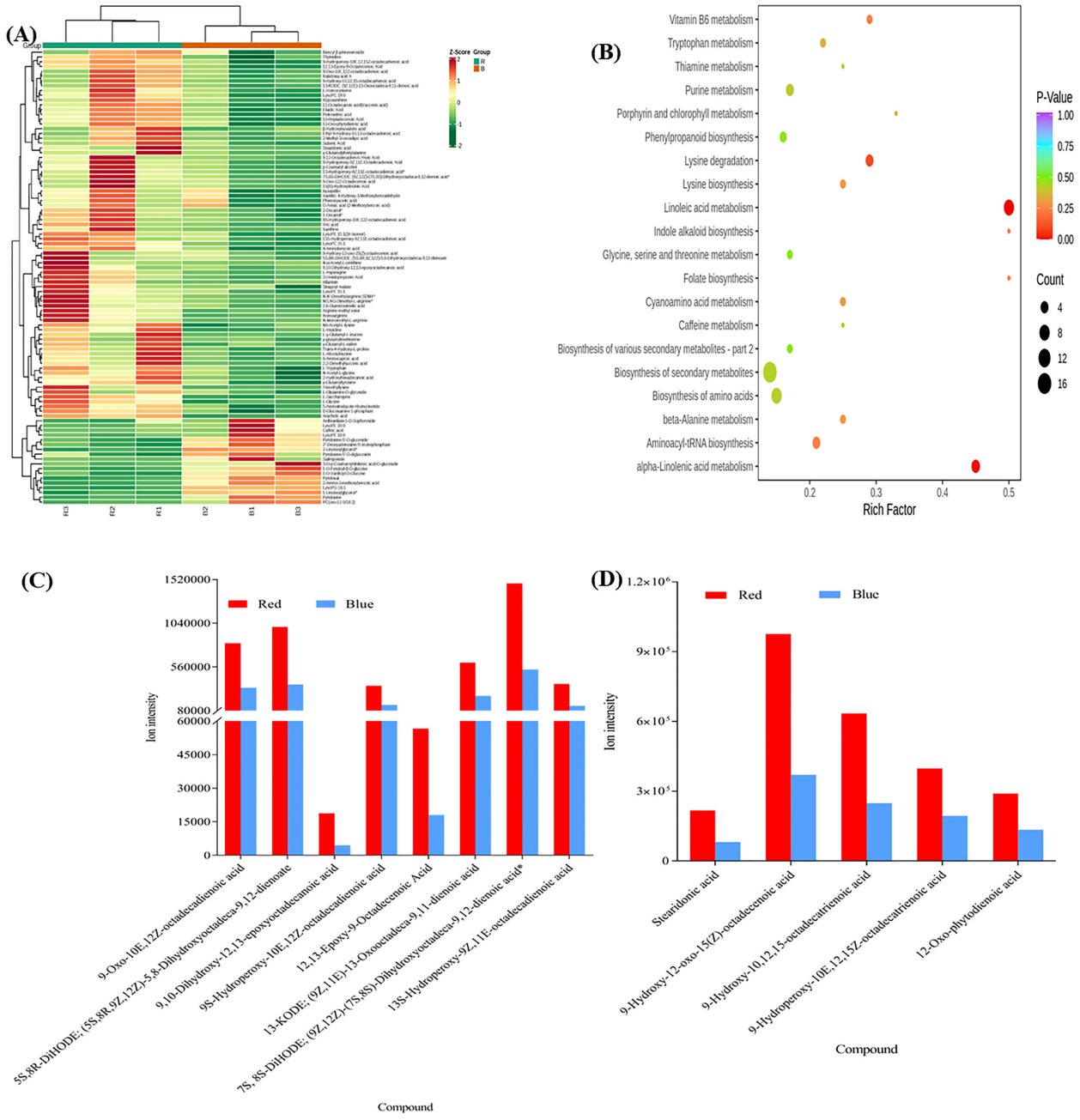

FIGURE 4
(A) The Differential metabolites clustering heatmap (R vs B) of sweet potato (*I. batatas* (L.) Lam) leaves grown under red (R) and blue **(B)** LEDs. The bar above the heatmap corresponds to the sample clustering (group). The dendrogram on the left side of the heatmap represents the differential metabolite clustering. The annotation bar on the left side of the heat map corresponds to the first-level classification (Class) of the compounds, and different colors represent different compound categories. **(B)** The Kyoto encyclopedia of genes and genomes (KEGG) pathway enrichment analysis bubble plot of differentially accumulated metabolites. Each row represents a KEGG pathway. The color of the dots represents the p-value, and the size of the bubbles represents the number of differential metabolites annotated in that pathway. Those underlined had p-values< *0.05*, and the KEGG pathway significantly (p< 0.05) enriched with differentially accumulated metabolites in the sweet potato leaves. **(C)** Linoleic acid metabolism. **(D)** Alpha-Linolenic acid metabolism.

(Table 1). In contrast, Yousef et al. (2021) found a lower pigment concentration in two tomato seedlings grown under monochromatic red lights, indicating that PSII had been altered and may be compromised in functionality. However, earlier studies showed that combining blue and red light was more successful in fostering plant growth than monochromatic lighting (Liang et al., 2021). In addition, the photosynthetic rate is increased by red light, which affects the transport of carbohydrates from leaves to roots (Zhong et al., 2021).

LEDs have been used as substitutes for conventional light sources in controlled agricultural environments (Yousef et al., 2021). They emit specific wavelengths of light suitable for photosynthesis and photomorphogenesis (Bantis et al., 2018). In this study, leaves grown under blue LEDs showed enhanced accumulation of total phenols

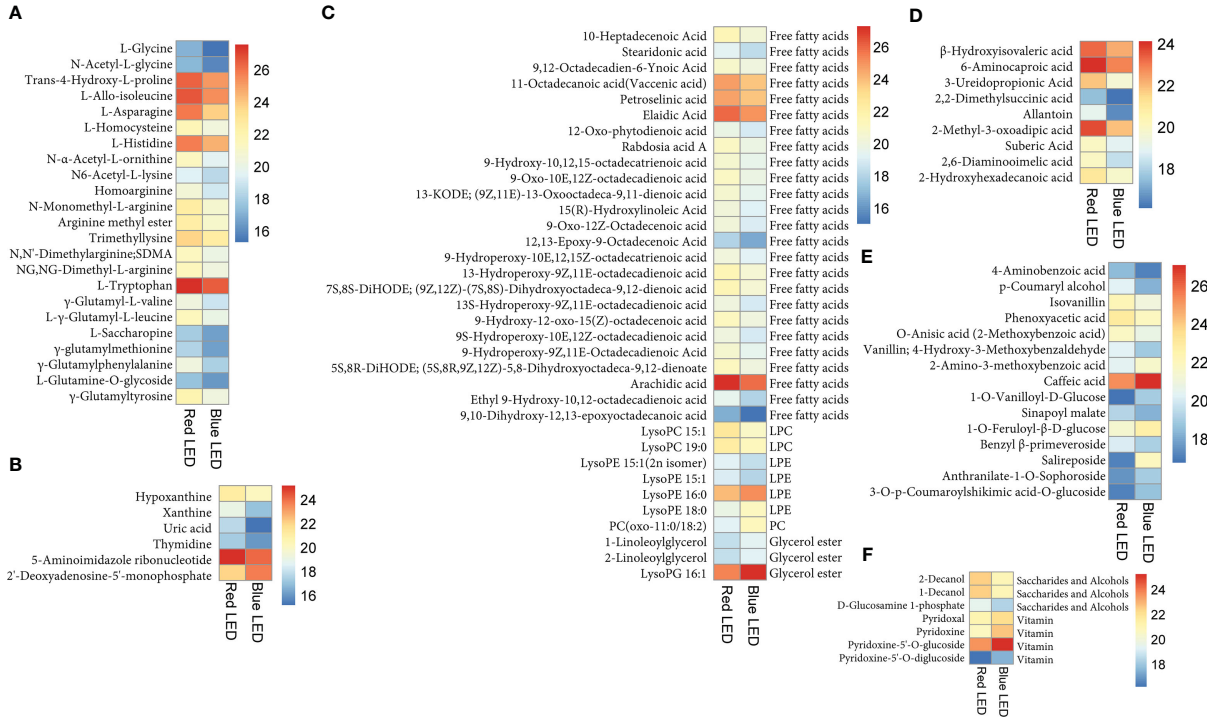

FIGURE 5
Heatmap of accumulation of different classes of compounds among the 95 differentially accumulated metabolites (DAMs) based on log2 transformed ion intensity of each compound between red (R) and blue **(B)** LEDs. **(A)** Amino acids and derivatives. **(B)** Nucleotides and derivatives. **(C)** Lipids. **(D)** Organic acids. **(E)** Phenolic acids. **(F)** Other classes. Each row represents one metabolite on the left-hand side of each heatmap. While in the case of lipids **(C)** and others **(F)** have sub-classes of compounds on the right-hand side of the heatmaps. The color gradients are shown on the right-hand side of each heatmap.

and flavonoids and increased antioxidant scavenging activity (Table 1). Tuladhar et al. (2021) reported that stressed plants showed increased biosynthesis of several compounds. In addition, the effects of red, blue, and far-red LEDs on phenol and flavonoid accumulation in diverse plant species have been well documented (Amoozgar et al., 2017; Nam et al., 2018). The roles of monochromatic red and blue LEDs depend on certain factors that need to be optimized. Studies have shown that blue and red light stimulate the activity of enzymes in the phenylpropanoid and shikimate pathways, including chalcone isomerase and synthases, leucoanthocyanidin dioxygenase, flavonol synthase, dihydroflavonol 4-reductase and stilbene (Gam et al., 2020), and phenylalanine ammonia-lyase (Wilawan et al., 2019). Light can affect plant total phenol and flavonoid contents by promoting the expression of genes involved in the biosynthesis of secondary compounds (Gam et al., 2020).

The identification of plant metabolites is an essential step for crop improvement. Therefore, it is vital to study key agronomic traits of crops. The UPLC–MS/MS was used in this study to analyze the metabolites in sweet potato leaves grown under red and blue LEDs. The detected metabolites based on their ion intensities grouped together biological replicates of a sample in the hierarchical heatmap clustering (Figure 2B); however, biological replicates of each sample, either red or blue LED clustered together with some discrepancies in PCA (Figure 2A). To overcome the discrepancies in the groupings seen in PCA and hierarchical heatmap clustering (Figures 2B, C), the DAMs and other downstream analyses were done based on average ion intensities of metabolites of the three biological repeats. The metabolite results showed that red light increased the abundance of metabolites in sweet potato leaves compared to sweet potato leaves grown under blue LEDs (Figure 4A). Similarly, red light has been shown to increase the content of amino acids in lettuce grown under red LEDs (Miyagi et al., 2017). In this study, red light significantly increased the accumulation of 23 amino acids and derivatives including eight essential amino acids. In addition, Hashim et al. (2021) reported that LEDs are useful in eliciting essential metabolites in plants for the nutrition and pharmaceutical industries. Besides, red light increased the abundance of 25 free fatty acids relative to blue LEDs. It has been reported that SDA acid is largely supplied to humans from marine sources (Banz et al., 2012), however; our results suggest that red light improve the abundance of SDA. This could serve as sustainable alternative means to curb type II diabetes mellitus (Banz et al., 2012). Red light increased the abundance of nine organic acid compounds in the sweet potato leaves. However, studies have shown that caffeic acid is found in abundance in many plants and foods, such as apples, potato, coffee and red wine. Coffee is the main source of caffeic acid in the diet. It is reported to have antioxidant and anti-inflammatory effects as well have potential to improve the immune system in humans (Zielińska et al., 2021).

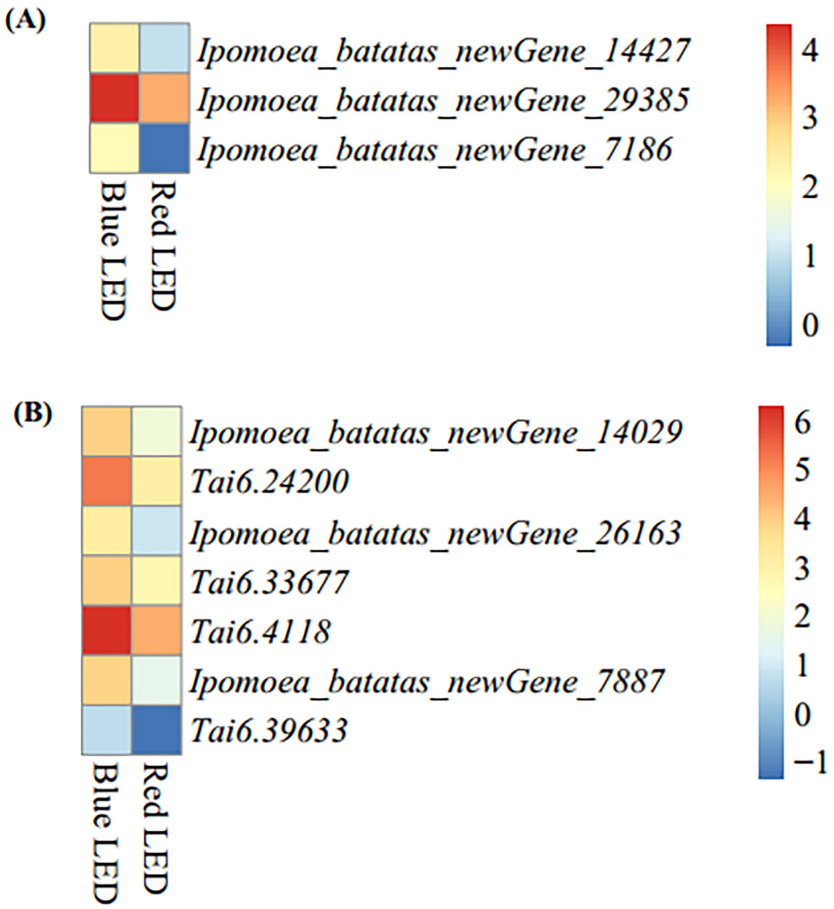

FIGURE 6
Heatmap of differentially expressed genes enriched in nutritionally-related KEGG pathways based log2 transformation of fragments kilobase of exon per million fragments mapped (FPKM) of sweet potato (*Ipomoea batatas* (L.) Lam) leaves grown with red and blue LEDs. **(A)** Anthocyanin biosynthesis with three structural genes (*Ipomoea_batatas_newGene_14427*, *Ipomoea_batatas_newGene_29385* and *Ipomoea_batatas_newGene_7186*) encode for anthocyanidin 3-O-glucosyltransferase [EC:24.1.115], Figure 5. **(B)** Carotenoid biosynthesis with seven structural genes, including two genes (*Ipomoea_batatas_newGene_14029* and *Tai6.24200*) encode carotenoid isomerase (crtH,crtISO) [EC:5.2.1.13], one gene (*Ipomoea_batatas_newGene_26163*) encode beta-carotene 9-cis-all-trans isomerase [EC:5.2.1.14], one gene (*Tai6.33677*) encode for zeaxanthin [EC:1.14.1521], one gene (*Tai6.4118*) encode for antheraxanthin [EC:1.23.5.1] and two genes (*Ipomoea_batatas_newGene_7887* and *Tai6.39633*) encode for abscisate [EC:1.14.14137] on Supplementary Figure B.

Both red and blue lights significantly affected the metabolites detected in the sweet potato leaves (Table 1, Figure 4). A total of 744 metabolites were identified, with leaves grown under red lights appearing more stressed and accumulating more metabolites than leaves produced under blue LEDs (Table S2). However, the total phenols and flavonoids were higher in leaves grown under blue light (Table 1). Simultaneously, most of the metabolites were induced and markedly accumulated under red light conditions (Figure 3A) as metabolite profiles are affected by differences in plant growth stage (Tamura et al., 2018; Wang et al., 2018). Consistent with our findings, previous studies have shown that red light increases the accumulation of phenolic acids and flavonoids in *M. communis* (Cioć et al., 2018) and *Silybum marianum* L. (Younas et al., 2018), while high levels of phenolics, flavonoids, and antioxidants were reported in tomato seedlings grown under blue LEDs (Kim et al., 2014). Specifically, eight essential amino acids (L-allo-isoleucine, L-histidine, N6-acetyl-L-lysine, L-tryptophan, γ-glutamyl-L-valine, L-γ-glutamyl-L-leucine, γ-glutamylmethionine and γ-glutamylphenylalanine) increased in abundance under red light (Figure 5A) and could be leveraged on to improve availability and accessibility of these essential amino acids for human health (Sá et al., 2020).

Transcriptome analysis has been used to elucidate the annotation of different gene functions and biosynthetic pathways (Zhong et al., 2021). Sweet potato, as a vegetable, is a source of essential nutritional compounds beneficial to human health, including carotenes, chlorophylls, vitamins, flavonoids and phenolics (Li et al., 2020). In this study, the transcript profiles revealed that genes involved in anthocyanin and carotenoid biosynthesis were more highly expressed under blue light than under red light conditions (Figure S3). These compounds work as antioxidants beneficial to human health (Li et al., 2020). Anthocyanins are phenolic (flavonoid) compounds. They are used as natural-coloring agents found in diverse plants as dietary antioxidants, and their consumption could help boost health by supplying several nutrients (Yousuf et al., 2016).

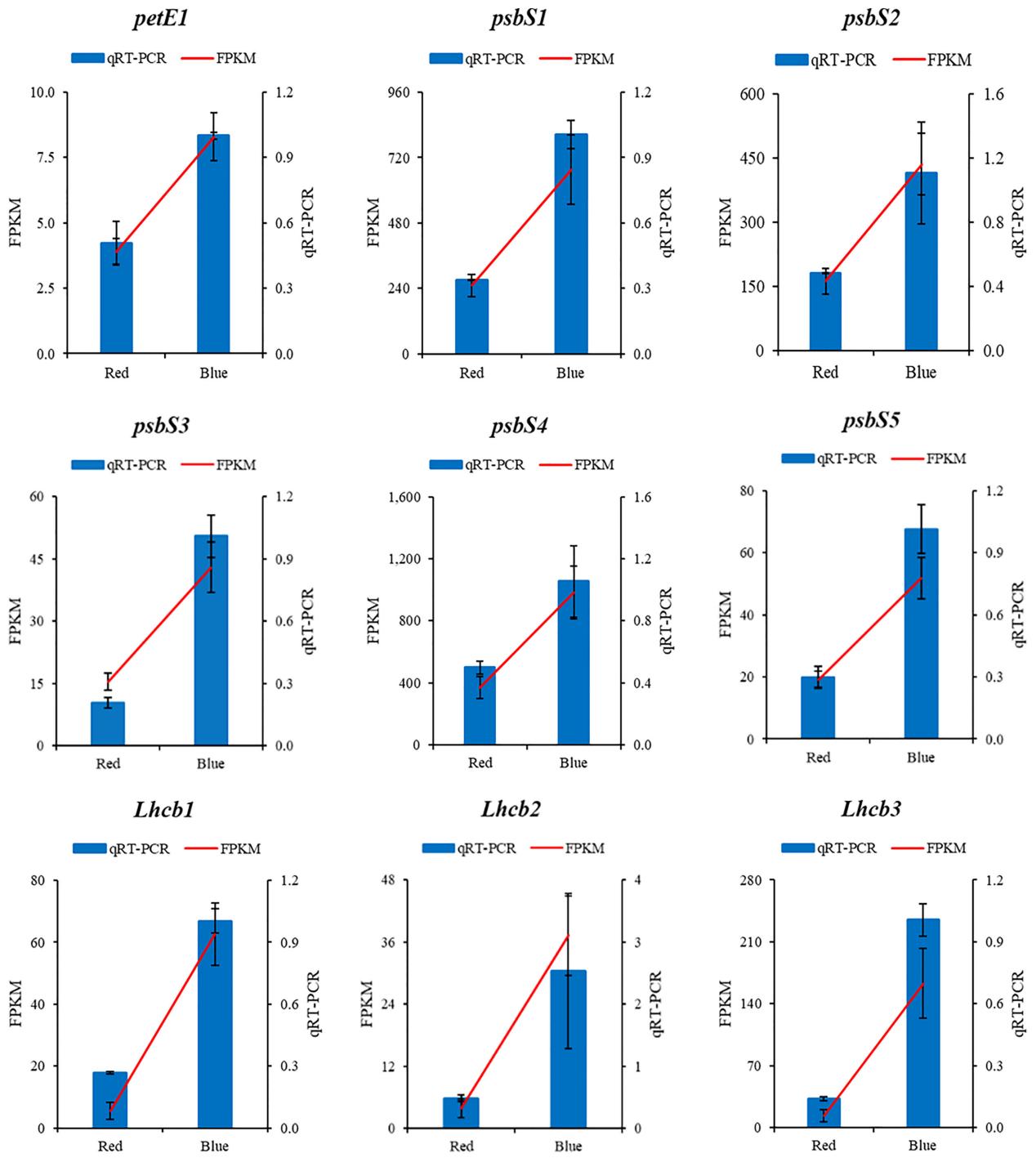

FIGURE 7
The qPCR validation of the RNA sequencing results of photosynthesis and photosynthesis-antenna proteins genes in sweet potato (I. batatas (L.) Lam) leaves grown under red and blue LEDs.

Also, studies have shown that anthocyanins possess antidiabetic, anticancer, anti-inflammatory, antimicrobial and anti-obesity effects, with the ability to prevent cardiovascular diseases (He et al., 2011). It has been shown that blue and UV-A light significantly increase the content of carotenoids and anthocyanins in Chinese kale and pak choi leaves (Li et al., 2020). Ouyang et al. (2015) reported that plant growth and development are regulated by light through altered gene expression. Also, the risk of developing cancer, cardiovascular disease, age-related macular degeneration, cataracts, disorders linked with inadequate immune function, and other degenerative diseases may be decreased by eating foods rich in carotenoids (Perera and Yen, 2007; Gammone et al., 2015). Genes identified in this study may be targeted for functional validation and verification to discover the regulatory role that they play in enhancing the nutritional profile of sweet potato leaves.

Our findings further explained the differences in the expression of light-regulated genes in sweet potato leaves in response to red and blue LEDs. Additionally, Chen et al. (2021) noted that the strength or weakness in synthesizing important metabolites is always indicated by the up- or downregulation of genes in certain metabolic pathways. Moreover, the development and metabolic changes in green plants are primarily thought to be regulated by changes in the expression of light-regulated genes (Ouyang et al., 2015). It has been reported that 16 hours of supplementation with blue lights increased the contents of carotenoids and anthocyanin, thereby increasing the antioxidant capacity of lettuce seedlings (Li et al., 2020). Earlier studies have shown that light significantly induces the production of phenolics, flavonoids, carotenoids and anthocyanin in several plants. For instance, UV-B, UV-A and blue light were cited to trigger the gene expression of some key enzyme functions in the biosynthesis of these metabolites (Li et al., 2020). Our results demonstrate a similar trend, where blue lights were shown to increase the expression of genes encoding anthocyanin and chlorophyll biosynthetic pathways. However, studies have shown that light quality significantly affects the accumulation of metabolites in crops grown in a controlled environment. Furthermore, the proportion of blue light supplied by LEDs affects the profiles of phytochemicals, depending on the species and the plant development stage of crops (Qinglu, 2021).

5 Conclusion

Sweet potato is a staple food and a critical food security crop in developing countries. However, previous studies have mainly focused on its production efficiency and tuber yield. The present study evaluates the influence of red and blue LEDs on sweet potato leaves. Blue light boosted dry matter accumulation, protein, total phenolics, flavonoids, and antioxidant scavenging activity relative to cultivation under red LEDs. Metabolite profiling using UPLC–MS/MS uncovered an abundance of 95 significant metabolites, where 77 compounds accumulated at higher levels in the leaf samples grown under red light and 18 metabolites at higher levels in leaves grown under blue light. KEGG pathway enrichment analysis revealed that nine and five DAMs were enriched in linoleic acid biosynthesis and alpha-linolenic acid metabolism.

Moreover, RNA sequencing identified 17,995 genes, out of which 14,039 novel genes were annotated. Most of the genes were upregulated in leaves grown under blue LEDs. The downregulation of the photosynthetic genes may account for the abscission and edema in leaves grown under red LEDs, and potentially serve as a putative mechanism of red and blue LED

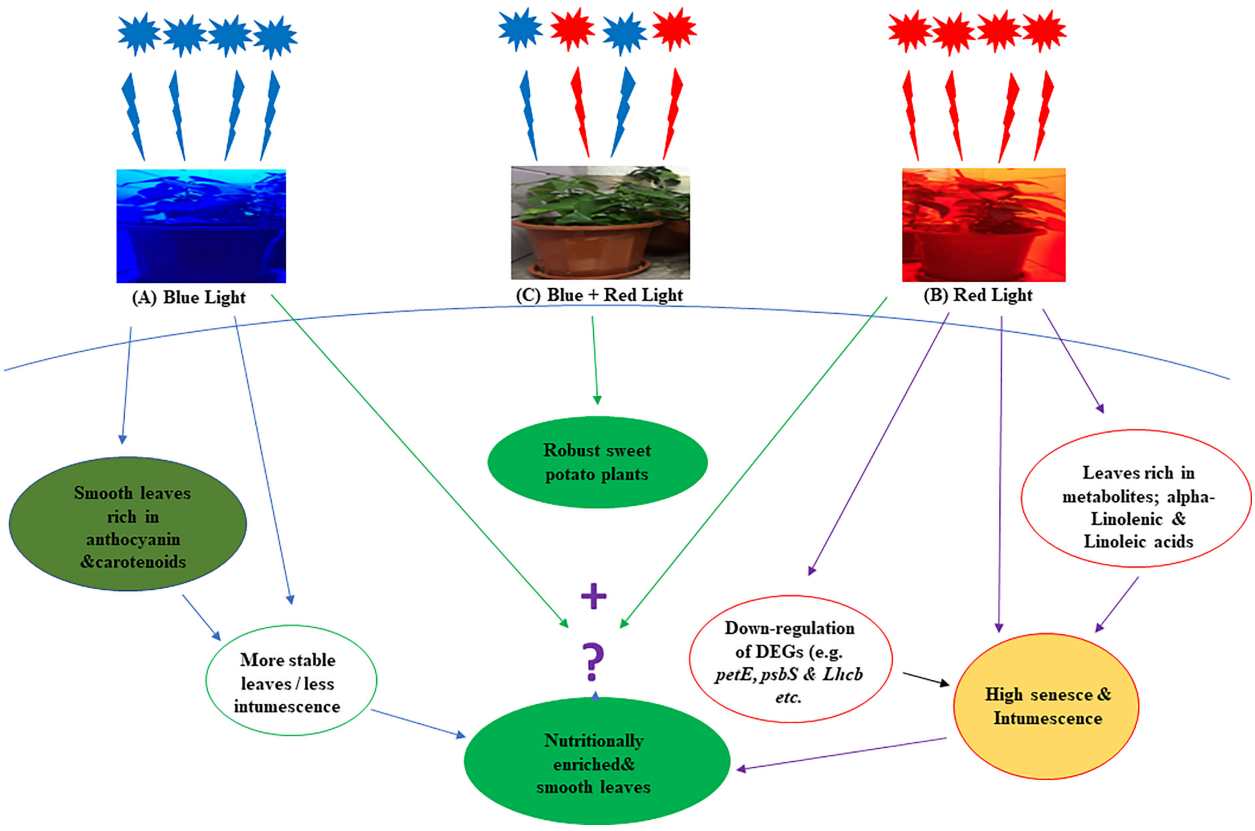

FIGURE 8
A hypothetical overview of the effect of red and blue LEDs on the production of sweet potato (I. batatas (L.) Lam) leaves. The leaves grown with monochromatic blue light were more stable **(A)** They have less intumescence and are rich in anthocyanin and carotenoids than those grown with monochromatic red lights, which have more abscission and intumescence **(B)** More DEGs were down-regulated under red light, and the leaves exhibit high metabolites (alpha-Linolenic and Linoleic acids) content. Hence, we proposed that a right proportion of red and blue light **(C)** may produce smooth leaves rich in metabolites.

regulation of metabolites in sweet potato leaves was summarized in Figure 8. The results could guide breeders and agronomists in improving the quality of sweet potato leaves through breeding and improved production practices.

Data availability statement

The datasets presented in this study can be found in online repositories. The names of the repository/repositories and accession number(s) can be found below: (http://www.ncbi.nlm.nih.gov/bioproject/947576), PRJNA947576.

Author contributions

SAT: Designed and executed the experiment, analyzed the data, and wrote the original manuscript. JKA and BK re-analyzed the data, revised and formatted the manuscript. CL, JD, JL, JW, HH, QF, LC, and PH, helped experimenting and data collection. XC and DQ conceptualization, supervised the work and finalized the manuscript. All authors contributed to the article and approved the submitted version.

Funding

This work was supported by the Fujian Provincial Department of Science and Technology, China (Grant numbers: 2020N5013; 2020N003; and 2019N0050); the 'Social service team' Support Program Project of FAFU (Grant numbers: 11899170108, and 11899170113).

Acknowledgments

We would like to thank the Fujian Agriculture and Forestry University, the Fujian Provincial Government, the Chinese Government, and DQ and XC for providing the financial support and enabling environment to conduct this research.

Conflict of interest

The authors declare that the research was conducted in the absence of any commercial or financial relationships that could be construed as a potential conflict of interest.

Publisher's note

Supplementary material

The Supplementary Material for this article can be found online at: https://www.frontiersin.org/articles/10.3389/fpls.2023.1181680/full#supplementary-material

References

Ahsen, M. A., Naqvi, S. A., Jaskani, M. J., Waseem, M., Khan, I. A., Hussnain, K., et al. (2019). Evaluation of exotic citrus rootstocks against *Fusarium spp. J. Global Innov. Agric. Soc. Sci.* 7, 151–156. doi: 10.22194/JGIASS/7.874

Alara, O. R., Abdurahman, N. H., and Olalere, O. A. (2020). Ethanolic extraction of flavonoids, phenolics and antioxidants from *Vernonia amygdalina* leaf using two-level factorial design. *J. King Saud Univ. - Sci.* 32, 7–16. doi: 10.1016/j.jksus.2017.08.001

Amoozgar, A., Mohammadi, A., and Sabzalian, M. R. (2017). Impact of light-emitting diode irradiation on photosynthesis, phytochemical composition and mineral element content of lettuce cv. grizzly. *Photosynthetica* 55, 85–95. doi: 10.1007/s11099-016-0216-8

Bantis, F., Smirnakou, S., Ouzounis, T., Koukounaras, A., Ntagkas, N., and Radoglou, K. (2018). Current status and recent achievements in the field of horticulture with the use of light-emitting diodes (LEDs). *Sci. Hortic.* 235, 437–451. doi: 10.1016/j.scienta.2018.02.058

Banz, W. J., Davis, J. E., Clough, R. W., and Cheatwood, J. L. (2012). Stearidonic acid: is there a role in the prevention and management of type 2 diabetes Mellitus?123. *J. Nutr.* 142, 635S–640S. doi: 10.3945/jn.111.146829

Benjamini, Y., and Hochberg, Y. (1995). Controlling the false discovery rate: a practical and powerful approach to multiple testing. *J. R. Stat. Soc.: Ser. B (Methodol.)* 57, 289–300. doi: 10.1111/j.2517-6161.1995.tb02031.x

Bennett, A. A., Mahood, E. H., Fan, K., and Moghe, G. D. (2021). Untargeted metabolomics of purple and orange-fleshed sweet potatoes reveals a large structural diversity of anthocyanins and flavonoids. *Sci. Rep.* 11, 16408–16408. doi: 10.1038/s41598-021-95901-y

Chen, L.-L., Wang, H.-Y., Gong, X.-C., Zeng, Z.-H., Xue, X.-Z., and Hu, Y.-G. (2021). Transcriptome analysis reveals effects of red and blue light-emitting diodes (LEDs) on the growth, chlorophyll fluorescence and endogenous plant hormones of potato (*Solanum tuberosum* L.) plantlets cultured *in vitro*. *J. Integr. Agric.* 20, 2914–2931. doi: 10.1016/S2095-3119(20)63393-7

Cioć, M., Szewczyk, A., Żupnik, M., Kalisz, A., and Pawłowska, B. (2018). LED lighting affects plant growth, morphogenesis and phytochemical contents of *Myrtus communis* L. *in vitro*. *Plant Cell Tissue Organ Cult. (PCTOC)* 132, 433–447. doi: 10.1007/s11240-017-1340-2

Craver, J. K., Miller, C. T., Williams, K. A., and Bello, N. M. (2014). Ultraviolet radiation affects intumescence development in ornamental sweetpotato (*Ipomoea batatas*). *HortScience* 49, 1277–1283. doi: 10.21273/HORTSCI.49.10.1277

Cui, L., Liu, C., Li, D., and Song, J. (2011). Effect of processing on taste quality and health-relevant functionality of sweet potato tips. *Agric. Sci. China* 10, 456–462. doi: 10.1016/S1671-2927(11)60025-4

Dwivedi, S. K., Arora, A., Singh, V. P., and Singh, G. P. (2018). Induction of water deficit tolerance in wheat due to exogenous application of plant growth regulators: membrane stability, water relations and photosynthesis. *Photosynthetica* 56, 478–486. doi: 10.1007/s11099-017-0695-2

Eguchi, T., Hernández, R., and Kubota, C. (2016). Far-red and blue light synergistically mitigate intumescence injury of tomato plants grown under ultraviolet-deficit light environment. *HortSci. horts* 51, 712–719. doi: 10.21273/HORTSCI.51.6.712

Fraga, C. G., Clowers, B. H., Moore, R. J., and Zink, E. M. (2010). Signature-discovery approach for sample matching of a nerve-agent precursor using liquid chromatography–mass spectrometry, XCMS, and chemometrics. *Anal. Chem.* 82, 4165–4173. doi: 10.1021/ac1003568

Gam, D. T., Khoi, P. H., Ngoc, P. B., Linh, L. K., Hung, N. K., Anh, P. T. L., et al. (2020). LED lights promote growth and flavonoid accumulation of anoectochilus roxburghii and are linked to the enhanced expression of several related genes. *Plants* 9, 1344. doi: 10.3390/plants9101344

Gammone, M. A., Riccioni, G., and D'orazio, N. (2015). Carotenoids: potential allies of cardiovascular health? *Food Nutr. Res.* 59, 26762. doi: 10.3402/fnr.v59.26762

Ghatak, A., Chaturvedi, P., and Weckwerth, W. (2018). Metabolomics in plant stress physiology. *Adv. Biochem. Eng. Biotechnol.* 164, 187–236. doi: 10.1007/10_2017_55

Gowda, G. A., and Djukovic, D. (2014). Overview of mass spectrometry-based metabolomics: opportunities and challenges. *Methods Mol. Biol.* 1198, 3–12. doi: 10.1007/978-1-4939-1258-2_1

Guo, X., Shang, X., Zhou, X., Zhao, B., and Zhang, J. (2017). Ultrasound-assisted extraction of polysaccharides from rhododendron aganniphum: antioxidant activity and rheological properties. *Ultrasonics Sonochem.* 38, 246–255. doi: 10.1016/j.ultsonch.2017.03.021

Hashim, M., Ahmad, B., Drouet, S., Hano, C., Abbasi, B. H., and Anjum, S. (2021). Comparative effects of different light sources on the production of key secondary metabolites in plants *In vitro* cultures. *Plants (Basel Switzerland)* 10, 1521. doi: 10.3390/plants10081521

He, K., Li, X., Chen, X., Ye, X., Huang, J., Jin, Y., et al. (2011). Evaluation of antidiabetic potential of selected traditional Chinese medicines in STZ-induced diabetic mice. *J. Ethnopharmacol.* 137, 1135–1142. doi: 10.1016/j.jep.2011.07.033

He, L., Liu, X., Liu, S., Zhang, J., Zhang, Y., Sun, Y., et al. (2020). Transcriptomic and targeted metabolomic analysis identifies genes and metabolites involved in anthocyanin accumulation in tuberous roots of sweetpotato (*Ipomoea batatas* L.). *Plant Physiol. Biochem.* 156, 323–332. doi: 10.1016/j.plaphy.2020.09.021

He, J., and Qin, L. (2020). Growth and photosynthetic characteristics of sweet potato (*Ipomoea batatas*) leaves grown under natural sunlight with supplemental LED lighting in a tropical greenhouse. *J. Plant Physiol.* 252, 153239. doi: 10.1016/j.jplph.2020.153239

Hua, Y., Liu, X., and Xie, F. (2021). Comparison of chemical constituents in pseudostellariae radix with different dosage forms based on HPLC-Q-Exactive Orbitrap/MS combined with multivariate statistical analysis. *Evid Based Complement Alternat Med.* 2021, 6644127. doi: 10.1155/2021/6644127

Iese, V., Holland, E., Wairiu, M., Havea, R., Patolo, S., Nishi, M., et al. (2018). Facing food security risks: the rise and rise of the sweet potato in the pacific islands. *Global Food Secur.* 18, 48–56. doi: 10.1016/j.gfs.2018.07.004

Kanehisa, M., Araki, M., Goto, S., Hattori, M., Hirakawa, M., Itoh, M., et al. (2008). KEGG for linking genomes to life and the environment. *Nucleic Acids Res.* 36, D480–D484. doi: 10.1093/nar/gkm882

Kim, E.-Y., Park, S.-A., Park, B.-J., Lee, Y., and Oh, M.-M. (2014). Growth and antioxidant phenolic compounds in cherry tomato seedlings grown under monochromatic light-emitting diodes. *Horticult. Environ. Biotechnol.* 55, 506–513. doi: 10.1007/s13580-014-0121-7

Kolde, R. (2012). "Pheatmap: pretty heatmaps," in *R package version 1*, 747. doi: 10.3389/fgene.2022.964684

Kui, X., Li, M., Yang, H., Tadda, A. S., Sun, Y., Ma, C., et al. (2020). Comparison of physico-chemical characteristics of myrtle at different ripening stages. *Folia Hortic.* 32, 125–133. doi: 10.2478/fhort-2020-0012

Kusano, M., Tohge, T., Fukushima, A., Kobayashi, M., Hayashi, N., Otsuki, H., et al. (2011). Metabolomics reveals comprehensive reprogramming involving two independent metabolic responses of arabidopsis to UV-b light. *Plant J.* 67, 354–369. doi: 10.1111/j.1365-313X.2011.04599.x

Lamers, P. P., Van De Laak, C. C., Kaasenbrood, P. S., Lorier, J., Janssen, M., De Vos, R. C., et al. (2010). Carotenoid and fatty acid metabolism in light-stressed *Dunaliella salina*. *Biotechnol. Bioeng.* 106, 638–648. doi: 10.1002/bit.22725

Li, M., Jang, G. Y., Lee, S. H., Kim, M. Y., Hwang, S. G., Sin, H. M., et al. (2017). Comparison of functional components in various sweet potato leaves and stalks. *Food Sci. Biotechnol.* 26, 97–103. doi: 10.1007/s10068-017-0013-6

Li, Q., and Kubota, C. (2009). Effects of supplemental light quality on growth and phytochemicals of baby leaf lettuce. *Environ. Exp. Bot.* 67, 59–64. doi: 10.1016/j.envexpbot.2009.06.011

Li, Y., Zheng, Y., Zheng, D., Zhang, Y., Song, S., Su, W., et al. (2020). Effects of supplementary blue and UV-a LED lights on morphology and phytochemicals of brassicaceae baby-leaves. *Molecules (Basel Switzerland)* 25, 5678. doi: 10.3390/molecules25235678

Liang, D., Yousef, A. F., Wei, X., Ali, M. M., Yu, W., Yang, L., et al. (2021). Increasing the performance of passion fruit (Passiflora edulis) seedlings by LED light regimes. *Sci. Rep.* 11, 20967. doi: 10.1038/s41598-021-00103-1

Lichtenthaler, H. K., and Babani, F. (2022). Contents of photosynthetic pigments and ratios of chlorophyll a/b and chlorophylls to carotenoids (a+b)/(x+c) in C4 plants as compared to C3 plants. *Photosynthetica* 60, 3–9. doi: 10.32615/ps.2021.041

Lisec, J., Schauer, N., Kopka, J., Willmitzer, L., and Fernie, A. R. (2006). Gas chromatography mass spectrometry–based metabolite profiling in plants. *Nat. Protoc.* 1, 387–396. doi: 10.1038/nprot.2006.59

Livak, K. J., and Schmittgen, T. D. (2001). Analysis of relative gene expression data using real-time quantitative PCR and the 2–ΔΔCT method. *Methods* 25, 402–408. doi: 10.1006/meth.2001.1262

Lobiuc, A., Vasilache, V., Pintilie, O., Stoleru, T., Burducea, M., Oroian, M., et al. (2017). Blue and red LED illumination improves growth and bioactive compounds contents in acyanic and cyanic *Ocimum basilicum* L. microgreens. *Mol. (Basel Switzerland)* 22, 2111. doi: 10.3390/molecules22122111

Lv, Z., Zhang, S., and Lu, G. (2021). Effect of light regulation on the quality of sweetpotato sprouts. *HortSci. horts* 56, 374. doi: 10.21273/HORTSCI15625-20

Ma, C., Dastmalchi, K., Flores, G., Wu, S. B., Pedraza-Peñalosa, P., Long, C., et al. (2013). Antioxidant and metabolite profiling of north American and neotropical blueberries using LC-TOF-MS and multivariate analyses. *J. Agric. Food Chem.* 61, 3548–3559. doi: 10.1021/jf400515g

Mao, X., Cai, T., Olyarchuk, J. G., and Wei, L. (2005). Automated genome annotation and pathway identification using the KEGG orthology (KO) as a controlled vocabulary. *Bioinformatics* 21, 3787–3793. doi: 10.1093/bioinformatics/bti430

Miyagi, A., Uchimiya, H., and Kawai-Yamada, M. (2017). Synergistic effects of light quality, carbon dioxide and nutrients on metabolite compositions of head lettuce under artificial growth conditions mimicking a plant factory. *Food Chem.* 218, 561–568. doi: 10.1016/j.foodchem.2016.09.102

Motsa, N. M., Modi, A. T., and Mabhaudhi, T. (2015). Sweet potato (*Ipomoea batatas* L.) as a drought tolerant and food security crop. *South Afr. J. Sci.* 111, 1–8. doi: 10.17159/sajs.2015/20140252

Nadeem, M., Abbasi, B. H., Younas, M., Ahmad, W., Zahir, A., and Hano, C. (2019). LED-enhanced biosynthesis of biologically active ingredients in callus cultures of ocimum basilicum. *J. Photochem. Photobiol. B: Biol.* 190, 172–178. doi: 10.1016/j.jphotobiol.2018.09.011

Nam, T. G., Kim, D. O., and Eom, S. H. (2018). Effects of light sources on major flavonoids and antioxidant activity in common buckwheat sprouts. *Food Sci. Biotechnol.* 27, 169–176. doi: 10.1007/s10068-017-0204-1

Ouyang, F., Mao, J. F., Wang, J., Zhang, S., and Li, Y. (2015). Transcriptome analysis reveals that red and blue light regulate growth and phytohormone metabolism in Norway spruce [*Picea abies* (L.) karst]. *PloS One* 10, e0127896. doi: 10.1371/journal.pone.0127896

Perera, C. O., and Yen, G. M. (2007). Functional properties of carotenoids in human health. *Int. J. Food Properties* 10, 201–230. doi: 10.1080/10942910601045271

Qinglu, Y. (2021). The proportion of blue light from light-emitting diodes alters microgreen phytochemical profiles in a species-specific manner. *HortScience* 56, 13–20-2021. doi: 10.21273/HORTSCI15371-20

Sá, A. G. A., Moreno, Y. M. F., and Carciofi, B. (2020). Plant proteins as high-quality nutritional source for human diet. *Trends Food Sci. Technol.* 97, 170–184. doi: 10.1016/j.tifs.2020.01.011

Sakuraba, Y. (2021). Light-mediated regulation of leaf senescence. *Int. J. Mol. Sci.* 22, 3291. doi: 10.3390/ijms22073291

Shannon, P., Markiel, A., Ozier, O., Baliga, N. S., Wang, J. T., Ramage, D., et al. (2003). Cytoscape: a software environment for integrated models of biomolecular interaction networks. *Genome Res.* 13, 2498–2504. doi: 10.1101/gr.1239303

Suematsu, K., Tanaka, M., Kurata, R., and Kai, Y. (2020). Comparative transcriptome analysis implied a ZEP paralog was a key gene involved in carotenoid accumulation in yellow-fleshed sweetpotato. *Sci. Rep.* 10, 20607. doi: 10.1038/s41598-020-77293-7

Tamura, Y., Mori, T., Nakabayashi, R., Kobayashi, M., Saito, K., Okazaki, S., et al. (2018). Metabolomic evaluation of the quality of leaf lettuce grown in practical plant factory to capture metabolite signature. *Front. Plant Sci.* 9. doi: 10.3389/fpls.2018.00665

Tang, C., Ameen, A., Fang, B.-P., Liao, M.-H., Chen, J.-Y., Huang, L.-F., et al. (2020). Nutritional composition and health benefits of leaf-vegetable sweet potato in south China. *J. Food Composition Anal.* 96, 103714. doi: 10.1016/j.jfca.2020.103714

Tuladhar, P., Sasidharan, S., and Saudagar, P. (2021). *Biocontrol agents and secondary metabolites* (The Netherlands: Elsevier Amsterdam).

Wang, S., Alseekh, S., Fernie, A. R., and Luo, J. (2019). The structure and function of major plant metabolite modifications. *Mol. Plant* 12, 899–919. doi: 10.1016/j.molp.2019.06.001

Wang, A., Li, R., Ren, L., Gao, X., Zhang, Y., Ma, Z., et al. (2018). A comparative metabolomics study of flavonoids in sweet potato with different flesh colors (*Ipomoea batatas* (L.) lam). *Food Chem.* 260, 124–134. doi: 10.1016/j.foodchem.2018.03.125

Wang, S., Nie, S., and Zhu, F. (2016a). Chemical constituents and health effects of sweet potato. *Food Res. Int.* 89, 90–116. doi: 10.1016/j.foodres.2016.08.032

Wang, S., Wang, X., Shi, X., Wang, B., Zheng, X., Wang, H., et al. (2016b). Red and blue lights significantly affect photosynthetic properties and ultrastructure of mesophyll cells in senescing grape leaves. *Hortic. Plant J.* 2, 82–90. doi: 10.1016/j.hpj.2016.03.001

Wei, C., Li, J., Ma, Z., Qiao, J., Zhao, W., and Liu, Y. (2019). Study on the best extraction technology of total flavonoids from piper sarmentosum roxb. leaves and evaluation of antioxidant activity. *IOP Conf. Series: Earth Environ. Sci.* 330, 042061. doi: 10.1088/1755-1315/330/4/042061

Wei, T., Simko, V., Levy, M., Xie, Y., Jin, Y., and Zemla, J. (2017). Package 'corrplot'. *Statistician* 56, e24.

Wilawan, N., Ngamwonglumlert, L., Devahastin, S., and Chiewchan, N. (2019). Changes in enzyme activities and amino acids and their relations with phenolic compounds contents in okra treated by LED lights of different colors. *Food Bioprocess Technol.* 12, 1945–1954. doi: 10.1007/s11947-019-02359-y

Williams, K. A., Miller, C. T., and Craver, J. K. (2016). "Light quality effects on intumescence (Oedema) on plant leaves," in *LED lighting for urban agriculture* (Singapore: Springer), 275–286. doi: 10.1007/978-981-10-1848-0_20

Wu, M.-C., Hou, C.-Y., Jiang, C.-M., Wang, Y.-T., Wang, C.-Y., Chen, H.-H., et al. (2007). A novel approach of LED light radiation improves the antioxidant activity of pea seedlings. *Food Chem.* 101, 1753–1758. doi: 10.1016/j.foodchem.2006.02.010

Xie, D., Chen, L., Zhou, C., Tarin, M. W. K., Yang, D., Ren, K., et al. (2020). Transcriptomic and metabolomic profiling reveals the effect of LED light quality on morphological traits, and phenylpropanoid-derived compounds accumulation in *Sarcandra glabra* seedlings. *BMC Plant Biol.* 20, 476. doi: 10.1186/s12870-020-02685-w

Xu, T.-F., Yang, X., Zhang, M., Guo, S.-H., Fu, W.-J., Zhou, B.-J., et al. (2022). The use of widely targeted metabolite profiling to reveal the senescence changes in postharvest 'Red globe' (*Vitis vinifera*) grape berries. *J. Integr. Agric.* 21, 1028–1043. doi: 10.1016/S2095-3119(21)63725-5

Yeshitila, M., and Taye, M. (2016). Non-destructive prediction models for estimation of leaf area for most commonly grown vegetable crops in Ethiopia. *Sci. J. Appl. Math. Stat* 4, 202–216. doi: 10.11648/j.sjams.20160405.13

Younas, M., Drouet, S., Nadeem, M., Giglioli-Guivarc'h, N., Hano, C., and Abbasi, B. H. (2018). Differential accumulation of silymarin induced by exposure of *Silybum marianum* L. callus cultures to several spectres of monochromatic lights. *J. Photochem. Photobiol. B: Biol.* 184, 61–70. doi: 10.1016/j.jphotobiol.2018.05.018

Young, M. D., Wakefield, M. J., Smyth, G. K., and Oshlack, A. (2010). Gene ontology analysis for RNA-seq: accounting for selection bias. *Genome Biol.* 11, R14. doi: 10.1186/gb-2010-11-2-r14

Yousef, A. F., Ali, M. M., Rizwan, H. M., Tadda, S. A., Kalaji, H. M., Yang, H., et al. (2021). Photosynthetic apparatus performance of tomato seedlings grown under various combinations of LED illumination. *PloS One* 16, e0249373. doi: 10.1371/journal.pone.0249373

Yousuf, B., Gul, K., Wani, A. A., and Singh, P. (2016). Health benefits of anthocyanins and their encapsulation for potential use in food systems: a review. *Crit. Rev. Food Sci. Nutr.* 56, 2223–2230. doi: 10.1080/10408398.2013.805316

Yue, C., Wang, Z., and Yang, P. (2021). Review: the effect of light on the key pigment compounds of photosensitive etiolated tea plant. *Bot. Stud.* 62, 21. doi: 10.1186/s40529-021-00329-2

Zheng, L., and Van Labeke, M. C. (2017). Long-term effects of red- and blue-light emitting diodes on leaf anatomy and photosynthetic efficiency of three ornamental pot plants. *Front. Plant Sci.* 8, 917. doi: 10.3389/fpls.2017.00917

Zhong, Y., Wang, L., Ma, Z., and Du, X. (2021). Physiological responses and transcriptome analysis of *Spirodela polyrhiza* under red, blue, and white light. *Planta* 255, 11. doi: 10.1007/s00425-021-03764-4

Zielińska, D., Zieliński, H., Laparra-Llopis, J. M., Szawara-Nowak, D., Honke, J., and Giménez-Bastida, J. A. (2021). Caffeic acid modulates processes associated with intestinal inflammation. *Nutrients* 13, 554. doi: 10.3390/nu13020554

frontiers | Frontiers in Plant Science

TYPE Original Research
PUBLISHED 02 June 2023
DOI 10.3389/fpls.2023.1185622

OPEN ACCESS

EDITED BY
Genhua Niu,
Texas A&M University, United States

REVIEWED BY
Shoko Hikosaka,
Chiba University, Japan
Yujin Park,
Arizona State University, United States

*CORRESPONDENCE
Paul Kusuma
paul.kusuma@wur.nl

†PRESENT ADDRESS
Paul Kusuma,
Horticulture and Product Physiology,
Department of Plant Sciences,
Wageningen University and Research,
Wageningen, Netherlands

RECEIVED 13 March 2023
ACCEPTED 10 May 2023
PUBLISHED 02 June 2023

CITATION
Kusuma P and Bugbee B (2023) On the contrasting morphological response to far-red at high and low photon fluxes.
Front. Plant Sci. 14:1185622.
doi: 10.3389/fpls.2023.1185622

On the contrasting morphological response to far-red at high and low photon fluxes

Paul Kusuma[1,2*†] and Bruce Bugbee[2]

[1]Department of Plant Sciences, Horticulture and Product Physiology, Wageningen University and Research, Wageningen, Netherlands, [2]Crop Physiology Laboratory, Department of Plants Soils and Climate, Utah State University, Logan, UT, United States

Plants compete for sunlight and have evolved to perceive shade through both relative increases in the flux of far-red photons (FR; 700 to 750 nm) and decreases in the flux of all photons (intensity). These two signals interact to control stem elongation and leaf expansion. Although the interacting effects on stem elongation are well quantified, responses for leaf expansion are poorly characterized. Here we report a significant interaction between far-red fraction and total photon flux. Extended photosynthetic photon flux density (ePPFD; 400 to 750 nm) was maintained at three levels (50/100, 200 and 500 µmol m^{-2} s^{-1}), each with a range of 2 to 33% FR. Increasing FR increased leaf expansion in three cultivars of lettuce at the highest ePPFD but decreased expansion at the lowest ePPFD. This interaction was attributed to differences in biomass partitioning between leaves and stems. Increased FR favored stem elongation and biomass partitioning to stems at low ePPFD and favored leaf expansion at high ePPFD. In cucumber, leaf expansion was increased with increasing percent FR under all ePPFD levels showing minimal interaction. The interactions (and lack thereof) have important implications for horticulture and warrant further study for plant ecology.

KEYWORDS

far-red, phytochrome, shade avoidance, shade tolerance, photosynthetic photon flux density, leaf expansion

1 Introduction

Limited resources limit plant growth (El-Sharkawy, 2011). As sessile organisms, plants must modulate their growth and development to compete for access to critical resources – one of which is sunlight. This has led to the evolution of a high degree of plant plasticity in response to shaded environments.

Before plants experience a decrease in the flux of photons within photosynthetically active radiation (PAR; 400 to 700 nm) in competitive environments, the flux of far-red photons (FR; 700 to 750 nm) will increase due to reflection from neighboring vegetation

primarily in the horizontal direction (Ballaré et al., 1987; Ballaré et al., 1991; Casal, 2012). This increase in FR (decrease in the R:FR ratio) is caused by preferential absorption of photons in the PAR region for photosynthesis and scattering of FR photons by leaf tissue. As plants grow, they begin to overlap, which decreases the overall flux of photons in both the PAR and FR regions, although the percentage of FR [100×FR/(PAR + FR)] remains enriched compared to sunlight. Many plant species adjust their morphology in response to both FR and PAR to maximize survival in a process called shade avoidance (Ballaré et al., 1991; Schmitt, 1997; Kurepin et al., 2007a; Pierik and de Wit, 2014). Shade avoidance responses are often defined as increased stem and petiole elongation, increased biomass allocation to stems, increased specific leaf area (SLA; leaf area divided by leaf mass), and increased apical dominance (Casal, 2012; Gommers et al., 2013; Pierik and de Wit, 2014).

Biomass accumulation is highly correlated with leaf area, especially before canopy closure when plants are young and a high fraction of photons fall between the plants (Monteith, 1977; Gifford et al., 1984; Zhen and Bugbee, 2020b). Furthermore, leaves are the primary photon-collecting organs of a plant with higher photosynthetic capacity than other organs (Xu et al., 1997). Increasing leaf area increases the area over which photons can be intercepted, and thus, leaf area/expansion in response to shade is a vital parameter for the competitiveness, survival, and fitness of a plant. Specific leaf area, which is often reported to increase in shade, only indicates a change in leaf area given the biomass partitioning to the leaves. Thus, total plant leaf area is dependent on both the SLA and the biomass partitioning, the latter of which tends to favor stems over leaves in shaded environments (Morgan and Smith, 1979; Ballaré et al., 1987; Ballaré et al., 1991; Poorter et al., 2012).

The literature has been inconsistent regarding the effect of increasing FR on leaf expansion. We summarize these contrasting responses across 41 studies spanning 46 years in Table S1. Within these 41 studies, 14 show that increasing percent far-red or end-of-day far-red can decrease leaf area (Holmes and Smith, 1975; Holmes and Smith, 1977; Frankland and Letendre, 1978; Child et al., 1981; Kwesiga and Grace, 1986; Robson et al., 1993; Devlin et al., 1999; Franklin et al., 2003; Carabelli et al., 2007; Kurepin et al., 2007a; Kurepin et al., 2007b; Qaderi et al., 2015; Park and Runkle, 2019; Kong and Nemali, 2021), 28 studies show increases (Child et al., 1981; Kwesiga and Grace, 1986; Casal et al., 1987; López-Juez et al., 1990; Pausch et al., 1991; Heraut-Bron et al., 1999; Franklin et al., 2003; Kurepin et al., 2006; Kurepin et al., 2007a; Boccalandro et al., 2009; Kurepin et al., 2012a; Kurepin et al., 2012b; Patel et al., 2013; Lee et al., 2016; Shibuya et al., 2016; Bae et al., 2017; Park and Runkle, 2017; Park and Runkle, 2018; Kalaitzoglou et al., 2019; Park and Runkle, 2019; Shibuya et al., 2019; Zou et al., 2019; Zhen and Bugbee, 2020b; Jin et al., 2021; Kong and Nemali, 2021; Kusuma and Bugbee, 2021; Legendre and van Iersel, 2021; Zou et al., 2021), and 14 studies show no effect (Child et al., 1981; Pausch et al., 1991; Barreiro et al., 1992; Miyashita et al., 1995; Heraut-Bron et al., 1999; Kurepin et al., 2006; Kurepin et al., 2010; Kurepin et al., 2012b; Patel et al., 2013; Lee et al., 2015; Park and Runkle, 2017; Park and Runkle, 2018; Park and Runkle, 2019; Zhang et al., 2020). These contrasting responses are well noted in the literature (see Casal and Smith, 1989; Casal, 2012; Demotes-Mainard et al., 2016), and have been attributed to species/cultivar differences (Casal et al., 1987; Boccalandro et al., 2009; Kurepin et al., 2012b), as well as interactions with vapor pressure deficit (Shibuya et al., 2019), temperature (Franklin et al., 2003; Patel et al., 2013), blue photon flux (Park and Runkle, 2019), and PAR intensity (Kurepin et al., 2007a; Park and Runkle, 2018; Zou et al., 2019).

One confounding factor with many of these studies is that FR photons are usually added to a constant flux of traditionally defined PAR. Recent evidence has demonstrated that FR photons are photosynthetic when combined with shorter wavelengths (Zhen and Bugbee, 2020a; Zhen and Bugbee, 2020b) through excitation of PSI (Zhen and van Iersel, 2017). Because many studies add FR on top of traditionally defined PAR, the flux of total photosynthetic photons is increased in these studies. This potentially leads to an increase in leaf area through an increase in photosynthesis and biomass accumulation rather than through a morphological adjustment to increase light capture. It is thus important to properly separate the two effects. The conclusion that FR is photosynthetic has resulted in the development of the term extended photosynthetically active radiation (ePAR), which considers the photons between 400 to 750 nm photosynthetic (Zhen et al., 2021). This metric has been increasingly adopted over the past few years (Kusuma and Bugbee, 2021; Shelford and Both, 2021; Veazie et al., 2023; Warner et al., 2023). Maintaining extended photosynthetic photon flux density (ePPFD; the photon flux of ePAR; 400 to 750 nm), while adjusting levels of FR, is one way to separate the photosynthetic and morphological responses.

Plant morphological responses to increases in FR are modulated by phytochrome photoreceptors (Holmes and Smith, 1975; Franklin et al., 2003; Casal, 2012), while responses to decreases in ePPFD are modulated by phytochromes (Millenaar et al., 2009; Trupkin et al., 2014), cryptochromes (Keller et al., 2011; Pedmale et al., 2016), and possibly photosynthetic signals (Millenaar et al., 2009). Cryptochromes and phytochromes interact with many of the same transcription factors to modulate gene expression (de Wit et al., 2016), but cryptochrome effects (low blue photon fluxes) have been shown to regulate genes related to cell wall elasticity, while FR was associated with auxin genes (Pedmale et al., 2016). Phytochrome responses depend on the ePPFD because thermal reversion (the light independent conversion of Pfr back to Pr) significantly affects phytochrome dynamics at lower photon fluxes (Sellaro et al., 2019). Additionally, hormonal signals in response to FR have different patterns of expression at low and high ePPFD (Hersch et al., 2014).

Altogether, the signaling pathways in response to changes in photon quality and quantity are complex, as photoreceptor-controlled responses have appeared both additive/independent (Neff and Chory, 1998; Keller et al., 2011; Pedmale et al., 2016) but also synergistic (Casal and Mazzella, 1998; Sellaro et al., 2009; de Wit et al., 2016). It has been hypothesized that one of the reasons FR decreases leaf expansion in some species is because of competition for resources between stems and leaves (Casal et al., 1987). If FR and PAR interact to control stem elongation, and if increased stem elongation induces more biomass partitioning to the stems (de Wit et al., 2018), then FR and PAR ought to be expected to interact to

predict leaf expansion, potentially showing opposite responses to FR at high and low ePPFD. The response may depend on the basic architecture of the specific species, especially regarding rosette versus upright plant architecture.

We investigated the interactions of FR and ePPFD on plant morphology, with specific interest in leaf expansion, in two diverse species, lettuce and cucumber (rosette and upright plant architecture, respectively). We hypothesize that increasing the percentage of FR will have contrasting effects at different levels of ePPFD. We show that increasing FR in lettuce increases leaf area and dry mass accumulation at high intensities but decreases leaf area and dry mass accumulation at lower intensities, while in cucumber leaf expansion increased with increasing FR at all intensities.

2 Materials and methods

2.1 Plant material and cultural conditions

Green butterhead lettuce (*Lactuca sativa* 'Rex') and cucumber (*Cucumis sativa* 'Straight Eight') seeds were direct seeded then thinned for uniformity after emergence leaving four plants per root module. Two supplemental studies with lettuce cultivars 'Waldmann's Dark Green' (replicated once) and 'Green Salad Bowl' (replicated three times) were conducted following the same methods as 'Rex' lettuce to determine the consistency of the responses across cultivars. Root modules measured 20 × 18 × 13 cm (4680 cm^3) and contained a 1:1 ratio of peat and vermiculite by volume with 0.75 g per L wetting agent (AquaGro G), 1 g per L hydrated lime, and 1 g per L of uniformly mixed slow-release fertilizer (Nutricote total; 18-6-8, N-P-K, type 70). Planted root modules were randomly placed into the 12 treatment chambers. Each chamber had dimensions of 20 × 23 × 30 cm (L × W × H, 13800 cm^3) with gloss white walls. Fans provided an air velocity of 0.5 m s^{-1} at the top of the canopy. Root modules were watered to 10% excess as needed with dilute fertilizer solution at a rate of 100 mg N per L (21-5-20; Peters Excel; EC = 1 dS m^{-1}) and allowed to passively drain. Type-E Thermocouples connected to a data logger (CR1000, Campbell Scientific, Logan UT) continuously monitored ambient air temperature. Day/night temperature averaged 23.4 ± 1.2/20.9 ± 0.8 °C, with less than a 1°C variation among chambers. CO_2 concentration was continuously monitored and was identical for all treatments and varied over time between 450 to 500 ppm.

2.2 Treatments

The system included 12 chambers with four percentages of FR (Figures 1, 2) at three levels of ePPFD (4×3 = 12 treatments). Light was provided over a 16 h photoperiod. In the cucumber study the three levels of ePPFD were 50, 200 and 500 µmol m^{-2} s^{-1} (Daily light integral, DLI: 2.88, 11.52 and 28.8 mol m^{-2} d^{-1}). In the lettuce studies, the lowest ePPFD treatment (50 µmol m^{-2} s^{-1}) was increased to 100 µmol m^{-2} s^{-1} (DLI: 5.76 mol m^{-2} d^{-1}) because 50 µmol m^{-2} s^{-1} was below the light compensation point.

Treatments were developed using white (2700 K and 6500 K), red (peak about 658 nm) and far-red (peak 726 nm) LEDs (Lumileds LLC, San Jose, CA) to output 20% blue, 40% green, and 40% red photons as a proportion of PAR. Treatments reduced

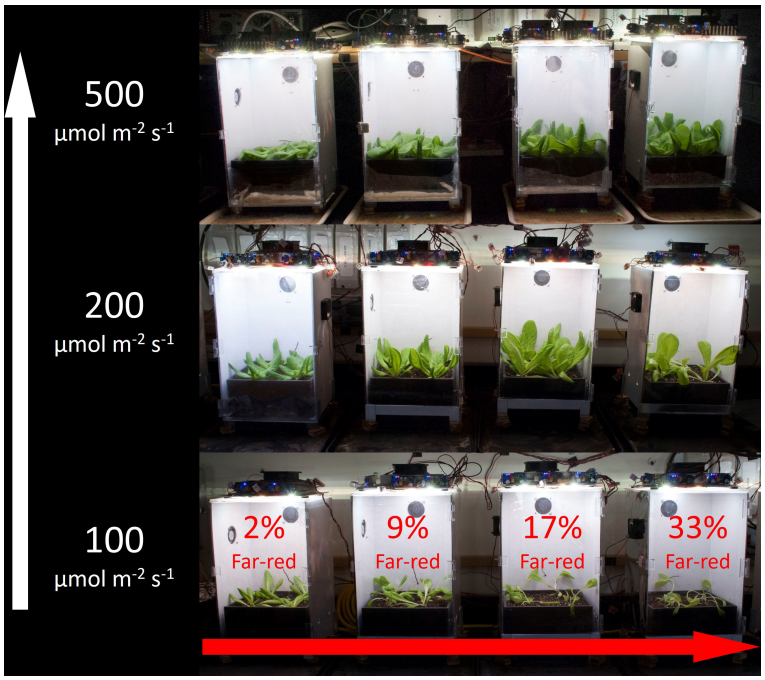

FIGURE 1
Experimental design of the study. Treatments included four percentages of far-red at three levels of extended photosynthetic photon flux density (ePPFD). The lowest ePPFD in the cucumber study was 50, instead of 100, µmol m^{-2} s^{-1}.

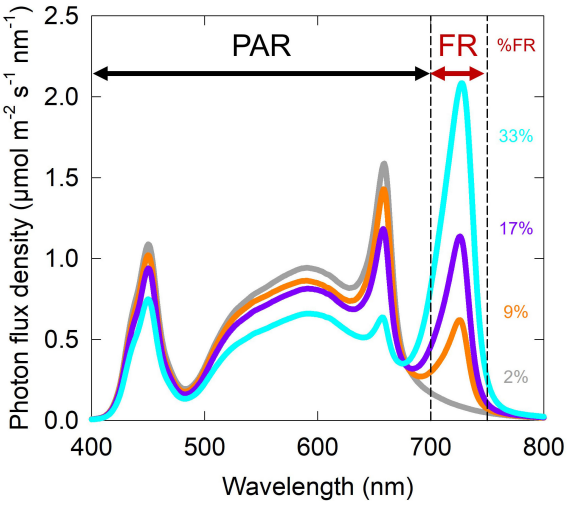

FIGURE 2
Representative spectral photon distributions for the four fractions of far-red (FR) from the ePPFD = 200 µmol m^{-2} s^{-1} intensity treatments. Spectral photon distributions from the other two intensities had the same shape with different scales on the y-axis. Photon fluxes of blue, green and red were maintained at 20, 40 and 40%, respectively, as a percent of photosynthetically active radiation (PAR; 400 to 700 nm) for each treatment of FR. Percent FR (%FR) treatments included 2% (grey), 9% (orange), 17% (purple), and 33% (cyan).

traditionally defined PAR while increasing FR photon flux density. Percent FR, calculated by dividing the FR photon flux density by the ePPFD and multiplying by 100, was 2, 9, 17 and 33% (Figures 1, 2). Spectral photon distributions of the treatments were measured before each replicate study with a spectroradiometer (model PS-300; Apogee Instruments, Logan UT). ePPFD was measured with an ePAR sensor (MQ-610, Apogee Instruments, Logan UT) at the top of the plant canopy throughout the study, and chambers were adjusted to maintain ePPFD at ± 5% of the setpoint. Root modules were rotated every three days to increase the uniformity of treatments within the chamber.

2.3 Plant measurements

Plants were harvested at canopy closure. This occurred 17 or 18 days after emergence in lettuce and 9, 10, or 11 days after emergence in cucumber. At harvest, stem length, leaf area, and fresh mass were measured. Leaf area was measured using a leaf area meter (LI-3000; LI-COR, Lincoln NE). Petiole length was measured in the cucumber study and leaf length and leaf width were measured in the lettuce study. Leaves and stems (and cotyledons in cucumber) were separated, and dry mass (DM) of each organ was measured after the tissue was dried at 80 ˚C for 48 hours. Percent stem mass was calculated by dividing stem dry mass by total shoot dry mass, multiplied by 100; roots were not included. Specific leaf area (SLA, m^2_{LA} kg DM_{leaf}^{-1}) was calculated by dividing the leaf area by the leaf dry mass.

2.4 Statistical analysis

The lettuce study was replicated three times and the cucumber study was replicated five times. Every replicate in time contained four plants in each treatment. All data was analyzed using R statistical software (R Foundation for Statistical Computing; Vienna, Austria). ePPFD was treated as a categorical variable with three levels for all analysis. Percent FR was treated as either a continuous variable or a categorical variable depending on the general response of the parameter. Responses that were linear with increasing percent FR were analyzed with linear mixed-effects regression analysis (percent FR treated as a continuous variable) and non-linear responses were analyzed with two-way ANOVA analysis (percent FR treated as a categorical variable). Replicates in time were treated as random factors in all statistical analyses. Significant effects were determined at the $p < 0.05$ level. Detailed statistical analysis for specific parameters are provided below.

3 Results

Figure 3 shows the overhead view of all the plants from each treatment in one replicate study, and Figure 4 shows the side view of the plants from each treatment in one replicate study. Figure S1 shows the overhead view of both the 'Waldmann's Dark Green' and 'Green Salad Bowl' supplementary lettuce studies. These photos show approximate plant diameters and heights in each treatment.

3.1 Biomass accumulation

The effect of percent FR on total shoot dry mass was non-linear in both lettuce and cucumber (Figures 5A, B), thus two-way ANOVA analysis and Tukey's *post hoc* test were used (with percent FR as a categorical variable) to separate the significant differences between treatments. The smaller values and variance of

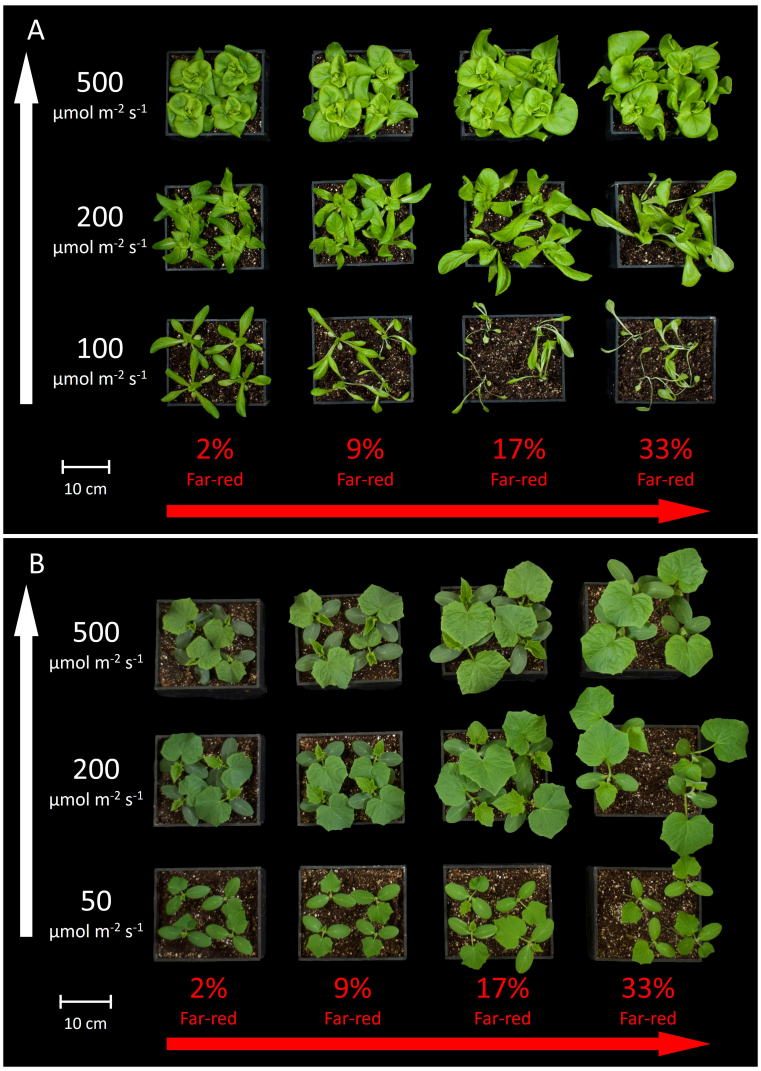

FIGURE 3
Overhead view of all the treatments in one replicate for **(A)** lettuce and **(B)** cucumber. The white arrow on the left indicates increasing extended photosynthetic photon flux density (ePPFD) and the red arrow on the bottom indicates increasing percent far-red.

total dry mass in the low ePPFD treatment resulted in reduced statistical power to determine significant difference between percent FR treatments. Therefore, the data of each replicate in time was normalized to its respective 2% FR (no added FR) control, and this normalized response was analyzed with 1) two-way ANOVA analysis/Tukey's *post hoc* test to determine significant differences between treatments and 2) a student's t-test to determine if the normalized response was statistically different from one, which represented the response of no added FR (Figures 5C, D).

Higher ePPFD produced more biomass in both species. In lettuce, percent FR and ePPFD interacted to predict biomass accumulation, where increasing percent FR increased dry mass at high ePPFD, but decreased dry mass at low ePPFD. This decrease occurred in both the 100 and 200 µmol m^{-2} s^{-1} ePPFD treatments. There was also an interaction between percent FR and ePPFD in cucumber, where the highest percent FR at the lowest ePPFD had no effect compared to higher ePPFD (Figure 5D), but in general the interaction was far less pronounced when compared to lettuce. In general, the response of cucumber shoot dry mass showed no effect of increasing percent FR from 2 to 9%, an increase between 9 and 17% FR, and little response between 17 and 33% FR.

3.2 Total leaf area

The effect of percent FR and ePPFD on total leaf area was similar to the effects on shoot dry mass (Figure 6). This indicates that the effects of percent FR on biomass accumulation in Figure 5 were likely driven by the ability of the plant to capture photons (leaf area is highly correlated with growth before canopy closure). Due to the similar non-linear response of leaf area to percent FR and ePPFD, this response was analyzed with the same methods as total dry mass.

Because leaf area/leaf expansion significantly contributes to the rate of biomass accumulation, it is valuable to better understand the interaction between the FR and ePPFD in controlling this response

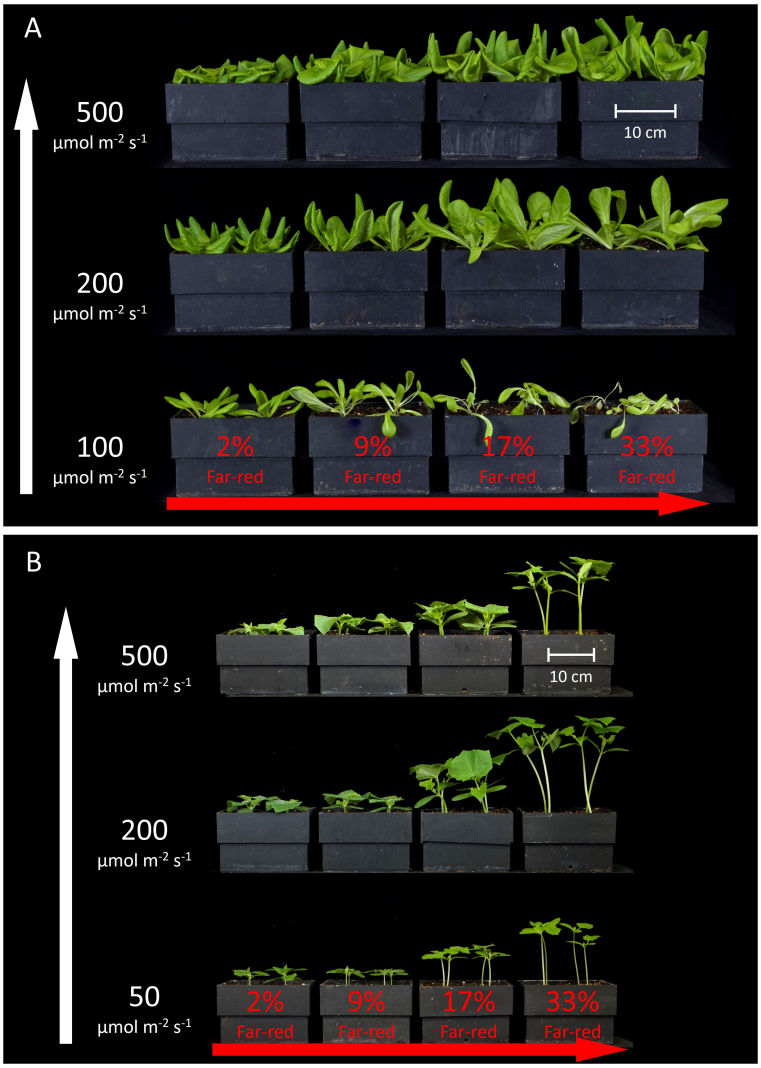

FIGURE 4
Side view of all the treatments in one replicate for **(A)** lettuce and **(B)** cucumber. The white arrow on the left indicates increasing extended photosynthetic photon flux density (ePPFD) and the red arrow on the bottom indicates increasing percent far-red.

in lettuce. Leaf lengths increased with percent FR at all three levels of ePPFD, while the response of leaf width was similar to the response of leaf area (Figures S2A, B). This resulted in longer, narrower leaves rather than rounder leaves at higher percent FR (Figure S2C). Although an increase in leaf length is generally expected under shaded conditions, the change in leaf shape does not fully explain the interaction between percent FR and ePPFD in predicting total leaf area in lettuce.

3.3 Specific leaf area

Specific leaf area (SLA) is a measure of leaf area given the biomass partitioning to the leaves, and it is widely reported to increase with shade. Compared to the responses of dry mass and total leaf area, the response of SLA to percent FR appeared linear. Thus, this parameter was analyzed with linear mixed-effects regression with percent FR as a continuous variable and ePPFD as a categorical variable. Increasing the percent FR and decreasing the ePPFD increased SLA in both species (Figures 6A, B).

Because ePPFD had a large effect on SLA (the lowest ePPFD induced a 2.5 to 3 times higher SLA than the highest ePPFD in both species), the best way to determine if there is an interaction between percent FR and ePPFD was to normalize the response. This is because the non-normalized response could indicate an interaction even if the effect of percent FR induced the same fractional change at all three levels of ePPFD. Figures 6C, D normalizes the SLA response to the average 2% FR response at each ePPFD. Linear mixed-effects regression analysis was then performed on this normalized data, which found no interaction between ePPFD and percent FR for either species, although the interaction approached significance in cucumber ($p = 0.11$; Figure 6D).

Increases in SLA in response to both increasing percent FR and decreasing ePPFD has often been observed in previous studies. However, because there was no interaction between the two treatments to predict SLA, this parameter (SLA) does not explain

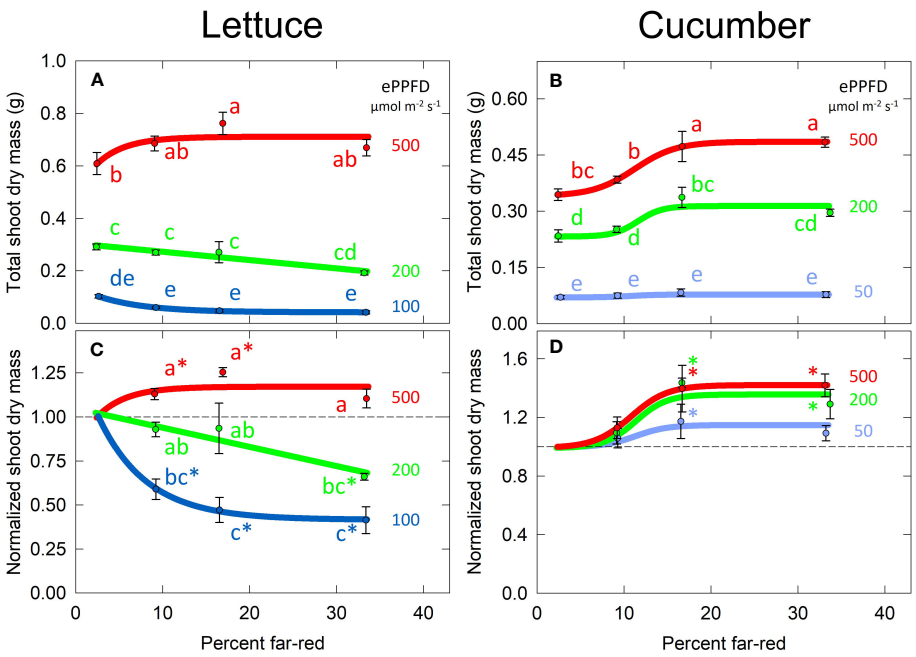

FIGURE 5
Effects of percent far-red (FR) and extended photosynthetic photon flux density (ePPFD) on shoot dry mass in lettuce **(A, C)** and cucumber **(B, D)**. **(A, B)** represent the original values of dry mass and **(C, D)** are the normalized response, where data from each replicate in time was normalized to its respective 2% FR (no added FR) control treatment for each ePPFD. In **(C, D)**, * indicates that the treatment is statistically different from 1 (using a student's t-test), which represents the response of the 2% FR control. Trend lines are included to guide the eye, and not meant to be used as a statistical representation. Error bars represent standard error for n = 3 replicates in lettuce and n = 5 replicates in cucumber. Letters are not included in **(D)** because the treatments were determined to be insignificantly different from each other, although several treatments were significantly different from their respective controls.

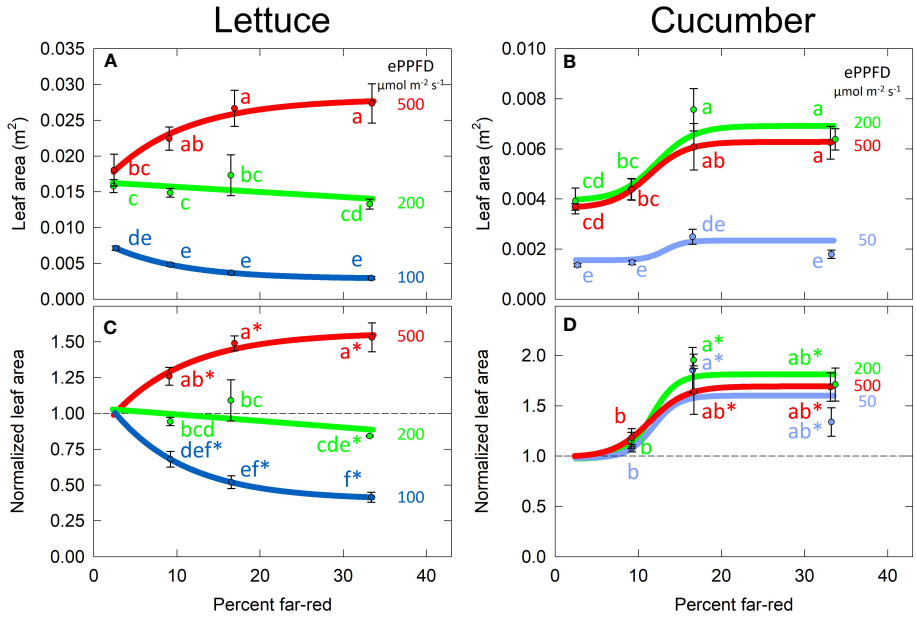

FIGURE 6
Effect of percent far-red (FR) at different levels of extended photosynthetic photon flux density (ePPFD) on specific leaf area (SLA) in lettuce **(A, C)** and cucumber **(B, D)**. **(A, B)** represent the original values of SLA, while **(C, D)** are the normalized response, where data has been normalized to the average response in the 2% FR control treatment for each ePPFD. Increasing the percent FR and decreasing the ePPFD increased SLA in both species. Error bars represent standard error for n = 3 replicates in lettuce and n = 5 replicates in cucumber.

the interaction between the two treatments to predict total leaf area in lettuce (Figures 7A, C).

3.4 Biomass partitioning

Increased shade is often reported to increase stem lengths, and this is often associated with an increase in biomass partitioning to stems. Percent stem mass, a metric that assesses partitioning to stems, is calculated by dividing stem dry mass by total shoot dry mass and multiplying by 100. Subtracting percent stem mass from 100 is the shoot biomass allocation to leaves (and cotyledons for cucumber).

In lettuce, the effects of percent FR and ePPFD on percent stem mass were analyzed with linear mixed-effects regression following the same procedure as SLA (Figure 6A). In cucumber, the effect of percent FR on percent stem mass was non-linear. Using two-way ANOVA analysis and Tukey's *post hoc* test, it was determined that there was no difference between 2 and 9% FR for the three levels of ePPFD (Figure 8B, dotted lines), but percent stem mass was significantly higher at the lowest ePPFD for both the 2% and 9% FR treatments (Figure 8B). Since there was no difference between 2 and 9% FR, to simplify the model, the 2% FR treatments were removed for analysis and the remaining data (9, 17 and 33% FR) were analyzed with linear mixed-effects regression analysis, similar to lettuce.

Increasing FR from 9 to 33% increased biomass partitioning to stems at all three levels of ePPFD in cucumber. Additionally, there was an effect of ePPFD on biomass partitioning to the stems with an increase in percent stem mass at lowest ePPFD. Finally, there was an interaction between the two treatments, meaning that there was a difference in the slopes of the lines among the levels of ePPFDs ($p < 0.001$). Unlike SLA, this interaction was determined for non-normalized data, although normalized data also showed an interaction (this is the case for both percent stem mass and stem length in both species). The interaction between percent FR and ePPFD resulted in a decreased response of percent stem mass to percent FR at the at the highest ePPFD (Figure 8B).

In lettuce, there was also an effect of percent FR, ePPFD and an interaction between the two treatments in the prediction of percent stem mass ($p < 0.001$). The most striking impact of the interaction between percent FR and ePPFD in lettuce was that increasing percent FR from 2 to 33% increased percent stem mass by 2.5-fold at the lowest ePPFD but had no effect at the highest ePPFD (Figure 8A). Similar to the effect of ePPFD at the lowest percent FR in cucumber (dotted lines in Figure 8B), percent stem mass in lettuce tended to be higher at 100 µmol m^{-2} s^{-1} compared to the higher two intensities at 2% FR. But, this was not statistically significant at the $p = 0.05$ level using Tukey's *post hoc* test from a two-way ANOVA ($p = 0.09$ and 0.06 for 100 compared to 200 and 100 compared to 500 µmol m^{-2} s^{-1}, respectively).

The striking interaction between percent FR and ePPFD in the prediction of percent stem mass in lettuce explains the interaction between the two treatments in the prediction of total plant leaf area. As percent stem mass (shoot biomass allocation to stems) increases, percent leaf mass (shoot biomass allocation to leaves) decreases. Because SLA increased with increasing percent FR at all levels of ePPFD (Figure 6C), and because biomass partitioning to leaves was

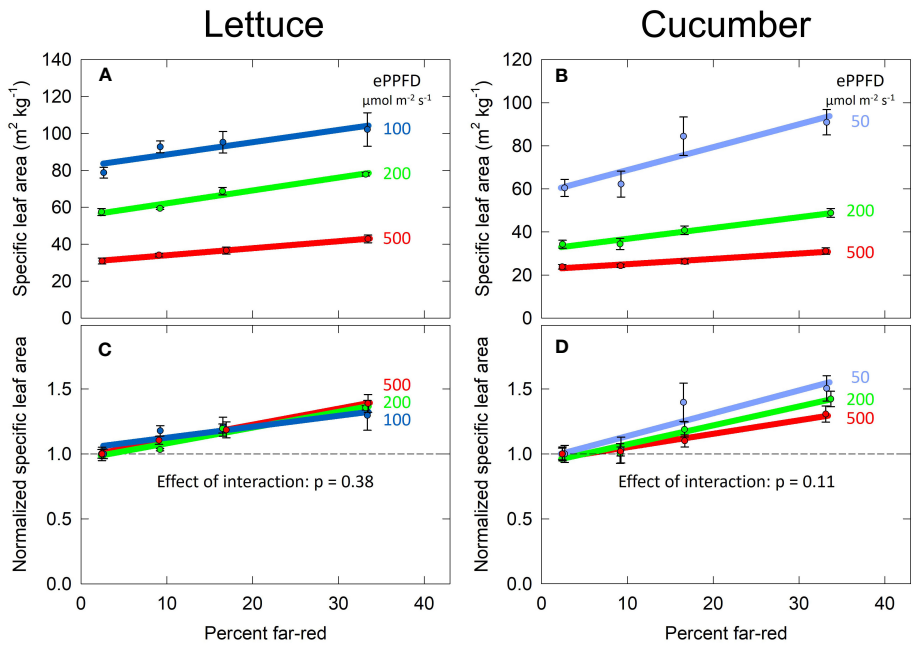

FIGURE 7
Effect of percent far-red (FR) and extended photosynthetic photon flux density (ePPFD) on leaf area in lettuce **(A, C)** and cucumber **(B, D)**. **(A, B)** represent the original values of leaf area and **(C, D)** are the normalized response, where data from each replicate in time has been normalized to its respective 2% FR control treatment for each level of ePPFD. In **(C, D)**, * indicates that the treatment is statistically different from 1 (using a student's t-test), which represents the effect of the 2% FR control. Trend lines are included to guide the eye, and not meant to be used as a statistical representation. Error bars represent standard error for n = 3 replicates in lettuce and n = 5 replicates in cucumber.

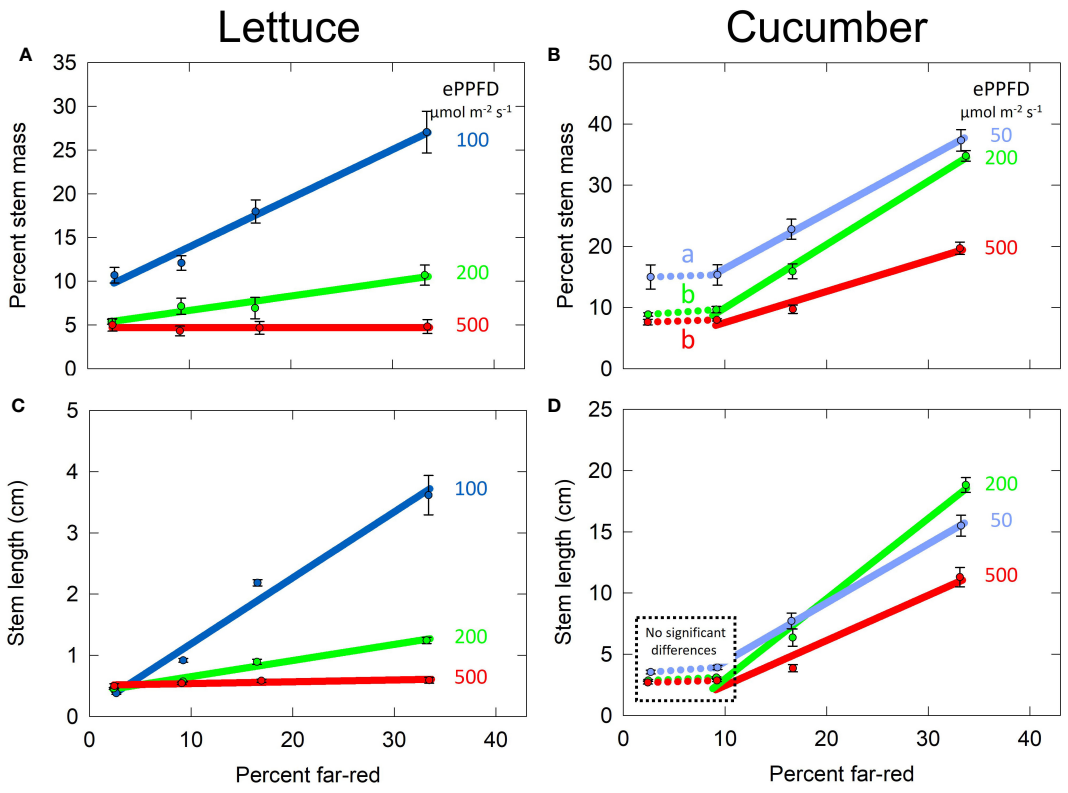

FIGURE 8
Effect of percent far-red (FR) at different levels of extended photosynthetic photon flux density (ePPFD) on stems. **(A)** Percent stem mass in lettuce, representative of biomass partitioning to stems, **(B)** percent stem mass in cucumber, **(C)** stem length in lettuce, and **(D)** stem length in cucumber. A two-way ANOVA analysis and Tukey's *post hoc* test indicated no difference in percent stem mass between 2 and 9% FR for all three levels of ePPFD, but it was significantly higher at the lowest ePPFD for both the 2% and 9% FR treatments. The letters indicate this effect showing percent stem mass was significantly higher at 2 and 9% FR at an ePPFD of 50 µmol m^{-2} s^{-1} than 2 and 9% FR at an ePPFD of either 200 or 500 µmol m^{-2} s^{-1}. Because the 2% data was removed to simplify the model and all remaining data was analysed with linear mixed-effects regression analysis. Error bars represent standard error for n = 3 replicates in lettuce and n = 5 replicates in cucumber. No significant differences

unaffected by percent FR at the highest ePPFD, overall total leaf area was increased with increasing percent FR. However, at the lowest ePPFD, even though increasing FR increased SLA by about 30%, biomass accumulation was redirected away from the leaves to a significant enough degree to reduce total leaf area.

Due to thermal reversion of phytochrome, ePPFD and FR have been combined into one unifying model called the cellular model, which accounts for both increased thermal reversion at higher temperatures and the larger contribution of thermal reversion on phytochrome dynamics at lower ePPFD. This model was unable to explain the response of percent stem mass in cucumber (Figure S3), indicating a contribution of other factors (e.g. cryptochrome and/or photosynthate signals, see discussion).

3.5 Stem length

The responses of lettuce and cucumber stem lengths to percent FR and ePPFD were similar to the response of percent stem mass, and thus the data for each species was analyzed using the same methods (Figure 8). There was an effect of percent FR, ePPFD and an interaction between the two ($p < 0.001$), in the prediction of stem length in both species. In cucumber, the tallest plants at the highest percent FR occurred at the middle ePPFD instead of the lowest ePPFD. A similar response was observed in longest petiole length (Figure S4). This is likely a direct result of lower photosynthesis resulting in reduced growth rate.

3.6 Responses of other lettuce cultivars

We investigated the same five parameters (biomass accumulation, total leaf area, specific leaf area, percent stem mass, and stem length) in two additional cultivars of lettuce: 'Waldmann's Dark Green' and 'Green Salad Bowl' (Figures S5–S8). Because 'Green salad bowl' was replicated the same number of times as 'Rex' (n = 3), it was analyzed following the same statistical approach. 'Waldmann's dark green' was only replicated once, and thus, no statistical analysis was performed, but the trends are consistent.

In all three cultivars, increasing percent FR resulted in an increase in biomass accumulation at the high ePPFD, but a decrease in accumulation at the low ePPFD. At the intermediate ePPFD, 'Waldmann's dark green' showed a general downward trend with increasing percent FR, while 'Green salad bowl' showed an increase followed by a decrease (Figure S5). As

expected, the response of total leaf area was similar to the response of total shoot dry mass (Figures S1, S6). In general, the responses of SLA were similar between all three cultivars (Figure S7), although FR appeared to have a larger effect at the high ePPFD in 'Waldmann's dark green', but this was likely due to reduced growth in the no added FR treatment. Additionally, at the lowest ePPFD in 'Green salad bowl' increasing FR appeared to increase SLA up to a threshold, then decrease it. Finally, there was a clear interaction between percent FR and ePPFD in predicting percent stem mass and stem length in all three cultivars (Figure S8). One notable difference from 'Rex' is that increasing percent FR had a small effect on percent stem mass and stem length at the high ePPFD in 'Green salad bowl'. These results indicate that the general interaction between ePPFD and percent FR on the prediction of leaf area and biomass accumulation may be observed across many lettuce cultivars.

4 Discussion

Leaves are the primary organs responsible for carbon gain as these organs have higher photosynthetic capacity than stems, petioles, and fruits (Xu et al., 1997). Despite the importance of leaves, the response of total leaf area to shade signals has been inconsistent (Casal and Smith, 1989; Casal, 2012; Demotes-Mainard et al., 2016). Here, we show that the effect of percent FR on leaf area/expansion can depend on the ePPFD (Figures 7A, C; S6). We conclude that this interaction is a byproduct of the differences in biomass allocation between stems and leaves under these conditions, and not a response of SLA, which increased with FR under all levels of ePPFD (Figures 6; S7). This potential dependency of leaf expansion on biomass allocation was previously noted by Casal et al. (1987) who observed that, in contrast to many other reports at the time, *Petunia axilaris*, *Taraxacum officinale*, *Terminalia ivorensis*, and numerous grass species all showed increased leaf area at low R:FR ratios (higher fraction of FR), while stem length in these species was relatively unaffected. Although we agree that FR effects on leaf area are highly dependent on biomass partitioning between stems and leaves, we observed an increase in both leaf area and stem length with increasing percent FR in cucumber.

The simultaneous increase in leaf area and stem length in cucumber may be explained by 1) the effect of increasing FR on percent stem mass was reduced at the highest ePPFD (Figure 8B); and 2) there was an insignificant ($p = 0.11$, Figure 6D) trend of a larger effect of increasing percent FR on SLA at lower levels of ePPFD in cucumber. Collectively, these factors may have allowed the overall leaf area in cucumber to increase despite a simultaneous increase in stem length. Additional studies are warranted.

Increased percent stem mass was associated with increased stem length (Figure 8). Biomass allocation between leaves and stems has been reported to be sensitive to both FR and ePPFD (Morgan and Smith, 1979; Morgan and Smith, 1981; Ballaré et al., 1987; Poorter et al., 2012; Yang et al., 2018). Faster rates of stem elongation may require an increase in sugars to support the upregulated metabolism. As such, increases in percent FR have been associated with 1) a decrease in hypocotyl (but not cotyledon) expression of genes related to photosynthesis, the Calvin cycle, and sucrose/starch biosynthesis in *Arabidopsis*, suggesting a decrease in local sugar production in the hypocotyl and thus an increase in stem sink strength; and 2) an increase in the transport of radiolabeled carbon from cotyledons to hypocotyls (de Wit et al., 2018). This transported carbon was allocated to multiple pools of carbon within the hypocotyl including amino acids, lipids, neutral sugars, proteins and cell walls. Of these, the insoluble portion—cell walls and proteins—and the ethanol soluble portion—lipids/cell membranes—both increased over 3-fold from the high R:FR (low percent FR) to the low R:FR (high percent FR) treated seedlings. The increases in these two pools indicate an increase to structural components, meaning an increase in hypocotyl/stem biomass accumulation. In addition to this change in carbon transport, shade- induced upregulation of auxin inhibits cytokinin expression in leaf primordia (Carabelli et al., 2007), which leads to an inhibition of cell proliferation in leaves causing reduced leaf area (Riefler et al., 2006; Wu et al., 2017). This provides a second mechanism by which biomass allocation to leaves decreases in shade. In a meta-analysis, Poorter et al. (2012) concluded that low ePPFD decreases the root mass fraction while increasing the stem and leaf mass fractions, and low R:FR (high percent FR) increases the stem mass fraction with little effect on root mass fraction. We did not measure root mass fraction, and it is possible that it increased under low ePPFD, but this would not change the conclusion that increasing the percent FR had a larger effect on stem biomass partitioning at lower ePPFD.

Shade symptoms are often reported to increase in response to both decreases in photon intensity and increases in FR. The response to photon intensity is often associated with a decrease in blue photons specifically (de Wit et al., 2016; Pedmale et al., 2016), although this is not always the case (Millenaar et al., 2009). Previous studies have shown interactions between low blue (low photon intensity) and increased FR, with synergistic shade-induced stem elongation under both conditions compared to one shade condition alone (de Wit et al., 2016). These previous results are very similar to the results obtained in this study (Figure 8). This interaction is hypothesized to be related to both the PHYTOCHROME INTERACTING FACTOR (PIF) family of transcription factors and the E3 ubiquitin ligase formed by CONSTITUTIVELY PHOTOMORPHOGEIC 1 (COP1) and SUPRESSOR OF PHYA-105(SPA) proteins (Su et al., 2017), both of which are regulated by the phytochrome and cryptochrome photoreceptors (Legris et al., 2019).

The highest FR treatments in the two highest ePPFD treatments had overlapping leaves resulting in inter-plant competition for light and thus decreased growth rates of individual plants. This leaf overlap means that the effect of FR would be underestimated if the results were applied to single spaced plants. This may explain the saturated effect of FR on leaf expansion in lettuce between 9 and 33% FR at the highest ePPFD treatment (Figure 7). However, the increased shade signals induced by the plant competition would have continued to increase SLA (Figure 6). A similar response was observed in the lowest ePPFD treatments: the effect of FR on leaf expansion saturated between 9 to 33% FR, but SLA, stem length and percent stem mass continued to increase in response to FR (Figures 7, 8). In this case, plant competition does not explain the

saturation, and therefore there may be some minimum leaf expansion that the plant maintains to allow for some photon capture and continued elongation.

4.1 Ecological significance

Ballaré et al. (1987) demonstrated that in competitive light environments FR can increase in the horizontal direction prior to a decrease in PAR. This is notable because it means that in certain circumstances there can be increases in FR in the natural environment even at high PAR. These FR signals are the first indication of oncoming shade and they have been shown to increase internode elongation prior to the subsequent decrease in PAR in *Sinapis alba* and *Datura ferox* (Ballaré et al., 1987). These two species have an upright plant architecture, similar to cucumber, in comparison to the rosette architecture of lettuce and *Arabidopsis*. Perhaps plants with an upright architecture, like cucumber, *Sinapis alba*, and *Datura ferox*, will always elongate in response to increasing FR no matter the ePPFD. We did not investigate the highest intensities that occur in the middle of a summer day, above 2000 μmol m^{-2} s^{-1}, but perhaps there would have been no effect of FR on stem elongation in cucumber at this intensity. It is interesting that cucumber increased leaf area at all three levels of ePPFD, meaning that in the natural environment FR would be likely to increase leaf expansion from both neighboring plants at high ePPFD and from true shade at low ePPFD.

For lettuce, and perhaps other species with a rosette architecture, the increase in FR from neighboring vegetation could actually increase leaf expansion in ecosystems with more light. This is further notable because in this study we substituted PAR for FR, but in the natural environment FR can increase with no change in PAR (Ballaré et al., 1987), and this could lead to additional increases in growth through photosynthesis. However, the increase in FR in most shaded environments would be much more likely induce decreases in leaf expansion, as the plants attempt to reach out of the shade.

The lowest two FR treatments (2 and 9%) are probably not entirely comparable to sunlight. Leaf expansion was not significantly different between 17 and 33% FR; thus, it could be argued that no such increases in leaf expansion would occur in the natural environment. However, FR LEDs have a peak that closely matches the peak of the Pfr form of phytochrome. Therefore, lower percentages of FR from FR LEDs may be comparable to higher percentages of FR in sunlight, but such comparisons are difficult.

4.2 Photosynthetic considerations

Often, studies investigating plant responses to FR typically add FR photons on top of a constant intensity of PAR instead of decreasing the photon intensity within PAR while increasing FR. Maintaining a constant ePPFD removes the potential impact of photosynthesis on leaf expansion. Assuming PAR and FR photons both drive photosynthesis with equal efficiencies, then the studies performed here (substituting PAR with FR) would at most result in equal leaf-level photosynthesis. However, this 1:1 assumption is likely not the case. Zhen and Bugbee (2020a) noted that the photosynthetic relationship of PAR photons and FR photons began to deviate from a 1:1 equivalency when FR was added in excess of 40% of PAR (29% FR based on the definition used here). Furthermore, Zhen et al. (2019) showed that photons at 752 nm did not increase the quantum yield of PSII (the fraction of absorbed photons used for photochemistry), indicating that photons at 752 nm did not contribute to photosynthesis (the next lowest wavelength measured was 731 nm). These considerations indicate that 1) extending the definition of photosynthetic photons out to 750 nm may overestimate the photosynthetic response, and b) 33% FR used in this study would have deviated from a 1:1 photosynthetic relationship FR and PAR. Perhaps this also explains the saturating effect of FR on shoot dry mass and leaf area (Figures 5, 7).

Despite this limitation of our experiment, both of these factors indicate that the higher FR treatments in this study would have resulted in lower leaf level photosynthesis, which further highlights the effect increasing percent FR can have on leaf expansion and thus photon capture in cucumber and lettuce (at high photon fluxes in the latter).

4.3 Implications for horticulture

The results presented here have substantial implications for the horticultural industry – especially in sole-source lighting environments, where electric lighting from LEDs has been rapidly expanding. Providing photons for crop production is expensive, especially when considering the electrical power required to operate the LEDs. FR LEDs are among the highest efficacy LEDs (μmol of photons per joule input electrical energy), primarily because of the lower energy of the photons (Kusuma et al., 2020). Interest in FR for horticultural environments has expanded in the past decade where studies have often found that adding FR increases leaf area or plant diameter in lettuce, resulting in an increase in fresh and dry mass (Lee et al., 2016; Meng and Runkle, 2019; Zou et al., 2019; Zhen and Bugbee, 2020b; Legendre and van Iersel, 2021). But, many of these studies supplemented FR rather than substituting PAR photons for FR. The addition of FR LEDs in fixtures increases costs for two reasons: 1) FR LEDs are in lower demand, meaning they are more expensive, and 2) increasing the total photon output of a fixture increases the power requirement. Thus, substitution of PAR with FR is much more reasonable for practical applications. Zhen and Bugbee (2020b) found that substituting 14% of PAR with FR at an ePPFD of 350 μmol m^{-2} s^{-1} resulted in similar quantum yields for CO_2 fixation in 'Waldmann's dark green' lettuce, but increased biomass accumulation by about 30% *via* an increase in photon capture (leaf expansion). We observed a similar response with 'Waldmann's dark green' in our experimental chambers; adding 9, 17 and 33% FR at an ePPFD of 500 μmol m^{-2} s^{-1} resulted in 31 to 33% increase in biomass accumulation. However, at lower ePPFD (100 and 200 μmol m^{-2} s^{-1}), increasing percent FR resulted in a decrease in biomass accumulation (Figures S5-S8).

In another similar study, Legendre and van Iersel (2021) concluded that FR photons were between 57 to 183% more effective at increasing photon capture than PAR photons in 'Green salad bowl' lettuce and were thus 93 to 162% more effective at increasing biomass accumulation. Interestingly, they observed no interaction between PPFD and FR when PPFD varied between 111 and 245 μmol m^{-2} s^{-1}. In this cultivar, we observed an increase in leaf expansion and shoot

dry mass with an increase in percent FR at 500 μmol m^{-2} s^{-1}, but a decrease at an ePPFD of 100 μmol m^{-2} s^{-1} and little effect at 200 μmol m^{-2} s^{-1} (Figures S5, S6). Interestingly at 200 μmol m^{-2} s^{-1} shoot dry mass was higher at 9% FR compared to 2% FR (Figure S5F), but at higher levels of FR, dry mass decreased. The contradictions between our study and Legendre and van Iersel (2021) are difficult to parse, as many of the environmental conditions were similar.

Producers can increase yields of lettuce by including FR LEDs in lighting fixtures because FR photons will increase leaf expansion and photon capture, while decreasing electrical input (depending on operating conditions and other LEDs in the fixture). However, caution must be taken as increases will only occur at high enough ePPFD. For cucumber, including more FR appears to be beneficial no matter the ePPFD, but the increase in leaf expansion appears to be accompanied by increases in stem elongation. This may be manageable in greenhouse environments but may be undesirable in sole-source lighting environments. Additionally, the added FR may only benefit cucumber plants when they are young.

Based on current definitions, FR photons are not considered in the calculation of photosynthetic photon efficacy, which is the flux of photosynthetic photons (μmol s^{-1}) divided by the input power (W), resulting in μmol per J. Currently, photosynthetic photons are considered to only be those with wavelengths between 400 to 700 nm based on studies by McCree (1972a); McCree (1972b). Because this definition excludes photons between 700 to 750 nm, the benefits of photons from FR LEDs, both on leaf expansion and photosynthesis are excluded. These definitions ought to be reconsidered (Zhen et al., 2021), but at the same time, FR must be used with caution, as we have shown it can be detrimental in some conditions.

Data availability statement

The raw data supporting the conclusions of this article will be made available by the authors, without undue reservation.

Author contributions

PK and BB contributed to the design of the study, analysis of data, and writing of the manuscript. Both authors approved the submitted version.

Funding

This work was supported by the Utah Agricultural Experiment Station, Utah State University (journal paper number 9664), the USDA-NIFA-SCRI (Grant Number 2018-51181-28365) (LAMP Project) NASA-CUBES (Grant Number NNX17AJ31G).

Acknowledgments

Expert technical assistance was provided by Erik Sargent and Alec Hay. We thank Brendan Fatzinger, William Wheeler, Shuyang Zhen, Mitchell Westmoreland, Boston Swan, Logan Banner, Jakob Johnson, Terri Manwaring, Matthew Hardy, Kahlin Wacker, Julie Hershkowitz, Wyatt Johnson for harvesting and maintaining the plants in this study, and we thank Hikari Skabelund for assistance formatting the manuscript.

Conflict of interest

The authors declare that the research was conducted in the absence of any commercial or financial relationships that could be construed as a potential conflict of interest.

Publisher's note

Supplementary material

The Supplementary Material for this article can be found online at: https://www.frontiersin.org/articles/10.3389/fpls.2023.1185622/full#supplementary-material

References

Bae, J. H., Park, S. Y., and Oh, M. M. (2017). Supplemental irradiation with far-red light-emitting diodes improves growth and phenolic contents in *Crepidiastrum denticulatum* in a plant factory with artificial lighting. *Hortic. Environ. Biotechnol.* 58, 357–366. doi: 10.1007/s13580-017-0331-x

Ballaré, C. L., Sanchez, R. A., Scopel, A. L., Casal, J. J., and Ghersa, C. M. (1987). Early detection of neighbor plants by phytochrome perception of spectral changes in reflected sunlight. *Plant Cell Environ.* 10, 551–557. doi: 10.1111/j.1365-3040.1987.tb01835.x

Ballaré, C. L., Scopel, A. L., and Sanchez, R. A. (1991). Photocontrol of stem elongation in plant neighborhoods - effects of photon fluence rate under natural conditions of radiation. *Plant Cell Environ.* 14, 57–65. doi: 10.1111/j.1365-3040.1991.tb01371.x

Barreiro, R., Guiamét, J. J., Beltrano, J., and Montaldi, E. R. (1992). Regulation of the photosynthetic capacity of primary bean leaves by the red:far-red ratio and photosynthetic photon flux density of incident light. *Physiol. Plant* 85, 97–101. doi: 10.1111/j.1399-3054.1992.tb05269.x

Boccalandro, H. E., Rugnone, M. L., Moreno, J. E., Ploschuk, E. L., Serna, L., Yanovsky, M. J., et al. (2009). Phytochrome b enhances photosynthesis at the expense of water-use efficiency in *Arabidopsis*. *Plant Physiol.* 150, 1083–1092. doi: 10.1104/pp.109.135509

Carabelli, M., Possenti, M., Sessa, G., Ciolfi, A., Sassi, M., Morelli, G., et al. (2007). Canopy shade causes a rapid and transient arrest in leaf development through auxin-induced cytokinin oxidase activity. *Genes Dev.* 21, 1863–1868. doi: 10.1101/gad.432607

Casal, J. J. (2012). Shade avoidance. *Arabidopsis Book* 10, e0157. doi: 10.1199/tab

Casal, J. J., Aphalo, P. J., and Sanchez, R. A. (1987). Phytochrome effects on leaf growth and chlorophyll content in *Petunia axilaris*. *Plant Cell Environ.* 10, 509–514. doi: 10.1111/j.1365-3040.1987.tb01829.x

Casal, J. J., and Mazzella, M. A. (1998). Conditional synergism between cryptochrome 1 and phytochrome b is shown by the analysis of *phyA*, *phyB*, and *hy4* simple, double, and triple mutants in arabidopsis. *Plant Physiol.* 118, 19–25. doi: 10.1104/pp.118.1.19

Casal, J. J., and Smith, H. (1989). The function, action and adaptive significance of phytochrome in light-grown plants. *Plant Cell Environ.* 12, 855–862. doi: 10.1111/j.1365-3040.1989.tb01966.x

Child, R., Morgan, D. C., and Smith, H. (1981). Control of development in chenopodium album l. by shade light the effect of light quality (red: far-red ratio) on morphogenesis. *New Phytol.* 89, 545–555. doi: 10.1111/j.1469-8137.1981.tb02334.x

Demotes-Mainard, S., Péron, T., Corot, A., Bertheloot, J., Le Gourrierec, J., Pelleschi-Travier, S., et al. (2016). Plant responses to red and far-red lights, applications in horticulture. *Environ. Exp. Bot.* 121, 4–21. doi: 10.1016/j.envexpbot.2015.05.010

Devlin, P. F., Robson, P. R., Patel, S. R., Goosey, L., Sharrock, R. A., and whitelam, G. C. (1999). Phytochrome d acts in the shade-avoidance syndrome in arabidopsis by controlling elongation growth and flowering time. *Plant Physiol.* 119, 909–916. doi: 10.1104/pp.119.3.909

de Wit, M., George, G. M., Ince, Y.Ç, Dankwa-Egli, B., Hersch, M., Zeeman, S. C., et al. (2018). Changes in resource partitioning between and within organs support growth adjustment to neighbor proximity in brassicaceae seedlings. *Proc. Natl. Acad. Sci. U.S.A.* 115, E9953–E9961. doi: 10.1073/pnas.1806084115

de Wit, M., Keuskamp, D. H., Bongers, F. J., Hornitschek, P., Gommers, C. M., Reinen, E., et al. (2016). Integration of phytochrome and cryptochrome signals determines plant growth during competition for light. *Curr. Biol.* 26, 3320–3326. doi: 10.1016/j.cub.2016.10.031

El-Sharkawy, M. A. (2011). Overview: early history of crop growth and photosynthesis modeling. *Biosystems* 103, 205–211. doi: 10.1016/j.biosystems.2010.08.004

Frankland, B., and Letendre, R. J. (1978). Phytochrome and effects of shading on growth of woodland plants. *Photochem. Photobiol.* 27, 223–230. doi: 10.1111/j.1751-1097.1978.tb07592.x

Franklin, K. A., Davis, S. J., Stoddart, M. W., Vierstra, R. D., and Whitelam, G. C. (2003). Mutant analyses define multiple roles for phytochrome c in arabidopsis photomorphogenesis. *Plant Cell* 15, 1981–1989. doi: 10.1105/tpc.015164

Gifford, R. M., Thorne, J. H., Hitz, W. D., and Giaquinta, R. T. (1984). Crop productivity and photoassimilate partitioning. *Science* 225, 801–808. doi: 10.1126/science.225.4664.801

Gommers, C. M., Visser, E. J., St Onge, K. R., Voesenek, L. A., and Pierik, R. (2013). Shade tolerance: when growing tall is not an option. *Trends Plant Sci.* 18, 65–71. doi: 10.1016/j.tplants.2012.09.008

Heraut-Bron, V., Robin, C., Varlet-Grancher, C., Afif, D., and Guckert, A. (1999). Light quality (red: far-red ratio): does it affect photosynthetic activity, net CO_2 assimilation, and morphology of young white clover leaves? *Can. J. Bot.* 77, 1425–1431. doi: 10.1139/b99-099

Hersch, M., Lorrain, S., de Wit, M., Trevisan, M., Ljung, K., Bergmann, S., et al. (2014). Light intensity modulates the regulatory network of the shade avoidance response in *Arabidopsis*. *Proc. Natl. Acad. Sci. U.S.A.* 111, 6515–6520. doi: 10.1073/pnas.1320355111

Holmes, M. G., and Smith, H. (1975). The function of phytochrome in plants growing in the natural environment. *Nature* 254, 512–514. doi: 10.1038/254512a0

Holmes, M. G., and Smith, H. (1977). The function of phytochrome in the natural environment–IV. light quality and plant development. *Photochem. Photobiol.* 25, 551–557. doi: 10.1111/j.1751-1097.1977.tb09127.x

Jin, W. Q., Urbina, J. L., Heuvelink, E., Marcelis,, and Leo, F. M. (2021). Adding far-red to red-blue light-emitting diode light promotes yield of lettuce at different planting densities. *Front. Plant Sci.* 11. doi: 10.3389/fpls.2020.609977

Kalaitzoglou, P., Van Ieperen, W., Harbinson, J., van der Meer, M., Martinakos, S., Weerheim, K., et al. (2019). Effects of continuous or end-of-day far-red light on tomato plant growth, morphology, light absorption and fruit production. *Front. Plant Sci.* 10. doi: 10.3389/fpls.2019.00322

Keller, M. M., Jaillais, Y., Pedmale, U. V., Moreno, J. E., Chory, J., and Ballare, C. L. (2011). Cryptochrome 1 and phytochrome b control shade-avoidance responses in arabidopsis *via* partially independent hormonal cascades. *Plant J.* 67, 195–207. doi: 10.1111/j.1365-313X.2011.04598.x

Kong, Y., and Nemali, K. (2021). Blue and far-red light affect area and number of individual leaves to influence vegetative growth and pigment synthesis in lettuce. *Front. Plant Sci.* 12. doi: 10.3389/fpls.2021.667407

Kurepin, L. V., Emery, R. J., Pharis, R. P., and Reid, D. M. (2007a). Uncoupling light quality from light irradiance effects in helianthus annuus shoots: putative roles for plant hormones in leaf and internode growth. *J. Exp. Bot.* 58, 2145–2157. doi: 10.1093/jxb/erm068

Kurepin, L. V., Joo, S. H., Kim, S. K., Pharis, R. P., and Back, T. G. (2012a). Interaction of brassinosteroids with light quality and plant hormones in regulating shoot growth of young sunflower and arabidopsis seedlings. *J. Plant Growth Regul.* 31, 156–164. doi: 10.1007/s00344-011-9227-7

Kurepin, L. V., Shah, S., and Reid, D. M. (2007b). Light quality regulation of endogenous levels of auxin, abscisic acid and ethylene production in petioles and leaves of wild type and ACC deaminase transgenic brassica napus seedlings. *Plant Growth Regul.* 52, 53–60. doi: 10.1007/s10725-007-9176-0

Kurepin, L. V., Walton, L. J., Hayward, A., Emery, R. J. N., Pharis, R. P., and Reid, D. M. (2012b). Interactions between plant hormones and light quality signaling in regulating the shoot growth of *Arabidopsis thaliana* seedlings. *Botany* 90, 237–246. doi: 10.1139/b11-108

Kurepin, L. V., Walton, L. J., Reid, D. M., Pharis, R. P., and Chinnappa, C. C. (2006). Growth and ethylene evolution by shade and sun ecotypes of *Stellaria longipes* in response to varied light quality and irradiance. *Plant Cell Environ.* 29, 647–652. doi: 10.1111/j.1365-3040.2005.01443.x

Kurepin, L. V., Yip, W. K., Fan, R., Yeung, E. C., and Reid, D. M. (2010). The roles and interactions of ethylene with gibberellins in the far-red enriched light-mediated growth of *Solanum lycopersicum* seedlings. *Plant Growth Regul.* 61, 215–222. doi: 10.1007/s10725-010-9465-x

Kusuma, P., and Bugbee, B. (2021). Improving the predictive value of phytochrome photoequilibrium: consideration of spectral distortion within a leaf. *Front. Plant Sci.* 12. doi: 10.3389/fpls.2021.596943

Kusuma, P., Pattison, P. M., and Bugbee, B. (2020). From physics to fixtures to food: current and potential LED efficacy. *Hortic. Res.* 7, 56. doi: 10.1038/s41438-020-0283-7

Kwesiga, F., and Grace, J. (1986). The role of the Red/Far-red ratio in the response of tropical tree seedlings to shade. *Ann. Bot.* 57, 283–290. doi: 10.1093/oxfordjournals.aob.a087108

Lee, M. J., Park, S. Y., and Oh, M. M. (2015). Growth and cell division of lettuce plants under various ratios of red to far-red light-emitting diodes. *Hortic. Environ. Biotechnol.* 56, 186–194. doi: 10.1007/s13580-015-0130-1

Lee, M.-J., Son, K.-H., and Oh, M.-M. (2016). Increase in biomass and bioactive compounds in lettuce under various ratios of red to far-red LED light supplemented with blue LED light. *Hortic. Environ. Biotechnol.* 57, 139–147. doi: 10.1007/s13580-016-0133-6

Legendre, R., and van Iersel, M. W. (2021). Supplemental far-red light stimulates lettuce growth: disentangling morphological and physiological effects. *Plants* 10, 166. doi: 10.3390/plants10010166

Legris, M., Ince, Y.Ç, and Fankhauser, C. (2019). Molecular mechanisms underlying phytochrome-controlled morphogenesis in plants. *Nat. Commun.* 10, 5219. doi: 10.1038/s41467-019-13045-0

López-Juez, E., Buurmeijer, W. F., Heeringa, G. H., Kendrick, R. E., and Wesselius, J. C. (1990). Response of light-grown wild-type and long hypocotyl mutant cucumber plants to end-of-day far-red light. *Photochem. Photobiol.* 52, 143–149. doi: 10.1111/j.1751-1097.1990.tb01767.x

McCree, K. J. (1972a). The action spectrum, absorptance and quantum yield of photosynthetisis in crop plants. *Agric. Meterol.* 9, 191–216. doi: 10.1016/0002-1571(71)90022-7

McCree, K. (1972b). Test of current definitions of photosynthetically active radiation against leaf photosynthesis data. *Agric. Meteorol* 10, 443–453. doi: 10.1016/0002-1571(72)90045-3

Meng, Q., and Runkle, E. S. (2019). Far-red radiation interacts with relative and absolute blue and red photon flux densities to regulate growth, morphology, and pigmentation of lettuce and basil seedlings. *Sci. Hortic.* 255, 269–280. doi: 10.1016/j.scienta.2019.05.030

Millenaar, F. F., Van Zanten, M., Cox, M. C. H., Pierik, R., Voesenek, L., and Peeters, A. J. M. (2009). Differential petiole growth in *Arabidopsis thaliana*: photocontrol and hormonal regulation. *New Phytol.* 184, 141–152. doi: 10.1111/j.1469-8137.2009.02921.x

Miyashita, Y., Kitaya, Y., Kozai, T., and Kimura, T. (1995). Effects of red and far-red light on the growth and morphology of potato plantlets *in vitro*: using light emitting diode as a light source for micropropagation. *Acta Hortic.* 393, 189–194. doi: 10.17660/ActaHortic.1995.393.22

Monteith, J. L. (1977). Climate and efficiency of crop production in Britain. *Philos. Trans. R. Soc Lond. B Biol. Sci.* 281, 277–294. doi: 10.1098/rstb.1977.0140

Morgan, D. C., and Smith, H. (1979). A systematic relationship between phytochrome controlled development and species habitat. *Planta* 145, 253–258. doi: 10.1007/BF00454449

Morgan, D. C., and Smith, H. (1981). Control of development in *Chenopodium album* l. by shadelight: the effect of light quantity (total fluence rate) and light quality (red:far-red ratio). *New Phytol.* 88, 239–248. doi: 10.1111/j.1469-8137.1981.tb01720.x

Neff, M. M., and Chory, J. (1998). Genetic interactions between phytochrome a, phytochrome b, and cryptochrome 1 during arabidopsis development. *Plant Physiol.* 118, 27–35. doi: 10.1104/pp.118.1.27

Park, Y., and Runkle, E. S. (2017). Far-red radiation promotes growth of seedling by increasing leaf expansion and whole-plant net assimilation. *Environ. Exp. Bot.* 136, 41–49. doi: 10.1016/j.envexpbot.2016.12.013

Park, Y., and Runkle, E. S. (2018). Far-red radiation and photosynthetic photon flux density independently regulate seedling growth but interactively regulate flowering. *Environ. Exp. Bot.* 155, 206–216. doi: 10.1016/j.envexpbot.2018

Park, Y., and Runkle, E. S. (2019). Blue radiation attenuates the effects of the red to far-red ratio on extension growth but not on flowering. *Environ. Exp. Bot.* 168, 103871. doi: 10.1016/j.envexpbot.2019.103871

Patel, D., Basu, M., Hayes, S., Majláth, I., Hetherington, F. M., Tschaplinski, T. J., et al. (2013). Temperature-dependent shade avoidance involves the receptor-like kinase ERECTA. *Plant J.* 73, 980–992. doi: 10.1111/tpj.12088

Pausch, R. C., Britz, S. J., and Mulchi, C. L. (1991). Growth and photosynthesis of soybean (*Glycine max* (L.) merr.) in simulated vegetation shade: influence of the ratio of red to far-red radiation. *Plant Cell Environ.* 14, 647–656. doi: 10.1111/j.1365-3040.1991.tb01537.x

Pedmale, U. V., Huang, S. S., Zander, M., Cole, B. J., Hetzel, J., Ljung, K., et al. (2016). Cryptochromes interact directly with PIFs to control plant growth in limiting blue light. *Cell* 164, 233–245. doi: 10.1016/j.cell.2015

Pierik, R., and de Wit, M. (2014). Shade avoidance: phytochrome signalling and other aboveground neighbour detection cues. *J. Exp. Bot.* 65, 2815–2824. doi: 10.1093/jxb/ert389

Poorter, H., Niklas, K. J., Reich, P. B., Oleksyn, J., Poot, P., and Mommer, L. (2012). Biomass allocation to leaves, stems and roots: meta-analyses of interspecific variation and environmental control. *New Phytol.* 193, 30–50. doi: 10.1111/j.1469-8137.2011.03952.x

Qaderi, M. M., Godin, V. J., and Reid, D. M. (2015). Single and combined effects of temperature and Red:Far-red light ratio on evening primrose (*Oenothera biennis*). *Botany* 93, 475–483. doi: 10.1139/cjb-2014-0194

Riefler, M., Novak, O., Strnad, M., and Schmülling, T. (2006). *Arabidopsis* cytokinin receptor mutants reveal functions in shoot growth, leaf senescence, seed size, germination, root development, and cytokinin metabolism. *Plant Cell* 18, 40–54. doi: 10.1105/tpc.105.037796

Robson, P., Whitelam, G. C., and Smith, H. (1993). Selected components of the shade-avoidance syndrome are displayed in a normal manner in mutants of *Arabidopsis thaliana* and *Brassica rapa* deficient in phytochrome b. *Plant Physiol.* 102, 1179–1184. doi: 10.1104/pp.102.4.1179

Schmitt, J. (1997). Is photomorphogenic shade avoidance adaptive? perspectives from population biology. *Plant Cell Environ.* 20, 826–830. doi: 10.1046/j.1365-3040.1997.d01-96.x

Sellaro, R., Hoecker, U., Yanovsky, M., Chory, J., and Casal, J. J. (2009). Synergism of red and blue light in the control of *Arabidopsis* gene expression and development. *Curr. Biol.* 19, 1216–1220. doi: 10.1016/j.cub.2009.05.062

Sellaro, R., Smith, R. W., Legris, M., Fleck, C., and Casal, J. J. (2019). Phytochrome b dynamics departs from photoequilibrium in the field. *Plant Cell Environ.* 42, 606–617. doi: 10.1111/pce.13445

Shelford, T. J., and Both, A. J. (2021). On the technical performance characteristics of horticultural lamps. *AgriEngineering* 3, 716–727. doi: 10.3390/agriengineering3040046

Shibuya, T., Endo, R., Kitaya, Y., and Hayashi, S. (2016). Growth analysis and photosynthesis measurements of cucumber seedlings grown under light with different red to far-red ratios. *HortScience* 51, 843–846. doi: 10.21273/HORTSCI.51.7.843

Shibuya, T., Kishigami, S., Endo, R., and Matsuda, R. (2019). Interaction between red to far-red ratio of light and vapor-pressure deficit on extension growth of cucumber seedlings. *Sci. Hortic.* 248, 98–104. doi: 10.1016/j.scienta.2018.12.049

Su, J., Liu, B., Liao, J., Yang, Z., Lin, C., and Oka, Y. (2017). Coordination of cryptochrome and phytochrome signals in the regulation of plant light responses. *Agronomy* 7, 25. doi: 10.3390/agronomy7010025

Trupkin, S. A., Legris, M., Buchovsky, A. S., Rivero, M. B. T., and Casal, J. J. (2014). Phytochrome b nuclear bodies respond to the low red to far-red ratio and to the reduced irradiance of canopy shade in *Arabidopsis*. *Plant Physiol.* 165, 1698–1708. doi: 10.1104/pp.114.242438

Veazie, P., Ballance, M. S., and Whipker, B. (2023). Supplemental lighting spectrum impact on sweet potato cutting production and rooting. *Crop Forage Turfgrass Manage.* 9, e20202. doi: 10.1002/cft2.20202

Warner, R., Wu, B. S., MacPherson, S., and Lefsrud, M. (2023). How the distribution of photon delivery impacts crops in indoor plant environments: a review. *Sustainability* 15, 4645. doi: 10.3390/su15054645

Wu, Y., Gong, W., and Yang, W. (2017). Shade inhibits leaf size by controlling cell proliferation and enlargement in soybean. *Sci. Rep.* 7, 9259. doi: 10.1038/s41598-017-10026-5

Xu, H. L., Gauthier, L., Desjardin, Y., and Gosselin, A. (1997). Photosynthesis in leaves, fruits, stem and petioles of greenhouse-grown tomato plants. *Photosynthetica* 33, 113–123. doi: 10.1023/A:1022135507700

Yang, F., Fan, Y., Wu, X., Cheng, Y., Liu, Q., Feng, L., et al. (2018). Auxin-to-gibberellin ratio as a signal for light intensity and quality in regulating soybean growth and matter partitioning. *Front. Plant Sci.* 9. doi: 10.3389/fpls.2018.00056

Zhang, M., Park, Y., and Runkle, E. S. (2020). Regulation of extension growth and flowering of seedlings by blue radiation and the red to far-red ratio of sole-source lighting. *Sci. Hortic.* 272, 109478. doi: 10.1016/j.scienta

Zhen, S., and Bugbee, B. (2020a). Far-red photons have equivalent efficiency to traditional photosynthetic photons: implications for redefining photosynthetically active radiation. *Plant Cell Environ.* 43, 1259–1272. doi: 10.1111/pce.13730

Zhen, S., and Bugbee, B. (2020b). Substituting far-red for traditionally defined photosynthetic photons results in equal canopy quantum yield for CO_2 fixation and increased photon capture during long-term studies: implications for redefining PAR. *Front. Plant Sci.* 11. doi: 10.3389/fpls.2020.581156

Zhen, S., Haidekker, M., and van Iersel, M. W. (2019). Far-red light enhances photochemical efficiency in a wavelength-dependent manner. *Physiol. Plant* 167, 21–33. doi: 10.1111/ppl.12834

Zhen, S., and van Iersel, M. W. (2017). Far-red light is needed for efficient photochemistry and photosynthesis. *J. Plant Physiol.* 209, 115–122. doi: 10.1016/j.jplph.2016.12.004

Zhen, S., van Iersel, M., and Bugbee, B. (2021). Why far-red photons should be included in the definition of photosynthetic photons and the measurement of horticultural fixture efficacy. *Front. Plant Sci.* 12. doi: 10.3389/fpls.2021.693445

Zou, J., Fanourakis, D., Tsaniklidis, G., Cheng, R., Yang, Q., and Li, T. (2021). Lettuce growth, morphology and critical leaf trait responses to far-red light during cultivation are low fluence and obey the reciprocity law. *Sci. Hortic.* 289, 110455. doi: 10.1016/j.scienta.2021.110455

Zou, J., Zhang, Y., Zhang, Y., Bian, Z., Fanourakis, D., Yang, Q., et al. (2019). Morphological and physiological properties of indoor cultivated lettuce in response to additional far-red light. *Sci. Hortic.* 257, 108725. doi: 10.1016/j.scienta.2019.108725

frontiers | Frontiers in Plant Science

TYPE Original Research
PUBLISHED 20 June 2023
DOI 10.3389/fpls.2023.1184664

OPEN ACCESS

EDITED BY
Jung Eek Son,
Seoul National University,
Republic of Korea

REVIEWED BY
Antonio Cellini,
University of Bologna, Italy
Georgios Liakopoulos,
Agricultural University of Athens, Greece

*CORRESPONDENCE
Carl E. Sams
carlsams@utk.edu

RECEIVED 12 March 2023
ACCEPTED 30 May 2023
PUBLISHED 20 June 2023

CITATION
Hammock HA and Sams CE (2023) Variation in supplemental lighting quality influences key aroma volatiles in hydroponically grown 'Italian Large Leaf' basil. *Front. Plant Sci.* 14:1184664. doi: 10.3389/fpls.2023.1184664

Variation in supplemental lighting quality influences key aroma volatiles in hydroponically grown 'Italian Large Leaf' basil

Hunter A. Hammock and Carl E. Sams*

Department of Plant Sciences, The University of Tennessee, Knoxville, TN, United States

The spectral quality of supplemental greenhouse lighting can directly influence aroma volatiles and secondary metabolic resource allocation (i.e., specific compounds and classes of compounds). Research is needed to determine species-specific secondary metabolic responses to supplemental lighting (SL) sources with an emphasis on variations in spectral quality. The primary objective of this experiment was to determine the impact of supplemental narrowband blue (B) and red (R) LED lighting ratios and discrete wavelengths on flavor volatiles in hydroponic basil (*Ocimum basilicum* var. Italian Large Leaf). A natural light (NL) control and different broadband lighting sources were also evaluated to establish the impact of adding discrete and broadband supplements to the ambient solar spectrum. Each SL treatment provided 8.64 mol·m^{-2}·d^{-1} (100 µmol·m^{-2}·s^{-1}, 24 h·d^{-1}) photon flux. The daily light integral (DLI) of the NL control averaged 11.75 mol·m^{-2}·d^{-1} during the growth period (ranging from 4 to 20 mol·m^{-2}·d^{-1}). Basil plants were harvested 45 d after seeding. Using GC-MS, we explored, identified, and quantified several important volatile organic compounds (VOCs) with known influence on sensory perception and/or plant physiological processes of sweet basil. We found that the spectral quality from SL sources, in addition to changes in the spectra and DLI of ambient sunlight across growing seasons, directly influence basil aroma volatile concentrations. Further, we found that specific ratios of narrowband B/R wavelengths, combinations of discrete narrowband wavelengths, and broadband wavelengths directly and differentially influence the overall aroma profile as well as specific compounds. Based on the results of this study, we recommend supplemental 450 and 660 nm (± 20 nm) wavelengths at a ratio of approximately 10B/90R at 100-200 µmol·m^{-2}·s^{-1}, 12-24 h·d^{-1} for sweet basil grown under standard greenhouse conditions, with direct consideration of the natural solar spectrum and DLI provided for any given location and growing season. This experiment demonstrates the ability to use discrete narrowband wavelengths to augment the natural solar spectrum to provide an optimal light environment across variable growing seasons. Future experiments should investigate SL spectral quality for the optimization of sensory compounds in other high-value specialty crops.

KEYWORDS

controlled environment agriculture, light-emitting diodes, narrowband LEDs, spectral quality, *Ocimum basilicum*, supplemental lighting, secondary metabolism, terpenes

Introduction

Light plays a crucial role in the growth, yield, and metabolic processes of plants (Schmitt and Wulff, 1993; Massa et al., 2008; Olle and Viršile, 2013). It is one of the most important abiotic factors that regulate various physiological signals as well as primary (Darko et al., 2014; Thoma et al., 2020) and secondary (Ouzounis et al., 2015; Landi et al., 2020) metabolic responses in plants. The quality, intensity, and photoperiod of light all directly impact plant growth and development (Smith, 1982; Fausey et al., 2005; Jiao et al., 2007). Photosynthetically active radiation (PAR) is composed of different wavelengths within the visible spectrum (400-700 nm) (McCree, 1973), but ultraviolet (Behn et al., 2010; Sakalauskaite et al., 2013; Santin et al., 2021) and far-red (Halaban, 1969; Mokvist et al., 2014; Kalaitzoglou et al., 2019; Zhen and Bugbee, 2020) wavelengths can be perceived and utilized by many species of higher plants.

The roles of light in activating pathways that shape plant growth and development are multifaceted and complex (Fankhauser and Chory, 1997; Chen et al., 2004). Plants possess a unique array of photoreceptors that sense various wavebands across the spectrum (Fankhauser and Chory, 1997; Folta and Carvalho, 2015; Galvao and Fankhauser, 2015). These include phytochromes which detect red and far-red light, cryptochromes which detect ultraviolet, blue, and green light; and phototropins, which respond primarily to blue light (Casal, 2000; Briggs and Olney, 2001). These sensors initiate downstream physiological and metabolic changes (Chen et al., 2004; Casal and Yanovsky, 2005; Rockwell et al., 2006). For example, isoprenoid and phenylpropanoid synthesis are differentially affected by the spectral quality of light received (Bourgaud et al., 2001; Vranova et al., 2012; Lu et al., 2017). Overlapping interactions between narrowband wavelengths have been shown to cause synergistic or antagonistic effects on primary and secondary metabolic pathways (Colquhoun et al., 2013; Carvalho et al., 2016; Pennisi et al., 2019a).

Discrete narrowband wavelengths within the natural solar spectrum are known to play an important role in the quality of plants, affecting flavor, aroma, color, texture, and other human sensory aspects (Kelly and Runkle, 2020; Hammock et al., 2021; Paradiso and Proietti, 2021). Altering the spectral quality of light provided to greenhouse crops, whether that be using filters or supplemental lighting (SL), can directly influence secondary metabolic pathways (Ouzounis et al., 2015; Pennisi et al., 2019a). Different wavelengths of light have been shown to produce other effects in high-value specialty crops such as herbs (Dou et al., 2017; Pennisi et al., 2019b; Larsen et al., 2020), spices (Dou et al., 2017), flowers (Colquhoun et al., 2010; Currey et al., 2012; Colquhoun et al., 2013), strawberries (Kasperbauer et al., 2001), tomatoes (Gómez and Mitchell, 2014; Kaiser et al., 2018; Dannehl et al., 2021), and tea leaves (Fu et al., 2015); all of these crops could utilize variable light exposure to modify volatile metabolites responsible for their sensory qualities (Carvalho et al., 2016). For example, narrowband red and blue wavelengths are known to improve the sensory quality of certain crops. Manipulating the spectral quality of greenhouse crops using SL has been shown to enhance the production of secondary metabolites, which can be used for culinary, medicinal, and commercial purposes (Holopainen et al., 2018).

Horticultural lighting systems are sometimes employed in greenhouse operations when natural light intensity and/or spectral quality are insufficient for sustained plant growth and development (Faust et al., 2005; Sipos et al., 2020). It is well known that solar spectral quality, irradiance, daily light integral (DLI), and photoperiod are variable depending on the time of day, the year, location, and local weather patterns (Korczynski et al., 2002; Thorne et al., 2009; Faust and Logan, 2018). Numerous studies have proven that such SL can noticeably improve both the yield and quality of various high-value specialty crops (Morrow, 2008; Singh et al., 2015). However, it is important to use the correct spectral qualities for each application to maximize plant performance, as many light responses are species-specific (Taulavuori et al., 2016a; Kyriacou et al., 2019; Santin et al., 2021). Despite being costly to purchase, maintain, and operate, commercial greenhouses lighting systems can be used to create the best possible conditions for growth. They can also be used to enhance the natural solar spectrum and impart desirable metabolic effects, such as the accumulation of aroma compounds and phytonutrients with known human health benefits (Rao and Rao, 2007; Poiroux-Gonord et al., 2010; Petrovic et al., 2019). By analyzing the impact of specific wavelengths created by existing greenhouse lighting systems on plant metabolism, we can develop energy-efficient SL strategies to enhance yields and the overall sensory quality of many high-value specialty crops.

One of the most popular and highly valued annual culinary herbs is sweet basil. It has a complex and unique aroma profile desired by professional chefs and restaurants worldwide (Putievsky and Galambosi, 1999; Hiltunen and Holm, 2003). It has a high harvest index and profit margin, is relatively easy to grow, and is well adapted for commercial greenhouse hydroponics and other controlled environment agriculture (CEA) systems (Sipos et al., 2021). The use of greenhouse hydroponics to cultivate basil can provide ideal climate and nutrient conditions that could help diminish any changes in plant growth or development caused by seasonal variations in environmental conditions (Kopsell et al., 2005; Kiferle et al., 2013). Basil is rich in phenolic and terpenoid compounds, many of which are important for human sensory perception and possess human health benefits (Pattison et al., 2018). The 'Italian Large Leaf' variety is known for its strong and intense flavor, vigorous growth, and large leaves, with extensive use in Western and Mediterranean cuisines (Shanmugam et al., 2018). Because of its popularity, demand, and intense VOC profile, sweet basil makes for an excellent model crop to explore the interactions of SL, the natural solar spectrum, and secondary metabolic resource allocation.

The intricacy of sweet basil's taxonomy is due to its hybridization, mislabeling, and abundance of cultivars (Sipos et al., 2021). Recent studies have highlighted that even though these cultivars may look alike and often share the same name, they are genetically distinct from one another. Variations in the genetic background will profoundly impact light-mediated responses associated with secondary metabolism and aroma volatiles (De Masi et al., 2006; Bernhardt et al., 2015). The optimization of

basil production in controlled environments depends on many factors, specifically the intensity and spectral quality of light provided.

Light-emitting diodes (LEDs) allow growers to precisely provide discrete narrowband wavelengths to their crops compared to traditional broadband lighting systems (i.e., high-pressure sodium). Spectral manipulation using LEDs can be used to alter the traits of basil, including its biomass and morphology, as well as its biochemical composition during growth and post-harvest (Hasan et al., 2017; Sipos et al., 2020). The potential for this physiological manipulation has been demonstrated with increases in total phenolic and isoprenoid concentrations when using narrowband blue and red light supplements. Research has shown that the addition of yellow and/or green wavelengths to blue and red wavelengths increased several monoterpenes, sesquiterpenes, and phenylpropanoids in basil compared with blue and red wavelength spectra (Stagnari et al., 2018; Sipos et al., 2020; Kivimaenpa et al., 2022). Further, many studies have demonstrated the species-specific (in some cases, even variety-specific) nature of secondary metabolic responses to narrowband wavelengths, warranting further investigation of both phenolics and terpenoids in basil and other high-value specialty crops (Kyriacou et al., 2019; Toscano et al., 2021). Because of their importance in human sensory perception, the phenolic and terpenoid pathways should be thoroughly evaluated using various analytical and molecular techniques, since light-mediated secondary metabolic resource allocation will impact the expression/bioaccumulation of certain compounds as well as entire secondary metabolic pathways. To date, no published scientific investigations have explored the impact of discrete supplemental narrowband wavelengths and broadband lighting sources on the aroma volatile profile of 'Italian Large Leaf' basil across the changing natural solar spectrum under glass greenhouses across growing seasons.

With this in mind, we designed a set of experiments to determine the overall impact of spectral quality variation of SL on a common variety of greenhouse-produced hydroponically grown basil. The goals of this project were to (1) explore, identify, and quantify plant volatile organic compounds with known impacts on sensory perception or plant physiological processes of basil using headspace gas chromatography-mass spectrometry (HS GC-MS); (2) determine the impact of spectral quality from ambient sunlight and SL sources on aroma volatile concentrations, including specific ratios of narrowband blue/red wavelengths, combinations of discrete narrowband wavelengths, and broadband wavelength; and (3) provide physiology-based recommendations for lighting regimes (spectral quality of supplemental horticultural lighting systems) for commercial greenhouse basil production.

We hypothesize that discrete waveband supplements will differentially influence specific aroma volatiles and secondary metabolic resource allocation (i.e., particular compounds and classes of compounds). We predict this experiment will confirm that manipulating the spectral quality of SL has a considerable impact on basil volatiles and can potentially enhance the human olfactory experience.

Materials and methods

Cultural techniques and environmental growing conditions

This project was conducted at The University of Tennessee Institute of Agriculture (UTIA) in Knoxville, TN, USA (35° 56'44.5"N, 83°56'17.3"W). Growing dates for these four experimental runs occurred from January 2019 to October 2019 and have been labeled as growing seasons. *Ocimum Basilicum* var. Italian Large Leaf basil seeds (Johnny's Select Seeds, Winslow, ME, United States) were germinated in peat moss-based cubes (2 × 2 × 6 cm) (Park's Bio Dome Sponges, Hodges, SC, United States) at 28.3°C and 95% RH. The 'Italian Large Leaf' variety of sweet basil was specifically chosen because of its unique flavor profile, high market demand, high yields, and preference among professional chefs. After two weeks, seedlings were transferred to nutrient film technique (NFT) hydroponic systems with full-strength general mix nutrient solution; the fertility regime was kept constant across the duration of all seasons. The nutrient solution was kept consistent at 5.9 pH and changed weekly. Elemental nutrient concentrations were as follows (ppm): Nitrogen (207.54), Phosphorous (50.87), Potassium (298.23), Calcium (180.15), Magnesium (77.10), Sulfur (136.45), Iron (3.95), Manganese (0.90), Zinc (0.40), Molybdenum (0.09), Copper (0.90), and Boron (0.90). Water samples were analyzed using Inductively Coupled Plasma Mass Spectrometry (Agilent Technologies, Santa Clara, CA, United States) throughout each experiment to ensure consistent nutrient composition. Total growth time lasted approximately 45 d across all four experimental runs (growing seasons). Relative humidity during the growth period averaged 52.5%. Day temperatures averaged 28.5°C, and night temperatures averaged 21.2°C. The DLI of the natural light control averaged 11.75 $mol \cdot m^{-2} \cdot d^{-1}$ during the growth period (ranging from 4 to 20 $mol \cdot m^{-2} \cdot d^{-1}$). Specific growing parameters for each of the seasons may be found in Table 1.

This experiment evaluated the impact of discrete narrowband wavelength combinations from SL systems on tissue concentrations of plant volatile organic compounds (PVOCs) pertinent to flavor/aroma profile and human sensory perception. A total of 12 lighting treatments were used in this experiment, which included one non-supplemented natural light (NL) control (Figure 1) and eleven supplemental lighting (SL) treatments of equal intensity with varying spectral distributions (Figures 2A–K). LEDs (Fluence Bioengineering, Austin, TX) and HPS lamps (Hortilux DE, Mentor OH) provided 8.64 $mol \cdot m^{-2} \cdot d^{-1}$ (equal intensity of 100 $\mu mol \cdot m^{-2} \cdot s^{-1}$ for 24 $h \cdot d^{-1}$) for each SL treatment, in addition to natural sunlight (Figure 1). Lighting treatments are denoted by their wavelengths applied, and each wavelength in series was applied at equal intensities (i.e., a ratio of 1:1:1, with target intensities of 33.3/33.3/33.3 $\mu mol \cdot m^{-2} \cdot s^{-1}$). The intensity and duration of the lighting treatments in this experiment were selected based on current literature with the intention of maximizing the production of key secondary metabolites known to influence flavor perception in basil.

Four treatments applied narrowband red wavelengths across varying narrowband blue wavelengths (ratio of 1B:2R as 660/400/

TABLE 1 Important environmental parameters across growing cycles.

Growing Period	"January"	"April"	"June"	"September"
	1/7/19-2/18/19	3/25/19-5/08/19	5/15/19-7/02/19	9/3/19-10/14/19
Average Day Temp (°C)	27.8	28.1	29.4	28.9
Average Night Temp (°C)	20.2	21.7	22.2	21.3
Average Relative Humidity	55%	50%	50%	55%
Average Daily Light Integral (DLI) ($mol \cdot m^{-2} \cdot d^{-1}$)	7.81	10.29	15.65	13.87
Average Day Length (h)	10:02	13:08	14:29	12:11

All crops grown under greenhouse conditions at The University of Tennessee Institute of Agriculture (UTIA) in Knoxville, TN, USA (35°56'44.5"N, 83°56'17.3"W).

660, 660/420/660, 660/450/660, and 660/470/660) (Fluence Bioengineering, Austin, TX). One treatment applied a high dose of only narrowband blue wavelengths (470/450/420) (Fluence Bioengineering, Austin, TX), while another applied a moderated amount of narrowband blue wavelengths with some narrowband red wavelengths (ratio of 2B:1R as 450/660/470) (Fluence Bioengineering, Austin, TX). Two PhysioSpec lighting systems (Fluence Bioengineering, Austin, TX) were used to evaluate the ratio of narrowband blue and red wavelengths (ratios of 3B:47R and 3B:22R, as 6B/94R and 12B/88R, respectively). Finally, three broadband supplemental treatments of various color temperatures were used, which included a high blue (450/W/470) (Fluence Bioengineering, Austin, TX), a neutral white (W/W/W) (Fluence Bioengineering, Austin, TX), and a high orange/red (HPS) (Hortilux DE, Mentor OH). As previously stated, all SL treatments were provided at equal intensity and duration. Treatments were measured with an Apogee PS-200 spectroradiometer (Apogee Instruments, Logan UT) multiple times per week (after dark) and regularly adjusted to ensure consistent SL intensities and spectral distributions across growing seasons.

Each SL treatment was physically separated to ensure no bleed-over effects between treatments (average of 1.1 ± 0.6 $\mu mol \cdot m^{-2} \cdot s^{-1}$ SL bleed-over at the treatment edges). 1.2 m x 1.2 m sections of basil were grown, with 1.2 m separation between treatments (i.e., measurement edge-to-edge of hydroponic systems within the greenhouse). Tissue samples were only harvested from within the middle 0.6 m of each treatment to ensure further reduction of SL contamination between treatments (0.3 m around the edge of each treatment was considered the buffer zone and was not used for sampling). SL bleed-over was <0.1 $\mu mol \cdot m^{-2} \cdot s^{-1}$ within the harvest zone of each treatment (i.e., below the instrumentation detection limit). Harvests occurred directly after sunrise, and samples were immediately sealed and frozen in liquid nitrogen, then transferred

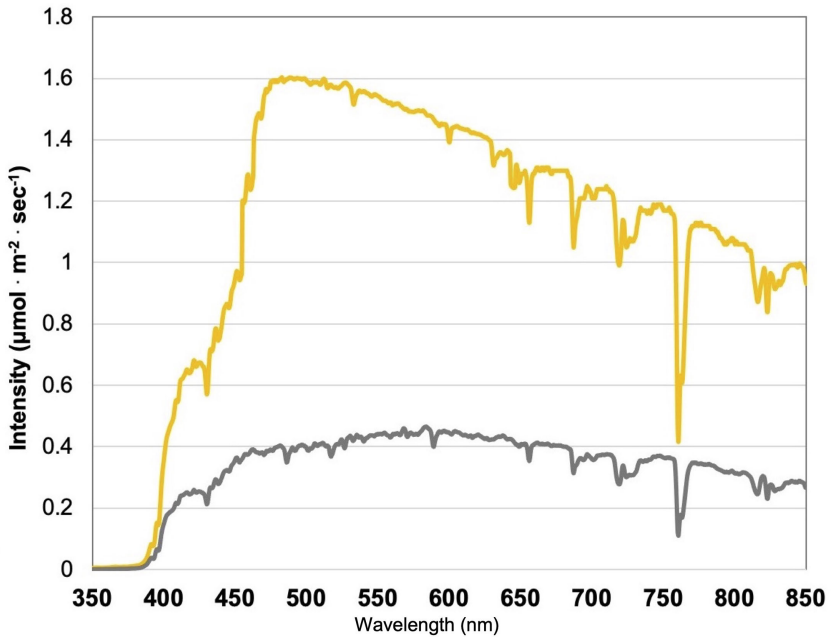

FIGURE 1
Natural light (NL) spectra under greenhouse glass, averaged across all four growing seasons, ranging from 350 nm to 850 nm. Values were taken at solar noon with three replicates for full sun (yellow) and overcast (gray) for each experimental run. The daily light integral (DLI) of the NL control averaged 11.75 $mol \cdot m^{-2} \cdot d^{-1}$ across all growing cycles (ranging from 4 to 20 $mol \cdot m^{-2} \cdot d^{-1}$).

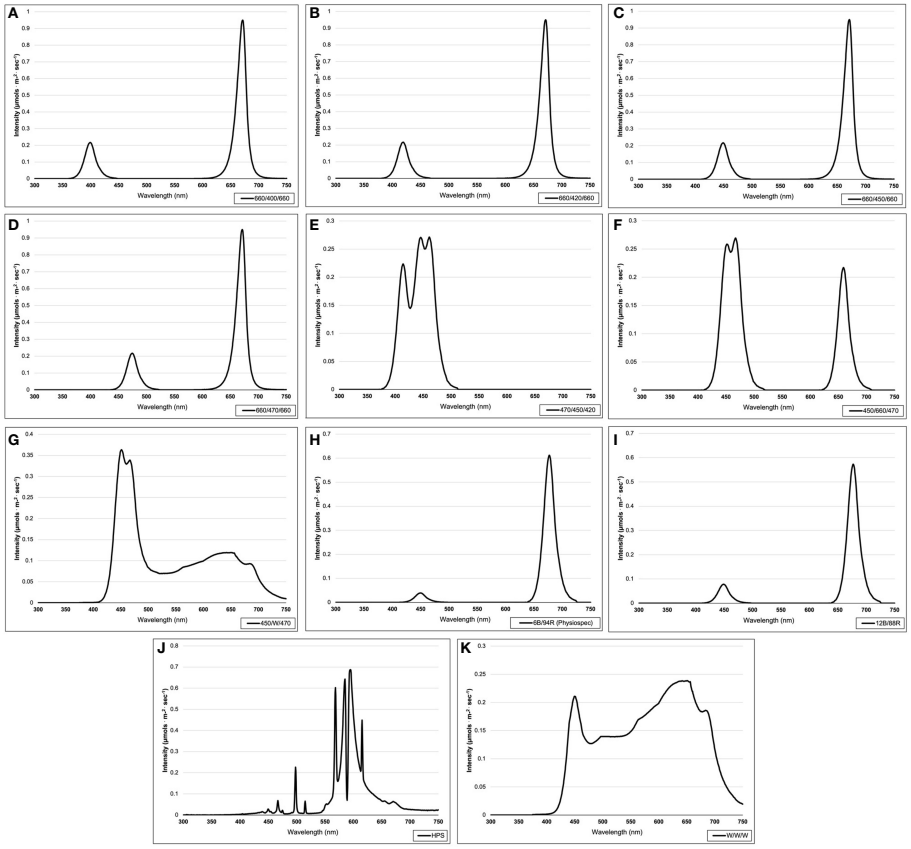

FIGURE 2
Emission spectra of supplemental lighting (SL) treatments from 300 nm to 750 nm: **(A)** 660/400/660; **(B)** 660/420/660; **(C)** 660/450/660; **(D)** 660/470/ 660; **(E)** 470/450/420; **(F)** 450/660/470; **(G)** 450/W/470; **(H)** 6B/94R; **(I)** 12B/88R; **(J)** HPS; **(K)** W/W/W. All SL treatments provided 8.64 mol·m^{-2}·d^{-1} (continuous 100 µmol·m^{-2}·s^{-1}; 24 h·d^{-1}). All lighting treatments were measured with a PS-200 Apogee Spectroradiometer to confirm the intensity of specific treatment wavelengths throughout each growing season. Readings were taken at midnight in order to exclude underlying natural solar spectra.

to a -80°C freezer until the time of analysis to preserve all volatile compounds and inhibit post-harvest changes to metabolism.

Gas chromatography and mass spectrometry method

Three g of fresh leaf tissue (two basil plants per sample rep, 1.5 g of representative material from each plant, nodes four and eight) were placed in 20 mL borosilicate glass vials, then immediately frozen in liquid nitrogen, and stored in a -80 °C freezer until time of analysis. Samples were run within 72 hours of collection. Frozen samples were placed onto a Network Headspace Sampler (Agilent G1888, Santa Clara, CA, United States). Ten sample reps were used per treatment. Samples were heated to 80 °C for 10 min and pressurized with Helium (Air Gas, analytical purity) to 95.21 kPa for 1 min. The tube was then vented for 1 min into the headspace transfer line (110 °C) and injected (port at 250 °C) into the GC (Agilent Technologies 6890N Network GC System). The volatiles were separated by an HP-5MS capillary column ((5%-Phenyl)-methylpolysiloxane, length: 30 m, ID: 0.250 mm, film thickness: 1 µm, Agilent Technologies) using analytical purity Helium carrier gas at 95.21 kPa with constant column pressure. At the start of data acquisition, the temperature was held at 40 °C for 5 min, ramped up from 40 °C to 250 °C (5 °C per min), then held constant for the duration of the run. The total run time was 70 min, including post-run and cool-down phases. After sample separation and column elution, the analytes were passed through a mass selective detector (Agilent Technologies 5973 Network Mass Selective Detector) at 250 °C and collected over the course of the sample run. The transfer line, ion source, and quadrupole temperatures were 250 °C, 230 °C, and 170 °C, respectively. The full scan mass range was set to 40-550 m/z (threshold: 150).

Agilent ChemStation was used for data collection and processing. Over 200 separate compounds were identified throughout this experiment, but emphasis was placed on key aroma compounds (i.e., shown in the literature to be essential for human sensory perception and/or plant metabolic processes) that have been calibrated to our GC-MS and HP-5MS column using pure analytical standards (Sigma-Aldrich, St. Louis, MO) to determine leaf tissue emissions of key VOCs on a fresh plant weight basis. The MS spectra from pure analytical standards and fresh samples were compared to NIST, ADMIS, and our custom basil reference library created from calibrated analytical standards to confirm peak identity and retention times. MassHunter Workstation Software Version B.06.00 (Agilent Technologies,

Inc., 2012) was used to integrate peaks automatically. Relative peak areas and retention times were automatically adjusted based on authentic analytical standards and multiple library references. Over 200 compounds were identified in this experiment, with approximately 50 of those being quantified using pure analytical standards.

All volatile concentration units are reported in micro molarity of analyte concentration (suspended in a known volume of gaseous headspace matrix) per g of fresh leaf tissue ($\mu M \cdot g^{-1}$ FM) to represent VOC emissions most accurately from the collected headspace sample above fresh plant tissues under specific reproducible analytical conditions (Tables 2–4; Figures 3, 4). This unit (compared to $\mu mol \cdot g^{-1}$ FM) was utilized because of its commonality in biological headspace GC-MS sampling and incorporates the concentration of each analyte per unit volume of headspace gas above the plant tissue (i.e., samples the dynamic and complex gaseous matrix which contains numerous pertinent VOCs), which is important for sensory-based studies. This provides the foundation for future sensory panel experiments aimed at determining the influence of light on consumer acceptance and preference of basil aroma profiles.

Statistical analyses

A Randomized Complete Block Design was used for this experiment. All data sets were analyzed by Generalized Linear Model (GLM) and Mixed Model Analysis of Variance (p = 0.05) procedures using the statistical software SAS (version 9.4, SAS Institute, Cary, NC). Design and Analysis macro (DandA.sas), created by Dr. Arnold Saxton, was utilized in addition to Tukey's adjustment, regression analysis, and univariate/normalization procedures to provide additional statistical insights on the complete data set. Treatments were separated by least significant difference (LSD) at α=0.05. Principal component analysis was performed using JMP Pro 17 (SAS Institute, Cary, NC). Due to the overwhelming number of compounds analyzed, only statically significant separations of compounds with known plant physiological function and/or human sensory impact were reported in this study. Key volatiles were analyzed and presented on a fresh mass (FM) basis as compared to calibration curves created from pure analytical standards.

Results

Plant volatile organic compound (PVOC) leaf tissue concentrations were evaluated in this experiment, many of which were influenced by growing season, lighting treatment, and season*treatment interactions. Total VOC concentrations of basil leaf tissues were found to be statistically significant across both lighting treatment (F=103.01; $P \leq 0.0001$) (Figure 3) and season (F=391.62; $P \leq 0.0001$) (Figure 4). Statistical summary for individual compounds evaluated in this study are included (Table 1) and separated by category based on chemical class and metabolic origin. Categories include alcohols, aldehydes, benzyl aldehydes, amides and furans, hydrocarbons, acyclic monoterpenes, bicyclic monoterpenes, cyclic monoterpenes, sesquiterpenes, organosulfur, and phenylpropanoids.

TABLE 2 Summary of statistical results for pertinent aroma volatile compounds detected using headspace gas chromatography-mass spectrometry.

Compound Name	CAS Number	F Value			Pr > F		
		Experiment	Treatment	Experiment*Treatment	Experiment	Treatment	Experiment*Treatment
Alcohols							
(E)-3-Hexen-1-ol	928-96-1	18.44	0.81	0.67	<0.0001	0.6264	0.8682
1-Octen-3-ol	3391-86-4	23.16	3.47	2.32	<0.0001	0.0001	<0.0001
2-Octyn-1-ol	20739-58-6	36.42	10.78	3.58	<0.0001	<0.0001	<0.0001
2-Phenylethanol	60-12-8	44.24	11.18	3.90	<0.0001	<0.0001	<0.0001
Aldehydes							
2-Ethyl-2-butenal	19780-25-7	44.87	1.60	2.26	<0.0001	0.0977	0.0002
2-Hexenal	6728-26-3	47.52	2.94	2.11	<0.0001	0.0009	0.0005
Nonanal	124-19-6	199.07	5.41	2.83	<0.0001	<0.0001	<0.0001
Hexanal	66-25-1	7.82	0.98	0.91	<0.0001	0.4703	0.6094
Benzyl Aldehydes							
3-Ethylbenzaldehyde	34246-54-3	140.11	9.66	3.95	<0.0001	<0.0001	<0.0001
Benzeneacetaldehyde	122-78-1	196.22	19.32	7.76	<0.0001	<0.0001	<0.0001
Amides and Furans							
Benzamide	55-21-0	345.39	2.49	2.14	<0.0001	0.0049	0.0003

(Continued)

TABLE 2 Continued

Compound Name	CAS Number	F Value			Pr > F		
		Experiment	Treatment	Experiment*Treatment	Experiment	Treatment	Experiment*Treatment
N-phenyl-Formamide	103-70-8	143.66	1.95	2.31	<0.0001	0.0323	<0.0001
2-Ethyl-furan	3208-16-0	16.32	1.48	1.83	<0.0001	0.1380	0.0045
2-Pentyl-furan	3777-69-3	4.82	2.63	0.90	0.0026	0.0029	0.6374
Hydrocarbons							
1,4-Cyclohexadiene	628-41-1	80.31	8.46	2.74	<0.0001	<0.0001	<0.0001
2-Cyclopropyl-2-pentene	5457-40-9	58.30	9.00	1.98	<0.0001	<0.0001	0.0013
Decane	124-18-5	158.69	5.79	2.66	<0.0001	<0.0001	<0.0001
(E)-3-Methyl-1,3,5-hexatriene	24587-26-6	6.53	1.78	1.04	0.0003	0.0558	0.4103
1,3-cis,5-cis-Octatriene	40087-62-5	42.07	8.62	1.71	<0.0001	<0.0001	0.0100
1,4-Octadiene	5675-25-2	27.54	3.60	2.18	<0.0001	<0.0001	0.0003
2-Methyl-2-hepten-4-yne	58275-91-5	31.70	9.23	2.07	<0.0001	<0.0001	0.0006
1-Methylcyclohexene	591-49-1	135.93	1.92	1.04	<0.0001	0.0356	0.4174
Cycloheptene	628-92-2	3.18	0.67	1.05	0.0258	0.7661	0.4110
Acyclic Monoterpenes							
2,6-Dimethyl-2,4,6-octatriene	673-84-7	65.54	12.59	3.43	<0.0001	<0.0001	<0.0001
cis-β-Ocimene	3338-55-4	48.61	3.18	1.81	<0.0001	0.0004	0.0048
Citronellyl Acetate	150-84-5	13.31	2.70	1.75	<0.0001	0.0024	0.0085
Linalool	78-70-6	47.53	2.17	1.57	<0.0001	0.0152	0.0262
trans-β-Ocimene	3779-61-1	80.44	6.97	3.19	<0.0001	<0.0001	<0.0001
α-Ocimene	6874-44-8	195.03	1.29	2.00	<0.0001	0.2295	0.0011
β-Myrcene	123-35-3	268.90	5.15	2.83	<0.0001	<0.0001	<0.0001
Bicyclic Monoterpenes							
3-Caren-10-al	14595-13-2	17.21	2.24	1.06	<0.0001	0.0123	0.3871
(+)-4-Carene	29050-33-7	27.75	7.00	1.57	<0.0001	<0.0001	0.0254
3-Carene	498-15-7	24.28	4.53	2.35	<0.0001	0.0521	0.0005
Camphene	79-92-5	70.69	9.41	1.52	<0.0001	<0.0001	0.0356
Isoborneol	507-70-0	22.21	3.85	1.51	<0.0001	<0.0001	0.0367
trans-Pinocarveol	5947-36-4	7.36	3.32	1.89	<0.0001	0.0002	0.00027
trans-Sabinene hydrate	17699-16-0	158.38	5.80	2.66	<0.0001	<0.0001	<0.0001
α-Pinene	80-56-8	73.74	9.40	1.65	<0.0001	<0.0001	0.0152
β-Pinene	127-91-3	49.46	5.93	1.86	<0.0001	<0.0001	0.0032
Cyclic Monoterpenes							
3-Menthene	500-00-5	10.23	4.23	2.34	<0.0001	<0.0001	<0.0001
d-Limonene	5989-27-5	29.80	7.17	1.74	<0.0001	<0.0001	0.0076
Fenchyl acetate	13851-11-1	14.98	1.58	0.62	<0.0001	0.1019	0.9467
p-Menth-1-en-8-ol	98-55-5	173.75	10.61	2.56	<0.0001	<0.0001	<0.0001
Sesquiterpenes							
a-Humulene	6753-98-6	19.58	1.87	1.12	<0.0001	0.0420	0.3001

(Continued)

TABLE 2 Continued

Compound Name	CAS Number	F Value			Pr > F		
		Experiment	Treatment	Experiment*Treatment	Experiment	Treatment	Experiment*Treatment
Organosulfur							
Isothiocyanatocyclopropane	56601-42-4	9.92	1.69	0.85	<0.0001	0.0752	0.7103
2-Isobutylthiazole	18640-74-9	10.79	1.90	1.23	<0.0001	0.0391	0.2101
Diallyl Disulfide	2179-57-9	1.69	0.40	0.67	0.1684	0.9559	0.9145
Dimethyl Sulfide	75-18-3	25.15	4.30	2.09	<0.0001	<0.0001	0.0005
Phenylpropanoids							
Eugenol	97-53-0	130.10	9.94	4.43	<0.0001	<0.0001	<0.0001
Methyl Eugenol	93-15-2	7.95	1.70	1.50	0.0010	0.0997	0.1545

Alcohols

(E)-3-Hexen-1-ol concentrations were significantly impacted by season (F=18.44; $P \leq 0.0001$), but not by lighting treatment (F=0.81; P=0.6264) or season*treatment interactions (F=0.67; P=0.8682) (Table 2). When averaged across all treatments, June and September had higher average concentrations, as compared to the January and April seasons. Season concentrations ranged from 2.27 $\mu M \cdot g^{-1}$ FM to 6.24 $\mu M \cdot g^{-1}$ FM (Table 3).

1-Octen-3-ol concentrations were significantly influenced by season (F=23.16; $P \leq 0.0001$), lighting treatment (F=3.47; $P \leq 0.0001$), and season*treatment interactions (F=2.32; $P \leq 0.0001$) (Table 2). The June growing season had the highest concentration averages as compared to any other season. September had the lowest but did not separate from January. Season concentrations ranged from 13.03 $\mu M \cdot g^{-1}$ FM to 39.72 $\mu M \cdot g^{-1}$ FM (Table 3). When averaged across all seasons, treatments 450/W/470 and 660/470/660 statistically separated from the 660/420/660 treatment, but the others did not show clear separation. Treatment concentration averages ranged from 15.15 $\mu M \cdot g^{-1}$ FM to 35.65 $\mu M \cdot g^{-1}$ FM (Table 4).

2-Octyn-1-ol concentrations were significantly impacted by season (F=36.42; $P \leq 0.0001$), lighting treatment (F=10.78; $P \leq 0.0001$), and season*treatment interactions (F=3.58; $P \leq 0.0001$) (Table 2). June again had the highest concentration as compared to any other season. September again had the lowest concentration. Season concentrations ranged from 395.22 $\mu M \cdot g^{-1}$ FM to 653.76 $\mu M \cdot g^{-1}$ FM (Table 3). While there was statistical separation for the two compounds across lighting treatments, no clear patterns were evident (Table 4).

2-Phenylethanol concentrations were significantly influenced by season (F=44.24; $P \leq 0.0001$), lighting treatment, (F=11.18; $P \leq 0.0001$) and season*treatment interactions (F=3.9; $P \leq 0.0001$) (Table 2). June again had the highest concentration as compared to any other season. September again had the lowest concentration but did not statistically separate from January. Season concentrations ranged from 19.56 $\mu M \cdot g^{-1}$ FM to 58.43 $\mu M \cdot g^{-1}$ FM (Table 3). The 6B/94R treatment had the highest concentration and statistically separated from all other treatments. The lowest concentration was found in the 660/420/660 and HPS treatments, but they were not statistically separate from many other treatments. Treatment concentrations ranged from 19.62 $\mu M \cdot g^{-1}$ FM to 74.13 $\mu M \cdot g^{-1}$ FM (Table 4).

Benzyl aldehydes

3-Ethylbenzaldehyde concentrations were significantly influenced by season (F=140.11; $P \leq 0.0001$), lighting treatment (F=9.66; $P \leq 0.0001$), and season*treatment interactions (F=3.95; $P \leq 0.0001$) (Table 2). The June growing season had the highest concentration and was statistically separated from the lowest seasons, which were January and September. The season concentrations ranged from 4.28 $\mu M \cdot g^{-1}$ FM to 17.15 $\mu M \cdot g^{-1}$ FM (Table 3). The 6B/94R treatment had the highest concentration and was statistically separated from many other treatments; this includes 660/420/660, 660/450/660, and the NL control, which had three of the lowest concentrations and did not statistically separate. The treatment concentrations ranged from 5.35 $\mu M \cdot g^{-1}$ FM to 15.18 $\mu M \cdot g^{-1}$ FM (Table 4).

Benzeneacetaldehyde concentrations were significantly influenced by season (F=196.22; $P \leq 0.0001$), lighting treatment (F=19.32; $P \leq 0.0001$), and season*treatment interactions (F=7.76; $P \leq 0.0001$) (Table 2). The June growing season had the highest concentration and was statistically separated from the lowest season, which was September. The season concentrations had a considerable range, from 9.92 $\mu M \cdot g^{-1}$ FM to 250.85 $\mu M \cdot g^{-1}$ FM (Table 3). The 6B/94R again had the highest concentration and statistically separated from all other treatments. In general, the narrowband treatments had higher concentrations than the broadband treatments. NL control had the lowest concentration, but did not separate from the 660/420/660, HPS, and W/W/W treatments. The treatment concentrations ranged from 69.70 $\mu M \cdot g^{-1}$ FM to 276.22 $\mu M \cdot g^{-1}$ FM (Table 4).

Hydrocarbons

1,4-Cyclohexadiene concentrations were significantly influenced by growing season (F=80.31; $P \leq 0.0001$), lighting treatment (F=8.46; $P \leq 0.0001$), and season*treatment interactions (F=2.74; $P \leq 0.0001$) (Table 2). June and September growing seasons had statistically higher

TABLE 3 Influence of growing season on aroma volatile tissue concentrations in hydroponically grown greenhouse sweet basil (*Ocimum basilicum* var. Italian Large Leaf).

Compound Name	Growing Season			
	January	April	June	September
Alcohols				
(E)-3-Hexen-1-ol	2.27^{b}	2.07^{b}	6.24^{a}	5.99^{a}
1-Octen-3-ol	16.43^{bc}	23.23^{b}	39.72^{a}	13.03^{c}
2-Octyn-1-ol	408.20^{c}	547.80^{b}	653.76^{a}	395.22^{d}
2-Phenylethanol	19.56^{c}	35.55^{b}	58.43^{a}	26.41^{bc}
Aldehydes				
2-Ethyl-2-butenal	0.87^{c}	1.11^{bc}	1.37^{bc}	2.32^{a}
2-Hexenal	3.39^{c}	4.43^{bc}	5.39^{b}	9.69^{a}
Nonanal	10.05^{c}	20.82^{b}	37.32^{a}	5.26^{d}
Hexanal	128.96^{c}	130.21^{bc}	131.06^{ab}	132.15^{a}
Benzyl Aldehydes				
3-Ethylbenzaldehyde	5.82^{c}	10.14^{b}	17.15^{a}	4.28^{c}
Benzeneacetaldehyde	76.12^{c}	181.19^{b}	250.85^{a}	9.92^{d}
Amides and Furans				
Benzamide	2.92^{b}	3.30^{b}	3.49^{b}	36.32^{a}
N-phenyl-Formamide	6.92^{b}	6.32^{b}	9.05^{b}	39.48^{a}
2-Ethyl-furan	27.51^{c}	29.83^{b}	29.59^{b}	32.22^{a}
2-Pentyl-furan	4.83^{b}	5.97^{ab}	6.33^{a}	5.27^{ab}
Hydrocarbons				
1,4-Cyclohexadiene	6.00^{c}	10.31^{b}	17.34^{a}	16.76^{a}
2-Cyclopropyl-2-pentene	12.09^{c}	20.43^{b}	24.59^{a}	25.58^{a}
Decane	9.99^{c}	20.71^{b}	37.07^{a}	10.61^{c}
(E)-3-Methyl-1,3,5-hexatriene	2.00^{b}	2.15^{b}	2.67^{ab}	3.19^{a}
1,3-cis,5-cis-Octatriene	5.41^{b}	6.27^{b}	8.84^{a}	8.20^{a}
1,4-Octadiene	16.63^{bc}	23.04^{b}	40.63^{a}	7.28^{c}
2-Methyl-2-hepten-4-yne	6.56^{b}	6.80^{b}	8.85^{a}	9.08^{a}
1-Methylcyclohexene	23.40^{b}	29.14^{b}	32.83^{b}	89.07^{a}
Cycloheptene	0.73^{b}	0.81^{b}	1.02^{a}	1.09^{a}
Acyclic monoterpenes				
2,6-Dimethyl-2,4,6-octatriene	1.77^{d}	4.16^{c}	6.30^{a}	5.15^{b}
cis-β-Ocimene	370.45^{c}	538.33^{b}	754.18^{a}	145.81^{d}
Citronellyl Acetate	188.27^{c}	190.24^{bc}	193.66^{a}	191.75^{b}
Linalool	925.12^{a}	876.30^{a}	870.25^{a}	239.32^{b}
trans-β-Ocimene	106.90^{c}	279.90^{b}	351.14^{a}	57.16^{c}
α-Ocimene	45.66^{b}	27.88^{b}	75.23^{b}	493.99^{a}
β-Myrcene	281.89^{b}	371.46^{a}	407.65^{a}	9.36^{c}

(Continued)

TABLE 3 Continued

Compound Name	Growing Season			
	January	April	June	September
Bicyclic monoterpenes				
3-Caren-10-al	1.79^{b}	1.21^{c}	1.52^{bc}	2.51^{a}
(+)-4-Carene	16.93^{d}	26.22^{c}	61.46^{a}	40.74^{b}
3-Carene	379.21^{b}	507.44^{a}	559.24^{a}	535.31^{a}
Camphene	23.41^{c}	29.25^{bc}	32.83^{bc}	55.77^{a}
Isoborneol	28.97^{bc}	23.53^{c}	32.50^{b}	49.74^{a}
trans-Pinocarveol	3.60^{b}	4.89^{ab}	5.87^{a}	6.13^{a}
trans-Sabinene hydrate	10.04^{c}	20.71^{b}	37.07^{a}	10.60^{c}
α-Pinene	17.27^{c}	22.81^{b}	25.94^{b}	46.27^{a}
β-Pinene	99.30^{c}	137.69^{b}	152.76^{b}	208.12^{a}
Cyclic monoterpenes				
3-Menthene	24.22^{b}	36.08^{a}	46.11^{a}	39.59^{a}
d-Limonene	234.61^{c}	311.32^{b}	378.51^{a}	315.24^{b}
Fenchyl acetate	132.80^{a}	149.80^{a}	127.37^{a}	81.12^{b}
p-Menth-1-en-8-ol	5.44^{d}	9.75^{c}	19.69^{a}	13.33^{b}
Sesquiterpenes				
α-Humulene	53.69^{b}	54.88^{b}	58.92^{a}	59.58^{a}
Organosulfur				
Isothiocyanatocyclopropane	1.28^{b}	1.20^{b}	1.78^{ab}	2.28^{ab}
2-Isobutylthiazole	5.57^{b}	6.74^{b}	8.86^{a}	8.94^{a}
Diallyl Disulfide	0.65^{a}	0.87^{a}	1.05^{a}	1.60^{a}
Dimethyl Sulfide	43.42^{c}	121.98^{a}	68.87^{b}	69.76^{b}
Phenylpropanoids				
Eugenol	43.16^{d}	139.70^{c}	280.02^{a}	212.33^{b}
Methyl Eugenol	131.23^{b}	138.51^{b}	160.17^{a}	172.11^{a}

All concentrations are presented in micro molarity of analyte per gram of fresh mass (μM·g^{-1} FM). Mean values represent two plants per replication and ten replications per treatment. Values for each season are averaged across all treatments within that season. Values were analyzed using Tukey's protected least significant difference. Data in the same row followed by the same letter are not significantly different (α = 0.05).

tissue concentrations than those in January and April. The January growing season had the lowest concentrations. The growing season concentrations ranged from 6.00 μM·g^{-1} FM to 17.34 μM·g^{-1} FM (Table 3). The treatment 6B/94R again had the highest tissue concentration, statistically greater than many of the narrowband and broadband SL treatments. The 660/420/660 again had the lowest tissue concentration of any treatment, and did not statistically separate from the NL control. The treatment tissue concentrations ranged from 6.38 μM·g^{-1} FM to 18.66 μM·g^{-1} FM (Table 4).

2-Cyclopropyl-2-pentene concentrations were significantly influenced by season (F=58.3; $P \leq 0.0001$), treatment (F=9.00; $P \leq 0.0001$), and season*treatment interactions (F=1.98; P=0.0013) (Table 2). This compound showed similar seasonal patterns to previous hydrocarbons. June and September growing seasons had statistically higher tissue concentrations than those in January and April. The January growing season again had the lowest concentrations. The season concentrations ranged from 12.09 μM·g^{-1} FM to 25.58 μM·g^{-1} FM (Table 3). The 6B/94R treatment again had the highest tissue concentration, separating from some of the other treatments. The 660/420/660 had the lowest tissue concentration of any treatment, and did not statistically separate from the NL control and some of the SL treatments. The treatment concentrations ranged from 14.51 μM·g^{-1} FM to 27.61 μM·g^{-1} FM (Table 4).

Decane concentrations were significantly influenced by season (F=158.69; $P \leq 0.0001$), treatment (F=5.79; $P \leq 0.0001$), and season*treatment interactions (F=2.66; $P \leq 0.0001$) (Table 2). June growing season had the highest tissue concentration, which statistically separated from all other seasons. The two seasons with the lowest concentrations were January and September. The season concentrations ranged from 9.99 μM·g^{-1} FM to 37.07 μM·g^{-1} FM

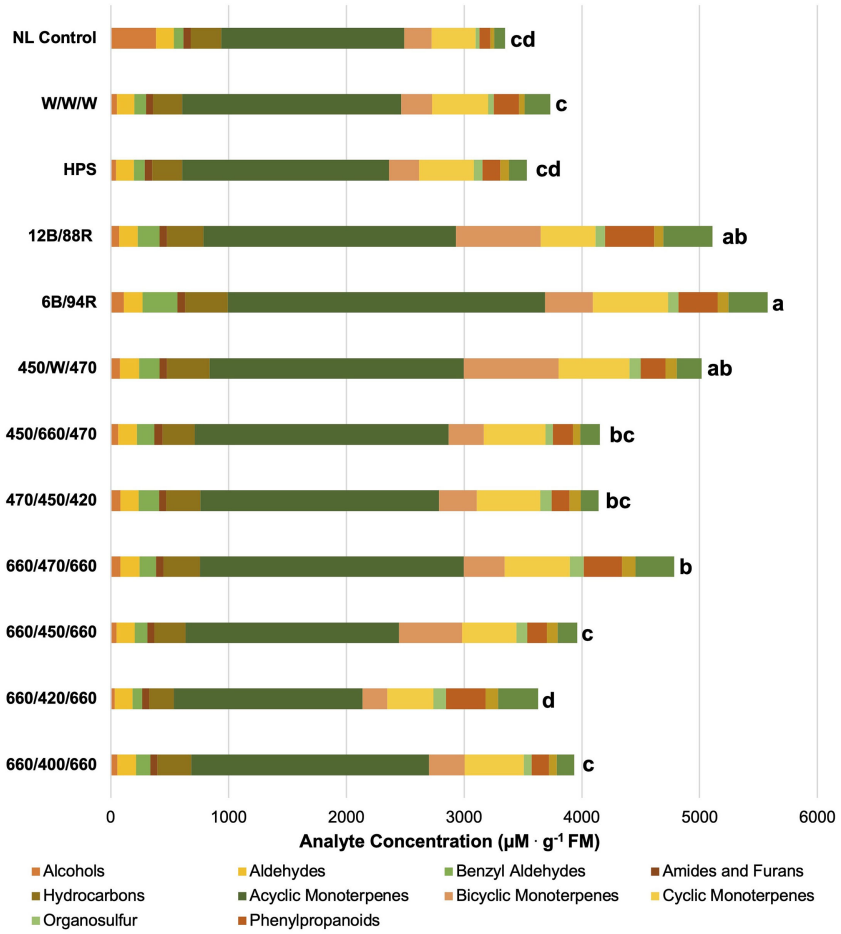

FIGURE 3
Impact of lighting treatment on tissue accumulation of each compound class. All concentrations are presented in micro molarity of analyte per gram of fresh mass (µM·g^{-1} FM). Mean values represent two plants per replication and ten replications per treatment. Values for each treatment are averaged across all seasons within that treatment. Total volatile organic compound concentration was analyzed using Tukey's protected least significant difference. Data followed by the same letter are not significantly different (α = 0.05).

(Table 4). The 660/470/660 and 6B/94R treatments had the two highest tissue concentrations, and did not separate from each other. The broadband treatments generally did not have as high concentrations as the narrowband treatments; the HPS and W/W/W treatments did not separate from the NL control, which had the lowest concentration. The treatment concentrations ranged from 13.10 µM·g^{-1} FM to 25.92 µM·g^{-1} FM (Table 4).

(E)-3-Methyl-1,3,5-hexatriene concentrations were significantly influenced by season (F=6.53; *P*=0.0003), but not by lighting treatment (F=1.78; *P*=0.0558) or season*treatment interactions (F=1.04; *P*=0.4103) (Table 2). The September growing season had the highest tissue concentration, but did not statistically separate from the June season. The January growing season had the lowest tissue concentration but did not separate from the April or June seasons. The season concentrations ranged from 2.00 µM·g^{-1} FM to 3.19 µM·g^{-1} FM (Table 3).

1,3-cis,5-cis-Octatriene concentrations were significantly influenced by season (F=42.07; $P \leq 0.0001$), lighting treatment (F=8.62; $P \leq 0.0001$), and season*treatment interactions (F=1.71; *P*=0.01) (Table 2). The June growing season had the highest tissue concentration, but did not statistically separate from the September season. The January growing season had the lowest tissue concentration but did not separate from the April season. The season concentrations ranged from 5.41 µM·g^{-1} FM to 8.84 µM·g^{-1} FM (Table 3). The 6B/94R treatment had the highest tissue concentration, but did not separate from the 450/W/470 or 12B/88R treatments. The 660/420/660 again had the lowest tissue concentration of any other treatment, and did not statistically separate from the NL control and some of the LED treatments. The treatment concentrations ranged from 5.08 µM·g^{-1} FM to 9.77 µM·g^{-1} FM (Table 4).

1,4-Octadiene concentrations were significantly influenced by season (F=27.54; $P \leq 0.0001$), lighting treatment (F=3.60; $P \leq 0.0001$), and season*treatment interactions (F=2.18; *P*=0.0003) (Table 2). The June growing season had the highest tissue concentration. The September growing season had the lowest tissue concentration but did not separate from the January season. The season concentrations ranged from 7.28 µM·g^{-1} FM to 40.63 µM·g^{-1} FM (Table 3). The treatments 660/470/660 and 450/W/470 had the highest two tissue concentrations and did not

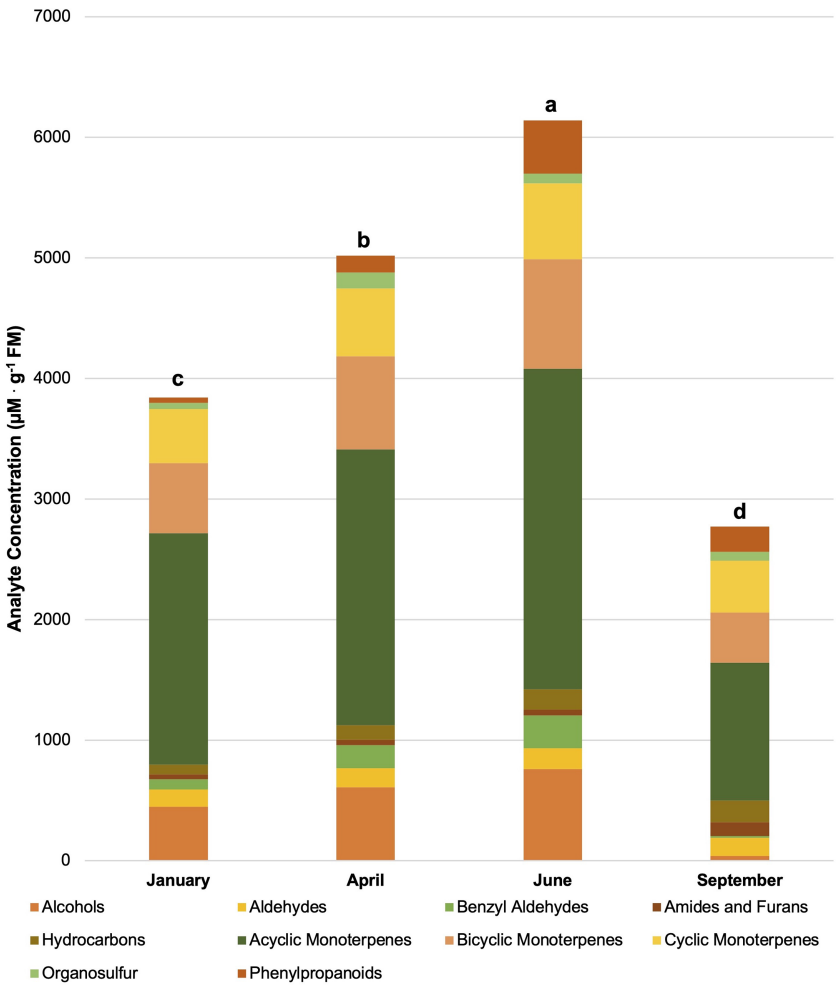

FIGURE 4
Influence of season on compound classes pertinent for aroma perception. All concentrations are presented in micro molarity of analyte per gram of fresh mass (µM·g^{-1} FM). Mean values represent two plants per replication and ten replications per treatment. Values for each season are averaged across all treatments within that season. Total volatile organic compound concentration was analyzed using Tukey's protected least significant difference. Data followed by the same letter are not significantly different (α = 0.05).

statistically from each other, as well many of the other treatments and control. The lowest tissue concentrations were found in the 660/420/660 treatment, which only statistically separated from the highest two treatments in addition to the 6B/94R treatment. The treatment concentrations ranged from 8.98 µM·g^{-1} FM to 35.66 µM·g^{-1} FM (Table 4).

2-Methyl-2-hepten-4-yne concentrations were significantly influenced by season (F=31.70; $P \leq 0.0001$), lighting treatment (F=9.23; $P \leq 0.0001$), and season*treatment interactions (F=2.07; P=0.0006) (Table 2). The September growing season had the highest tissue concentration, but did not statistically separate from the June season. The January growing season had the lowest tissue concentration but did not separate from the April season. The season concentrations ranged from 6.56 µM·g^{-1} FM to 9.08 µM·g^{-1} FM (Table 3). The treatment 6B/94R had the highest tissue concentration, but did not separate from the 450/W/470 and 12B/88R treatments. The lowest tissue concentrations were again found in the 660/420/660 treatment, which did not separate from the NL control and some of the LED treatments. The treatment concentrations ranged from 5.52 µM·g^{-1} FM to 10.20 µM·g^{-1} FM (Table 4).

1-Methylcyclohexene concentrations were significantly influenced by season (F=135.93; $P \leq 0.0001$) and lighting treatment (F=1.92; P=0.0356), but not by season*treatment interactions (F=1.04; P=0.4174) (Table 2). The September growing season had the highest tissue concentrations, which separated from all other seasons. The lowest tissue concentrations were found during the January growing season, but did not separate from the April and June seasons. The season concentrations ranged from 23.40 µM·g^{-1} FM to 89.07 µM·g^{-1} FM (Table 3). The treatment concentrations ranged from 179.01 µM·g^{-1} FM to 235.55 µM·g^{-1} FM; while the p-value from ANOVA did pass the 0.05 threshold, Tukey's protected LSD test did not indicate separation of means across treatments (Tables 2, 4).

Cycloheptene concentrations were significantly influenced by season (F=3.18; P=0.0258), but not by lighting treatment (F=0.67; P=0.7661) or season*treatment interactions (F=1.05; P=0.411) (Table 2). This compound was found in very low concentrations.

TABLE 4 Influence of light treatment on aroma volatile tissue concentrations in hydroponically grown greenhouse sweet basil (*Ocimum basilicum* var. Italian Large Leaf).

Compound Name	Lighting Treatments											
	660/400/660	660/420/660	660/450/660	660/470/660	470/450/420	450/660/470	450/W/470	6B/94R	12B/88R	HPS	W/W/W	NL Control
Alcohols												
(E)-3-Hexen-1-ol	4.45^{a}	2.90^{a}	5.78^{a}	3.32^{a}	28.15^{a}	4.57^{a}	4.06^{a}	3.66^{a}	1.97^{a}	4.33^{a}	2.88^{a}	2.54^{a}
1-Octen-3-ol	20.48^{abc}	10.40^{c}	15.17^{bc}	36.11^{a}	16.03^{bc}	24.75^{abc}	35.65^{a}	31.25^{ab}	24.65^{abc}	18.57^{abc}	20.41^{abc}	24.70^{abc}
2-Phenylethanol	29.64^{bcd}	20.70^{d}	28.35^{bcd}	42.26^{bc}	36.71^{bcd}	33.43^{bcd}	37.98^{bcd}	74.13^{a}	44.78^{b}	19.62^{d}	26.80^{bcd}	24.47^{cd}
Aldehydes												
2-Ethyl-2-butenal	1.51^{a}	1.12^{a}	1.14^{a}	1.36^{a}	1.70^{a}	1.26^{a}	1.42^{a}	1.43^{a}	1.26^{a}	1.39^{a}	1.47^{a}	2.15^{a}
2-Hexenal	5.84^{ab}	4.35^{b}	4.72^{b}	5.98^{ab}	4.85^{b}	5.26^{b}	6.15^{ab}	5.82^{ab}	5.03^{b}	5.55^{b}	5.84^{ab}	9.00^{a}
Nonanal	20.31^{abcd}	15.37^{cde}	16.10^{bcde}	24.48^{a}	18.40^{abcde}	18.82^{abcde}	23.03^{abc}	24.14^{ab}	18.75^{bcde}	14.58^{de}	14.18^{de}	12.02^{e}
Hexanal	131.48^{a}	131.12^{a}	130.58^{a}	130.03^{a}	131.23^{a}	132.24^{a}	131.00^{a}	129.98^{a}	130.56^{a}	131.11^{a}	128.63^{a}	130.84^{a}
Benzyl Aldehydes												
3-Ethylbenzaldehyde	8.94^{bcd}	5.35^{d}	7.71^{cd}	11.48^{abc}	8.96^{bcd}	8.44^{bcd}	10.98^{bc}	15.18^{a}	11.80^{abc}	7.98^{bcd}	8.36^{bcd}	6.91^{d}
Benzeneacetaldehyde	112.53^{bcde}	72.21^{e}	97.43^{cde}	126.75^{bcde}	161.13^{b}	136.60^{bcd}	158.82^{bc}	276.22^{a}	172.59^{b}	83.91^{de}	86.51^{de}	69.70^{e}
Amides and Furans												
Benzamide	9.97^{ab}	8.40^{b}	9.94^{ab}	10.23^{ab}	14.69^{ab}	12.25^{ab}	16.33^{a}	14.29^{ab}	11.89^{ab}	9.73^{ab}	11.13^{ab}	9.49^{ab}
N-phenyl-Formamide	12.85^{ab}	16.24^{ab}	15.69^{ab}	16.85^{ab}	9.87^{b}	22.42^{a}	11.66^{ab}	15.04^{ab}	15.37^{ab}	15.91^{ab}	14.69^{ab}	18.73^{ab}
2-Ethyl-furan	29.05^{a}	29.77^{a}	28.40^{a}	28.63^{a}	31.32^{a}	31.16^{a}	30.66^{a}	29.05^{a}	28.99^{a}	29.68^{a}	30.07^{a}	30.75^{a}
2-Pentyl-furan	5.74^{ab}	4.80^{ab}	5.02^{ab}	6.52^{ab}	5.38^{ab}	5.02^{ab}	6.79^{ab}	7.04^{a}	6.19^{ab}	5.51^{ab}	4.81^{ab}	4.54^{b}
Hydrocarbons												
1,4-Cyclohexadiene	12.21^{bcd}	6.38^{d}	10.39^{cd}	14.17^{abc}	12.84^{bcd}	11.24^{bcd}	16.01^{ab}	18.66^{a}	15.92^{ab}	10.67^{cd}	11.74^{bcd}	9.16^{d}
2-Cyclopropyl-2-pentene	19.42^{cdef}	14.51^{f}	17.05^{def}	24.41^{abc}	23.26^{abcd}	20.81^{bcdef}	26.17^{ab}	27.61^{a}	22.97^{abcde}	17.43^{def}	17.71^{def}	16.74^{ef}
Decane	21.66^{abc}	17.05^{bcd}	16.91^{bcd}	25.92^{a}	19.65^{abcd}	19.96^{abcd}	24.46^{ab}	25.57^{a}	19.90^{abcd}	15.52^{cd}	15.58^{cd}	13.10^{d}
(E)-3-Methyl-1,3,5-hexatriene	2.33^{a}	1.78^{a}	2.25^{a}	2.28^{a}	2.50^{a}	2.81^{a}	2.59^{a}	3.37^{a}	3.38^{a}	2.30^{a}	1.95^{a}	2.56^{a}
1,3-cis,5-cis-Octatriene	6.81^{cd}	5.08^{d}	5.97^{cd}	7.67^{bc}	7.42^{bc}	6.61^{cd}	8.82^{ab}	9.77^{a}	7.86^{abc}	6.49^{cd}	7.55^{bc}	6.19^{cd}
1,4-Octadiene	19.76^{abc}	8.98^{c}	14.86^{bc}	35.66^{a}	16.99^{abc}	24.25^{abc}	35.60^{a}	31.24^{ab}	22.96^{abc}	17.61^{abc}	20.19^{abc}	14.70^{abc}
2-Methyl-2-hepten-4-yne	7.40^{cde}	5.52^{e}	6.74^{de}	8.27^{bcd}	7.92^{bcd}	7.34^{cde}	9.44^{ab}	10.20^{a}	8.72^{abc}	7.30^{cde}	7.96^{bcd}	7.17^{cde}
1-Methylcyclohexene	198.20^{a}	153.05^{a}	190.83^{a}	191.56^{a}	200.03^{a}	181.60^{a}	235.55^{a}	234.54^{a}	207.13^{a}	179.01^{a}	163.04^{a}	188.81^{a}
Acyclic Monoterpenes												
2,6-Dimethyl-2,4,6-octatriene	3.89^{bcde}	2.62^{e}	3.41^{cde}	4.15^{bcde}	5.39^{b}	4.76^{bcd}	5.27^{bc}	7.65^{a}	5.56^{b}	3.20^{de}	3.78^{bcde}	2.55^{e}
cis-β-Ocimene	454.45^{b}	345.75^{b}	474.37^{ab}	435.78^{b}	442.53^{b}	526.31^{ab}	446.03^{b}	756.25^{a}	489.82^{ab}	380.42^{b}	331.10^{b}	343.47^{b}
Citronellyl Acetate	191.03^{ab}	189.75^{b}	190.81^{ab}	189.65^{b}	189.24^{b}	191.93^{ab}	191.62^{ab}	194.78^{a}	190.54^{b}	191.23^{ab}	191.00^{ab}	190.14^{ab}
Linalool	753.22^{ab}	602.95^{b}	628.48^{ab}	924.86^{a}	696.32^{ab}	714.47^{ab}	767.72^{ab}	848.92^{ab}	779.51^{ab}	650.81^{ab}	778.87^{ab}	586.82^{ab}

(Continued)

10.3389/fpls.2023.1184664

TABLE 4 Continued

Compound Name	Lighting Treatments											
	660/400/660	660/420/660	660/450/660	660/470/660	470/450/420	450/660/470	450/W/470	6B/94R	12B/88R	HPS	W/W/W	NL Control
trans-β-Ocimene	195.86^{bcd}	111.37^{d}	168.39^{bcd}	239.57^{abc}	216.57^{bcd}	232.42^{bcd}	262.02^{ab}	357.86^{a}	205.60^{bcd}	119.00^{cd}	158.82^{bcd}	117.86^{cd}
α-Ocimene	152.20^{a}	144.29^{a}	122.17^{a}	140.02^{a}	186.90^{a}	212.20^{a}	186.24^{a}	183.96^{a}	173.81^{a}	164.77^{a}	163.11^{a}	98.66^{a}
β-Myrcene	268.91^{abcd}	203.27^{d}	225.35^{bcd}	308.12^{ab}	287.72^{abcd}	271.36^{abcd}	301.56^{abc}	345.31^{a}	301.92^{abc}	245.65^{bcd}	235.39^{bcd}	216.54^{cd}
Bicyclic Monoterpenes												
3-Caren-10-al	1.70^{ab}	1.54^{ab}	1.54^{ab}	1.77^{ab}	1.61^{ab}	1.66^{ab}	2.31^{a}	2.40^{a}	1.58^{ab}	1.75^{ab}	1.95^{ab}	1.32^{b}
(+)-4-Carene	24.34^{bc}	18.67^{c}	22.85^{bc}	35.92^{ab}	32.04^{abc}	31.81^{abc}	40.76^{a}	45.46^{a}	30.60^{abc}	21.72^{bc}	21.06^{bc}	20.90^{bc}
Camphene	35.12^{bcd}	22.72^{d}	30.86^{bcd}	41.10^{ab}	35.81^{bcd}	30.27^{bcd}	51.23^{a}	51.21^{a}	38.04^{abc}	28.27^{bcd}	32.50^{bcd}	26.70^{cd}
Isoborneol	32.04^{abc}	22.05^{c}	29.66^{bc}	37.27^{abc}	28.57^{bc}	33.55^{abc}	44.80^{ab}	51.35^{a}	32.38^{abc}	30.87^{bc}	37.14^{abc}	24.62^{c}
trans-Pinocarveol	4.77^{ab}	3.12^{b}	3.67^{b}	4.68^{ab}	5.39^{ab}	5.68^{ab}	6.46^{ab}	6.36^{ab}	7.30^{a}	4.19^{ab}	3.66^{b}	6.27^{ab}
trans-Sabinene hydrate	21.66^{abc}	17.05^{bcd}	16.98^{bcd}	25.92^{a}	19.65^{abcd}	19.91^{abcd}	24.47^{ab}	25.63^{a}	19.90^{abcd}	15.51^{cd}	15.57^{cd}	13.09^{d}
α-Pinene	28.39^{bcd}	16.60^{d}	23.75^{bcd}	32.82^{ab}	29.58^{bc}	24.52^{bcd}	41.75^{a}	41.74^{a}	30.10^{abc}	22.02^{bcd}	25.19^{bcd}	20.42^{cd}
β-Pinene	155.77^{abcd}	111.86^{d}	117.45^{cd}	167.90^{abc}	170.62^{ab}	153.17^{abcd}	190.27^{a}	187.17^{a}	158.70^{abcd}	134.33^{bcd}	125.50^{bcd}	120.90^{bcd}
Cyclic Monoterpenes												
3-Menthene	35.99^{abcd}	20.38^{d}	25.47^{bcd}	31.81^{abcd}	41.70^{abcd}	39.30^{abcd}	45.50^{abc}	48.01^{ab}	53.10^{a}	29.57^{bcd}	24.96^{cd}	42.28^{abcd}
d-Limonene	308.17^{bcd}	224.30^{d}	271.77^{cd}	343.69^{abc}	331.01^{abc}	301.89^{bcd}	371.93^{ab}	401.22^{a}	341.25^{abc}	281.49^{cd}	278.99^{cd}	263.32^{cd}
Fenchyl acetate	92.03^{a}	81.94^{a}	97.62^{a}	111.13^{a}	95.53^{a}	115.00^{a}	109.94^{a}	111.16^{a}	112.12^{a}	86.90^{a}	105.84^{a}	81.22^{a}
p-Menth-1-en-8-ol	10.99^{cdef}	7.78^{f}	9.53^{ef}	13.32^{bcd}	12.78^{bcde}	11.46^{bcdef}	15.01^{ab}	17.03^{a}	14.39^{abc}	10.77^{cdef}	11.64^{bcde}	10.02^{def}
Sesquiterpene												
a-Humulene	55.29^{a}	55.99^{a}	55.79^{a}	56.25^{a}	59.41^{a}	59.01^{a}	57.52^{a}	58.82^{a}	56.25^{a}	56.05^{a}	54.51^{a}	56.36^{a}
Organosulfur												
Isothiocyanatocyclopropane	1.22^{a}	1.51^{a}	2.03^{a}	1.71^{a}	1.88^{a}	1.67^{a}	1.88^{a}	2.32^{a}	1.66^{a}	1.40^{a}	1.40^{a}	0.99^{a}
Diallyl Disulfide	0.87^{a}	0.70^{a}	0.88^{a}	0.95^{a}	0.99^{a}	1.02^{a}	1.21^{a}	1.36^{a}	0.97^{a}	0.80^{a}	2.05^{a}	0.76^{a}
Dimethyl Sulfide	64.89^{abc}	104.39^{a}	88.73^{ab}	112.47^{a}	93.37^{ab}	59.82^{abc}	88.37^{ab}	86.28^{ab}	70.26^{abc}	65.26^{abc}	45.70^{bc}	32.68^{c}
Phenylpropanoids												
Eugenol	146.53^{bcd}	178.05^{bc}	166.69^{bc}	164.96^{bc}	151.49^{bcd}	116.37^{cd}	208.47^{b}	283.16^{a}	202.84^{b}	151.32^{bcd}	165.70^{bc}	90.09^{d}
Methyl Eugenol	158.96^{a}	159.54^{a}	158.58^{a}	165.77^{a}	159.72^{a}	159.72^{a}	160.49^{a}	160.12^{a}	160.38^{a}	162.91^{a}	158.11^{a}	162.05^{a}

All concentrations are presented in micro molarity of analyte per gram of fresh mass (μM·g^{-1} FM). Mean values represent two plants per replication and ten replications per treatment. Values for each treatment are averaged across all four growing seasons. Values were analyzed using Tukey's protected least significant difference. Data in the same row followed by the same letter are not significantly different (α = 0.05).

10.3389/fpls.2023.1184664

The June and September growing seasons had the two highest concentrations and did not statistically separate. The January and April growing seasons had the two lowest concentrations and did not statistically separate. The season concentrations ranged from 0.73 μM·g^{-1} FM to 1.09 μM·g^{-1} FM (Table 3). Treatment concentrations ranged from 0.70 μM·g^{-1} FM to 1.01 μM·g^{-1} FM (Table 4).

Acyclic monoterpenes

2,6-Dimethyl-2,4,6-octatriene concentrations were significantly influenced by season (F=65.54; $P \leq 0.0001$), lighting treatment (F=12.59; $P \leq 0.0001$), and season*treatment interactions (F=3.43; $P \leq 0.0001$) (Table 2). The June growing season had the highest tissue concentration, while the lowest concentration was found in January. Each of the growing seasons statistically separated. The season concentrations ranged from 1.77 μM·g^{-1} FM to 6.30 μM·g^{-1} FM (Table 3). The 6B/94R treatment had the highest tissue concentration, which statistically separated from all other treatments. The NL control had the lowest concentration of any treatment, and did not statistically separate from many of the LED treatments as well as the HPS and W/W/W treatments. The treatment tissue concentrations ranged from 2.55 μM·g^{-1} FM to 7.65 μM·g^{-1} FM (Table 4).

cis-β-Ocimene concentrations were significantly influenced by season (F=48.61; $P \leq 0.0001$), lighting treatment (F=3.18; P=0.0004), and season*treatment interactions (F=1.81; P=0.0048) (Table 2). The June growing season had the highest tissue concentration, while the lowest concentration was found in September. Each of the growing seasons statistically separated. The season concentrations ranged from 145.81 μM·g^{-1} FM to 754.18 μM·g^{-1} FM (Table 3). The 6B/94R treatment again had the highest tissue concentrations, and statistically separated from some of the LED treatments as well as the HPS and W/W/W treatments. The NL control had the lowest concentration, but did not separate from the broadband treatments and many of the LED treatments. The treatment tissue concentrations ranged from 343.47 μM·g^{-1} FM to 756.25 μM·g^{-1} FM (Table 4).

Citronellyl Acetate concentrations were significantly influenced by season (F=13.31; $P \leq 0.0001$), lighting treatment (F=2.7; P=0.0024), and season*treatment interactions (F=1.75; P=0.0085) (Table 2). The June growing season had the highest tissue concentration, while the lowest concentration was found in January. September statistically separated from June and January, but not from the April growing season. The season concentrations ranged from 188.27 μM·g^{-1} FM to 193.66 μM·g^{-1} FM (Table 3). The 6B/94R treatment had the highest tissue concentrations, and statistically separated from some of the LED treatments, but not the NL control or broadband treatments. The high blue 470/450/420 treatment had the lowest concentration, but only separated from the 6B/94R treatment. The treatment tissue concentrations ranged from 189.24 μM·g^{-1} FM to 194.78 μM·g^{-1} FM (Table 4).

Linalool concentrations were significantly influenced by season (F=47.53; $P \leq 0.0001$), lighting treatment (F=2.17; P=0.0152), and season*treatment interactions (F=1.57; P=0.0262) (Table 2). The January growing season had the highest tissue concentration, while the lowest concentration was found in September. January, April, and June all statistically separated from September, but not from each other. The season concentrations ranged from 239.32 μM·g^{-1} FM to 925.12 μM·g^{-1} FM (Table 3). The 660/470/660 treatment had the highest tissue concentrations, but only statistically separated from the 660/420/660 treatment; none of the other treatments showed statistical separation. The treatment tissue concentrations ranged from 602.95 μM·g^{-1} FM to 924.86 μM·g^{-1} FM (Table 4).

trans-β-Ocimene concentrations were significantly influenced by season (F=80.44; $P \leq 0.0001$), lighting treatment (F=6.97; $P \leq 0.0001$), and season*treatment interactions (F=3.19; $P \leq 0.0001$) (Table 2). The June growing season had the highest tissue concentration, while the lowest concentration was found in September. September statistically separated from June and April, but not from the January growing season. The season concentrations ranged from 57.16 μM·g^{-1} FM to 351.14 μM·g^{-1} FM (Table 3). The 6B/94R treatment had the highest tissue concentrations, and statistically separated from all the other treatments except for 450/W/470. Many of the LED treatments do not show separation among themselves. The lowest concentration was found in the 660/420/660 treatment, but it did not separate from the NL control, many narrowband treatments, and the HPS and W/W/W treatments. The treatment tissue concentrations ranged from 111.37 μM·g^{-1} FM to 357.86 μM·g^{-1} FM (Table 4).

α-Ocimene concentrations were significantly influenced by season (F=195.03; $P \leq 0.0001$) and season*treatment interactions (F=2.00; P=0.0011), but not by treatment (F=1.29; P=0.2295) (Table 2). The September growing season had the highest tissue concentration, while the lowest concentration was found in April. September separated from the other seasons, but the January, April, and June seasons did not separate amongst themselves. September had approximately 5-20x tissue concentrations compared to other seasons. The season concentrations ranged from 75.23 μM·g^{-1} FM to 493.99 μM·g^{-1} FM (Table 3). Treatments did not statistically separate, and tissue concentrations ranged from 98.66 μM·g^{-1} FM to 212.20 μM·g^{-1} FM (Table 4).

β-Myrcene concentrations were significantly influenced by season (F=268.9; $P \leq 0.0001$), lighting treatment (F=5.15; $P \leq 0.0001$), and season*treatment interactions (F=2.83; $P \leq 0.0001$) (Table 2). The June growing season had the highest tissue concentration, while the lowest concentration was found in September. June did not statistically separate from April; September statistically separated from all other treatments and had drastically lower concentrations when compared to other seasons. The season concentrations ranged from 9.36 μM·g^{-1} FM to 407.65 μM·g^{-1} FM (Table 3). The 6B/94R treatment had the highest tissue concentrations, and statistically separated from the NL control, HPS, and W/W/W treatments. The 660/420/660 treatment had the lowest concentration, which separated from the 660/470/660, 450/W/470, and PhysioSpec treatments. The treatment tissue concentrations ranged from 203.27 μM·g^{-1} FM to 345.31 μM·g^{-1} FM (Table 4).

Bicyclic monoterpenes

3-Caren-10-al concentrations were significantly influenced by season (F=17.21; $P \leq 0.0001$) and treatment (F=2.24; P=0.0123), but not by season*treatment interactions (F=1.06; P=0.3871) (Table 2). The September growing season had the highest concentration and was statistically separated from the lowest season, which was April. Season concentrations ranged from 1.21 μM·g^{-1} FM to 2.51 μM·g^{-1} FM (Table 3). The treatments 450/W/470 and 6B/94R were both significantly higher than the NL control, but the other treatments did not separate statistically. The treatment concentrations ranged from 1.32 μM·g^{-1} FM to 2.40 μM·g^{-1} FM (Table 4).

(+)-4-Carene concentrations were significantly influenced by season (F=27.75; $P \leq 0.0001$), lighting treatment (F=7.00; $P \leq 0.0001$), and season*treatment interactions (F=1.57; P=0.0254) (Table 2). The June growing season had the highest tissue concentration, while the lowest concentration was found in January. All of the season concentration averages statistically separated from each other. The season concentrations ranged from 16.93 μM·g^{-1} FM to 61.46 μM·g^{-1} FM (Table 3). The 6B/94R treatment had the highest tissue concentrations, and statistically separated from the NL control, HPS, and W/W/W treatments. The 660/420/660 treatment had the lowest concentration, which separated from the 660/470/660, 450/W/470, and 6B/94R treatments. The treatment tissue concentrations ranged from 18.67 μM·g^{-1} FM to 45.46 μM·g^{-1} FM (Table 4).

3-Carene concentrations were significantly influenced by season (F=24.28; $P \leq 0.0001$) and season*treatment interactions (F=2.35; P=0.0005), but not by lighting treatment (F=4.53; P=0.0521) (Table 2). The June growing season had the highest tissue concentration, but did not statistically separate from April or September. January growing season had the lowest concentration, separating from the other seasons. The season concentrations ranged from 379.21 μM·g^{-1} FM to 559.24 μM·g^{-1} FM (Table 3).

Camphene concentrations were significantly influenced by season (F=70.69; $P \leq 0.0001$), lighting treatment (F=9.41; $P \leq 0.0001$), and season*treatment interactions (F=1.52; P=0.0356) (Table 2). The September growing season had the highest tissue concentration, while the lowest concentration was found in January. The September season statistically separated from the other seasons, but January, April, and June did not separate amongst themselves. The season concentrations ranged from 23.41 μM·g^{-1} FM to 55.77 μM·g^{-1} FM (Table 3). The 450/W/470 treatment had the highest tissue concentrations, but did not statistically separate from the PhysioSpec and 660/470/660 treatments; the 450/W/470 did separate from the HPS, W/W/W, and NL control. The 660/420/660 treatment had the lowest concentration, which separated from the 660/470/660, 450/W/470, and PhysioSpec treatments. The treatment tissue concentrations ranged from 22.72 μM·g^{-1} FM to 51.23 μM·g^{-1} FM (Table 4).

Isoborneol concentrations were significantly influenced by season (F=22.21; $P \leq 0.0001$), lighting treatment (F=3.85; $P \leq 0.0001$), and season*treatment interactions (F=1.51; P=0.0367) (Table 2). The September growing season had the highest tissue concentration, while the lowest concentration was found in April. September, June, and April all statistically separated, but January did not separate from June and April. The season concentrations ranged from 23.53 μM·g^{-1} FM to 49.74 μM·g^{-1} FM (Table 3). The 6B/94R treatment had the highest tissue concentrations, and statistically separated from the NL control and HPS treatments, as well as some of the LED treatments. The 660/420/660 treatment had the lowest concentration, which did not separate from the NL control and the majority of LED treatments. The treatment tissue concentrations ranged from 22.05 μM·g^{-1} FM to 51.35 μM·g^{-1} FM (Table 4).

trans-Pinocarveol concentrations were significantly influenced by season (F=7.36; $P \leq 0.0001$), lighting treatment (F=3.32; P=0.0002), and season*treatment interactions (F=1.89; P=0.00027) (Table 2). The September growing season had the highest tissue concentration, while the lowest concentration was found in January. The season concentrations ranged from 3.60 μM·g^{-1} FM to 6.13 μM·g^{-1} FM (Table 3). The 6B/94R treatment again had the highest tissue concentrations, which separated from the 660/420/660, 660/450/660, and W/W/W treatments. The 660/420/660 treatment had the lowest concentration, but the only treatment that was statistically significantly different was the 6B/94R treatment. The treatment tissue concentrations ranged from 3.12 μM·g^{-1} FM to 7.30 μM·g^{-1} FM (Table 4).

trans-Sabinene hydrate concentrations were significantly influenced by season (F=158.38; $P \leq 0.0001$), lighting treatment (F=5.80; $P \leq 0.0001$), and season*treatment interactions (F=2.66; $P \leq 0.0001$) (Table 2). The June growing season had the highest tissue concentration, while the lowest concentration was found in January. September and January did not statistically separate. The season concentrations ranged from 10.04 μM·g^{-1} FM to 37.07 μM·g^{-1} FM (Table 3). The 660/470/660 treatment had the highest tissue concentrations, and statistically separated from the NL control, HPS, and W/W/W treatments. The 660/470/660 treatment did not separate from the 6B/94R treatment and some of the other LED treatments. The lowest concentration was found in the NL control, which did not separate from the HPS and W/W/W treatments. The treatment tissue concentrations ranged from 13.09 μM·g^{-1} FM to 25.92 μM·g^{-1} FM (Table 4).

α-Pinene concentrations were significantly influenced by season (F=73.74; $P \leq 0.0001$), lighting treatment (F=9.4; $P \leq 0.0001$), and season*treatment interactions (F=1.65; P=0.0152) (Table 2). The September growing season had the highest tissue concentration, while the lowest concentration was found in January. All of the season concentration averages statistically separated, except for April and June. The season concentrations ranged from 17.27 μM·g^{-1} FM to 46.27 μM·g^{-1} FM (Table 3). The 450/W/470 and 6B/94R treatments had the highest tissue concentrations and were not statistically separate. The 660/420/660 treatment again had the lowest concentration, which separated from the 660/470/660, 470/450/420, 450/W/470, and PhysioSpec treatments. The 660/420/660 treatment did not separate from the HPS, W/W/W, or the NL control. The treatment tissue concentrations ranged from 16.60 μM·g^{-1} FM to 41.75 μM·g^{-1} FM (Table 4).

β-Pinene concentrations were significantly influenced by season (F=49.46; $P \leq 0.0001$), lighting treatment (F=5.93; $P \leq 0.0001$), and season*treatment interactions (F=1.86; P=0.0032) (Table 2). β-Pinene followed a similar pattern to α-Pinene for both season

and lighting treatment concentration. In addition, the ratio of α-Pinene to β-Pinene varied less than 8% across all treatments and seasons, and did not show any discernable pattern. The September growing season had the highest tissue concentration, while the lowest concentration was found in January. All of the season concentration averages statistically separated, except for April and June. The season concentrations ranged from 99.30 $\mu M \cdot g^{-1}$ FM to 208.12 $\mu M \cdot g^{-1}$ FM (Table 3). The 450/W/470 and 6B/94R treatments again had the highest tissue concentrations and were not statistically separate. The 660/420/660 treatment again had the lowest concentration, which separated from the 660/470/660, 470/450/420, 450/W/470, and 6B/94R treatments. The 660/420/660 treatment did not separate from the HPS, W/W/W, or the NL control. The treatment tissue concentrations ranged from 111.86 $\mu M \cdot g^{-1}$ FM to 190.27 $\mu M \cdot g^{-1}$ FM (Table 4).

Cyclic monoterpenes

3-Menthene concentrations were significantly influenced by season (F=10.23; $P \leq 0.0001$), lighting treatment (F=4.23; $P \leq 0.0001$), and season*treatment interactions (F=2.34; $P \leq 0.0001$) (Table 2). The June growing season had the highest tissue concentration, while the lowest concentration was found in January. The January growing season separated from the other seasons, but April, June, and September did not separate amongst themselves. The season concentrations ranged from 24.22 $\mu M \cdot g^{-1}$ FM to 46.11 $\mu M \cdot g^{-1}$ FM (Table 3). The 12B/88R treatment had the highest tissue concentrations and separated from the HPS, and W/W/W, but not the NL control. The 660/420/660 treatment again had the lowest concentration, which separated from the 450/W/470 PhysioSpec treatments. The 660/420/660 treatment did not separate from the HPS, W/W/W, or the NL control. The treatment tissue concentrations ranged from 20.38 $\mu M \cdot g^{-1}$ FM to 53.10 $\mu M \cdot g^{-1}$ FM (Table 4).

d-Limonene concentrations were significantly influenced by season (F=29.8; $P \leq 0.0001$), lighting treatment (F=7.17; $P \leq 0.0001$), and season*treatment interactions (F=1.74; P=0.0076) (Table 2). The June growing season had the highest tissue concentration, while the lowest concentration was found in January. All of the season concentration averages statistically separated, except for April and September. The season concentrations ranged from 234.61 $\mu M \cdot g^{-1}$ FM to 387.51 $\mu M \cdot g^{-1}$ FM (Table 3). The 6B/94R treatment had the highest tissue concentration and was separated from the HPS, W/W/W, and NL control. The 660/420/660 treatment had the lowest concentration, which separated from the 660/470/660, 470/450/420, 450/W/470, and PhysioSpec treatments. The 660/420/660 treatment did not separate from the HPS, W/W/W, or the NL control. The treatment tissue concentrations ranged from 224.30 $\mu M \cdot g^{-1}$ FM to 401.22 $\mu M \cdot g^{-1}$ FM (Table 4).

Fenchyl acetate concentrations were significantly influenced by season (F=14.98; $P \leq 0.0001$), but not by lighting treatment (F=1.58; P=0.1019) or season*treatment interactions (F=0.62; P=0.9467) (Table 2). The April growing season had the highest tissue concentration, but it did not statistically separate from the January or June seasons. The lowest concentrations were found in the September season. The season concentrations ranged from 81.12 $\mu M \cdot g^{-1}$ FM to 149.80 $\mu M \cdot g^{-1}$ FM (Table 3). The treatment tissue concentrations did not statistically separate and ranged from 81.22 $\mu M \cdot g^{-1}$ FM to 115.00 $\mu M \cdot g^{-1}$ FM (Tables 2, 4).

p-Menth-1-en-8-ol concentrations were significantly influenced by season (F=173.75; $P \leq 0.0001$), lighting treatment (F=10.61; $P \leq 0.0001$) and season*treatment interactions (F=2.56; $P \leq 0.0001$) (Table 2). The June growing season had the highest tissue concentration, while the lowest concentration was found in January. All of the season concentration averages statistically separated. The season concentrations ranged from 5.44 $\mu M \cdot g^{-1}$ FM to 19.69 $\mu M \cdot g^{-1}$ FM (Table 3). The 6B/94R treatment had the highest tissue concentration and was separated from the HPS, W/W/W, and NL control. The 660/420/660 treatment had the lowest concentration, which separated from the 660/470/660, 470/450/420, 450/W/470, and PhysioSpec treatments. The 660/420/660 treatment did not separate from the HPS or the NL control, as well as a few LED treatments. The treatment tissue concentrations ranged from 7.78 $\mu M \cdot g^{-1}$ FM to 17.03 $\mu M \cdot g^{-1}$ FM (Table 4).

Sesquiterpenes

α-Humulene concentrations were significantly influenced by season (F=19.58; $P \leq 0.0001$) and lighting treatment (F=1.87; P=0.0420), but not by season*treatment interactions (F=1.12; P=0.3001) (Table 2). The September growing season had the highest tissue concentration, but did not separate from the June season. While the lowest concentration was found in January, it did not statistically separate from April. The season concentrations ranged from 53.69 $\mu M \cdot g^{-1}$ FM to 59.58 $\mu M \cdot g^{-1}$ FM (Table 3). The treatment tissue concentrations did not show statistical separation and ranged from 54.51 $\mu M \cdot g^{-1}$ FM to 59.41 $\mu M \cdot g^{-1}$ FM (Tables 2, 4).

Organosulfur

Isothiocyanatocyclopropane concentrations were significantly influenced by season (F=9.92; $P \leq 0.0001$), but not by lighting treatment (F=1.69; P=0.0752) or season*treatment interactions (F=0.85; P=0.7103) (Table 2). The September growing season had the highest tissue concentration, while the lowest concentration was found in April. The season concentrations ranged from 1.20 $\mu M \cdot g^{-1}$ FM to 2.28 $\mu M \cdot g^{-1}$ FM (Table 3). The treatment tissue concentrations did not show statistical separation, and ranged from 0.99 $\mu M \cdot g^{-1}$ FM to 2.32 $\mu M \cdot g^{-1}$ FM (Table 4).

2-Isobutylthiazole concentrations were significantly influenced by season (F=10.79; $P \leq 0.0001$), but not by lighting treatment (F=1.90; P=0.0591) or season*treatment interactions (F=1.23; P=0.2101) (Table 2). The September growing season had the highest tissue concentration, but did not statistically separate from the June season. The lowest concentration was found in January, but it did not separate from the April season. The season concentrations ranged from 5.57 $\mu M \cdot g^{-1}$ FM to 8.94 $\mu M \cdot g^{-1}$ FM (Table 3).

Dimethyl Sulfide concentrations were significantly influenced by season (F=25.15; $P \leq 0.0001$), lighting treatment (F=4.30; $P \leq 0.0001$), and season*treatment interactions (F=2.09; P=0.0005) (Table 2). The April growing season had the highest tissue concentration and statistically separated from all other seasons. The lowest season concentration was found in January, which also separated from all other seasons. The season concentrations ranged from 43.42 $\mu M \cdot g^{-1}$ FM to 121.98 $\mu M \cdot g^{-1}$ FM (Table 3). The 660/470/660 treatment had the highest tissue concentration and was separated from the W/W/W and NL control. The NL control had the lowest concentration, which separated from some of the narrowband treatments. The treatment tissue concentrations ranged from 32.68 $\mu M \cdot g^{-1}$ FM to 112.47 $\mu M \cdot g^{-1}$ FM (Table 4).

Phenylpropanoids

Eugenol concentrations were significantly influenced by season (F=130.1; $P \leq 0.0001$), lighting treatment (F=9.94; $P \leq 0.0001$), and season*treatment interactions (F=4.43; $P \leq 0.0001$) (Table 2). The June growing season had the highest tissue concentration, while the lowest concentration was found in January. All of the season tissue concentration averages statistically separated. The season concentrations ranged from 43.16 $\mu M \cdot g^{-1}$ FM to 280.02 $\mu M \cdot g^{-1}$ FM (Table 3). The 6B/94R treatment had the highest tissue concentration and separated from all other treatments. The NL control had the lowest concentration, which separated from the 660/420/660, 660/450/660, 660/470/660, 470/450/420, 450/W/470, W/W/W, and PhysioSpec treatments. The treatment tissue concentrations ranged from 90.09 $\mu M \cdot g^{-1}$ FM to 283.16 $\mu M \cdot g^{-1}$ FM (Table 4).

Methyl Eugenol concentrations were significantly influenced by season (F=7.95; $P \leq 0.0001$), but not by lighting treatment (F=1.7; P=0.0997) or season*treatment interactions (F=1.5; P=0.1545) (Table 2). The September growing season had the highest tissue concentration, but did not statistically separate from the June season. The lowest concentration was found in January, but did not separate from April. The season concentrations ranged from 131.23 $\mu M \cdot g^{-1}$ FM to 172.11$\mu M \cdot g^{-1}$ FM (Table 3). The treatment tissue concentrations ranged from 158.11 $\mu M \cdot g^{-1}$ FM to 165.77 $\mu M \cdot g^{-1}$ FM (Table 4).

Principal component analysis

A principal component analysis (PCA) comparison of key PVOCs and lighting treatments, represented using a biplot, revealed that two components with eigenvalues > 1 accounted for 60.0% of the total data variability (Figure 5). Component 1 accounted for 42.1% of the variability, while component 2 accounted for 17.9% of the data variability. Many key volatile compounds were positive discriminating factors for component 1 of varying magnitudes, while component 2 evenly separated compounds into positive and negative discriminating factors of various magnitudes. Quadrant I contained positive discriminating factors for both component 1 and component 2, which were the aroma compounds: (E)-2-Hexenal, α-Humulene, 3-Caren-10-al, Camphene, Linalool, α-Pinene, β-Pinene, d-Limonene, p-Menth-1-en-8-ol, 3-Carene, and Eugenol. Concentration increases of these compounds were generally associated with the narrowband LED treatments 470/450/420, 660/470/660, and 660/400/660. Quadrant II and Quadrant III do not contain any of the key aroma compounds and reveal that 450/660/470, 660/420/660, HPS, W/W/W, NL Control, and 660/450/660 are negatively associated with concentration increases of many key aroma volatiles, at various weights. Quadrant IV contained positive discriminating factors for component 1 and negative discriminating factors for component 2, which included the aroma compounds: 2-Phenyl Ethanol, 1-Octen-3-ol, 2-Octyn-1-ol, Benzeneacetaldehyde, trans-Sabinene hydrate, Nonanal, β-Myrcene, and Linalool. Concentration increases of these compounds were generally associated with the PhysioSpec (6B/94R, 12B/88R) and 450/W/470 treatments (Figure 5).

Discussion

Light plays a critical role in the growth and development of many crops, including sweet basil. Spectral quality has a significant impact on secondary metabolism, which can directly influence the concentration of flavor and aroma compounds in plant tissues. Leveraging environmental controls and applying abiotic stressors has the ability to influence the secondary metabolism of high-value specialty crops. The results of this study demonstrate that spectral quality manipulations of supplemental greenhouse lighting can directly influence tissue concentrations of key aroma volatiles and other secondary metabolites in sweet basil. Total basil tissue VOC concentrations, in addition to many of the concentrations of specific volatile compounds, were significantly impacted by the growing season and lighting treatment.

In Figure 3, total VOC concentrations are displayed based on lighting treatment and have been broken down into their respective compound classes. All of the SL treatments provide the same intensity (100 $\mu mol \cdot m^{-2} \cdot s^{-1}$) for the same duration (24 h); this isolates SL spectral quality as a primary independent variable, while the non-supplemented NL control provides a baseline to compare treatments. Statistical analysis reveals that total VOC concentrations separated across lighting treatments, and a few general patterns emerge.

First, the 6B/94R treatment had the highest total VOC concentration, but did not statistically separate from the 12B/88R treatment. The total VOC concentration of the 450/660/470 (i.e., 2B:1R or 66.6B/33.3R) was significantly lower than the 6B/94R treatment, but did not separate from the 12B/88R treatment. In one recent study with green basil (*Ocimum basilicum* L.), the chemical composition of essential oil and total phenolic content was improved by growing plants under 30B/70R light when compared to monochromatic, dichromatic, and broadband sources (Hosseini et al., 2018). Pennisi et al. also found that a ratio of 3 R:B (i.e., 1B:3R) was ideal for resource use efficiency and flavor volatile production in basil (*Ocimum basilicum* L.) (Pennisi et al., 2019a). Our group determined that for 'Genovese' sweet basil (*Ocimum basilicum* L.), maximum concentrations for key compounds varied among narrowband lighting treatment, but most monoterpenes and diterpenes evaluated were highest under a SL treatment of 20B/

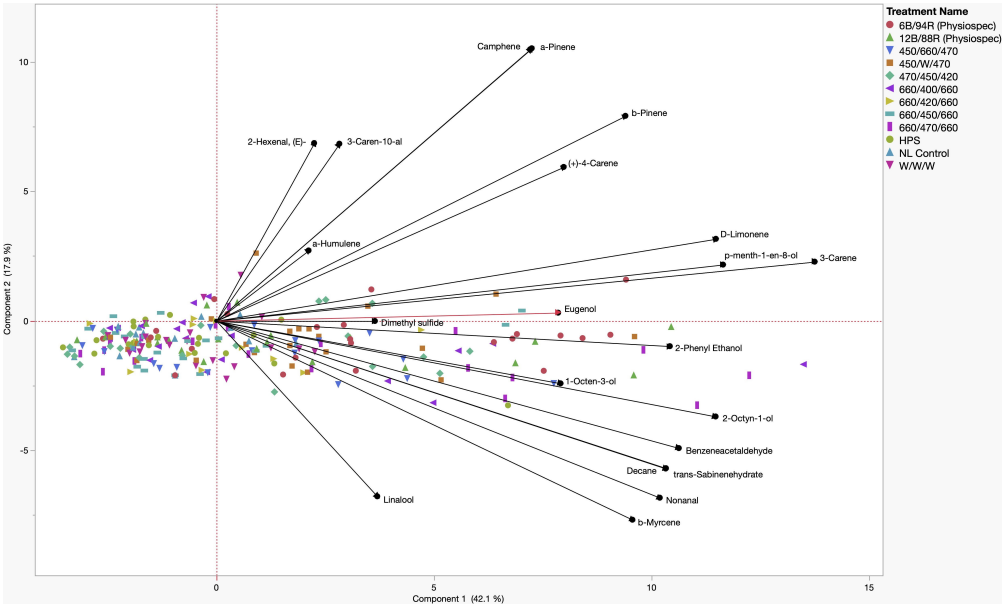

FIGURE 5
Principal Component Analysis (PCA) showing the biplot differentiation between sweet basil 'Italian Large Leaf' (*Ocimum basilicum* L.) aroma compound concentrations (black) grown under various supplemental lighting treatments.

80R to 50B/50R (Hammock et al., 2021). When comparing previous studies, it is clear that light-mediated responses (i.e., isoprenoid and phenylpropanoid metabolism changes based on B:R ratio) are species and even variety-specific (Taulavuori et al., 2016b; Toscano et al., 2021). Based on the results of this experiment and current literature, we recommend supplemental narrowband B:R ratios between 20B/80R and 5B/95R (i.e., 1B:4R to 1B:20R) with the intensity of 100-200 $\mu mol \cdot m^{-2} \cdot s^{-1}$ for 12-24 h daily for high-value specialty crops under standard greenhouse conditions, with direct consideration of the unique ambient spectra and DLI provided for any given location and growing season. Further studies should also be conducted on different varieties of basil and other high-value specialty crop species to determine ideal supplemental B:R ratios.

Second, the high blue treatment (470/450/420) performed as well as the 2B:1R narrowband treatment (450/660/470). It has generally been shown that high intensities of blue wavelengths promote the synthesis of many phenols and terpenoids (Colquhoun et al., 2013; Carvalho et al., 2016; Taulavuori et al., 2016b; Toscano et al., 2021; Kivimaenpa et al., 2022). That being said, it is likely that the ambient solar spectrum during the natural daylight hours was sufficient to provide additional wavelengths necessary for normal physiological function and secondary metabolite concentrations as observed in this experiment. Some studies have shown that monochromatic or dichromatic sole-source lighting can be detrimental to primary and secondary metabolic function (Carvalho et al., 2016; Jishi et al., 2016; Kong et al., 2019). Adding small amounts of discrete wavelengths relative to the total intensity of the ambient spectrum has potential to impart desirable secondary metabolic effects while minimizing electrical energy use.

Third, the total VOC concentrations of the four 1B:2R treatments (660/400/660, 660/420/660, 660/450/660, and 660/470/660) each statistically separated from each other. The 660/470/660 had the highest total concentrations, while the 660/420/660 had the lowest. This demonstrates the impact of discrete narrowband blue wavelengths (with the same spectra/intensity of red wavelengths) on total VOC concentration. The 660/470/660 treatment was the only 1B:2R treatment to statistically separate from the NL control. A sole-source lighting study found that several quality parameters and secondary metabolite concentrations in basil (*Ocimum basilicum* L.) and strawberry (*Fragaria x ananassa*) were improved by using a 0.7 R:B ratio (i.e., 1.4B:1R) (Piovene et al., 2015). A study comparing natural light under standard greenhouse conditions to indoor sole-source lighting treatments determined significant increases to monoterpene concentrations when using blue/red/yellow and blue/red/green in growth chambers (Carvalho et al., 2016). A similar indoor lighting study found that using broadband sources with higher intensities of blue wavelengths (i.e., 1B:2.5R vs. 1B:4R) influenced terpenoid and phenylpropanoid concentrations in relation to phenolic acids (Kivimaenpa et al., 2022). This further demonstrates the wide range of effects from sole source, and SL can be species and variety-specific.

This study differs from many previous studies evaluating basil aroma volatiles in that sole-source lighting is utilized as compared to supplementing the natural solar spectrum with specific wavebands. The ambient solar spectra, as well as differing species-specific light mediated responses it imparts, adds an additional layer of complexity. Determining the influence of varying light spectra with and without ambient solar spectra, as well as comparing both, will improve our understanding of plant/light interaction as well as help commercial growers in both indoor farm and greenhouse operations.

Based on this comparison of discrete blue wavelengths, if using supplemental narrowband B/R lighting for sweet basil production, we also recommend 450 nm blue additions to 660 nm red (± 20 nm) for ideal total VOC bioaccumulation in basil, using the aforementioned B:R ratio range (i.e., 1B:4R to 1B:20R). Further

evaluation is warranted on 420 nm in relation to VOC profiles. The wavelengths around 420 nm have been shown to promote VOCs and other secondary metabolites (Singh et al., 2015; Hasan et al., 2017; Ueda et al., 2021). The 660/420/660 actually produced the lowest total VOC concentration, and was statistically lower than many of the narrowband treatments. Further, it did not statistically separate from the NL control. It is likely that the 420 nm wavelengths promoted the production of other non-volatile secondary metabolites which are not detectable using HS GC-MS, such as carotenoids and flavonoids. Additional experiments evaluating the entire secondary metabolome with various analytical techniques in addition to metabolomics and/or transcriptomics would further elucidate the specific regulation of key pathways. It is also pertinent for future studies to incorporate both primary and secondary metabolic data to determine further resource allocation based on light responses.

Fourth, the broadband spectrum lighting treatments had mixed performance in terms of total VOC concentration. The HPS and W/W/W treatments did not statistically separate from the NL control. The high-blue broad-spectrum treatment (450/W/470) actually had the second-highest total VOC concentration, and did not statistically separate from the 6B/94R and 12B/88R treatments. Further exploration into specific intensities of discrete narrowband wavelengths within broad-spectrum supplement lighting, specifically blue wavelengths, is needed. Additionally, the color temperature (i.e., Kelvin) of broadband white light, should be evaluated in terms of secondary metabolic resource allocation.

Figure 4 shows total VOC concentrations based on the growing season and have been broken down into their respective compound classes. All of the total VOC concentrations statistically separated across the growing season. In the order of highest to lowest total VOC concentrations, June had the highest total VOC concentration (6140 $\mu M \cdot g^{-1}$ FM), April had the second highest total VOC concentration (5015 $\mu M \cdot g^{-1}$ FM), January had the third highest total VOC concentration (3840 $\mu M \cdot g^{-1}$ FM), and finally, September had the lowest concentration (2760 $\mu M \cdot g^{-1}$ FM). Greenhouse growing conditions and environmental parameters were similar for all four growing seasons in this experiment (Table 1). The non-supplemented NL control provides a baseline to compare across all seasons. Greenhouse day and night temperatures were held constant within 2 °C across all growing seasons, which isolates two of the primary independent variables utilized in this experiment: change in spectral quality from ambient sunlight across growing seasons and change in total DLI from ambient sunlight across growing seasons. It would generally be expected that increasing the DLI from ambient sunlight would indirectly increase total volatile concentration, due to the increased primary metabolic capacity and ability to allocate additional resources to secondary pathways (Faust et al., 2005; Garland et al., 2010; Currey and Lopez, 2015). That being said, it was interesting to see that September had the second-highest DLI, but the lowest total VOC concentration. Additionally, January had the lowest DLI, but had the third-highest total VOC concentration. June had the highest DLI, as well as the highest total VOC concentration (Table 4). This indicates that the change in both total DLI and spectral quality of the ambient sunlight across growing seasons directly influences total VOC concentrations.

The June growing seasons generally had the highest tissue concentrations of specific volatile compounds, while January generally had the lowest concentrations. Many of the compounds followed the trend of higher tissue concentrations as the average total growing season DLI increased. That being said, some notable exceptions do not trend with seasonal DLI, demonstrating the complex interaction between seasonal spectral quality and secondary metabolism. These exceptions can be separated into three groups. First, the compounds 2-Octyn-1-ol, Nonanal, cis-β-Ocimene, Linalool, and β-Myrcene had the lowest concentrations in the September growing season rather than the January growing season. Second, the compounds 3-Caren-10-al, Camphene, Isoborneol, α-Pinene, and β-Pinene all had the highest concentrations in the September growing season rather than June growing season. Third, Dimethyl Sulfide was the only compound in this experiment to have the highest tissue concentration in the April growing season, rather than the June growing season. It was interesting to observe the various effects on compounds across different classes and metabolic pathways, which warrants further exploration using analytical techniques as well as metabolomics.

For many of the statistically significant compounds evaluated in this study, the 6B/94R treatment produced the highest concentrations, while the lowest was generally observed in the 660/420/660 treatment. 16 VOCs were determined to be responsible for approximately 90% of the total response area as well as variations in the aromatic profile, which is in agreement with a similar experiment (Pennisi et al., 2019a). Four compounds deviated from this pattern, all of which have proven significant in sensory perception for sweet basil.

Nonanal has a strong and unmistakable scent. Its aroma is described as fatty, citrusy orange peel with notes of sweet floral and rose petals. It adds warmth to fragrances, boosts freshness in floral compositions, and offers a distinctive aldehydic odor. Nonanal rounds off the smell of perfumes and helps make them more palatable to the nose. It also has the ability to lend its waxy character to other flavors, giving it a unique sensorial appeal (Sell, 2019). The highest tissue concentration of Nonanal was found under the 660/470/660 treatment, which was more than double the concentration found in the NL control.

Linalool is a naturally occurring terpene found in many flowers, spices, and other higher plants. The aroma of linalool is described as sweet, fruity, floral, and herbaceous. It has citrus and spice notes, with a light woodsy character reminiscent of lavender and bergamot oil. Linalool is commonly found in herbs such as oregano, thyme, marjoram, rosemary, and basil (Meligaard et al., 2007; Sell, 2019). Linalool tissue concentrations were highest in the 660/470/660, while the lowest was under the 660/420/660 treatment; these were the only two treatments that statistically separated for Linalool.

Dimethyl Sulfide has a strong, pungent aroma that can be described as earthy, fishy, or sulfuric. It is often compared to the smell of cooked cabbage and is used as an ingredient in certain types of food flavorings. It has high bioactivity and can be detected in extremely small concentrations, even at concentrations below 0.1 ppm; relatively low concentrations can lead to negative sensory perception in humans (Meligaard et al., 2007; Sell, 2019). Interestingly, the highest concentration was found in the 660/470/

660, but was only statistically separate from the W/W/W and the NL control. It should be noted that the addition of narrowband LED treatments directly increased the concentration of this negatively perceived compound, while the same intensity of broad-spectrum white light (W/W/W) was statistically lower. The broad spectrum white and the NL control, despite different DLIs, did not statistically separate, suggesting that spectral quality has a greater influence on Dimethyl Sulfide tissue concentrations than DLI. Other sulfur compounds in this experiment did not show statistically significant differences in concentration across lighting treatments.

Eugenol is a phenylpropanoid with a sweet, spicy, nutty, and woody aroma, with notes of clove, cinnamon, and allspice. Its scent is reminiscent of bay leaf and is often used as a food flavoring. Eugenol is known for its antimicrobial properties and therapeutic properties. It has been used to create unique perfumes, adding depth and complexity to scents, especially those with a floral or citrus character. It is commonly used to flavor commercially produced food products (Lawless, 2010; Sell, 2019). The highest tissue concentrations were found under the 6B/94R treatment, while the lowest concentrations were found under the NL control, an almost 3.5x difference. The 660/420/660 treatment did not statistically separate from any of the other LED treatments or the NL controls. Additionally, Methyl Eugenol, the synthesis of which is directly related to Eugenol, was not statistically significant across lighting treatments.

Four terpenoid compounds of key aroma volatiles, consisting of different chemical classes at various points within the isoprenoid pathway, followed the same general pattern across lighting treatments. These include α-Pinene, β-Pinene, Camphene, and d-Limonene.

α-Pinene and β-Pinene are two isomers found ubiquitously in nature, most notably in the essential oils of coniferous trees. α-pinene has a sharp, piney aroma. β-pinene, on the other hand, has an earthy and herbaceous scent reminiscent of rosemary and sage. The main difference between these two terpenes is their perceived intensity, as α-Pinene's sharp and intense aroma stands out from β-pinene's more subtle earthy notes. Both terpenes have significant culinary and therapeutic potential (Sell, 2019).

Camphene has a strong, piney, camphoraceous aroma with hints of fir and spices. It is often described as having citrus notes with an underlying musky sweetness. Camphene is used in perfume creation to add a woody and earthy edge to fragrances, particularly those with fresh and herbal elements. Camphene accentuates other flavors like citrus, mint, and earthy notes in food flavorings (Lawless, 2010; Sell, 2019).

d-Limonene has a strong and distinct citrus scent reminiscent of oranges and lemons. It is often described as having a distinctive sweet orange aroma, with notes of lemon and lime. d-Limonene is used in the production of perfumes, cosmetics, food flavorings, and cleaning products due to its pleasant smell. Despite being an undernote of basil aroma, it still plays a significant role in the overall aroma perception of some sweet basil varieties (Lawless, 2010; Sell, 2019).

These four terpenoid compounds all have various physical and chemical properties and reside at different locations within the isoprenoid pathway, but generally maintain the same pattern across lighting treatments. This suggests that these pathways are receiving more upstream products to the biosynthesis of some terpenoid compounds (i.e., resource allocation is being shifted to terpenoid pathways due to light stress induced from discrete combinations of narrowband wavelengths), while other specific compounds within the isoprenoid and phenylpropanoid pathway are being differentially regulated based on varying spectral quality and/or DLIs.

Although basil is one of the most popular herbs globally, it can be challenging to characterize in terms of light-mediated sensory properties at the genomic and phenotypic levels. One limitation to evaluating the interaction of light and sensory quality is that there are over sixty varieties of *Ocimum basilicum*, each with specific light-mediated secondary metabolic responses; this complicates the comparison of studies found in current literature (Blank et al., 2004). These light-mediated responses cannot be easily generalized to other high-value specialty crops, which provides numerous unique research opportunities.

Headspace GC-MS is a commonly used analytical technique used to qualify and quantify VOCs from many types of biological samples. It is particularly useful for metabolomics and characterizing aroma profiles for plant tissues and food products. In this experiment, all volatile concentration units are reported in $\mu M \cdot g^{-1}$ FM. This unit (compared to $\mu mol \cdot g^{-1}$ FM) was utilized because it incorporates the concentration of each analyte per unit volume of headspace gas above the plant tissue (i.e., samples the dynamic and complex gaseous matrix which contains numerous pertinent VOCs), which is important for sensory-based studies. Further, VOCs are highly localized and typically require other GC-MS techniques (i.e., liquid solvent extraction/injection) to accurately quantify in terms of $\mu mol \cdot g^{-1}$ of homogenized plant tissue. HS analysis is an ideal GC-MS sampling technique involving sensory studies with plant flavor/aroma, because it accounts for the dynamic release of volatiles from plant tissues under repeatable conditions and can be incorporated with olfactometry (GC-O). Humans primarily detect aroma volatiles that have been volatilized (i.e., released from trichomes and other specialized structures), which then induces an olfactory response. By accurately calibrating analytical standards to known headspace concentrations, we can determine the micro molarity of each analyte, within a known volume of dynamic gaseous headspace matrix, under repeatable conditions (i.e., temperature and pressure using inert analytical grade He) to which a consumer would be exposed to during consumption. Future studies should use a variety of analytical as well as molecular techniques to determine the primary and secondary metabolic impacts of spectral quality. A multidisciplinary approach would allow for greater insight into the complex interactions between light and plant physiology. This could result in the development of light recipe guidelines based on location and weather conditions, to dynamically attenuate SL spectra to the natural solar spectra as it changes across seasons; season-specific lighting regimes have the potential to maintain consistent flavor and aroma quality throughout the year.

This experiment utilized continuous low-intensity light supplements, which have the potential to manipulate secondary metabolite bioaccumulation while efficiently increasing crop DLI (i.e., utilizing cheaper off-peak electrical rates during night hours). Because basil is grown to vegetative maturity and does not require a photoperiodic response, it tolerates 24 h SL very well; other crops

will experience deleterious effects when using this type of lighting regime. Increasing the intensity and/or manipulating the duration of SL also has the potential to differentially influence secondary metabolic profiles and should be further evaluated under greenhouse and growth chamber conditions.

While narrowband B/R wavelengths have been shown to increase total and specific VOC concentrations, varying levels of impact have been observed among different species and specific SL spectral qualities; further exploration into discrete narrowband wavelengths at varying ratios is warranted (i.e., +/- 2 nm within the ambient spectrum). This could be used to push certain secondary metabolic pathways that could be used to improve flavor, the concentration of phytonutrients, human health benefits, and marketability. Many studies have demonstrated the species-specific nature of secondary metabolic light-mediated responses, which provides a vast range of research opportunities. Factors such as yield, nutrition content, phytonutrient concentrations, texture, and visual characteristics should also be considered when selecting SL regimes. Certain niche markets may utilize the findings of this study to improve flavor quality or push certain metabolic pathways (i.e., terpenoid and phenylpropanoid).

This study utilizes free sunlight and is intended to inform greenhouse basil production with SL requirements. It would be valuable from a scientific perspective to further explore similar methodologies, analytical techniques, and narrowband wavelengths in growth chambers with sole source lighting to determine the influence of ambient solar spectra and if similar results occur without the ambient solar being present. The results of this study show the merit of supplementing broad-spectrum ambient sunlight with targeted discrete narrowband wavelengths to manipulate secondary metabolism. Utilizing growth chambers to manipulate photoperiods and DLI of distinct spectral quality supplements would also prove beneficial for growers, as it would eliminate potential confounding factors from variation in ambient sunlight (i.e., weather, growing location, etc.), as well as provide comparative data for operations that rely on sole-source lighting, such as indoor farms and other types of controlled environment agriculture operations.

The results of this experiment will provide useful information on how SL can be used to optimize the sensory characteristics of sweet basil and provide a baseline to explore other high-value specialty crops. It is possible to significantly alter secondary metabolism by using sole source narrowband lighting, as well as narrowband supplements to ambient sunlight. Further research is required to determine patterns within different specialty crops and how wavelengths can be optimized for daily and seasonal changes in the solar spectrum.

Conclusions

In this study, we explored, identified, and quantified several important volatile organic compounds with known influence on sensory perception and/or plant physiological processes of greenhouse-grown sweet basil. We determined that the spectral quality from SL sources, in addition to changes in the spectral quality and DLI of ambient sunlight across growing seasons, directly influence aroma volatile concentrations. Further, we found that specific ratios of narrowband blue/red wavelengths, combinations of discrete narrowband wavelengths, and broadband wavelengths directly influence the basil aroma profile as well as specific compounds. The results also show that variation in spectral quality and DLI across seasons can dramatically influence aroma concentrations. Narrowband treatments generally produced higher VOC compound concentrations; based on the results of this experiment and current literature, we suggest supplemental narrowband wavelengths blue (450-470 nm) and red (660-700 nm) at a ratio of approximately 10B/90R at 100-200 $\mu mol \cdot m^{-2} \cdot s^{-1}$ for 12-24 h for maximum total VOC concentration and key individual aroma volatile concentrations in greenhouse-grown 'Italian Large Leaf' sweet basil; future experiments should determine the influence of lighting regimes on VOC profiles in relation to consumer perception and preference. This experiment demonstrates the ability to use discrete narrowband wavelengths to augment the natural solar spectrum in order to provide an optimal light environment across growing seasons. Further, narrowband SL can be used to manipulate key flavor and aroma compound concentrations, which can directly impact human sensory perception. Future work should incorporate different analytical and metabolic techniques to determine the impact on important aroma volatiles as well as other primary and secondary metabolites; this includes any potential species-specific effects that spectral quality may have on plant physiology with the potential to indirectly impact sensory quality through light-mediated metabolic resource allocation.

Data availability statement

The raw data supporting the conclusions of this article will be made available by the authors, without undue reservation.

Author contributions

Conceptualization – HH and CS. Methodology – HH and CS. Software – HH and CS. Validation – HH. Formal analysis – HH. Investigation – HH. Resources – CS. Data curation – HH. Writing (original draft preparation) - HH. Writing (review and editing) – HH and CS. Visualization – HH. Supervision and project administration – CS. Funding acquisition – CS. All authors contributed to the article and approved the submitted version.

Funding

Funds were obtained by CS through our University. No grant funds were used for this experiment. This research was made possible through support from the University of Tennessee Institute of Agriculture.

Conflict of interest

The authors declare that the research was conducted in the absence of any commercial or financial relationships that could be construed as a potential conflict of interest.

Publisher's note

References

Behn, H., Albert, A., Marx, F., Noga, G., and Ulbrich, A. (2010). Ultraviolet-b and photosynthetically active radiation interactively affect yield and pattern of monoterpenes in leaves of peppermint (Mentha x piperita l.). *J. Agric. Food Chem.* 58 (12), 7361–7367. doi: 10.1021/jf9046072

Bernhardt, B., Sipos, L., Kokai, Z., Gere, A., Szabo, K., Bernath, J., et al. (2015). Comparison of different ocimum basilicum l. gene bank accessions analyzed by GC–MS and sensory profile. *Ind. Crops Prod* 67, 498–508. doi: 10.1016/j.indcrop.2015.01.013

Blank, A. F., Filho, C., Santos Neto, A., Alves, P. B., Arrigoni-Blank, M., Silva-Mann, R., et al. (2004). Caracterização morfológica e agronômica de acessos de manjericão e alfavaca. *Horticultura Bras.* 22 (1), 113–116. doi: 10.1590/s0102-05362004000100024

Bourgaud, F., Gravot, A., Milesi, S., and Gontier, E. (2001). Production of plant secondary metabolites: a historical perspective. *Plant Sci.* 161 (5), 839–851. doi: 10.1016/s0168-9452(01)00490-3

Briggs, W. R., and Olney, M. A. (2001). Photoreceptors in plant photomorphogenesis to date. five phytochromes, two cryptochromes, one phototropin, and one superchrome. *Plant Physiol.* 125 (1), 85–88. doi: 10.1104/pp.125.1.85

Carvalho, S. D., Schwieterman, M. L., Abrahan, C. E., Colquhoun, T. A., and Folta, K. M. (2016). Light quality dependent changes in morphology, antioxidant capacity, and volatile production in sweet basil (*Ocimum basilicum*). *Front. Plant Sci.* 7. doi: 10.3389/fpls.2016.01328

Casal, J. J. (2000). Phytochromes, cryptochromes, phototropin: photoreceptor interactions in plants. *Photochem. Photobiol.* 71 (1), 1–11. doi: 10.1562/0031-8655(2000)071<0001:pcppii>2.0.co;2

Casal, J. J., and Yanovsky, M. J. (2005). Regulation of gene expression by light. *Int. J. Dev. Biol.* 49 (5-6), 501–511. doi: 10.1387/ijdb.051973jc

Chen, M., Chory, J., and Fankhauser, C. (2004). Light signal transduction in higher plants. *Annu. Rev. Genet.* 38, 87–117. doi: 10.1146/annurev.genet.38.072902.092259

Colquhoun, T. A., Schwieterman, M. L., Gilbert, J. L., Jaworski, E. A., Langer, K. M., Jones, C. R., et al. (2013). Light modulation of volatile organic compounds from petunia flowers and select fruits. *Postharvest Biol. Technol.* 86, 37–44. doi: 10.1016/j.postharvbio.2013.06.013

Colquhoun, T. A., Verdonk, J. C., Schimmel, B. C., Tieman, D. M., Underwood, B. A., and Clark, D. G. (2010). Petunia floral volatile benzenoid/phenylpropanoid genes are regulated in a similar manner. *Phytochemistry* 71 (2-3), 158–167. doi: 10.1016/j.phytochem.2009.09.036

Currey, C. J., Hutchinson, V. A., and Lopez, R. G. (2012). Growth, morphology, and quality of rooted cuttings of several herbaceous annual bedding plants are influenced by photosynthetic daily light integral during root development. *HortScience* 47 (1), 25–30. doi: 10.21273/hortsci.47.1.25

Currey, C. J., and Lopez, R. G. (2015). Biomass accumulation and allocation, photosynthesis, and carbohydrate status of new Guinea impatiens, geranium, and petunia cuttings are affected by photosynthetic daily light integral during root development. *J. Am. Soc. Hortic. Sci.* 140 (6), 542–549. doi: 10.21273/jashs.140.6.542

Dannehl, D., Schwend, T., Veit, D., and Schmidt, U. (2021). Increase of yield, lycopene, and lutein content in tomatoes grown under continuous PAR spectrum LED lighting. *Front. Plant Sci.* 12. doi: 10.3389/fpls.2021.611236

Darko, E., Heydarizadeh, P., Schoefs, B., and Sabzalian, M. R. (2014). Photosynthesis under artificial light: the shift in primary and secondary metabolism. *Philos. Trans. R Soc. Lond B Biol. Sci.* 369 (1640), 20130243. doi: 10.1098/rstb.2013.0243

De Masi, L., Siviero, P., Esposito, C., Castaldo, D., Siano, F., and Laratta, B. (2006). Assessment of agronomic, chemical and genetic variability in common basil (Ocimum basilicum l.). *Eur. Food Res. Technol.* 223 (2), 273–281. doi: 10.1007/s00217-005-0201-0

Dou, H., Niu, G., Gu, M., and Masabni, J. (2017). Effects of light quality on growth and phytonutrient accumulation of herbs under controlled environments. *Horticulturae* 3 (2). doi: 10.3390/horticulturae3020036

Fankhauser, C., and Chory, J. (1997). Light control of plant development. *Annu. Rev. Cell Dev. Biol.* 13, 203–229. doi: 10.1146/annurev.cellbio.13.1.203

Fausey, B. A., Heins, R. D., and Cameron, A. C. (2005). Daily light integral affects flowering and quality of greenhouse-grown achillea, gaura, and lavandula. *HortScience* 40 (1), 114–118. doi: 10.21273/hortsci.40.1.114

Faust, J. E., Holcombe, V., Rajapakse, N. C., and Layne, D. R. (2005). The effect of daily light integral on bedding plant growth and flowering. *HortScience* 40 (3), 645–649. doi: 10.21273/hortsci.40.3.645

Faust, J. E., and Logan, J. (2018). Daily light integral: a research review and high-resolution maps of the united states. *HortScience* 53 (9), 1250–1257. doi: 10.21273/HORTSCI13144-18

Folta, K. M., and Carvalho, S. D. (2015). Photoreceptors and control of horticultural plant traits. *HortScience* 50 (9), 1274–1280. doi: 10.21273/hortsci.50.9.1274

Fu, X., Chen, Y., Mei, X., Katsuno, T., Kobayashi, E., Dong, F., et al. (2015). Regulation of formation of volatile compounds of tea (Camellia sinensis) leaves by single light wavelength. *Sci. Rep.* 5, 16858. doi: 10.1038/srep16858

Galvao, V. C., and Fankhauser, C. (2015). Sensing the light environment in plants: photoreceptors and early signaling steps. *Curr. Opin. Neurobiol.* 34, 46–53. doi: 10.1016/j.conb.2015.01.013

Garland, K. F., Burnett, S. E., Stack, L. B., and Zhang, D. (2010). Minimum daily light integral for growing high-quality coleus. *HortTechnology* 20 (5), 929–933. doi: 10.21273/horttech.20.5.929

Gómez, C., and Mitchell, C. A. (2014). Supplemental lighting for greenhouse-grown tomatoes: intracanopy LED towers vs. overhead HPS lamps. *Acta Hortic.* 1037), 855–862. doi: 10.17660/ActaHortic.2014.1037.114

Halaban, R. (1969). Effects of light quality on the circadian rhythm of leaf movement of a short-day-plant. *Plant Physiol.* 44 (7), 973–977. doi: 10.1104/pp.44.7.973

Hammock, H. A., Kopsell, D. A., and Sams, C. E. (2021). Narrowband blue and red LED supplements impact key flavor volatiles in hydroponically grown basil across growing seasons. *Front. Plant Sci.* 12. doi: 10.3389/fpls.2021.623314

Hasan, M. M., Bashir, T., Ghosh, R., Lee, S. K., and Bae, H. (2017). An overview of LEDs' effects on the production of bioactive compounds and crop quality. *Molecules* 22 (9). doi: 10.3390/molecules22091420

Hiltunen, R., and Holm, Y. (2003). *Basil: the genus ocimum* (Amsterdam: CRC Press).

Holopainen, J. K., Kivimaenpaa, M., and Julkunen-Tiitto, R. (2018). New light for phytochemicals. *Trends Biotechnol.* 36 (1), 7–10. doi: 10.1016/j.tibtech.2017.08.009

Hosseini, A., Zare Mehrjerdi, M., and Aliniaeifard, S. (2018). Alteration of bioactive compounds in two varieties of basil (Ocimum basilicum) grown under different light spectra. *J. Essential Oil Bearing Plants* 21 (4), 913–923. doi: 10.1080/0972060x.2018.1526126

Jiao, Y., Lau, O. S., and Deng, X. W. (2007). Light-regulated transcriptional networks in higher plants. *Nat. Rev. Genet.* 8 (3), 217–230. doi: 10.1038/nrg2049

Jishi, T., Kimura, K., Matsuda, R., and Fujiwara, K. (2016). Effects of temporally shifted irradiation of blue and red LED light on cos lettuce growth and morphology. *Scientia Hortic.* 198, 227–232. doi: 10.1016/j.scienta.2015.12.005

Kaiser, E., Ouzounis, T., Giday, H., Schipper, R., Heuvelink, E., and Marcelis, L. F. M. (2018). Adding blue to red supplemental light increases biomass and yield of greenhouse-grown tomatoes, but only to an optimum. *Front. Plant Sci.* 9. doi: 10.3389/fpls.2018.02002

Kalaitzoglou, P., van Ieperen, W., Harbinson, J., van der Meer, M., Martinakos, S., Weerheim, K., et al. (2019). Effects of continuous or end-of-Day far-red light on tomato plant growth, morphology, light absorption, and fruit production. *Front. Plant Sci.* 10. doi: 10.3389/fpls.2019.00322

Kasperbauer, M. J., Loughrin, J. H., and Wang, S. Y. (2001). Light reflected from red mulch to ripening strawberries affects aroma, sugar and organic acid concentrations. *Photochem. Photobiol.* 74 (1), 103–107. doi: 10.1562/00318655(2001)074

Kelly, N., and Runkle, E. S. (2020). Spectral manipulations to elicit desired quality attributes of herbaceous specialty crops. *Eur. J. Hortic. Sci.* 85 (5), 339–343. doi: 10.17660/eJHS.2020/85.5.5

Kiferle, K., Maggini, R., and Pardossi, P. (2013). Influence of nitrogen nutrition on growth and accumulation of rosmarinic acid in sweet basil (Ocimum basilicum l.) grown in hydroponic culture. *Aust. J. Crop Sci.* 7 (3), 321–327.

Kivimaenpa, M., Mofikoya, A., Abd El-Raheem, A. M., Riikonen, J., Julkunen-Tiitto, R., and Holopainen, J. K. (2022). Alteration in light spectra causes opposite responses in volatile phenylpropanoids and terpenoids compared with phenolic acids in sweet basil (Ocimum basilicum) leaves. *J. Agric. Food Chem.* 70 (39), 12287–12296. doi: 10.1021/acs.jafc.2c03309

Kong, Y., Schiestel, K., and Zheng, Y. B. (2019). Pure blue light effects on growth and morphology are slightly changed by adding low-level UVA or far-red light: a comparison with red light in four microgreen species. *Environ. Exp. Bot.* 157, 58–68. doi: 10.1016/j.envexpbot.2018.09.024

Kopsell, D. A., Kopsell, D. E., and Curran-Celentano, J. (2005). Carotenoid and chlorophyll pigments in sweet basil grown in the field and greenhouse. *HortScience* 40 (5), 1230–1233. doi: 10.21273/hortsci.40.5.1230

Korczynski, P. C., Logan, J., and Faust, J. E. (2002). Mapping monthly distribution of daily light integrals across the contiguous united states. *HortTechnology* 12 (1), 12–16. doi: 10.21273/horttech.12.1.12

Kyriacou, M. C., El-Nakhel, C., Pannico, A., Graziani, G., Soteriou, G. A., Giordano, M., et al. (2019). Genotype-specific modulatory effects of select spectral bandwidths on the nutritive and phytochemical composition of microgreens. *Front. Plant Sci.* 10. doi: 10.3389/fpls.2019.01501

Landi, M., Zivcak, M., Sytar, O., Brestic, M., and Allakhverdiev, S. I. (2020). Plasticity of photosynthetic processes and the accumulation of secondary metabolites in plants in response to monochromatic light environments: a review. *Biochim. Biophys. Acta Bioenerg* 1861 (2), 148131. doi: 10.1016/j.bbabio.2019.148131

Larsen, D. H., Woltering, E. J., Nicole, C. C. S., and Marcelis, L. F. M. (2020). Response of basil growth and morphology to light intensity and spectrum in a vertical farm. *Front. Plant Sci.* 11. doi: 10.3389/fpls.2020.597906

Lawless, H. H. (2010). *Sensory evaluation of food* (New York: Springer Verlag).

Lu, N., Bernardo, E. L., Tippayadarapanich, C., Takagaki, M., Kagawa, N., and Yamori, W. (2017). Growth and accumulation of secondary metabolites in perilla as affected by photosynthetic photon flux density and electrical conductivity of the nutrient solution. *Front. Plant Sci.* 8. doi: 10.3389/fpls.2017.00708

Massa, G. D., Kim, H. H., Wheeler, R. M., and Mitchell, C. A. (2008). Plant productivity in response to LED lighting. *Hortscience* 43 (7), 1951–1956. doi: 10.21273/HORTSCI.43.7.1951

McCree, K. J. (1973). The measurement of photosynthetically active radiation. *Solar Energy* 15 (1), 83–87. doi: 10.1016/0038-092x(73)90010-8

Meligaard, M., Civile, G. V., and Carr, B. T. (2007). *Sensory evaluation techniques. 4th ed.* (Boca Raton: CRC Press).

Mokvist, F., Mamedov, F., and Styring, S. (2014). Defining the far-red limit of photosystem I: the primary charge separation is functional to 840 nm. *J. Biol. Chem.* 289 (35), 24630–24639. doi: 10.1074/jbc.M114.555649

Morrow, R. C. (2008). LED lighting in horticulture. *HortScience* 43 (7), 1947–1950. doi: 10.21273/hortsci.43.7.1947

Olle, M., and Viršile, A. (2013). The effects of light-emitting diode lighting on greenhouse plant growth and quality. *Agric. Food Sci.* 22, 223–234. doi: 10.23986/afsci.7897

Ouzounis, T., Rosenqvist, E., and Ottosen, C. O. (2015). Spectral effects of artificial light on plant physiology and secondary metabolism: a review. *Hortscience* 50 (8), 1128–1135. doi: 10.21273/HORTSCI.50.8.1128

Paradiso, R., and Proietti, S. (2021). Light-quality manipulation to control plant growth and photomorphogenesis in greenhouse horticulture: the state of the art and the opportunities of modern LED systems. *J. Plant Growth Regul.* 41 (2), 742–780. doi: 10.1007/s00344-021-10337-y

Pattison, P. M., Tsao, J. Y., Brainard, G. C., and Bugbee, B. (2018). LEDs For photons, physiology and food. *Nature* 563 (7732), 493–500. doi: 10.1038/s41586-018-0706-x

Pennisi, G., Blasioli, S., Cellini, A., Maia, L., Crepaldi, A., Braschi, I., et al. (2019a). Unraveling the role of red : blue LED lights on resource use efficiency and nutritional properties of indoor grown sweet basil. *Front. Plant Sci.* 10. doi: 10.3389/fpls.2019.00305

Pennisi, G., Sanyé-Mengual, E., Orsini, F., Crepaldi, A., Nicola, S., Ochoa, J., et al. (2019b). Modelling environmental burdens of indoor-grown vegetables and herbs as affected by red and blue LED lighting. *Sustainability* 11 (15). doi: 10.3390/su11154063

Petrovic, J., Stojkovic, D., and Sokovic, M. (2019). Terpene core in selected aromatic and edible plants: natural health improving agents. *Adv. Food Nutr. Res.* 90, 423–451. doi: 10.1016/bs.afnr.2019.02.009

Piovene, C., Orsini, F., Bosi, S., Sanoubar, R., Bregola, V., Dinelli, G., et al. (2015). Optimal red:blue ratio in led lighting for nutraceutical indoor horticulture. *Scientia Hortic.* 193, 202–208. doi: 10.1016/j.scienta.2015.07.015

Poiroux-Gonord, F., Bidel, L. P., Fanciullino, A. L., Gautier, H., Lauri-Lopez, F., and Urban, L. (2010). Health benefits of vitamins and secondary metabolites of fruits and vegetables and prospects to increase their concentrations by agronomic approaches. *J. Agric. Food Chem.* 58 (23), 12065–12082. doi: 10.1021/jf1037745

Putievsky, E., and Galambosi, B. (1999). *Production systems of basils* (Basil: The Genus Ocimum. Harwood Academic Publishers).

Rao, A. V., and Rao, L. G. (2007). Carotenoids and human health. *Pharmacol. Res.* 55 (3), 207–216. doi: 10.1016/j.phrs.2007.01.012

Rockwell, N. C., Su, Y. S., and Lagarias, J. C. (2006). Phytochrome structure and signaling mechanisms. *Annu. Rev. Plant Biol.* 57, 837–858. doi: 10.1146/annurev.arplant.56.032604.144208

Sakalauskaite, J., Viskelis, P., Dambrauskiene, E., Sakalauskiene, S., Samuoliene, G., Brazaityte, A., et al. (2013). The effects of different UV-b radiation intensities on morphological and biochemical characteristics in. *J. Sci. Food Agric.* 93 (6), 1266–1271. doi: 10.1002/jsfa.5879

Santin, M., Ranieri, A., and Castagna, A. (2021). Anything new under the sun? an update on modulation of bioactive compounds by different wavelengths in agricultural plants. *Plants (Basel)* 10 (7). doi: 10.3390/plants10071485

Schmitt, J., and Wulff, R. D. (1993). Light spectral quality, phytochrome and plant competition. *Trends Ecol. Evol.* 8 (2), 47–51. doi: 10.1016/0169-5347(93)90157-K

Sell, C. S. (2019). *Fundamentals of fragrance chemistry* (Hoboken, New Jersey: Wiley).

Shanmugam, K., Gimbun, J., Ranganathan, B., Suganthi, P., Srinivasan, R. P., and Purushothaman, B. (2018). A comprehensive review on ocimum basilicum. *J. Natural Remedies* 18 (3), 71–85. doi: 10.18311/jnr/2018/21324

Singh, D., Basu, C., Meinhardt-Wollweber, M., and Roth, B. (2015). LEDs For energy efficient greenhouse lighting. *Renewable Sustain. Energy Rev.* 49, 139–147. doi: 10.1016/j.rser.2015.04.117

Sipos, L., Balázs, L., Székely, G., Jung, A., Sárosi, S., Radácsi, P., et al. (2021). Optimization of basil (*Ocimum basilicum* l.) production in LED light environments – a review. *Scientia Hortic.* 289. doi: 10.1016/j.scienta.2021.110486

Sipos, L., Boros, I. F., Csambalik, L., Székely, G., Jung, A., and Balázs, L. (2020). Horticultural lighting system optimalization: a review. *Scientia Hortic.* 273. doi: 10.1016/j.scienta.2020.109631

Smith, H. (1982). Light quality, photoperception, and plant strategy. *Annu. Rev. Plant Physiol.* 33 (1), 481–518. doi: 10.1146/annurev.pp.33.060182.002405

Stagnari, F., Di Mattia, C., Galieni, A., Santarelli, V., D'Egidio, S., Pagnani, G., et al. (2018). Light quantity and quality supplies sharply affect growth, morphological, physiological and quality traits of basil. *Ind. Crops Products* 122, 277–289. doi: 10.1016/j.indcrop.2018.05.073

Taulavuori, K., Hyöky, V., Oksanen, J., Taulavuori, E., and Julkunen-Tiitto, R. (2016b). Species-specific differences in synthesis of flavonoids and phenolic acids under increased periods of enhanced blue light. *Environ. Exp. Bot.* 121 145, 150. doi: 10.1016/j.envexpbot.2015.04.002

Taulavuori, E., Taulavuori, K., Hyoky, V., Oksanen, J., and Julkunen-Tiitto, R. (2016a). Speciesspecific differences in synthesis of flavonoids and phenolic acids under increasing periods of enhanced blue light. *Environ. Exp. Bot.* 121, 145–150. doi: 10.1016/j.envexpbot.2015.04.002

Thoma, F., Somborn-Schulz, A., Schlehuber, D., Keuter, V., and Deerberg, G. (2020). Effects of light on secondary metabolites in selected leafy greens: a review. *Front. Plant Sci.* 11. doi: 10.3389/fpls.2020.00497

Thorne, H. C., Jones, K. H., Peters, S. P., Archer, S. N., and Dijk, D. J. (2009). Daily and seasonal variation in the spectral composition of light exposure in humans. *Chronobiol Int.* 26 (5), 854–866. doi: 10.1080/07420520903044315

Toscano, S., Cavallaro, V., Ferrante, A., Romano, D., and Patane, C. (2021). Effects of different light spectra on final biomass production and nutritional quality of two microgreens. *Plants (Basel)* 10 (8). doi: 10.3390/plants10081584

Ueda, T., Murata, M., and Yokawa, K. (2021). Single wavelengths of LED light supplement promote the biosynthesis of major cyclic monoterpenes in Japanese mint. *Plants (Basel)* 10 (7). doi: 10.3390/plants10071420

Vranova, E., Coman, D., and Gruissem, W. (2012). Structure and dynamics of the isoprenoid pathway network. *Mol. Plant* 5 (2), 318–333. doi: 10.1093/mp/sss015

Zhen, S., and Bugbee, B. (2020). Far-red photons have equivalent efficiency to traditional photosynthetic photons: implications for redefining photosynthetically active radiation. *Plant Cell Environ.* 43 (5), 1259–1272. doi: 10.1111/pce.13730

frontiers | Frontiers in Plant Science

TYPE Original Research
PUBLISHED 18 July 2023
DOI 10.3389/fpls.2023.1164768

OPEN ACCESS

EDITED BY
Roland Valcke,
University of Hasselt, Belgium

REVIEWED BY
Sachchidanand Tripathi,
University of Delhi, India
Juanjuan Fu,
Northwest A&F University, China

*CORRESPONDENCE
Houcheng Liu
liuhch@scau.edu.cn

RECEIVED 13 February 2023
ACCEPTED 21 April 2023
PUBLISHED 18 July 2023

CITATION
Liu X, Shi R, Gao M, He R, Li Y and Liu H (2023) Growth of tomato and cucumber seedlings under different light environments and their development after transplanting.
Front. Plant Sci. 14:1164768.
doi: 10.3389/fpls.2023.1164768

Growth of tomato and cucumber seedlings under different light environments and their development after transplanting

Xiaojuan Liu, Rui Shi, Meifang Gao, Rui He, Yamin Li and Houcheng Liu*

College of Horticulture, South China Agricultural University, Guangzhou, China

Selecting suitable light conditions according to the plant growth characteristics is one of the important approaches to cultivating high-quality vegetable seedlings. To determine the more favorable LED light conditions for producing high-quality tomato and cucumber seedlings in plant factories with artificial light (PFALS), the growth characteristics of tomato and cucumber seedlings under seven LED light environments (CK, B, UV-A, FR, B+UV-A, UV-A+FR, and B+FR) and the development of these seedlings after transplanting into a plastic greenhouse were investigated. The results showed that the seedling height and hypocotyl length increased in treatments with far-red light supplementation (FR, UV-A+FR, and B+FR), but decreased in the B treatment, in both varieties. The seedling index of tomato seedlings increased in the B+UV-A treatment, while that of cucumber seedlings increased in the FR treatment. After transplanting into a plastic greenhouse, tomato plants that radiated with UV-A had greater flower numbers on the 15th day after transplanting. In cucumber plants of the FR treatment, the flowering time was significantly delayed, and the female flower exhibited at a lower node position. By using a comprehensive scoring analysis of all detected indicators, light environments with UV-A and FR were more beneficial for improving the overall quality of tomato and cucumber seedlings, respectively.

KEYWORDS

light conditions, seedling quality, comprehensive evaluation, tomato, cucumber

Introduction

Seedling growth is fundamental to plant growth and important for vegetable yield and quality. Seedlings with poor quality often behave worse in terms of growth, development, yield, and quality after transplanting (Jeong et al., 2020). Therefore, it is necessary to adopt reasonable cultivation measures, such as changing the nutrient solution, temperature,

carbon dioxide concentration, and so on, light environment, to improve the quality of vegetable seedlings on the basis of the growth requirements of different vegetables (Balliu, 2017).

Light, which can provide energy and regulate multiple biological processes, is vital for plants. Plant factories with artificial light (PFALs) are indoor farms, which have gradually developed into stable and large-scale vegetable seedling production and cultivation facilities (Kozai, 2018). APFAL is composed of a soilless culture system, an artificial lighting system, and environmental regulatory devices, among which the artificial lighting system plays an essential role (Kozai, 2013). Since the late 2000s, LEDs have been introduced into PFALs for artificial lighting and applied progressively due to their increased effectiveness and lower electricity costs (Goto, 2012). In contrast to traditional lights, LED lamps have a smaller size, higher stable radiation efficiency, greater environmental friendliness, and longer lifetimes (Sabzalian et al., 2014). Moreover, LED lights can conveniently and accurately regulate plant growth and development by adjusting the light environment (light quality, intensity, and photoperiod) (Morrow, 2008).

In recent years, a wide range of research has revealed the influences of various LED spectra on the growth and development of different vegetable seedlings. For monochromic light, compared with pea seedlings treated with white light, red light radiation led to significantly higher stem length and leaf area, with increased antioxidant activity, while blue light radiation induced increases in seedling weight and chlorophyll content (Wu et al., 2007). Under exposure to the orange light treatment, tomato seedlings showed a higher and weaker phenotype than those under the control (white light) treatment (Liu et al., 2012). Although cucumber seedlings treated with monochromic red, blue, yellow, and green light displayed inhibited plant growth and decreased chlorophyll content compared to the white light, each monochromatic light played a special role in the regulation of plant morphogenesis and photosynthesis (Su et al., 2013). Meanwhile, research on the effects of combined spectra on plant growth and development is increasing. Being effectively absorbed by chloroplasts, red and blue light lead to improved plant photosynthesis (Carvalho et al., 2010; Chen et al., 2021). The positive effects of these two light spectral combinations on plant growth and development have been revealed in many vegetable varieties, including tomato, cucumber, and pepper (Hernández and Kubota, 2016; Son et al., 2018; Li et al., 2020). In terms of other light spectrum combinations, the RGB (red + green + blue) pepper seedlings had greater seedling height, stem diameter, and total leaf area than seedlings of the GB (green + blue) treatments (Claypool and Lieth, 2020). Supplementary light with UV-A or far-red affects the morphology of cabbage and kale seedlings grown under pure blue light (B), with different responses to the same light conditions in these two varieties (Kong et al., 2019). Even so, further exploration is still needed to determine the positive impacts of various monochromatic lights and their different combinations on the growth and development of different kinds of vegetable seedlings.

Tomatoes and cucumbers are two of the world's most popular fruit vegetables. With the enhancement of human awareness of healthy living, the demand for fresh vegetables (including tomatoes and cucumbers) continues to increase (Stanaway et al., 2022). Consequently, the demand for high-quality tomato and cucumber seedlings in the vegetable industry is also increasing. However, tomato and cucumber seedlings grown outdoors are easily affected by bad weather, poor soil quality, pests, etc., resulting in poor-quality seedlings, whereas those planted in plant factories are independent of these conditions (Kozai, 2013). To date, lots of investigations have reported the impacts of different LED light conditions on the growth and quality of tomato and cucumber seedlings (Nanya et al., 2012; Khoshimkhujaev et al., 2014; Hwang et al., 2020; Jeong et al., 2020; Hamedalla et al., 2022; Jin et al., 2023), but few of them have determined the relatively suitable LED light conditions for improving their seedling qualities in plant factories through comprehensive comparative analysis. Additionally, relatively few studies have displayed the effects of different light conditions on the post-transplantation growth performance of tomato and cucumber seedlings. Furthermore, the growth responses of tomato and cucumber seedlings to different combinations of different light qualities are still not fully known.

In this study, under conditions of similar light intensity (photosynthetic photon flux density, PPDF of 250 $\mu molm^{-2}$ s^{-1}), the various growth indices of tomato and cucumber seedlings supplemented with different LED light spectra (blue, UV-A, and far-red) and these light spectrum combinations, as well as the growth performance of these seedlings after transplant into a plastic greenhouse, were examined. A formula was established to comprehensively compare and analyze all measured indices, in order to select the more favorable LED light conditions for improving the growth quality of tomato and cucumber seedlings. These results will provide a theoretical basis for cultivating tomato and cucumber seedlings with high uniformity and quality in plant factories by altering the light environments.

Materials and methods

Plant material and growth conditions

All the seedlings in this experiment were grown in an indoor plant factory at South China Agricultural University (Guangzhou, China). Seeds of tomato (cv. Zhuanhong No. 2, Hunan Xingshu Seed Industry Co. Ltd.) and cucumber (cv. Zaoqing No. 2, Guangdong Kenong Vegetable Seed Industry Co. Ltd.) were sown in sponges of size 2 cm × 2 cm × 2 cm and pretreated under PPFD of 200 μmol m^{-2} s^{-1} white light for 2 days after germination. In the preliminary research, we discovered that white: red = 3:2 is superior to single white light for tomato and cucumber breeding. Tomato and cucumber seedlings were planted in the hydroponic systems after germination and divided into seven groups for different light treatments (CK: 3W2R (W:R=3:2); B: 3W2R+50 $\mu molm^{-2}$ s^{-1} B; UV-A: 3W2R+6 $\mu molm^{-2}$ s^{-1} UV-A; FR: 3W2R+30 $\mu molm^{-2}$ s^{-1}FR; B+UV-A: 3W2R+50 $\mu molm^{-2}$ s^{-1} B+6 $\mu molm^{-2}$ s^{-1} UV-A; UV-A+FR: 3W2R+6 $\mu molm^{-2}$ s^{-1} UV-A +30 $\mu molm^{-2}$ s^{-1} FR; B +FR: 3W2R+50 $\mu molm^{-2}$ s^{-1} B+30 $\mu molm^{-2}$ s^{-1} FR), respectively. The light sources were provided by stable and adjustable LED

panels (Chenghui Equipment Co., Ltd., Guangzhou, China; 150 cm × 30 cm). The seedling growth conditions were set to 24 ± 2°C, 75 ± 5% relative humidity (RH). All the seedlings were grown under a similar PPFD of 250 μmol m^{-2} s^{-1}, with a 12/12 h (light/dark) duration, and supplied with a 1/2 Hoagland solution (pH 5.5; EC, 1.30 mS cm^{-2}). The respective light intensities of the PPFD and light spectra (W: 400–700 nm; R: 660 ± 10 nm; B: 450 ± 10 nm, UV-A: 385 ± 10 nm, FR: 735 ± 10 nm) were determined by using the APL-01 machine (Asensetek, Taiwan) (Figure 1; Supplementary Table S1). To ensure the accuracy of light intensity and quality, we measured them twice a day using the APL-01 machine during plant treatment, once in the morning and once in the afternoon, respectively. After 15 days of light treatments, all the seedlings were transplanted into a plastic greenhouse (South China Agricultural University, Guangzhou, China).

Plant growth analysis and biomass determination

After 15 days of light treatment, 15 uniform seedlings of tomato and cucumber were selected to determine their growth indices. A measuring ruler was used to measure the seedling height (cm) and hypocotyl length (cm). The stem diameter (mm) was detected by using a vernier caliper.

The true leaf number of all treated seedlings was counted. The total leaf area (cm^2) of tomato and cucumber seedlings was measured using a leaf area meter (LI-3000A). The fresh weight (g/plant) was measured with an electronic balance (BCE224-1CCN, Sartorius, Beijing), and the dry weight (g/plant) was determined after drying at 105°C for 30 min and then dried at 75°C to a constant weight.

Determination of comprehensive seedling indices

The following formulas were used to calculate the comprehensive seedling indexes of tomato and cucumber seedlings:

Specific leaf weight = leaf dry weight/leaf area,

Plant compactness = shoot dry weight/plant height,

Root shoot ratio = root dry weight/shoot dry weight,

The seedling index = (stem diameter/plant height + root dry weight/shoot dry weight) * whole plant dry weight (Bai et al., 2014).

Determination of photosynthetic pigment content and chlorophyll fluorescence parameters

A total of 0.5 g fresh samples of tomato and cucumber seedlings was taken for photosynthetic pigment content (chlorophyll and carotenoids) determination. In brief, the sample was placed in the dark at room temperature with 8 ml of an acetone–alcohol mixture (acetone: alcohol = 1:1, v/v) overnight until it turned white. A UV spectrophotometer (Shimadzu UV-16A, Shimadzu, Corporation, Kyoto, Japan) was used to obtain the absorbance of the supernatant at 440, 645, and 663 nm. Chlorophyll a (mg/g), chlorophyll b (mg/g), total chlorophyll (mg/g), and carotenoid content (mg/g) were calculated according to the methods described by He et al. (He et al. 2021).

Using the third true leaf of each seedling as a sample, measurements of chlorophyll fluorescence parameters were performed using a fluorometer (MINI-PAM-II, Germany).

Evaluation of phytochemical substance and enzyme activities of seedlings

Following the experimental steps reported in He et al. (He et al. 2021), the total soluble protein content was determined by the Coomassie brilliant blue G-250 dye method. To detect the activities of the antioxidant enzymes [superoxide dismutase (SOD), peroxidase (POD), and catalase (CAT)], 0.5 g fresh leaf from seedlings was ground in 10 ml phosphate buffer (50 mM, pH 7.8) and centrifuged at 10,000 rpm for 20 min; then, the supernatant was collected and used for further analysis. The reaction solution consisted of 50 mM phosphate buffer, 13 mM methionine, 2 μM riboflavin, 10 μM EDTA-Na_2, 75 μM NBT, and 50 μl enzyme extract. The SOD activity was estimated at 560 nm following the method of Li and Yi (2012). The reaction mixture measuring POD activity contained 0.8 ml enzyme extract, 1.45 ml phosphate buffer, 0.5 ml guaiacol (50 mM/L), and 0.5 ml H_2O_2 (2%), and was

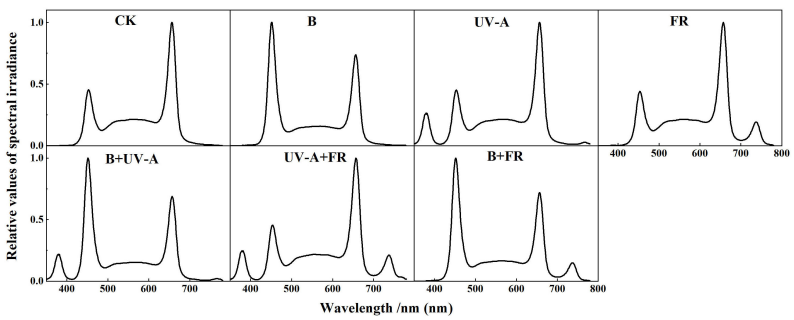

FIGURE 1
The light spectral of different light treatments used in this experiment.

determined at 470 nm. Changes in absorbance at 0.01 units min^{-1} were defined as one unit of POD activity (Raza et al., 2007). For CAT activity, the reaction mixture contained 0.2 ml enzyme extraction, 1.5 ml phosphate buffer, 1 ml distilled water, and 200 mM H_2O_2. By measuring at 240 nm, one unit of CAT activity was expressed as 0.1 units min^{-1} change in absorbance (Seckin et al., 2008).

To access the malondialdehyde (MDA) content, a total of 0.5 g fresh sample was homogenized in a 10-ml 10% trichloroacetic acid (TCA) solution. After centrifugation (4,000 rpm, 10 min), the supernatant was subjected to a further reaction. The reaction solution (contained 2 ml supernatant and 2 ml 0.6% TBA solution) was heated at 100°C for 15 min, followed by rapid cooling, and then centrifuged at 4,000 rpm for 10 min. After that, the supernatant was measured at 532, 600, and 450 nm using a UV spectrophotometer (Zhang et al., 2005).

Growth analysis of plant performance after transplanting

After 15 days of light treatment, 24 tomato and cucumber seedlings with uniform growth from each treatment were transplanted into a plastic greenhouse. All the seedlings were grown in coir tanks and fertilized with a drip irrigation system using the Yamazaki nutrient solution. For tomato plant growth indicators within 30 days after transplanting (DAT), the flowering time, the node position of the first flower, and the number of fruits per plant at 15 and 30 DAT were recorded. For cucumber plants of 20 DAT, growth parameters, including the flowering time, the node position of the first flower, the node position of the first female flower, the number of female flowers, and the total number of flowers within 15 nodes, were counted.

Statistical analysis

All statistical analyses were performed by using SPSS 26.0 and Origin 2021. The Duncan's multiple range test was used to determine the significant differences at the 0.05 significance level ($p < 0.05$) using SPSS 26.0. The graphing was conducted by Origin 2021.

Results

Impacts of diverse LED light qualities on the morphology and biomass of vegetable seedlings

Obviously, different LED light conditions had significant effects on the morphology of tomato and cucumber seedlings (Figures 2A, B). In the two species, the FR, UV-A+FR, and B+FR treatments significantly promoted seedling growth, including seedling height, stem diameter, and hypocotyl length (Figures 2A, B). Specifically, compared to the control, the seedling height, stem diameter, and hypocotyl diameter of tomato seedlings were increased by more than 102%, 19.0%, and 13.0%, respectively, while those in cucumber increased by more than 70%, 45.0%, and 17.0%, respectively (Figures 2C–E). However, the seedling height and hypocotyl length of cucumber and tomato seedlings significantly decreased in the B treatment (Figures 2C–E). In the UV-A treatment, the seedling height, hypocotyl length, and stem diameter of tomato seedlings were not affected, but those of cucumber seedlings obviously decreased (Figures 2C–E). Compared with the control, the B+UV-A treatment led to a noticeable decrease in the height of tomato seedlings and the hypocotyl length of cucumber seedlings, respectively (Figures 2C–E). In the aspects of leaf development, the true leaf number of tomato seedlings exhibited no significant difference among all treatments, while that of cucumber seedlings in the UV-A, FR, UV-A+FR, and B+FR treatments significantly increased (Figure 2F). The total leaf area of tomato seedlings grown under the B and B+UV-A treatments was 27.6% and 20.9% lower than those of seedlings grown under the control, respectively (Figure 2G). Compared to the control of cucumber seedlings, the total leaf area was the highest in the FR treatment, while no significant difference was found among the other treatments (Figure 2G).

As shown in Figure 3, the dry weight of the plant and shoot exhibited no significant difference among all the treatments in tomato seedlings (Figure 3A). Except for the significant reduction in the UV-A+FR and B+FR treatments, there was no significant difference in root dry weight of tomato seedlings between the other treatments and the control (Figure 3A). When irradiated under the FR treatment, cucumber seedlings exhibited a markable increase in the dry weight of the plant, shoot, and root (Figure 3B). In both varieties, the fresh weight of plant and shoot in the FR, UV-A+FR, and B+FR treatments was obviously elevated (Figure 3C). The cucumber seedlings in the B treatment showed a reduction in the shoot fresh weight, whereas those in the UV-A and B+UV-A treatments did not significantly differ from the control (Figure 3D). No significant difference was found in the root fresh weight among all the treatments in tomato seedlings (Figure 3D). The root fresh weight of tomato seedlings in the FR treatment was significantly higher than that in the control treatment (Figure 3D).

Influences of diverse LED light qualities on the comprehensive indices of seedling morphology

The effects of distinct LED light environments on comprehensive indices of seedling morphology were analyzed. In tomato seedlings, the plant compactness in the B and B+UV-A treatments was significantly higher than that in the control, whereas it was significantly decreased in the FR, UV-A+FR, and B+FR treatments (Table 1). The trend of alternation in plant compactness in cucumber seedlings under different light conditions followed the same pattern as that in tomato seedlings (Table 1). Tomato seedlings exposed to different LED light treatments showed no comparable difference in the root shoot ratio, while in cucumber, FR treatment induced a

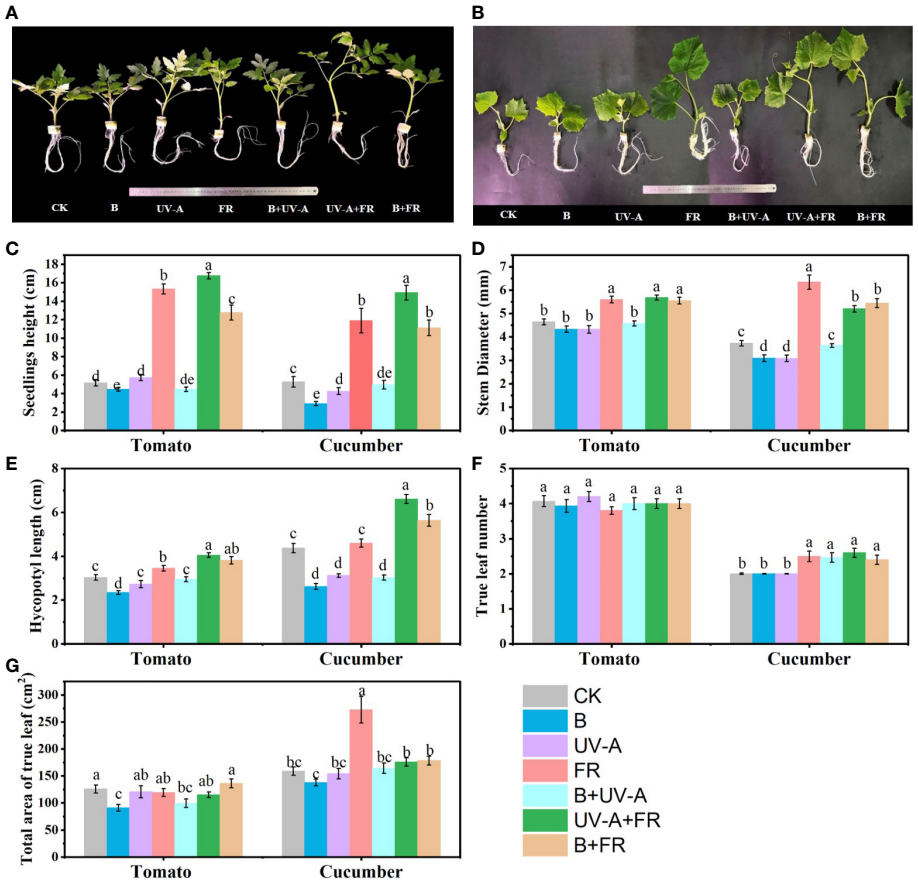

FIGURE 2
Influence of various light treatments on the growth of the tomato and cucumber seedlings. The morphology of **(A)** tomato seedlings and **(B)** cucumber seedlings cultivated under different light environments for 15 days. **(C)** The seedling height, **(D)** stem diameter, **(E)** hypocotyl length, **(F)** true leaf number, and **(G)** total leaf area of tomato and cucumber seedlings after light treatments. Data represent mean ± SE followed by the same letters do not differ significantly according to the Duncan's multiple range test.

significant decrease in the root shoot ratio compared to the control, which decreased by 37.1% (Table 1). When compared to the control, the specific leaf weight of tomato seedlings was clearly increased in the B and B+UV-A treatments but decreased in the UV-A+FR and B +FR treatments (Table 1). Cucumber seedlings in the FR, B+UV-A, and B+FR treatments showed obviously elevated specific leaf weight in comparison with the control (Table 1). For tomato seedlings, the highest seedling index was observed in the B+UV-A treatment, while the lowest occurred in the UV-A+FR treatment (Table 1). As for cucumber seedlings, the seedling index in the FR treatment was the highest, increasing by 54.1% compared with the control, although there was no significant difference between the other treatments and the control (Table 1).

Effects of different LED light qualities on photosynthetic pigment content and chlorophyll fluorescence parameters

In tomato, when compared to the control, the UV-A+FR and B +FR treatments reduced the contents of chlorophyll a, chlorophyll b, and total chlorophyll, but in other treatments, there was no significant difference in these three pigments (Table 2). The carotenoid content of tomato seedlings did not differ among all the treatments in our experiment (Table 2). As regards cucumber seedlings, a significant higher content of chlorophyll a and total chlorophyll was observed only in the B treatment (Table 2). The chlorophyll b content of all cucumber leaves was not obviously affected by different light treatments (Table 2). The carotenoid content decreased by 15.0% in the B+FR treatment compared to the control (Table 2).

For tomato, the Fv/Fm ratio significantly increased under the B+UV-A treatment, while no difference was found between the other treatments and the control (Table 2). In cucumber seedlings, the Fv/Fm value significantly increased in the B+FR treatment, but there was a decrease in the FR treatment compared with the control (Table 2). Interestingly, compared with the control, both the Y(II) and electron transportation rate (ETR) values of the other treatments in tomato seedlings decreased (Table 2), while in cucumber seedlings, the opposite trend was observed, showing that Y(II) and ETR values were the lowest in the control (Table 2).

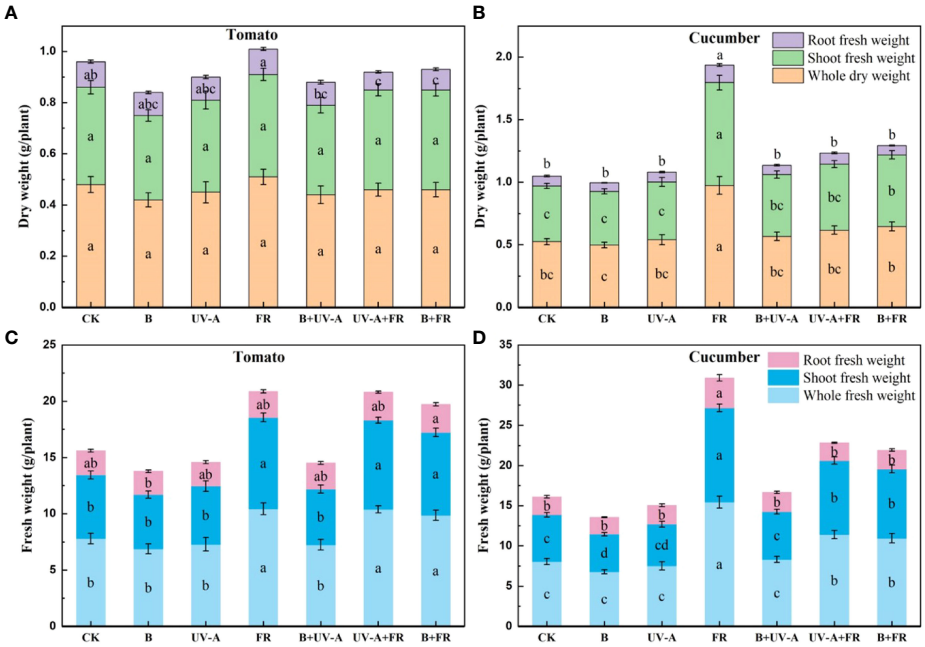

FIGURE 3
Changes of biomass in tomato and cucumber seedlings treated by different light environments. The dry weight of **(A)** tomato seedlings and **(B)** cucumber seedlings and **(C)** the fresh weight of tomato seedlings and **(D)** cucumber seedlings cultivated under different light environments. Data represent mean ± SE followed by the same letters do not differ significantly according to the Duncan's multiple range test.

TABLE 1 Comprehensive growth indexes of tomato and cucumber seedlings cultivated under different LED light environments.

Species	Treatment	Compactness	Root shoot ratio	Specific leaf weight	The seedling index
Tomato	CK	42.41 ± 2.87 b	0.28 ± 0.02 a	2.28 ± 0.080 b	0.35 ± 0.02 b
	B	50.39 ± 2.17 a	0.27 ± 0.01 a	3.40 ± 0.301 a	0.41 ± 0.02 ab
	UV-A	46.29 ± 3.30 ab	0.25 ± 0.01 a	2.39 ± 0.057 b	0.40 ± 0.03 ab
	FR	19.87 ± 0.91 c	0.26 ± 0.01 a	2.53 ± 0.158 b	0.26 ± 0.01 c
	B+UV-A	53.01 ± 3.06 a	0.24 ± 0.01 a	3.18 ± 0.278 a	0.43 ± 0.03 a
	UV-A+FR	18.52 ± 0.81 c	0.18 ± 0.01 b	1.98 ± 0.099 c	0.21 ± 0.01 c
	B+FR	22.54 ± 1.31 c	0.20 ± 0.01 b	1.98 ± 0.091 c	0.25 ± 0.02 c
Cucumber	CK	48.07 ± 3.26 c	0.94 ± 0.07 ab	2.09 ± 0.06 c	0.31 ± 0.03 bc
	B	77.95 ± 2.23 a	1.01 ± 0.04 a	2.37 ± 0.05 abc	0.36 ± 0.02 b
	UV-A	61.93 ± 2.43 b	1.00 ± 0.08 a	2.22 ± 0.08 bc	0.32 ± 0.02 bc
	FR	40.44 ± 3.71 d	0.59 ± 0.04 c	2.43 ± 0.07 ab	0.48 ± 0.05 a
	B+ UV-A	62.59 ± 2.66 b	0.90 ± 0.05 ab	2.61 ± 0.21 a	0.35 ± 0.02 b
	UV-A+FR	24.43 ± 0.77 e	0.86 ± 0.05 ab	2.32 ± 0.07 abc	0.25 ± 0.01 c
	B+FR	34.41 ± 1.51 d	0.78 ± 0.04 b	2.50 ± 0.08 ab	0.30 ± 0.02 bc

Data represent mean ± SE(n=20). Different letters indicate significant differences between treatments at the $p < 0.05$ using the Duncan's test. Plant compactness = shoot dry weight/plant height, specific leaf weight = leaf dry weight/leaf area, root shoot ratio = root dry weight/shoot dry weight, the seedling index = (stem diameter/plant height + root dry weight/shoot dry weight) × whole plant dry weight.

10.3389/fpls.2023.1164768

TABLE 2 The photosynthetic pigment content and photosynthetic characteristics of tomato and cucumber seedlings grown under various light environments.

Species	Treatment	Chlorophyll a (mg/g)	Chlorophyll b (mg/g)	Total Chlorophyll (mg/g)	Carotenoids (mg/g)	Fv/Fm	Y(II)	ETR
Tomato	CK	1.19 ± 0.01 a	0.53 ± 0.03 ab	1.74 ± 0.04 ab	0.04 ± 0.01 abc	0.79 ± 0.00 b	0.57 ± 0.00 a	13.24 ± 3.00 a
	B	1.21 ± 0.01 a	0.57 ± 0.04 ab	1.80 ± 0.05 ab	0.03 ± 0.01 bc	0.78 ± 0.00 b	0.50 ± 0.00 b	11.85 ± 6.03 b
	UV-A	1.22 ± 0.00 a	0.59 ± 0.01 a	1.83 ± 0.01 a	0.02 ± 0.00 c	0.78 ± 0.00 b	0.45 ± 0.00 b	10.50 ± 2.00 b
	FR	1.16 ± 0.03 abc	0.49 ± 0.03 bc	1.67 ± 0.06 bc	0.06 ± 0.01 ab	0.79 ± 0.00 b	0.50 ± 0.00 b	11.60 ± 3.00 b
	B+ UV-A	1.18 ± 0.01 ab	0.51 ± 0.01 abc	1.72 ± 0.02 abc	0.06 ± 0.01 ab	0.80 ± 0.00 a	0.51 ± 0.00 b	11.72 ± 3.00 b
	UV-A+FR	1.11 ± 0.04 c	0.44 ± 0.04 c	1.58 ± 0.07 c	0.08 ± 0.01 a	0.78 ± 0.00 b	0.51 ± 0.00 b	11.68 ± 3.00 b
	B+FR	1.13 ± 0.00 bc	0.44 ± 0.00 c	1.59 ± 0.01 c	0.07 ± 0.00 a	0.78 ± 0.00 b	0.51 ± 0.00 b	11.77 ± 5.00 b
Cucumber	CK	1.73 ± 0.01 bcd	0.55 ± 0.01 ab	2.31 ± 0.02 bcd	0.29 ± 0.00 a	0.77 ± 0.00 bc	0.40 ± 0.01 c	9.20 ± 0.30 c
	B	1.93 ± 0.03 a	0.62 ± 0.01 a	2.58 ± 0.04 a	0.28 ± 0.01 a	0.78 ± 0.00 ab	0.51 ± 0.01 a	11.80 ± 0.29 a
	UV-A	1.72 ± 0.03 cd	0.54 ± 0.01 b	2.28 ± 0.04 cd	0.30 ± 0.01 a	0.77 ± 0.00 c	0.47 ± 0.01 b	10.81 ± 0.27 b
	FR	1.70 ± 0.05 cd	0.52 ± 0.02 b	2.24 ± 0.07 cd	0.30 ± 0.00 a	0.75 ± 0.01 d	0.49 ± 0.00 ab	11.38 ± 0.08 ab
	B+ UV-A	1.90 ± 0.09 ab	0.63 ± 0.05 a	2.56 ± 0.14 ab	0.28 ± 0.01 a	0.77 ± 0.00 bc	0.46 ± 0.01 b	10.59 ± 0.35 b
	UV-A+FR	1.61 ± 0.06 d	0.52 ± 0.02 b	2.16 ± 0.08 d	0.29 ± 0.00 a	0.77 ± 0.00 bc	0.46 ± 0.01 b	10.72 ± 0.23 b
	B+FR	1.84 ± 0.06 abc	0.60 ± 0.03 ab	2.47 ± 0.09 abc	0.25 ± 0.00 b	0.79 ± 0.00 a	0.51 ± 0.01a	11.85 ± 0.24 a

Data represent mean ± SE (n=20). Different letters indicate significant differences between treatments at the $p < 0.05$ using the Duncan's test.

Influences of different LED light qualities on physiological characteristics and antioxidant enzyme activities of vegetable seedlings

In tomato seedlings, compared with the control, the soluble protein content was significantly higher in the B treatment, whereas it was significantly lower in the FR, UV-A+FR, and B+FR treatments (Figure 4A). Seedlings in the UV-A, FR, B+UV-A, UV-A+FR, and B+FR treatments showed a marked decrease in the activity of SOD compared to the control (Figure 4B). Relative to the control, a significant decrease in the POD activity was observed in all the other treatments (Figure 4C). In contrast to the control, the CAT activity increased in the B treatment, whereas it decreased in the UV-A+FR and B+FR treatments (Figure 4D). The MDA content was unaffected in the B, UV-A, FR, and B+UV-A treatments but decreased in the UV-A+FR and B+FR treatments (Figure 4E).

In the case of cucumber, the B, UV-A, and B+UV-A treatments led to noticeable increases in the soluble protein content compared with the control, whereas the soluble protein content significantly decreased in the FR, UV-A+FR, and B+FR treatments, respectively (Figure 4A). The B, UV-A, and B+UV-A treatments increased, while the UV-A+FR and B+FR treatments markedly decreased the activity of SOD when compared to the control (Figure 4B). In comparison with the control, increments in the activity of POD were noted under all the other treatments (Figure 4C). The highest activity of CAT was detected in the UV-A treatment, while the lowest occurred in the UV-A+FR treatment (Figure 4D). Seedlings grown under the B+UV-A treatment had the highest MDA content, while no significant difference was found between the other treatments and the control (Figure 4E).

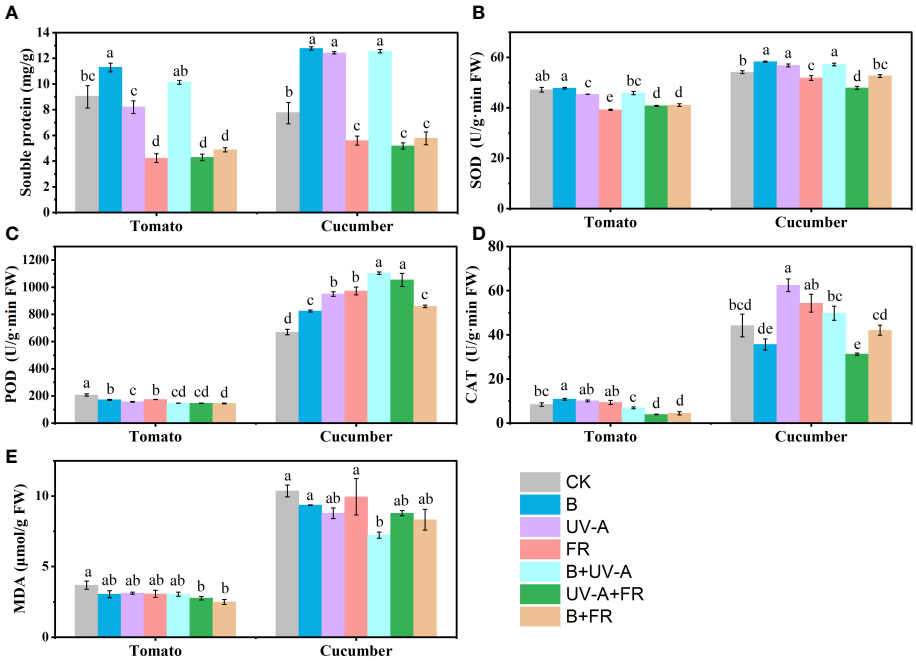

FIGURE 4
The differences in physiological characteristics and antioxidant enzyme activities in tomato and cucumber seedlings under different light conditions. **(A)** The soluble protein content, activity of SOD **(B)**, POD **(C)**, CAT **(D)**, and MDA content **(E)** in tomato and cucumber seedlings after 15 days of light treatments. Data represent mean ± SE followed by the same letters do not differ significantly according to the Duncan's multiple range test.

Effects of different LED light conditions on transplant development of different seedlings

We further assessed the growth and development of these plants treated differently after transplantation. In tomato, the flowering time of all the plants showed no notable difference under different light conditions, whereas it tended to be later in the B+UV-A, UV-A+FR, and B+FR treatments than in the UV-A treatment (Table 3). The first flower in seedlings treated with UV-A+FR and B+FR exhibited at higher node position, while no significant difference was observed between the other treatments and the control (Table 3). On the 15th DAT, the flower number of plants treated in the UV-A treatment was the highest (Table 3). The total fruit number of plants on the 30th DAT was not significantly affected by various LED light treatments (Table 3).

In cucumber plants, compared with the control, plants exposed to the UV-A and FR treatments flowered significantly earlier, but these was not affected in the other treatments (Table 4). The node position of the first flower did not differ among all the treatments (Table 4). However, on the 20th DAT, the node position of the first female flower in the FR treatment was the lowest, which is significantly different from the control (Table 4). In particular, the total flower number of seedlings grown in the UV-A+FR and B+FR treatments was clearly lower than that in the control (Table 4).

TABLE 3 Performance of transplant tomato plants treated with different light conditions at the seedling stage.

Species	Treatment	Time to first flower (day)	Node position of the first flower	Flower numbers at the 15th DAT	Fruit numbers at the 30th DAT
Tomato	CK	16.07 ± 0.27 ab	8.13 ± 0.09 cd	2.13 ± 0.19 b	2.07 ± 0.38 a
	B	16.60 ± 0.27 ab	8.27 ± 0.12 bc	2.20 ± 0.30 b	1.47 ± 0.41 a
	UV-A	15.87 ± 0.13 b	7.87 ± 0.09 d	3.13 ± 0.22 a	1.87 ± 0.34 a
	FR	16.60 ± 0.29 ab	8.47 ± 0.13 abc	1.87 ± 0.38 b	1.20 ± 0.24 a
	B+ UV-A	16.73 ± 0.28 a	7.87 ± 0.13 d	2.47 ± 0.34 ab	1.87 ± 0.39 a
	UV-A+FR	16.80 ± 0.28 a	8.53 ± 0.13 ab	1.60 ± 0.31 b	1.53 ± 0.42 a
	B+FR	16.80 ± 0.26 a	8.73 ± 0.12 a	2.00 ± 0.29 b	1.00 ± 0.32 a

Data represent mean ± SE (n=20). Different letters indicate significant differences between treatments at the $p < 0.05$ using the Duncan's test.

TABLE 4 Growth of cucumber seedlings grown under distinct light treatments after transplanting.

Species	Treatment	Time to first flower (day)	Node position of the first flower	At the 20th DAT (within 15 nodes)		
				Node position of the first female flower	Female flower numbers	Total flower numbers
Cucumber	CK	34.7 ± 0.2 ab	4.4 ± 0.5 a	6.3 ± 0.5 ab	2.0 ± 0.4 a	4.3 ± 0.4 a
	B	34.1 ± 0.2 bc	3.5 ± 0.4 a	6.4 ± 0.5 ab	1.5 ± 0.4 a	4.2 ± 0.3 ab
	UV-A	31.9 ± 0.1 d	3.5 ± 0.4 a	6.1 ± 0.7 abc	1.2 ± 0.4 a	4.2 ± 0.4 ab
	FR	33.9 ± 0.3 c	3.1 ± 0.4 a	4.7 ± 0.5 c	1.5 ± 0.3 a	3.9 ± 0.4 ab
	B+ UV-A	34.4 ± 0.2 abc	4.5 ± 0.7 a	7.3 ± 0.4 a	1.7 ± 0.2 a	4.1 ± 0.4 ab
	UV-A+FR	34.1 ± 0.3 bc	3.7 ± 0.3 a	5.2 ± 0.3 bc	1.6 ± 0.3 a	3.1 ± 0.3 bc
	B+FR	34.9 ± 0.1 a	4.1 ± 0.3 a	5.0 ± 0.4 bc	1.2 ± 0.3 a	2.5 ± 0.4 c

Data represent mean ± SE (n=20). Different letters indicate significant differences between treatments at the $p < 0.05$ using the Duncan's test.

Correlation analysis and comprehensive analysis

The Pearson correlation and principal component analysis (PCA) were performed to analyze the correlation between each examined growth index, and a formula was constructed to comprehensively analyze the growth quality of vegetable seedlings under different light environments.

Tomato seedlings

According to the results of Pearson correlation, a significant positive correlation was exhibited between the seedling index and compactness, true leaf number, total leaf area, whole dry weight, root dry weight, shoot dry weight, whole fresh weight, ETR, and MDA content, whereas no significant negative correlation was found between the seedling index and all of the examined indicators (Figure 5A).

Similarly, the results of PCA revealed that the seedling index was positively related to true leaf number, total leaf area, whole dry weight, shoot dry weight, root dry weight, and plant compactness, whereas it is negatively correlated with stem diameter, seedling height, hypocotyl length, and carotenoid content (Figure 6A). In addition, as can be seen, the seedling growth difference between the FR, UV-A+FR, and B+FR treatments was small. Analogously, a relatively small difference in seedling growth existed between the B, UV-A, B+UV-A, and CK treatments (Figure 6A).

To simplify these indices, OriginPro 2021 software was used to build a formula to simplify these evaluated indicators. Then, we constructed a comprehensive score model for comprehensively evaluating the performance of tomato seedlings grown under

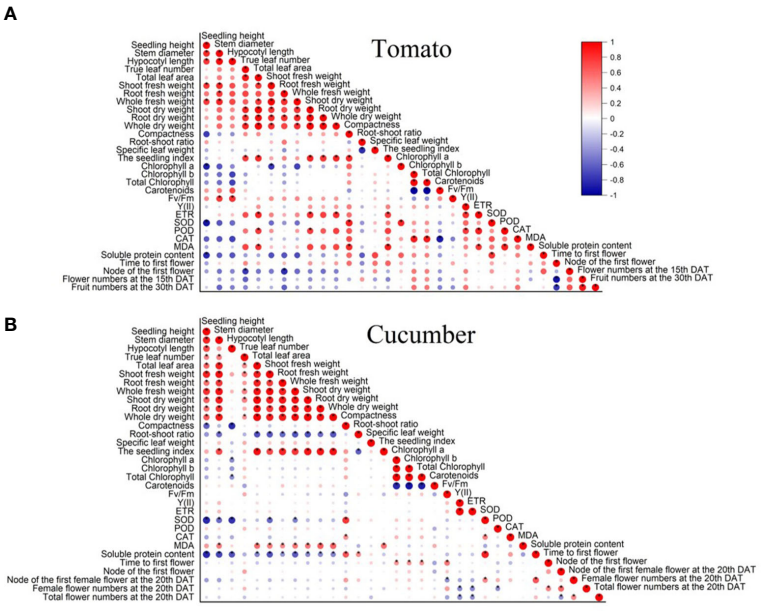

FIGURE 5
The Pearson correlation of **(A)** tomato and **(B)** cucumber seedlings under different light conditions. All examined indexes in each variety were involved in the analysis. * means significance level ($p < 0.05$).

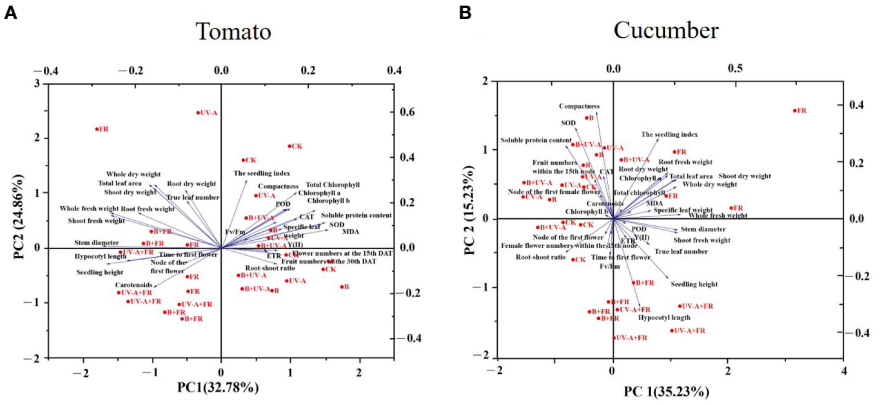

FIGURE 6
PCA analysis of **(A)** tomato and **(B)** cucumber seedlings grown under various light conditions.

various light conditions. With reference to the methods of Huang et al. (2021) and Sabzalian et al. (2014), the formula was Y = 32.78% Y1 +24.86% Y2 (Supplementary Table S2). Using this formula, the optimal light treatment for the growth and quality of tomato seedlings was UV-A > B > CK > B+UV-A > FR > B+FR > UV-A+FR.

Cucumber seedlings

In cucumber seedlings, the seedling index was positively correlated with the stem diameter, true leaf number, total leaf area, whole fresh weight, shoot fresh weight, root fresh weight, shoot dry weight, root dry weight, and MDA content (Figure 5B). However, it was negatively correlated with the root shoot ratio and had no significant correlation with the other examined indicators (Figure 5B).

As was shown, following the PCA, the seedling index was positively related with chlorophyll a, total leaf area, whole dry weight, shoot dry weight, root dry weight, whole fresh weight, root fresh weight, and MDA content (Figure 6B). In terms of growth performance, seedlings grown in the CK, B, UV-A, and B +UV-A treatments showed small growth differences, while the growth of those seedlings was significantly different from that in the UV-A+FR and B+FR treatments (Figure 6B).

By means of the above-described method, Y=35.23% Y1 +15.23% Y2 was the calculated formula of the comprehensive score model (Supplementary Table S3). According to this model, the optimal light quality for the growth and quality of cultivated cucumber seedlings was as follows: FR > UV-A+FR > B > B+UV-A > UV-A > B+FR > CK.

Discussion

Effects of different light qualities on the morphology and biomass of tomato and cucumber seedlings

The negative role of blue light in plant height has been previously described in many species, such as tomato, cucumber, and pepper (Nanya et al., 2012; Hamedalla et al., 2022; Liu et al., 2022). In this study, we also obtained similar results (Figure 2C). Adding 6.8 W-m^{-2} UV-A to monochromatic red light significantly reduced the height of tomato seedlings (Khoshimkhujaev et al., 2014). Differently, our data displayed that supplemental radiation of 6 μmol m^{-2} s^{-1} UV-A to the CK (white: red= 3:2) had no significant effect on the seedling height of tomato (Figure 2C). These might be due to the different responses of plants to different combinations of light wavelengths. However, unlike in tomato, supplementing with 6 μmol m^{-2} s^{-1} UV-A significantly inhibited the height of cucumber seedlings (Figure 2C), suggesting that the response of seedling height to supplemental UV-A light might vary in different vegetable varieties. When plant cryptochromes perceive UV-A and blue radiations, the synthesis or sensitivity of gibberellin and auxin in plants is affected, resulting in stem elongation inhibition (Huchéthélier et al., 2016). However, in both tomato and cucumber, seedlings in the UV-A+FR and B+FR treatments exhibited higher seedling height and hypocotyl length than those in the control (Figure 2C), meaning that when combined with blue or UV-A light, far-red light played a predominant role in the effect of seedling height and hypocotyl length. When exposed to far-red light, the increased seedling height in both tomato and cucumber might be due to the reduction in the R:FR ratio caused by supplementing far-red light, which is sensed by phytochrome and induces a shade-avoidance syndrome, including stem elongation (Franklin and Quail, 2010).

Previous studies demonstrated a reduction in total leaf area in tomato and cucumber seedlings when exposed to increased blue light (Yousef et al., 2021; Hamedalla et al., 2022). In this study, under the B and B+UV-A treatments, the total leaf area decreased in tomato seedlings but did not change in cucumber seedlings (Figure 2G). These might be because that the cucumber varieties used in this study (cv. Zaoqing No. 2) was relatively insensitive to blue light, resulting in different plant responses. Our results showed that the total leaf area of tomato seedlings in the UV-A treatment was not significantly different from that in the control (Figure 2G). These results were not in line with the result on tomato that supplementation of UV-A (daily UV-A dose > 1.17 kJ-m^{-2} · d^{-1})

increased the total leaf area (Kang et al., 2018), but the dose of UV-A light used in the study was different from our study. Under the R3B7+ UV-A treatment, the total leaf area of cucumber seedlings was evidently increased, while that in the R5B5+ UV-A treatment showed no comparable difference (Jeong et al., 2020). In this study, the total leaf area of cucumber seedlings in the 3W2R+ UV-A treatment did not differ from that of those in the control (3W2R treatment) (Figure 2G). These different effects of light quality on leaf development in these treatments might be due to the different light quality ratios or combinations. Interestingly, in our study, in cucumber seedlings under the far-red light supplement treatments (FR, UV-A+FR, and B+FR), the total leaf area was elevated only in the FR treatment (Figure 2G), suggesting that there might be an antagonism effect between far-red light and blue light or UV-A light on leaf development. To adapt to the low R:FR ratio caused by FR radiation, plants increased their total leaf area to harvest more light, but this hinged on species and growth conditions (Demotes-Mainard et al., 2016). Total leaf area has been considered a key parameter in determining plant growth (Weraduwage et al., 2015). Our Pearson analysis showed that the seedling index was positively correlated with the total leaf area in cucumber seedlings (Figure 5B). Among all treatments in cucumber, only the FR treatment showed a significant increase in the seedling index, and the total leaf area merely increased in the FR treatment (Figure 5G; Table 1). The highest total leaf area observed in the FR treatment might be attributed to the low R: FR radiation inducing rapid leaf development, resulting in increased leaf area and a large accumulation of photosynthetic products in the leaves (Park and Runkle, 2017).

The fresh and dry weights of the "Oxheart" tomato seedlings were increased, whereas those of the "Cherry" and "Roma" tomato seedlings were unaffected by adding UV-A light (Mariz-Ponte et al., 2018). Supplementation with far-red light and 25B (blue light) increased the total dry weight of the tomato plants, whereas 50–100B had no effect (Liang et al., 2021; Wang et al., 2021). Here, our data suggested that there was no obvious discrepancy in the dry weight of tomato seedlings among all the treatments (Figure 3A). These results demonstrated that the influence of supplemental light of different qualities on plant biomass is jointly determined by light quality, light intensity, and variety. The accumulation of plant dry matter is also affected by the total leaf area, since the light energy intercepted by plants will increase with the increase in total leaf area (Park and Runkle, 2018). In this paper, the total leaf area of tomato seedlings treated with UV-A, FR, UV-A+FR, and B+FR had no significant difference compared with the control (Figure 2G), which corresponds to the result that there was no significant difference in the total dry weight and the shoot dry weight between these four treatments and the control (Figure 3A). In the results of Pearson analysis and the PCA of cucumber seedlings, the seedling index was positively correlated with the plant dry weight, the shoot dry weight, and the root dry weight (Figure 5B). Under the FR treatment, the increase in total leaf area of cucumber seedlings may promote a marked increase in plant dry weight and shoot dry weight, thus enhancing the seedling index (Figures 2G, 3B).

With respect to a single growth index, like plant height, stem diameter, and biomass, comprehensive indexes, such as compactness and the seedling index, can more comprehensively reflect the overall growth quality of seedlings (Bai et al., 2014; Vu et al., 2014). Usually, the higher the seedling index and compactness, the higher the quality of the seedlings (Bai et al., 2014; An et al., 2020). Previous studies have revealed that more compact pepper and tomato seedlings were produced by appropriately increasing blue light (Hernández et al., 2016; Liu et al., 2022). In addition, exposure to UV-A increased the compactness of cucumber and pepper seedlings (Jeong et al., 2020; Liu et al., 2022). Consistently, the compactness of cucumber and tomato seedlings under B and B+UV-A treatments significantly increased (Table 1). In the UV-A treatment, being distinct from the increased compactness of cucumber seedlings, those of tomato seedlings did not differ from the control (Table 1). Since plant compactness represents the ratio of shoot dry weight to plant height, the unaffected shoot dry weight and plant height of tomato seedlings in the UV-A treatment might explain why there is no significant difference in compactness between the UV-A treatment and control (Table 1). The compactness of both cucumber and tomato seedlings grown under FR, B+FR, and UV-A+FR treatments significantly decreased, which might be due to the promotion of far-red light on the seedling height. According to the results of Pearson analysis and PCA in tomato seedlings, the seedling index was significantly positively correlated with compactness (Figure 5A). The increased seedling index and compactness of the B+UV-A treatment meant that the light quality of this treatment was advantageous for cultivating high-quality tomato seedlings. What's interesting is that although the seedling height, stem diameter, total leaf area, dry weight, fresh weight, the seedling index, compactness, and photosynthetic pigment content of tomato seedlings under the UV-A treatment were not significantly greater than those of the control, the comprehensive score of tomato seedlings obtained by comprehensive analysis in the UV-A treatment was higher than that in control, which indicated that the light condition of the UV-A treatment was more suitable for cultivating tomato seedlings. These results might be due to the relatively small component contribution value of each growth index in the comprehensive formula (Supplementary Table S2). In cucumber, the seedling height, stem diameter, total leaf area, whole dry weight, shoot dry weight, and the seedling index of cucumber seedlings under FR treatment significantly increased. Correspondingly, the comprehensive analysis in this study showed that FR treatment was the most favourable lighting condition for cultivating high-quality cucumber seedlings.

Furthermore, the results of the Pearson analysis indicated that the seedling growth difference between the B, UV-A, B+UV-B, and CK treatments and the FR, UV-A+FR, and B+FR treatments, no matter in tomato or cucumber, was small (Figures 6A, B). These suggested that the effects of different light qualities on different plants were similar to some extent; undoubtedly, more experiments should be conducted in the future to clarify these differences.

Effects of different light qualities on photosynthetic characteristics and photosynthetic pigments of tomato and cucumber seedlings

UV-A did not cause an evident influence on the chlorophyll content of cucumber and tomato plants (Brazaitytė et al., 2009; Brazaitytė et al., 2010), similar results in the UV-A and B+UV-A treatments were also observed in this work (Table 2). Supplementation of far-red light decreased the chlorophyll content in both tomato and cucumber plants (Wang et al., 2021). Our FR treatment did not affect the chlorophyll content of tomatoes and cucumbers, while the FR+B treatments reduced the chlorophyll content of tomatoes and the carotenoid content of cucumbers, respectively. Adding blue light promoted chlorophyll accumulation in cucumber (Hernández and Kubota, 2016). In this study, a stimulation of chlorophyll contents was only detected in the B treatment when supplemented with blue light. In tomato, the contents of chlorophyll a, chlorophyll b, and total chlorophyll were not affected in the B, UV-A, and FR treatments, whereas these significantly reduced in the UV-A+FR and B+FR treatments (Table 2). These results collectively suggested that the effect of different light spectral combinations on plant photosynthetic pigments was a complex response process, which might be a consequence of the interaction between different light spectra.

Fv/Fm represents the potential quantum efficiency of PSII; the smaller the value, the greater the photoinhibition of plants (Kumar et al., 2014). Generally, in normally growing plants, the maximum quantum yield of PSII (Fv/Fm value) is approximately 0.83 (Björkman and Demmig, 1987). The Fv/Fm values of seedlings in this study are approximately 0.78 (Table 2), which might be a result of the incomplete light spectral range of the used LED lights. UV radiation induces photosynthetic protein degradation, causing negative stress on the PSII (Greenberg et al., 1989). However, compared to the control, no significant differences in the Fv/Fm values were exhibited in tomato and cucumber seedlings under UV-A light (UV-A, B+UV-A, and UV-A+FR treatments) (Table 2), indicating that these seedlings were not under light stress. In tomato seedlings, the Fv/Fm values in the FR treatment were not significantly different from those in the control (Table 2); similar results were found in a previous report (Wang et al., 2021). In cucumber seedlings, the Fv/Fm were unaffected in the B treatment but remarkably decreased in the FR treatment in comparison with the control (Table 2), implying that the FR treatment led to inhibition of PSII in cucumber leaves. Surprisingly, the Fv/Fm values of cucumber seedlings in the B+FR treatment were significantly greater than those in the control (Table 2), which means that blue light in the B+FR treatment could alleviate the inhibition of PSII caused by far-red light, but the interaction between blue and far-red light needs further investigation.

In the six light treatments except CK, both the Y (II) and ETR values significantly reduced in tomato seedlings but markedly enhanced in cucumber seedlings (Table 2). These indicated that the actual quantum yield and electron transfer rate of the control were comparatively higher in tomato but lower in cucumber (Yousef et al., 2021). In cucumber seedlings, although the chlorophyll content was unaffected in the B+FR treatment, the photosynthesis rate significantly increased in the B+FR treatment (Table 2), which might be caused by the difference in leaf microstructures (Yao et al., 2017).

Effects of different light qualities on antioxidant system of tomato and cucumber seedlings

The antioxidant enzyme activity in plant tissues, which are affected by different light spectrums, clearly states a valid response to various stresses. Cucumber plants that radiated under blue light exhibited higher activities of SOD and CAT, with increased tolerance to Cd stress (Guo et al., 2022). Tomato seedlings supplemented with far-red light had elevated activities of SOD, POD, and CAT and enhanced salt resistance (Wang et al., 2021). However, in this study, in comparison with the control, the activity of SOD and POD decreased in the FR and UV-A+FR treatments of tomato seedlings (Figures 4B, C), which might be related to differences in the background light quality or the plant cultivars, causing different experimental results.

After being exposed to blue light, the content of chlorophyll and soluble protein in cucumber increased, which will indirectly balance the active oxygen in the species, thus increasing the activity of antioxidant enzymes (Wang et al., 2009). In this study, the increase in the content of chlorophyll and soluble protein in the B treatment might be contributed to the increased activities of SOD and POD in cucumber seedlings (Figures 4B, C). In contrast to the control seedlings, cucumber seedlings under the UV-A and B+UV-A treatments had significantly elevated activities of SOD and POD, with significantly decreased MDA content in the B+UV-A treatment (Figures 4B–E), suggesting that supplementation of blue and UV-A light alone and UV-A+B was beneficial to increasing the antioxidant level of cucumber seedlings, which needs further demonstration.

Effects of different light qualities on the growth and development of tomato and cucumber after transplanting

Our results showed that the flowering time was delayed significantly in cucumber seedlings grown under the FR treatments, but it was not affected in tomato plants (Table 3). Supplementation of FR radiation at the seedling stage had no effect on the flowering time of geranium (Park and Runkle, 2017). From these, the effect of far-red light radiation on the flowering of different species and its mechanism deserves further exploration. From the PCA results, in tomato, there was no significant correlation between the flowering time and measured physiological indices before transplanting (Figure 5A). In cucumber, the flowering time was positively correlated with Fv/Fm (Figures 5B, 6B), which was in agreement with the results that

Fv/Fm was significantly reduced and the flowering time was significantly delayed under the FR treatment. Certain correlations exist between the vegetative and reproductive growth of plants (Cremer, 1992). In the FR treatment, the decrease in Fv/Fm might result in insufficient nutrient growth, which may lead to the delay of flowering time in cucumber plants.

For cucumber, the node position of the first female flower in seedlings treated with FR treatment was lower (Table 4), indicating that adding far-red light alone could promote the formation of female flowers. It is known that the sexual differentiation of cucumber is affected by hormones such as ethylene and gibberellin (Zhang et al., 2017). In addition, far-red light can affect the synthesis of plant hormones (Islam et al., 2014). In this study, far-red light might influence female flower differentiation by affecting the synthesis of hormones. Despite that the total flower number was obviously unaffected within 20 DAT in the B, UV-A, and FR treatments, this was significantly reduced in the UV-A+FR and B+FR treatments (Table 4), implying that supplementing with UV-A+FR or B+FR at the seedling stage appears to be not good for flower development in cucumber plants. This phenomenon and its mechanism deserve in-depth research in the future.

Conclusion

This study investigated the growth of tomato and cucumber seedlings under different light treatments (CK, B, UV-A, FR, B +UV-A, UV-A+FR, and FR+BB+FR) and the development of these seedlings after transplanting. There are some similarities in the growth morphology of the two varieties under different lighting environments: the growth morphology was promoted under the FR, UV-A+FR, and B+FR treatments but was inhibited under the B treatment. The B+UV-A treatment and the FR treatment increased the seedling index of tomato and cucumber seedlings, respectively. The B treatment increased the chlorophyll content, Y (II), and ETR of cucumber. In the UV-A treatment, the activities of SOD and POD were repressed in tomatoes but enhanced in cucumbers. The UV-A and FR treatments were beneficial for the flower development of tomato and cucumber after transplantation, respectively. In the future, the correlation between light quality and environmental factors such as photoperiod and temperature can be conducted through multiple variables, in order to obtain a better environment for seedling growth and provide a reference for the development of the vegetable seedling industry in plant factories and greenhouses.

Data availability statement

The original contributions presented in the study are included in the article/Supplementary Material. Further inquiries can be directed to the corresponding author.

Author contributions

XL, RS, and MG performed the experiments and wrote the manuscript. RH and YL performed the experiments and statistical analyses. HL conceived and designed the experiments. HL acquired of funding and contributed to revised the manuscript. All authors have read and agreed to the published version of the manuscript.

Funding

This study was supported by grant from the Key Research and Development Program of Ningxia (2021BBF02024) and the National Key Research and Development Program of China (2017YFE0131000).

Conflict of interest

The authors declare that the research was conducted in the absence of any commercial or financial relationships that could be construed as a potential conflict of interest.

Publisher's note

Supplementary material

The Supplementary Material for this article can be found online at: https://www.frontiersin.org/articles/10.3389/fpls.2023.1164768/full#supplementary-material

References

An, S., Park, S. W., and Kwack, Y. (2020). Growth of cucumber scions, rootstocks, and grafted seedlings as affected by different irrigation regimes during cultivation of 'Joenbaekdadagi' and 'Heukjong' seedlings in a plant factory with artificial lighting. *Agronomy* 10 (12), 1943. doi: 10.3390/agronomy10121943

Bai, Y., Shi, W., Xing, X., Wang, Y., Jin, Y., Zhang, L., et al. (2014). Study on tobacco vigorous seedling indexes model. *Agric. Sci. China* 6, 1086–1098. doi: 10.3864/j.issn.0578-1752.2014.06.005

Balliu, A. (2017). Nursery management practices influence the quality of vegetable seedlings. *Italus Hortus* 24, 39–52. doi: 10.26353/j.itahort/2017.3.3952

Björkman, O., and Demmig, B. (1987). Photon yield of O2 evolution and chlorophyll fluorescence characteristics at 77 K among vascular plants of diverse origins. *Planta* 170, 489–504. doi: 10.1007/BF00402983

Brazaitytė, A., Duchovskis, P., Urbonavičiūtė, A., Samuolienė, G., Jankauskienė, J., Kasiulevičiūtė-Bonakėrė, A., et al. (2009). The effect of light-emitting diodes lighting on

cucumber transplants and after-effect on yield. *Zemdirbyste-Agriculture* 96 (3), 102-118. Available at: https://zemdirbyste-agriculture.lt/96(3)tomas/96_3_tomas_102_118.pdf.

Brazaitytė, A., Duchovskis, P., Urbonavičiūtė, A., Samuolienė, G., Jankauskienė, J., Sakalauskaitė, J., et al. (2010). The effect of light-emitting diodes lighting on the growth of tomato transplants. *Zemdirbyste-Agriculture* 97 (2), 89–98. doi: 10.1080/14620316.2005.11511934

Carvalho, R. F., Takaki, M., and Azevedo, R. A. (2010). Plant pigments: the many faces of light perception. *Acta Physiologiae Plantarum* 33 (2), 241–248. doi: 10.1007/s11738-010-0533-7

Chen, X. L., Li, Y. L., Wang, L. C., and Guo, W. Z. (2021). Red and blue wavelengths affect the morphology, energy use efficiency and nutritional content of lettuce (*Lactuca sativa* l.). *Sci. Rep.* 11 (1), 8374. doi: 10.1038/s41598-021-87911-7

Claypool, N. B., and Lieth, J. H. (2020). Physiological responses of pepper seedlings to various ratios of blue, green, and red light using LED lamps. *Scientia Hortic.* 268, 109371. doi: 10.1016/j.scienta.2020.109371

Cremer, K. W. (1992). Relations between reproductive growth and vegetative growth of pinus radiata. *For. Ecol. Manage.* 52 (1-4), 179–199. doi: 10.1016/0378-1127(92)90501-y

Demotes-Mainard, S., Péron, T., Corot, A., Bertheloot, J., Le Gourrierec, J., Pelleschi-Travier, S., et al. (2016). Plant responses to red and far-red lights, applications in horticulture. *Environ. Exp. Bot.* 121, 4–21. doi: 10.1016/j.envexpbot.2015.05.010

Franklin, K. A., and Quail, P. H. (2010). Phytochrome functions in arabidopsis development. *J. Exp. Bot.* 61 (1), 11–24. doi: 10.1093/jxb/erp304

Goto, E. (2012). Plant production in a closed plant factory with artificial lighting. *Acta Hortic.* 956, 37–49. doi: 10.17660/actahortic.2012.956.2

Greenberg, B. M., Gaba, V., Canaani, O., Malkin, S., Mattoo, A. K., and Edelman, M. (1989). Separate photosensitizers mediate degradation of the 32-kDa photosystem II reaction center protein in the visible and UV spectral regions. *Proc. Natl. Acad. Sci.* 86 (17), 6617–6620. doi: 10.1073/pnas.86.17.6617

Guo, Z., Lv, J., Zhang, H., Hu, C., Qin, Y., Dong, H., et al. (2022). Red and blue light function antagonistically to regulate cadmium tolerance by modulating the photosynthesis,antioxidant defense system and cd uptake in cucumber(*Cucumis sativus* l.). *J. Hazard Mater* 429, 128412. doi: 10.1016/j.jhazmat.2022.128412

Hamedalla, A. M., Ali, M. M., Ali, W. M., Ahmed, M. A. A., Kaseb, M. O., Kalaji, H. M., et al. (2022). Increasing the performance of cucumber (*Cucumis sativus* l.) seedlings by LED illumination. *Sci. Rep.* 12 (1), 852. doi: 10.1038/s41598-022-04859-y

He, R., Zhang, Y., Song, S., Su, W., Hao, Y., and Liu, H. (2021). UV-A and FR irradiation improves growth and nutritional properties of lettuce grown in an artificial light plant factory. *Food Chem.* 345, 128727. doi: 10.1016/j.foodchem.2020.128727

Hernández, R., Eguchi, T., Deveci, M., and Kubota, C. (2016). Tomato seedling physiological responses under different percentages of blue and red photon flux ratios using LEDs and cool white fluorescent lamps. *Scientia Hortic.* 213, 270–280. doi: 10.1016/j.scienta.2016.11.005

Hernández, R., and Kubota, C. (2016). Physiological responses of cucumber seedlings under different blue and red photon flux ratios using LEDs. *Environ. Exp. Bot.* 121, 66–74. doi: 10.1016/j.envexpbot.2015.04.001

Huang, Y., Li, Y., Gao, X., Zhang, Y., Chen, C., Wu, M., et al. (2021). Evaluation indexes of tomato seedling growth based on principal component analysis. *China Cucurbits Vegetables.* 34 (8), 32–37. doi: 10.16861/j.cnki.zggc.2021.0201

Huchéthélier, L., Crespel, L., Gourrierec, J. L., Morel, P., Sakr, S., and Leduc, N. (2016). Light signaling and plant responses to blue and UV radiations–perspectives for applications in horticulture. *Environ. Exp. Bot.* 121, 22–38. doi: 10.1016/j.envexpbot.2015.06.009

Hwang, H., An, S., Lee, B., and Chun, C. (2020). Improvement of growth and morphology of vegetable seedlings with supplemental far-red enriched LED lights in a plant factory. *Horticulturae* 6 (4), 109. doi: 10.3390/horticulturae6040109

Islam, M. A., Tarkowská, D., Clarke, J. L., Blystad, D.-R., Gislerød, H. R., Torre, S., et al. (2014). Impact of end-of-day red and far-red light on plant morphology and hormone physiology of poinsettia. *Scientia Hortic.* 174, 77–86. doi: 10.1016/j.scienta.2014.05.013

Jeong, H. W., Lee, H. R., Kim, H. M., Kim, H. M., Hwang, H. S., and Hwang, S. J. (2020). Using light quality for growth control of cucumber seedlings in closed-type plant production system. *Plants (Basel)* 9 (5), 639. doi: 10.3390/plants9050639

Jin, D., Su, X., Li, Y., Shi, M., Yang, B., Wan, W., et al. (2023). Effect of red and blue light on cucumber seedlings grown in a plant factory. *Horticulturae* 9 (2), 124. doi: 10.3390/horticulturae9020124

Kang, S., Zhang, Y., Zhang, Y., Zou, J., Yang, Q., and Li, T. (2018). Ultraviolet-a radiation stimulates growth of indoor cultivated tomato (*Solanum lycopersicum*) seedlings. *HortScience* 53 (10), 1429–1433. doi: 10.21273/hortsci13347-18

Khoshimkhujaev, B., Kwon, J. K., Park, K. S., Choi, H. G., and Lee, S. Y. (2014). Effect of monochromatic UV-a LED irradiation on the growth of tomato seedlings. *Horticulture Environment Biotechnol.* 55 (4), 287–292. doi: 10.1007/s13580-014-0021-x

Kong, Y., Schiestel, K., and Zheng, Y. (2019). Pure blue light effects on growth and morphology are slightly changed by adding low-level UVA or far-red light: a comparison with red light in four microgreen species. *Environ. Exp. Bot.* 157, 58–68. doi: 10.1016/j.envexpbot.2018.09.024

Kozai, T. (2013). Resource use efficiency of closed plant production system with artificial light: concept, estimation and application to plant factory. *Proc. Jpn Acad. Ser. B Phys. Biol. Sci.* 89 (10), 447–461. doi: 10.2183/pjab.89.447

Kozai, T. (2018). Plant factories with artificial lighting (PFALs) benefits, problems, and challenges: the next generation indoor vertical farms. *Smart Plant Factory* 2, 15-29. doi: 10.1007/978-981-13-1065-2_2

Kumar, K. S., Dahms, H. U., Lee, J. S., Kim, H. C., Lee, W. C., and Shin, K. H. (2014). Algal photosynthetic responses to toxic metals and herbicides assessed by chlorophyll a fluorescence. *Ecotoxicol Environ. Saf.* 104, 51–71. doi: 10.1016/j.ecoenv.2014.01.042

Li, Y., Xin, G., Liu, C., Shi, Q., Yang, F., and Wei, M. (2020). Effects of red and blue light on leaf anatomy, CO2 assimilation and the photosynthetic electron transport capacity of sweet pepper (*Capsicum annuum* l.) seedlings. *BMC Plant Biol.* 20 (1), 318. doi: 10.1186/s12870-020-02523-z

Li, L., and Yi, H. (2012). Effect of sulfur dioxide on ROS production, gene expression and antioxidant enzyme activity in arabidopsis plants. *Plant Physiol. Biochem.* 58, 46–53. doi: 10.1016/j.plaphy.2012.06.009

Liang, Y., Kang, C., Kaiser, E., Kuang, Y., Yang, Q., and Li, T. (2021). Red/blue light ratios induce morphology and physiology alterations differently in cucumber and tomato. *Scientia Hortic.* 281, 109995. doi: 10.1016/j.scienta.2021.109995

Liu, X., Guo, S., Chang, T., Xu, Z., and Tezuka, T. (2012). Regulation of the growth and photosynthesis of cherry tomato seedlings by different light irradiations of light emitting diodes (LED). *Afr. J. Biotechnol.* 11 (22), 6169-6177. doi: 10.5897/ajb11.1191

Liu, X., Shi, R., Gao, M., He, R., Li, Y., and Liu, H. (2022). Effects of LED light quality on the growth of pepper (*Capsicum* spp.) seedlings and the development after transplanting. *Agronomy* 12 (10), 2269. doi: 10.3390/agronomy12102269

Mariz-Ponte, N., Mendes, R. J., Sario, S., Melo, P., and Santos, C. (2018). Moderate UV-a supplementation benefits tomato seed and seedling invigoration: a contribution to the use of UV in seed technology. *Scientia Hortic.* 235, 357–366. doi: 10.1016/j.scienta.2018.03.025

Morrow, R. C. (2008). LED lighting in horticulture. *HortScience horts* 43 (7), 1947–1950. doi: 10.21273/HORTSCI.43.7.1947

Nanya, K., Ishigami, Y., Hikosaka, S., and Goto, E. (2012). Effects of blue and red light on stem elongation and flowering of tomato seedlings. *Acta Horticulturae.* 956, 261–266. doi: 10.17660/ActaHortic.2012.956.29

Park, Y., and Runkle, E. S. (2017). Far-red radiation promotes growth of seedlings by increasing leaf expansion and whole-plant net assimilation. *Environ. Exp. Bot.* 136, 41–49. doi: 10.1016/j.envexpbot.2016.12.013

Park, Y., and Runkle, E. S. (2018). Far-red radiation and photosynthetic photon flux density independently regulate seedling growth but interactively regulate flowering. *Environ. Exp. Bot.* 155, 206–216. doi: 10.1016/j.envexpbot.2018.06.033

Raza, S. H., Athar, H. R., Ashraf, M., and Hameed, A. (2007). Glycinebetaine-induced modulation of antioxidant enzymes activities and ion accumulation in two wheat cultivars differing in salt tolerance. *Environ. Exp. Bot.* 60 (3), 368–376. doi: 10.1016/j.envexpbot.2006.12.009

Sabzalian, M. R., Heydarizadeh, P., Zahedi, M., Boroomand, A., Agharokh, M., Sahba, M. R., et al. (2014). High performance of vegetables, flowers, and medicinal plants in a red-blue LED incubator for indoor plant production. *Agron. Sustain. Dev.* 34 (4), 879–886. doi: 10.1007/s13593-014-0209-6

Seckin, B., Sekmen, A. H., and Türkan, İ. (2008). An enhancing effect of exogenous mannitol on the antioxidant enzyme activities in roots of wheat under salt stress. *J. Plant Growth Regul.* 28 (1), 12–20. doi: 10.1007/s00344-008-9068-1

Son, K., Kim, E., and Oh, M. (2018). Growth and development of cherry tomato seedlings grown under various combined ratios of red to blue LED lights and fruit yield and quality after transplanting. *Protected horticulture Plant Factory* 27 (1), 54–63. doi: 10.12791/ksbec.2018.27.1.54

Stanaway, J. D., Afshin, A., Ashbaugh, C., Bisignano, C., Brauer, M., Ferrara, G., et al. (2022). Health effects associated with vegetable consumption: a burden of proof study. *Nat. Med.* 28 (10), 2066–2074. doi: 10.1038/s41591-022-01970-5

Su, N., Wu, Q., Shen, Z., Xia, K., and Cui, J. (2013). Effects of light quality on the chloroplastic ultrastructure and photosynthetic characteristics of cucumber seedlings. *Plant Growth Regul.* 73 (3), 227–235. doi: 10.1007/s10725-013-9883-7

Vu, N.-T., Kim, Y.-S., Kang, H.-M., and Kim, I.-S. (2014). Influence of short-term irradiation during pre- and post-grafting period on the graft-take ratio and quality of tomato seedlings. *Horticulture Environment Biotechnol.* 55 (1), 27–35. doi: 10.1007/s13580-014-0115-5

Wang, Y., Bian, Z., Pan, T., Cao, K., and Zou, Z. (2021). Improvement of tomato salt tolerance by the regulation of photosynthetic performance and antioxidant enzyme capacity under a low red to far-red light ratio. *Plant Physiol. Biochem.* 167, 806–815. doi: 10.1016/j.plaphy.2021.09.008

Wang, H., Gu, M., Cui, J., Shi, K., Zhou, Y., and Yu, J. (2009). Effects of light quality on CO2 assimilation, chlorophyll-fluorescence quenching, expression of Calvin cycle genes and carbohydrate accumulation in cucumis sativus. *J. Photochem. Photobiol. B* 96 (1), 30–37. doi: 10.1016/j.jphotobiol.2009.03.010

Weraduwage, S. M., Chen, J., Anozie, F. C., Morales, A., Weise, S. E., and Sharkey, T. D. (2015). The relationship between leaf area growth and biomass accumulation in arabidopsis thaliana. *Front. Plant Sci.* 6, 167. doi: 10.3389/fpls.2015.00167

Wu, M., Hou, C., Jiang, C., Wang, Y., Wang, C., Chen, H., et al. (2007). A novel approach of LED light radiation improves the antioxidant activity of pea seedlings. *Food Chem.* 101 (4), 1753–1758. doi: 10.1016/j.foodchem.2006.02.010

Yao, X., Liu, X., Xu, Z., and Jiao, X. (2017). Effects of light intensity on leaf microstructure and growth of rape seedlings cultivated under a combination of red and blue LEDs. *J. Integr. Agric.* 16 (1), 97–105. doi: 10.1016/s2095-3119(16)61393-x

Yousef, A. F., Ali, M. M., Rizwan, H. M., Tadda, S. A., Kalaji, H. M., Yang, H., et al. (2021). Photosynthetic apparatus performance of tomato seedlings grown under various combinations of LED illumination. *PloS One* 16 (4), e0249373. doi: 10.1371/journal.pone.0249373

Zhang, J., Huang, W., Liu, Y., and Pan, Q. (2005). Effects of temperature acclimation pretreatment on the ultrastructure of mesophyll cells in young grape plants (*Vitis vinifera* l. cv. jingxiu) under cross-temperature stresses. *J. Integr. Plant Biol.* 47 (8), 959–970. doi: 10.1111/j.1744-7909.2005.00109.x

Zhang, Y., Zhao, G., Li, Y., Mo, N., Zhang, J., and Liang, Y. (2017). Transcriptomic analysis implies that GA regulates sex expression *via* ethylene-dependent and ethylene-independent pathways in cucumber (*Cucumis sativus* l.). *Front. Plant Sci.* 8, 10. doi: 10.3389/fpls.2017.00010

frontiers | Frontiers in Plant Science

TYPE Original Research
PUBLISHED 29 August 2023
DOI 10.3389/fpls.2023.1199168

OPEN ACCESS

EDITED BY
Qingming Li,
Chinese Academy of Agricultural Sciences, China

REVIEWED BY
Mohammad Nauman Khan,
Huazhong Agricultural University, China
Fei Ni,
Shandong Agricultural University, China

*CORRESPONDENCE
Shizhou Du
dsz315@sina.com
Yuqiang Qiao
yuqiangqiao@163.com

RECEIVED 03 April 2023
ACCEPTED 02 August 2023
PUBLISHED 29 August 2023

CITATION
Zhang X, Xu Y, Du S, Qiao Y, Cao C and Chen H (2023) Optimized N application improves N absorption, population dynamics, and ear fruiting traits of wheat. *Front. Plant Sci.* 14:1199168. doi: 10.3389/fpls.2023.1199168

Optimized N application improves N absorption, population dynamics, and ear fruiting traits of wheat

Xiangqian Zhang[1], Yunji Xu[2], Shizhou Du[1]*, Yuqiang Qiao[1]*, Chengfu Cao[1] and Huan Chen[1]

[1]Crops Research Institute, Anhui Academy of Agricultural Sciences, Hefei, Anhui, China, [2]Joint International Research Laboratory of Agriculture and Agri-product Safety, The Ministry of Education of China, Yangzhou University, Yangzhou, Jiangsu, China

Optimizing the N application amount and topdressing ratio can increase crop yield and decrease N loss, but its internal mechanisms have not been well studied, especially from the aspects of population dynamics and structure, ear fruiting traits. Here, field experiments, with three N rates 120 (N1), 180 (N2), and 240 (N3) kg N ha^{-1} and three N topdressing ratios T1 (7:3), T2 (6:4), and T3 (5:5) were conducted. At the same N level, results showed that the N accumulation amounts in the leaf, grain, and plant in T2 were higher than in T3 and T1, and increasing 60 kg N ha^{-1} (N3 compared to N2, N2 compared to N1) significantly enhanced N accumulation amounts. The effect of the N topdressing ratio on partial factor productivity of applied N was consistently T2 > T3 > T1, but T1 was more conducive to improving N utilization efficiency for grain and biomass production. After the jointing stage, compared to T1 and T3, T2 was more conducive to increasing the population growth rate of plant height, leaf area index, leaf area growth rate, dry matter weight, dry matter accumulation rate, light interception rate, and spikelets of population, and the above-mentioned indexes of population could be significantly enhanced by increasing 120 kg N ha^{-1}. T2 increased the fruiting spikelets per ear, grains per ear, grain weight per ear, fruiting rate per ear, grain filling rate per ear, and yield but decreased the sterile spikelets at the top and bottom and imperfect grains per ear. Increasing N from 120 kg ha^{-1} to 180 kg ha^{-1} or from 180 kg ha^{-1} to 240 kg ha^{-1} significantly enhanced yield. The N accumulation amount in the grain, leaf, plant, leaf area growth rate, dry matter accumulation rate, light interception rate, population spikelets, fruiting spikelets per ear, grain filling rate, and yield were significantly positively correlated with each other. This study demonstrates a suitable N application rate with a N topdressing ratio 6:4 would more effectively improve N efficiency, population dynamics, structure, ear fruiting traits, and yield, but the effect of the N topdressing ratio is not as significant as that of increasing 60 kg N ha^{-1}.

KEYWORDS

N use efficiency, leaf area, light interception rate, ear fruiting traits, yield

Abbreviations: Three N rates, N1, 120 kg N ha^{-1}, N2, 180 kg N ha^{-1}, N3, 240 kg N ha^{-1}; Three ratios of basal N to topdressing: T1, 7:3, T2, 6:4, T3, 5:5.

1 Introduction

Wheat is one of the most important crops in the world, with figures showing a harvested area of 214.3 million ha and a global production of 734 million tons in 2018 (Illescas et al., 2020). As an essential nutrient for crop growth and development, nitrogen (N) is a major determinant of grain yield in wheat cropping systems, increasing the N application rate has contributed significantly to the increase of wheat yield in the world (Zörb et al., 2018). However, the rates of crop yield growth have slowed down in the past 20 years and have even become stagnated in some countries and regions despite enhanced N fertilizer input (Grassini et al., 2013; Che et al., 2015). The N fertilizer use efficiency in wheat production is abysmally low, i.e., around 30–35%, implying that only 30–35% of applied N is absorbed and utilized while the remaining 65–70% is lost into the environment (Sinha et al., 2020). The high rate and unsuitable timing of N application are major problems in wheat production. This has resulted in low N use efficiency, low yield and economic benefit, and high environmental costs (Lu et al., 2015).

Given the key indexes of yield formation and N application rate are not always positively correlated, to achieve high yield and N use efficiency many useful N application techniques have been developed and researched, and these N application technologies mainly focus on optimizing the total N input, adjusting the topdressing time, and decreasing the N losses. Ravier et al. (2017) found that decreasing the N application rate at the seedling stage had no impact on yield, grain protein content, and dry matter weight but increased N uptake rate and NUE (N use efficiency), as wheat has a strong low-N tolerance at the seedling stage. Sui et al. (2013) observed that optimizing N topdressing strategies enhanced rice yield by 8.2–12.6% and NUE by 57.14–138.3% when compared to local farmers' fertilization practices. Likewise, others also successfully improved crop yield, NUE, and grain quality by optimizing the N application amount and topdressing ratio (Qu et al., 2018; Liu et al., 2019; Sun et al., 2020). Therefore, in terms of optimizing N rates and its splitting during the crop growth cycle, split application of N, where some N is applied before sowing and some is applied at later growth periods, contributes to synchronize N supply with crop N demand and reduce N loss. However, an unsuitable N application rate and time will usually cause a lack of N in a certain crop growth periods, and the N deficiency has been proved to make leaf area, biomass accumulation, plant N concentration, plant photosynthetic capacity, and crop growth rate decrease, which are strongly associated with the grain filling rate, yield, and harvest index (Liu et al., 2019; Dong et al., 2022).

Increasing N rates is unlikely to be effective in increasing crop yields; excessive use of N fertilizers and inappropriate application methods will cause excessive amounts of N in the soil since it cannot be absorbed by crops, limiting instead plant growth and reducing N use efficiency due to the asynchrony between N supply and N requirements (Ercoli et al., 2013; Liu et al., 2019);. Better management and appropriate use of N fertilizers are a convenient and effective way to improve crop growth, population structure, N accumulation, N use efficiency, and yield components (Peng et al., 2010; Ciampitti and Vyn, 2012). Although a suitable N application amount and topdressing ratio can obviously increase wheat yield (Shi et al., 2007; Zhao and Si, 2015), the internal mechanisms of yield formation or increase have not been well studied, especially from the aspects of population dynamics and structure, ear fruiting traits, N absorption and utilization, and the potential relationships of mutual inhibition and promotion among them. Therefore, a relevant field experiment was conducted (i) to clarify the variation trend of N accumulation, N use efficiency, population dynamics and structure, ear fruiting traits and wheat yield, which respond to different N application amounts and N topdressing ratios; (ii) to reveal the suitable N application amount and topdressing ratio with which N efficiency, population dynamics, and yield are effectively improved so as to maximize the yield and N benefits; and (iii) to identify the potential relationships among the above-mentioned key indexes of yield formation.

2 Materials and methods

2.1 Site description

Field experiments were conducted in a Baihu farm (31°53' N, 117°14' E; 29.8 m a.s.l.), Lujiang County, Anhui Province in China from November 2019 to May 2021 (the climate being basically the same over the 3 years). The 3-year experimental site (in the same location) is located in the southeast of the country with an annual single rice-wheat rotation system. The region is classified as having a subtropical monsoon climate. The annual mean temperature (2019~2021) is 16.0°C, accumulated temperatures above 10°C are about 5100°C, and annual mean precipitation is about 1150 mm. Soil samples were collected from the research field at a depth of 0–20 cm for analyzing soil properties before wheat sowing and basal fertilizers application. The soil's physical and chemical properties at depths of 0–20 cm at the beginning of the experiment were as follows: available N 98.09 mg kg^{-1}, available P 7.46 mg kg^{-1}, available K 93.8 mg kg^{-1}, total N 1.19 g kg^{-1}, total P 0.61 g kg^{-1}, organic matter 18.31 g kg^{-1}, and pH 5.8.

2.2 Experimental design

The field experiment was laid out in a two-factor completely randomized design with three replicates for each treatment. One factor was the N application level, consisting of three N levels, i.e., 120, 180, and 240 kg ha^{-1} (referred as N1, N2, and N3, and the highest N application rate in this study was slightly lower than the conventional N application rate in the test area). Another factor was the ratio of basal N to topdressing, including three N topdressing ratios, i.e., 7:3, 6:4, and 5:5 (referred to as T1, T2, and T3). Therefore, nine treatments were established, namely N1T1, N1T2, N1T3, N2T1, N2T2, N2T3, N3T1, N3T2, and N3T3. For all plots, 120 kg P ha^{-1} and 120 kg K ha^{-1} were applied as basal fertilizer before sowing, and the topdressing N was applied at the jointing stage of wheat, N was applied as urea (46.4% N), and P and K were supplied as calcium superphosphate (12% P_2O_5) and potassium chloride (60% K_2O), respectively. The plot size was 3 m × 4 m with a row space of 25 cm, and the distance between neighboring plots was 50 cm. A local wheat variety of "Ningmai 13" (widely planted

in the region) was selected and planted on 6 November with a density 300×10^4 ha^{-1} for basic seedlings and was harvested on 24 May of the following year.

2.3 Sampling and measurements

N accumulation: at the maturity stage, 1-m rows of consecutive plants in each experimental plot were clipped at soil surface, and separated into three fractions: leaves, stems plus petioles, and grains. The plant samples were oven-dried at 80°C until reaching a constant weight, and then we calculated aboveground dry matter (ADM) weight at the maturity stage. Each ADM sample (leaves, stems plus petioles, and grains) was ground separately using 1mm of screen mesh. Total N content in the above-ground parts were determined using the semi-micro Kjeldahl method (FOSS-2300, FOSS Analytical A/S, Denmark) where total N accumulation = dry matter weight of tissues × total N content (Shi and Yan, 2013).

N utilization efficiency: partial factor productivity of applied N (PFP) = kg grain yield with N application/kg N applied); N utilization efficiency for grain production (kg kg^{-1}) = grain yield/total N content in the above-ground plant; N utilization efficiency for biomass production (kg kg^{-1}) = dry matter weight of population at maturity stage/total N content in the above-ground plant.

Dynamic changes of plant population height: the average height of wheat population was measured at jointing and flowering stages, the height of wheat plants was the distance from soil surface to the top of leaves, and the population growth rate of plant height = average plant height (mm)/number of days during the measurement of two growth periods (d).

Dynamic changes of population leaf area: leaf area was measured using a portable leaf area meter (Model Li-3000C, Li-cor, Lincoln, Nebraska, USA), and then LAI (leaf area index) was calculated as leaf area per unit land area. In total, 20 wheat plants in each treatment were sampled and measured at the jointing, flowering, and middle of filling stages in 2020 and 2021. Leaf area growth rate = population leaf area (m^2)/number of days during the measurement of two growth periods (d).

Dynamic changes of dry matter accumulation of population: to obtain the dry matter weight, 20 wheat plants in each plot were sampled (at the jointing, flowering, and maturity stages) and oven dried at 80°C for 72 h till they reached a constant weight. The dry matter accumulation rate of population = dry matter weight of population (kg)/number of days during the measurement of two growth periods (d).

Dynamic changes of the light interception rate of the population: photosynthetically active radiation (PAR) was measured by a SUNSCAN Canopy Analysis System (Delta company, Britain) at the booting, flowering, initial of filling, and end of filing stages of wheat in 2020 and 2021, respectively. The PAR was calculated according to the difference value between the PAR of the top and bottom of the wheat population, and the measurements were performed at 9:30–12:00 h, Beijing standard time, on sunny days. The measurement locations were chosen randomly, and 10 replications were performed for each plot. LI (light interception rate) was calculated using the following formula (Xue et al., 2015; Tsujimoto et al., 2017): LI = (1-Io/lt)×100%, where LI is the percentage of light that is intercepted, and Io and It are the PAR of wheat population at top and bottom, respectively.

Spikelet number of population, fruiting spikelets per ear, sterile spikelets, grains per ear, grain weight per ear, imperfect grains, and fruiting rate per ear were determined at harvesting for an area of 2 square meters for each plot in 2020 and 2021. The percentage of fruiting spikelets was calculated by dividing the number of fruiting spikelets based on the number of total spikelets panicle^{-1}.

2.4 Data analysis

All data was expressed as means over three replicates. ANOVA was conducted by using SPSS 21.0 software with the general linear model-univariate procedure (IBM, Armonk, New York, USA). A one-way analysis of variance (ANOVA) was performed on each measurement index in the paper to compare differences among N level and N topdressing treatments for each year. All treatment means were compared for any significant differences by the Duncan's multiple range tests at the 5%level using the SPSS 21.0 software package for Windows.

3 Result

3.1 Effects of optimizing N application on N absorption and utilization

3.1.1 Plant N uptake and accumulation

At (Figure 1) the same N level (N1, N2, or N3), the total amount of N accumulation in the stem plus petiole in T3 was higher than that in T1 and T2, and the differences between T3 and T2 were insignificant, while the differences between T3 and T1 were significant at N2 and N3 in 2020. The effect of the N topdressing ratio on the amount of N accumulation in leaf, grain, and plant were consistently T2 > T3 > T1, and the differences between T2 and T1 were significant (except for grain at N1 in 2020), while the differences between T2 and T3 were insignificant. With the same N topdressing ratio (T1, T2, or T3), the effect of N application amount on N accumulation in the stem plus petiole, leaf, grain, and plant were consistently N3 > N2 > N1, and the differences between N2 and N1, N3, and N2 were significant, indicating that increasing 60 kg N ha^{-1} (N3 compared to N2, N2 compared to N1) significantly enhanced N accumulation amount in wheat. In addition, we also found that the amount of N accumulation at maturity stage were consistently plant > grain > stem plus petiole > leaf.

3.1.2 N utilization efficiency

As shown in Figure 2, at the same N level (N1, N2, or N3), the effect of the N topdressing ratio on partial factor productivity of applied N was consistently T2 > T3 > T1 in 2020 and 2021, and the values of N utilization efficiency for grain production and N utilization efficiency for biomass production were the highest in T1. However, at the same N level, the differences in partial factor productivity of applied N, N utilization efficiency for grain production, and N utilization efficiency for biomass production

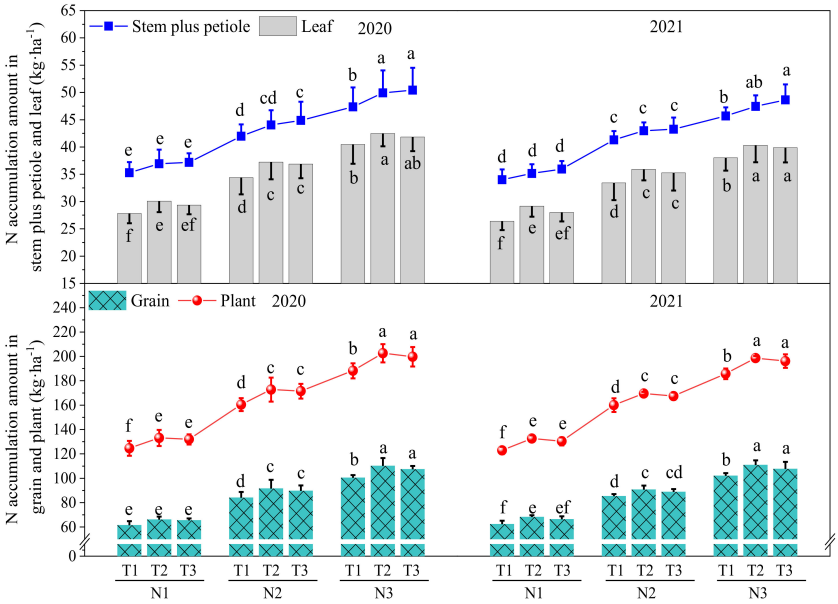

FIGURE 1
The Effect of optimizing N application on plant N uptake and accumulation at maturity stage. Values were means ± SD. Different letters indicate a significant difference within the same year under the treatments of three N levels and three N topdressing ratios by Duncan test (ANOVA) at the 5% level. Three N fertilization levels: N1, 120 kg ha^{-1}; N2, 180 kg ha^{-1}; and N3, 240 kg ha^{-1}. Three N topdressing ratios: T1, 7:3; T2, 6:4; and T3, 5:5.

among T1, T2, and T3 were insignificant. With the same N topdressing ratio (T1, T2, or T3), the effect of N application amount on partial factor productivity of applied N, N utilization efficiency for grain production, and N utilization efficiency for biomass production were consistently N1 > N2 > N3. The partial factor productivity of applied N in N1 were significantly higher than in N2 and in N2 significantly higher than that in N3, indicating that increasing 60 kg N ha^{-1} significantly decreased partial factor productivity of applied N. Compared to N3, N1 for T1, T2, and T3 significantly decreased N utilization efficiency for biomass

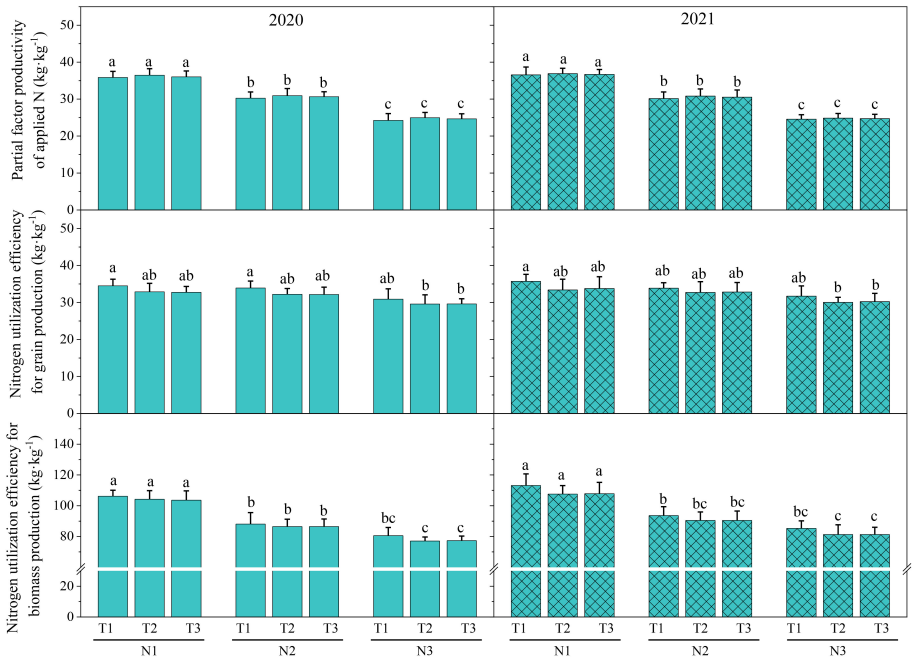

FIGURE 2
The Effect of optimizing N application on N use efficiency. Values were means ± SD. Different letters indicated significant difference within the same year under the treatments of three N levels and three N topdressing ratios by Duncan test (ANOVA) at the 5% level. Three N fertilization levels: N1, 120 kg ha^{-1}; N2, 180 kg ha^{-1}; and N3, 240 kg ha^{-1}. Three N topdressing ratios: T1, 7:3; T2, 6:4; and T3, 5:5.

production in 2020 and 2021, indicating that increasing 120 kg N ha^{-1} would significantly decrease N utilization efficiency for biomass production. With the same N topdressing ratio, the differences in N utilization efficiency for grain production among N1, N2, and N3 were insignificant.

3.2 Effects of optimizing N application on population dynamics

3.2.1 Dynamic changes of plant population height

At (Figure 3) the same N level, the population growth rate of plant height from sowing date to jointing stage in T1 was higher than that in T2 and T3; however, the population growth rate of plant height from jointing stage to flowering stage was consistently T2 > T3 > T1 in 2020 and 2021, and the differences among T1, T2, and T3 were insignificant. With the same N topdressing ratio (T1, T2, or T3), the population growth rate of plant height was consistently N3 > N2 > N1, and the differences between N3 and N1 were significant. The results indicated that N topdressing ratio had no significant effect on the population growth rate of plant height, while increasing 120 kg N ha^{-1} significantly enhanced the population growth rate of plant height.

3.2.2 Dynamic changes of population leaf area

At the same N level (Table 1), the leaf area index at the flowering and middle of filling stages and the leaf area growth rate from the jointing stage to flowering stage were consistently T2 > T3 > T1, while the leaf area index at jointing stage and leaf area growth rate from sowing date to jointing stage were consistently T1 > T2 > T3, indicating that increasing the basal N application amount was beneficial to increasing leaf area index and leaf area growth rate of wheat before the jointing stage, and T2 was the most beneficial to improving the leaf area index and leaf area growth rate after the jointing stage. At the same N level, the differences in leaf area index and leaf area growth rate were insignificant between T2 and T3. With the same N topdressing ratio, the leaf area index and leaf area growth rate in N3 were higher than in N2 and significantly higher than that in N1 (except for leaf area growth rate from jointing to flowering stages between N3T1 and N1T1 in 2020). Therefore, increasing the N application amount appropriately with the N topdressing ratio T2 was relatively more helpful for enhancing leaf area index and leaf area growth rate after jointing stage.

3.2.3 Dynamic changes of dry matter accumulation of population

At the same N level (Table 2), the dry matter weight of the population at the jointing stage were consistently T1 > T2 > T3, while the dry matter weight of the population at the flowering and maturity stages as well as the dry matter accumulation rate from sowing date to flowering stage and from flowering to maturity stage were consistently T2 > T3 > T1, indicating that increasing the basal N application amount was beneficial to increasing the dry matter weight of population before the jointing stage, and the T2 treatment was the most beneficial to improving the dry matter weight and dry matter accumulation rate of the population after the jointing stage. The differences in the dry matter accumulation rate among T1, T2,

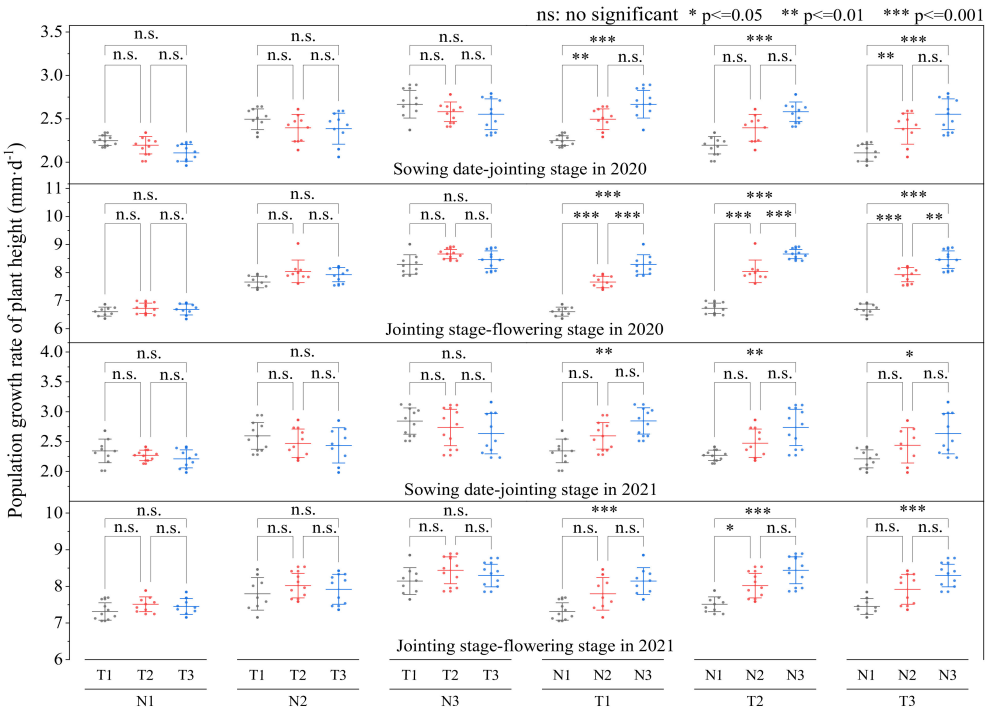

FIGURE 3
The Effect of optimizing N application on population growth rate of plant height. Values were means ± SD. Different letters indicated significant difference within the same year under the treatments of three N levels and three N topdressing ratios by Duncan test (ANOVA) at the 5% level. Three N fertilization levels: N1, 120 kg ha^{-1}; N2, 180 kg ha^{-1}; and N3, 240 kg ha^{-1}. Three N topdressing ratios: T1, 7:3; T2, 6:4; and T3, 5:5.

10.3389/fpls.2023.1199168

TABLE 1 The effect of optimizing N application on dynamic changes of population leaf area.

N fertilization	N topdressing ratio	Leaf area index			Leaf area growth rate ($m^2 \cdot ha^{-1} d^{-1}$)	
		Jointing stage	Flowering stage	Middle of filling stage	From sowing date to jointing stage	From jointing stage to flowering stage
2020						
N1	T1	3.25 ± 0.15 b	5.38 ± 0.16 f	3.26 ± 0.17 c	282.32 ± 13.20 b	417.65 ± 36.31 c
	T2	3.22 ± 0.11 b	5.53 ± 0.06 def	3.43 ± 0.13 bc	280.29 ± 9.22 b	452.29 ± 10.06 bc
	T3	3.19 ± 0.14 b	5.43 ± 0.13 ef	3.33 ± 0.20 c	277.68 ± 12.34 b	439.22 ± 21.96 c
N2	T1	3.54 ± 0.22 ab	5.66 ± 0.17 cde	3.49 ± 0.04 bc	307.54 ± 18.70 ab	416.34 ± 61.71 c
	T2	3.48 ± 0.07 ab	5.82 ± 0.14 c	3.65 ± 0.13 ab	302.90 ± 5.79 ab	458.82 ± 18.91 bc
	T3	3.45 ± 0.21 ab	5.73 ± 0.08 cd	3.60 ± 0.10 ab	299.71 ± 18.27 ab	447.06 ± 37.56 c
N3	T1	3.68 ± 0.20 a	6.07 ± 0.14 b	3.67 ± 0.15 ab	319.71 ± 17.27 a	468.63 ± 35.46 bc
	T2	3.63 ± 0.24 a	6.38 ± 0.14 a	3.81 ± 0.09 a	315.36 ± 20.84 a	540.52 ± 57.91 a
	T3	3.61 ± 0.23 a	6.27 ± 0.15 ab	3.77 ± 0.14 a	313.91 ± 19.66 a	521.57 ± 14.14 ab
2021						
N1	T1	3.22 ± 0.15 cde	5.29 ± 0.11 d	3.24 ± 0.21 c	282.16 ± 12.84 cde	398.08 ± 10.71 e
	T2	3.14 ± 0.16 de	5.54 ± 0.11 bcd	3.38 ± 0.16 bc	275.73 ± 13.31 de	461.54 ± 8.81 cd
	T3	3.09 ± 0.15 e	5.47 ± 0.20 cd	3.35 ± 0.29 bc	271.35 ± 12.93 e	456.41 ± 10.94 cd
N2	T1	3.43 ± 0.15 abcd	5.68 ± 0.11 bcd	3.53 ± 0.37 abc	300.88 ± 13.10 abcd	433.33 ± 36.61 d
	T2	3.34 ± 0.19 bcde	5.86 ± 0.17 abc	3.71 ± 0.38 abc	293.27 ± 16.93 bcde	484.62 ± 12.01 bc
	T3	3.30 ± 0.22 bcde	5.78 ± 0.17 abc	3.66 ± 0.34 abc	289.47 ± 19.24 bcde	477.56 ± 10.59 c
N3	T1	3.67 ± 0.13 a	5.97 ± 0.18 ab	3.84 ± 0.34 ab	321.93 ± 10.99 a	442.95 ± 22.78 d
	T2	3.59 ± 0.17 ab	6.24 ± 0.14 a	3.99 ± 0.33 a	315.20 ± 14.61 ab	509.62 ± 13.87 ab
	T3	3.50 ± 0.20 abc	6.19 ± 0.19 a	3.91 ± 0.34 a	307.31 ± 17.11 abc	516.03 ± 7.28 a

values were means ± SD. Means followed by different letters in the same column indicated significant difference within the same year under the treatments of three N levels and three N topdressing ratios by Duncan test (ANOVA) at the 5% level. Three N fertilization levels: N1, 120 kg ha^{-1}; N2, 180 kg ha^{-1}; and N3, 240 kg ha^{-1}. Three N topdressing ratios: T1, 7:3; T2, 6:4; and T3, 5:5.

T3 were insignificant (except between N3T1 and N3T2, N3T3 from sowing date to flowering stage in 2021). With the same N topdressing ratio, the dry matter weight of the population in N2 was significantly higher than that in N1, and in N3 it was significantly higher than that in N2 (except at maturity in 2021), indicating that increasing 60 kg N ha^{-1} significantly enhanced the dry matter weight of population. The dry matter accumulation rate in N3 was higher than that in N2 and significantly higher than that in N1.

3.2.4 Dynamic changes of population light interception rate

At (Figure 4) the same N level (N1, N2, or N3), the population light interception rate in T2 was higher than that in T1 and T3 at the

10.3389/fpls.2023.1199168

TABLE 2 The effect of optimizing N application on the population dynamics of dry matter accumulation.

N fertilization	N topdressing ratio	Dry matter weight of population (kg·ha^{-1})			Dry matter accumulation rate (kg·ha^{-1}d^{-1})	
		Jointing stage	Flowering stage	Maturity stage	From sowing date to flowering stage	From flowering to maturity stage
2020						
N1	T1	4001.03 ± 95.26 c	8617.23 ± 120.70 d	13236.13 ± 235.55 e	51.91 ± 1.67 e	131.97 ± 4.47 d
	T2	3943.40 ± 72.56 cd	8763.03 ± 74.89 d	13873.40 ± 274.22 d	52.79 ± 0.45 de	146.01 ± 6.35 bcd
	T3	3839.30 ± 55.06 d	8709.10 ± 62.87 d	13681.87 ± 279.34 de	52.46 ± 2.34 de	142.08 ± 6.23 cd
N2	T1	4219.60 ± 107.59 b	9097.60 ± 65.02 c	14142.47 ± 142.32 cd	54.80 ± 0.39 cde	144.14 ± 2.25 cd
	T2	4163.63 ± 79.47 b	9196.27 ± 57.59 c	14645.13 ± 407.20 bc	55.40 ± 2.22 bcd	155.68 ± 16.53 abc
	T3	4087.70 ± 24.55 bc	9138.30 ± 106.66 c	14468.70 ± 478.71 c	55.05 ± 0.64 cde	152.30 ± 10.78 abc
N3	T1	4457.57 ± 106.72 a	9509.13 ± 46.64 b	15162.37 ± 128.63 ab	57.28 ± 2.21 abc	161.52 ± 2.41 ab
	T2	4419.30 ± 85.06 a	9808.00 ± 55.43 a	15617.80 ± 372.23 a	59.08 ± 2.32 a	165.99 ± 9.39 a
	T3	4365.63 ± 50.20 a	9714.27 ± 82.00 a	15445.27 ± 55.43 a	58.52 ± 0.49 ab	163.74 ± 3.69 a
2021						
N1	T1	3992.57 ± 22.09 ef	8734.67 ± 113.33 e	13903.10 ± 583.78 e	52.62 ± 0.68 e	152.01 ± 13.96 d
	T2	3943.43 ± 69.43 ef	8920.77 ± 108.56 de	14270.97 ± 340.60 de	53.74 ± 0.65 de	157.36 ± 7.26 bcd
	T3	3820.80 ± 71.87 f	8877.37 ± 99.26 e	14165.07 ± 526.57 de	53.48 ± 0.60 e	155.52 ± 12.57 cd
N2	T1	4287.57 ± 149.28 cd	9081.10 ± 152.89 cd	14985.43 ± 797.25 cd	54.71 ± 0.92 cd	173.66 ± 19.10 abc
	T2	4238.53 ± 104.94 cd	9245.00 ± 115.95 c	15336.63 ± 450.55 abc	55.69 ± 0.70 c	179.17 ± 10.41 a
	T3	4113.37 ± 81.83 de	9190.23 ± 144.25 c	15141.43 ± 271.10 bc	55.36 ± 0.87 c	175.04 ± 4.31 abc
N3	T1	4553.80 ± 83.60 a	9612.40 ± 155.45 b	15636.13 ± 189.41 abc	57.91 ± 0.94 b	177.17 ± 2.99 ab
	T2	4484.13 ± 136.17 ab	9871.50 ± 82.57 a	16153.97 ± 258.94 a	59.47 ± 0.50 a	184.78 ± 5.62 a
	T3	4360.47 ± 73.15 bc	9831.70 ± 116.84 a	15950.87 ± 529.15 ab	59.23 ± 0.70 a	179.98 ± 12.70 a

values were means ± SD. Means followed by different letters in the same column indicated significant difference within the same year under the treatments of three N levels and three N topdressing ratios by Duncan test (ANOVA) at the 5% level. Three N fertilization levels: N1, 120 kg ha^{-1}; N2, 180 kg ha^{-1}; and N3, 240 kg ha^{-1}. Three N topdressing ratios: T1, 7:3; T2, 6:4; and T3, 5:5.

same growth stage, but the differences among T1, T2, and T3 were insignificant, indicating that an appropriate N topdressing ratio was beneficial to increasing population light interception rate, but its effect was insignificant. Increasing the N application amount enhanced the population light interception rate; with the same N topdressing ratio, the population light interception rate in N3 was higher than that in N2 and significantly higher than that in N1. The results showed that increasing 120 kg N ha^{-1} significantly enhanced the population light interception rate.

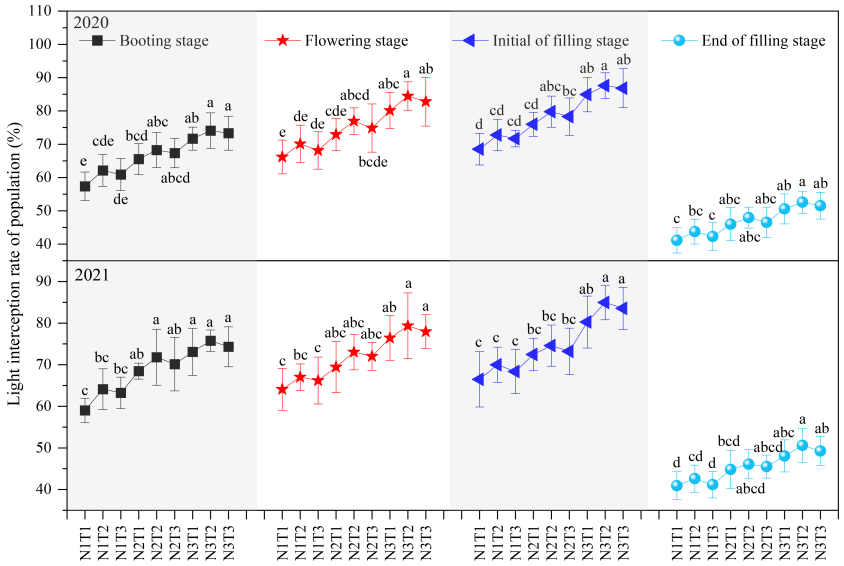

FIGURE 4
The Effect of optimizing N application on population light interception rate. Values were means ± SD. Different letters indicated significant difference within the same year under the treatments of three N levels and three N topdressing ratios by Duncan test (ANOVA) at the 5% level. Three N fertilization levels: N1, 120 kg ha^{-1}; N2, 180 kg ha^{-1}; and N3, 240 kg ha^{-1}. Three N topdressing ratios: T1, 7:3; T2, 6:4; and T3, 5:5.

3.2.5 Dynamic changes of population spikelet number

The total (Figure 5) number of spikelets in T2 were higher than that in T1 and T3 at the same N level (N1, N2 or N3), but the differences among T1, T2, and T3 were insignificant. With the same N topdressing ratio, the total number of spikelets in N3 were higher than that in N2, and significantly higher than that in N1. We can draw that N topdressing ratio had no significant effect on total number of spikelets, while increasing 120 kg N ha^{-1} significantly enhanced the total number of population spikelets.

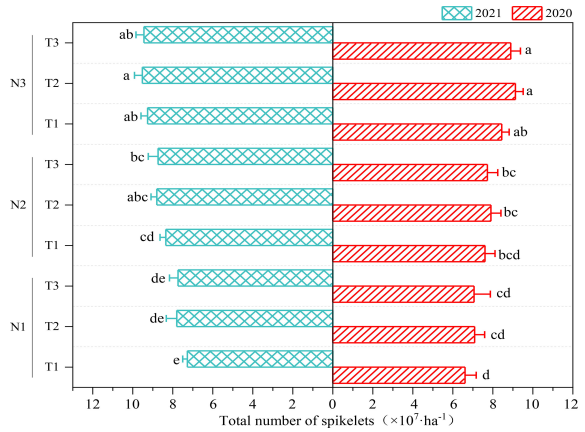

FIGURE 5
The Effect of optimizing N application on total number of population spikelets. Values were means ± SD. Different letters indicated significant difference within the same year under the treatments of three N levels and three N topdressing ratios by Duncan test (ANOVA) at the 5% level. Three N fertilization level: N1, 120 kg ha^{-1}; N2, 180 kg ha^{-1}; and N3, 240 kg ha^{-1}. Three N topdressing ratios: T1, 7:3; T2, 6:4; and T3, 5:5.

3.3 Effects of optimizing N application on ear fruiting traits and yield

At the same N level (Table 3), the fruiting spikelets per ear, grains per ear, grain weight per ear, fruiting rate per ear, grain filling rate per ear, and yield were consistently T2 > T3 > T1, while the sterile spikelets at the top and bottom and imperfect grains per ear were consistently T1 > T3 > T2, indicating that T2 was not only beneficial to increasing the fruiting spikelets per ear, grains per ear, grain weight per ear, fruiting rate per ear, grain filling rate per ear and yield, but also helpful for decreasing the sterile spikelets at the top and bottom and imperfect grains per ear. Increasing the N application amount enhanced the fruiting spikelets per ear, grains per ear, grain weight per ear, fruiting rate per ear, grain filling rate per ear and yield, while it decreased the sterile spikelets at the top and bottom and imperfect grains per ear. The differences in fruiting spikelets per ear, sterile spikelets at the top and bottom, grains per ear, grain weight per ear, imperfect grains per ear, fruiting rate per ear, and grain filling rate per ear between N3 and N1 were significant. In addition, the yield in N3 was significantly higher than that in N2, and in N2 it was significantly higher than that in N1.

3.4 Correlation analysis

As shown in Figure 6, the NAG (N accumulation amount in grain), NAL (N accumulation amount in leaf), NAP (N accumulation amount in plant), LAGR (leaf area growth rate), DMAR (dry matter accumulation rate), LIR (light interception rate of population), NS(number of population spikelets), FSE (fruiting spikelets per ear), GFRE (grain filling rate per ear), and Y (yield)

10.3389/fpls.2023.1199168

TABLE 3 The effect of optimizing N application on ear fruiting traits (average value of 2020 and 2021) and yield of wheat.

N fertilization	Ratio of basal to topdressing	Fruiting spikelets per ear	Sterile spikelets at the top	Sterile spikelets at the bottom	Grains per ear	Grain weight per ear (g)
N1	T1	12.19 ± 0.57 d	0.60 ± 0.04 a	1.92 ± 0.06 a	27.93 ± 1.04 c	1.03 ± 0.08 e
	T2	13.37 ± 0.45 cd	0.53 ± 0.04 bc	1.79 ± 0.08 abc	28.53 ± 0.77 c	1.08 ± 0.07 de
	T3	13.17 ± 0.89 cd	0.54 ± 0.03 b	1.83 ± 0.08 ab	28.07 ± 0.60 c	1.06 ± 0.05 e
N2	T1	13.86 ± 0.90 bc	0.50 ± 0.03 bcd	1.73 ± 0.08 bc	30.71 ± 1.25 b	1.19 ± 0.05 cd
	T2	14.48 ± 0.52 bc	0.46 ± 0.03 def	1.66 ± 0.09 cde	31.89 ± 1.24 ab	1.26 ± 0.05 abc
	T3	14.10 ± 1.34 bc	0.48 ± 0.04 cde	1.69 ± 0.07 bcd	31.57 ± 2.31 ab	1.24 ± 0.07 bc
N3	T1	15.24 ± 0.23 ab	0.43 ± 0.04 efg	1.58 ± 0.09 def	32.22 ± 1.43 ab	1.30 ± 0.05 abc
	T2	16.59 ± 0.90 a	0.39 ± 0.03 g	1.51 ± 0.06 f	33.11 ± 0.76 a	1.36 ± 0.05 a
	T3	16.18 ± 0.69 a	0.40 ± 0.02 fg	1.53 ± 0.05 ef	32.75 ± 0.77 ab	1.34 ± 0.08 ab
		Imperfect grains per ear	Fruiting rate per ear (%)	Grain filling rate per ear ($mg \cdot d^{-1}$)	Yield in 2020 ($kg \cdot ha^{-1}$)	Yield in 2021 ($kg \cdot ha^{-1}$)
N1	T1	2.45 ± 0.12 a	86.41 ± 0.80 e	36.79 ± 2.14 d	4300.73 ± 50.86 e	4386.27 ± 43.52 d
	T2	2.26 ± 0.12 b	88.38 ± 1.86 cde	38.57 ± 2.74 d	4378.07 ± 20.91 e	4427.80 ± 60.60 d
	T3	2.28 ± 0.09 ab	87.72 ± 1.16 de	37.98 ± 2.58 d	4322.60 ± 38.07 e	4404.77 ± 86.37 d
N2	T1	2.03 ± 0.08 c	89.50 ± 0.96 bcd	42.38 ± 2.51 c	5444.83 ± 46.90 d	5423.60 ± 54.85 c
	T2	1.88 ± 0.09 cd	90.77 ± 1.40 ab	44.88 ± 3.77 bc	5566.50 ± 49.19 c	5548.87 ± 69.08 b
	T3	1.92 ± 0.10 c	90.15 ± 1.40 bc	44.17 ± 2.78 bc	5516.57 ± 71.00 cd	5493.80 ± 78.71 bc
N3	T1	1.74 ± 0.12 de	91.60 ± 1.30 ab	46.31 ± 2.03 ab	5814.80 ± 100.25 b	5894.17 ± 86.70 a
	T2	1.60 ± 0.08 e	92.99 ± 1.24 a	48.69 ± 1.95 a	5995.53 ± 111.67 a	5963.50 ± 72.98 a
	T3	1.64 ± 0.08 e	92.59 ± 1.42 a	47.86 ± 2.07 ab	5917.73 ± 53.19 ab	5930.30 ± 80.24 a

values were means ± SD. Means followed by different letters in the same column indicated significant difference within the same year under the treatments of three N levels and three N topdressing ratios by Duncan test (ANOVA) at the 5% level. Three N fertilization levels: N1, 120 kg ha^{-1}; N2, 180 kg ha^{-1}; and N3, 240 kg ha^{-1}. Three N topdressing ratios: T1, 7:3; T2, 6:4; and T3, 5:5.

were all significantly ($p<0.05$) positively correlated with each other, indicating that there were positive (significant or markedly significant) mutual promotion interactions among each factor. The SST (sterile spikelets at the top), SSB (sterile spikelets at the bottom), and IGE (imperfect grains per ear) were all significantly negatively correlated with NAG, NAL, NAP, LAGR, DMAR, LIR, NS, FSE, GFRE, and Y (except for the relationships between SSB with DMAR, NS, FSE, and between SST with DMAR). The relationships between SST, SSB, and IGE were significant, indicating that the increase of sterile spikelets would lead to an obvious enhancement of imperfect grains per ear. Therefore, to increase N accumulation amount in grain, leaf, and plant, and the rate of leaf area growth, dry matter accumulation and population light interception by optimizing N application amount and

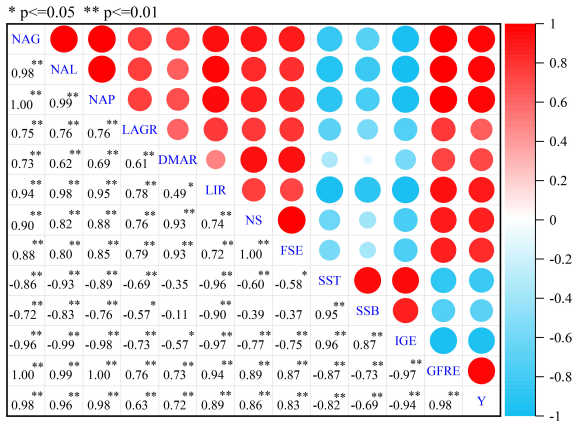

FIGURE 6
Correlation analyses among NAG (N accumulation amount in grain), NAL (N accumulation amount in leaf), NAP (N accumulation amount in plant), LAGR (leaf area growth rate) and DMAR (dry matter accumulation rate), LIR (light interception rate of population), NS (number of population spikelets), FSE (fruiting spikelets per ear), SST (sterile spikelets at the top), SSB (sterile spikelets at the bottom), IGE (imperfect grains per ear), GFRE (grain filling rate per ear), and Y (yield). *Correlation is significant (p<0.05); **Correlation is markedly significant (p<0.01).

topdressing ratio have great significance on reducing the number of sterile spikelets and imperfect grains and increasing the number of fruiting spikelets per ear, grain filling rate, and yield.

4 Discussion

Precise N fertilization management is important in improving plant N uptake and N use efficiency (NUE), while increasing the N fertilization level is unlikely to be effective in enhancing potential N benefits and NUE (Wu et al., 2019). Better management and appropriate use of N fertilizers are a convenient and effective way to improve crop productivity and N use efficiency with minimum N loss (Yin et al., 2019). Therefore, optimizing N application strategies should consider adopting an appropriate N fertilization rate and splitting the fertilizer dose into different fertilization or topdressing application times based on crop requirements so as to enhance N use efficiency while decrease N inputs. Liu et al. (2019) indicated that in the split application of N, where some N was applied before sowing and some N was applied at later growth periods, N concentration in the grain, total N accumulation at harvest, and N use efficiency increased. Sun et al. (2020) found that compared with one-time basal fertilization, optimized N topdressing ratios (especially the 4:3:3 and 5:3:2 ratios) significantly increased N use efficiency and aboveground N accumulation. In this study, we found that T3 was more beneficial to increasing total N accumulation in the stem plus petiole compared with T1 and T2, while T1 was more beneficial to enhancing N use efficiency for grain and biomass production compared with T2 and T3, and the effect of the N topdressing ratio on N accumulation amount in leaf, grain, plant, and partial factor productivity of applied N were consistently T2 > T3 > T1. In addition, we also proved that increasing 60 kg N ha^{-1} significantly enhanced N accumulation amount in the stem plus petiole, leaf, grain, and plant, while partial factor productivity of applied N (within the range of N application in this experiment) significantly decreased, and a similar conclusion was also drawn by Zhao and Si (2015). Di Paolo and Rinaldi (2008) found that N use efficiency (NUE) decreased gradually as the N level increased from 0 to 300 kg ha^{-1}, while excessive N application did not enhance N uptake. Jia et al. (2011) also reported that the optimal ratio of basal-N to topdress-N could lead to higher N accumulation in wheat, higher N recovery efficiency, NUE, and decreased loss of fertilizer-N. Optimizing the N application rate and N topdressing ratio could have a significant impact on plant N accumulation and NUE, which is mainly due to the fact that (i) as the rate of N application relative to plant N requirement increases, the N use efficiency normally decreases; and (ii) delaying N application until the later growth stage or applying N with a suitable topdressing ratio is an effective strategy for improving the synchrony among N supply, soil N availability, and crop N demand (Gu et al., 2019; Liu et al., 2019).

Plant height, leaf area, dry matter weight and spikelet number of population are important agronomic traits of cereal crops that not only determine plant architecture but also contribute significantly to grain yield. For instance, Machado et al. (2002) indicated that plant height explained 61% of the variation in the grain yield of corn. Viña et al. (2011) reported that leaf area was an important parameter controlling many biological and physical processes of the crop, including the interception of light and water, autotrophic respiration, dry matter accumulation, and carbon and nutrient cycles. Therefore, it is of great significance to study and reveal the effects of N application amount and topdressing ratio on agronomic characters, especially on the growth rate of plant height, leaf area, dry matter weight, and spikelet number of population. Chen et al. (2016) reported that maize plants with 220 kg N ha^{-1} had a higher dry matter accumulation, green leaf number and leaf area index than plants with 55 kg N ha^{-1}. Ye et al. (2019) indicated that increasing tiller N could help promote tillering during the early growth stage, and increasing panicle N could help increase the number of differentiated spikelets (prevent differentiated spikelets from degeneration), as well as enhance dry matter accumulation and the percentage of filled grains. In this study we found that increasing basal N application amount(T1)was beneficial to increasing the population growth rate of plant height, leaf area index, leaf area growth rate, and dry matter weight (from sowing date to jointing stage), while after the jointing stage, T2 showed more advantages in increasing the population growth rate of plant height, leaf area index, leaf area growth rate, dry matter weight, dry matter accumulation rate, and spikelets of population. In addition, we also found that the dry matter weight of population was significantly enhanced by increasing 60 kg N ha^{-1}, and the population growth rate of plant height, leaf area index, leaf area growth rate, dry matter accumulation rate, and spikelets of population were significantly enhanced by increasing 120 kg N ha^{-1}. The effect of increasing 60 kg N ha^{-1} on improving the above-mentioned indexes were more obvious than that of N topdressing ratio. Some studies (Tian et al., 2017; Ye et al., 2019; Xu et al., 2021) also proved that the population dynamics or population structure of crops were significantly influenced by N fertilization level and N

topdressing ratio, for which the results presented in this paper provided further evidence. Therefore, we can obtain ideal population dynamics (structure) of crops by choosing a suitable combination of N application rate and N topdressing ratio.

Crop yield formation is closely related to the efficient use of radiation resources, and enhancing crop ability to capture radiation resources is an effective strategy for increasing crop productivity. Xue et al. (2015) indicated that the amount of light intercepted by the crop population reflected the physiological processes that occur in the population, and that the interception of light by the crop population was complicated and was affected by some agricultural measures. Zhao et al. (2022) reported that a fraction of intercepted photosynthetic active radiation (FIPAR) could be regulated through an N application method, which was lower in the N limiting treatments than in the N non-limiting treatments. In this study we found that an appropriate N topdressing ratio (T2) was conductive to increasing the light interception rate of population, but the effect was insignificant. In addition, increasing 120 kg N ha^{-1} significantly enhanced the light interception rate of population within the amount of N application in this experiment. These results were similar to those of Tsujimoto et al. (2017) who also proved that suitable N application methods could obviously improve crop population development and increase both radiation use efficiency and light interception. N application amount and topdressing ratio can obviously affect the light interception rate of population mainly due to plant density and leaf area expansion not being closely related to the intercepted PAR within the population but also significantly affected by N supply status and period (Tao et al., 2018; Zhao et al., 2022).

Agronomically optimizing the timing and rates of N fertilizer application can enhance crop yield and coordinate yield component parameters. Liu et al. (2019) indicated that by applying N fertilizer with three splits and delaying topdressing fertilization until the booting stage of winter wheat, the total grain yield and spike number, kernel number per spike, and 1000-kernel weight could increase. In some similar studies, it is also reported that by dividing N fertilizer application into basal and topdressing applications, the source–sink relationship could be regulated, further improving yield component parameters and increasing crop yields (Ercoli et al., 2013; Sui et al., 2013; Lyu et al., 2021). In this study, we found that N topdressing ratio T2 was not only beneficial to increasing fruiting spikelets per ear, grains per ear, grain weight per ear, fruiting rate per ear, grain filling rate per ear, and yield but was also helpful for decreasing sterile spikelets at the top and bottom and imperfect grains per ear. In addition, enhancing the N application rate from 120 kg ha^{-1} to 180 kg ha^{-1} or from 180 kg ha^{-1} to 240 kg ha^{-1} significantly increased yield and obviously improved the above-mentioned yield component parameters. A suitable N application rate and N topdressing ratio can obviously increase crop yield and improve yield component parameters mainly because (i) compared with one-time basal fertilization, aboveground N accumulation and NUE of crops can be significantly enhanced with an optimized N application rate and N topdressing ratio (Liu et al., 2019; Yin et al., 2019); (ii) N supply is better synchronized with crop N demand (Shi et al., 2012; Gu et al., 2019); (iii) physiological characteristics, population dynamics, and structures closely related to yield formation are effectively improved.

5 Conclusions

The effects of N topdressing ratio on increasing N accumulation amounts in leaf, grain, and plant and partial factor productivity of applied N were consistently 6:4 > 5:5 > 7:3, but N topdressing ratio 7:3 was more conducive to improving N use efficiency for grain and biomass production, and increasing 60 kg N ha^{-1} significantly enhanced the N accumulation amount in the stem plus petiole, leaf, grain, and plant. After the jointing stage, a N topdressing ratio 6:4 was more beneficial to enhancing the population growth rate of plant height, leaf area index, leaf area growth rate, dry matter weight, dry matter accumulation rate, light interception rate, and the total number of population spikelets; meanwhile, the above-mentioned indexes of population could be significantly enhanced by increasing 120 kg N ha^{-1}. N3T2 was more conducive to improving yield and yield component parameters, and increasing 60 kg N ha^{-1} significantly enhanced yield. Therefore, we suggested that a moderate N application rate N3 with a suitable N topdressing ratio might be an environmentally friendly mode for wheat cropping for high yield (T2) and N use efficiency (T1).

Data availability statement

The original contributions presented in the study are included in the article/supplementary material. Further inquiries can be directed to the corresponding authors.

Author contributions

XZ conducted the field experiments and wrote the manuscript. SD, YX, and CC provided advice on experimental implementation. HC and YQ prepared the materials for the experiment. YQ and SD conceived and supervised the field experiments and revised manuscript. YX, CC, and HC participated data collection and data analysis. All authors contributed to the article and approved the submitted version.

Funding

This research was funded by the National Key Research and Development Program of China (2016YFD0300408), the Transformation and Application Special Project in Agricultural Scientific and Technological Achievements of Anhui Province (2021ZH002), the Anhui Natural Science Foundation of China (2108085QC111), and the Open Project from Joint International Research Laboratory of Agriculture and Agri-Product Safety of Yangzhou University (JRK2018004).

Conflict of interest

The authors declare that the research was conducted in the absence of any commercial or financial relationships that could be construed as a potential conflict of interest.

Publisher's note

References

Che, S. G., Zhao, B. Q., Li, Y. T., Liang, Y. U. A. N., Wei, L. I., Lin, Z. A., et al. (2015). Review grain yield and nitrogen use efficiency in rice production regions in China. *Agric. Sci. China* 14 (12), 2456–2466. doi: 10.1016/S2095-3119(15)61228-X

Chen, K., Camberato, J. J., Tuinstra, M. R., Kumudini, S. V., Tollenaar, M., and Vyn, T. J. (2016). Genetic improvement in density and nitrogen stress tolerance traits over 38 years of commercial maize hybrid release. *Field Crops Res.* 196, 438–451. doi: 10.1016/j.fcr.2016.07.025

Ciampitti, I. A., and Vyn, T. J. (2012). Physiological perspectives of changes over time in maize yield dependency on nitrogen uptake and associated nitrogen efficiencies: A review. *Field Crops Res.* 133, 48–67. doi: 10.1016/j.fcr.2012.03.008

Di Paolo, E., and Rinaldi, M. (2008). Yield response of corn to irrigation and nitrogen fertilization in a Mediterranean environment. *Field Crops Res.* 105 (3), 202–210. doi: 10.1016/j.fcr.2007.10.004

Dong, S., Zhang, X., Chu, J., Zheng, F., Fei, L., Dai, X., et al. (2022). Optimized seeding rate and nitrogen topdressing ratio for simultaneous improvement of grain yield and bread-making quality in bread wheat sown on different dates. *J. Sci. Food Agr.* 102 (1), 360–369. doi: 10.1002/jsfa.11366

Ercoli, L., Masoni, A., Pampana, S., Mariotti, M., and Arduini, I. (2013). As durum wheat productivity is affected by nitrogen fertilization management in Central Italy. *Eur. J. Agron.* 44, 38–45. doi: 10.1016/j.eja.2012.08.005

Grassini, P., Eskridge, K. M., and Cassman, K. G. (2013). Distinguishing between yield advances and yield plateaus in historical crop production trends. *Nat. Commun.* 4, 2918–2928. doi: 10.1038/ncomms3918

Gu, X., Ding, M., Lu, W., and Lu, D. (2019). Nitrogen topdressing at the jointing stage affects the nutrient accumulation and translocation in rainfed waxy maize. *J. Plant Nutr.* 42 (6), 657–672. doi: 10.1080/01904167.2019.1567773

Illescas, M., Rubio, M. B., Hernández-Ruiz, V., Morán-Diez, M. E., Martínez de Alba, A. E., Nicolás, C., et al. (2020). Effect of inorganic N top dressing and Trichoderma harzianum seed-inoculation on crop yield and the shaping of root microbial communities of wheat plants cultivated under high basal N fertilization. *Front. Plant Sci.* 1658. doi: 10.3389/fpls.2020.575861

Jia, S., Wang, X., Yang, Y., Dai, K., Meng, C., Zhao, Q., et al. (2011). Fate of labeled urea-^{15}N as basal and topdressing applications in an irrigated wheat–maize rotation system in North China Plain: I winter wheat. *Nutr. Cycl. Agroecosys.* 90 (3), 331–346. doi: 10.1007/s10705-011-9433-5

Liu, Z., Gao, F., Liu, Y., Yang, J., Zhen, X., Li, X., et al. (2019). Timing and splitting of nitrogen fertilizer supply to increase crop yield and efficiency of nitrogen utilization in a wheat–peanut relay intercropping system in China. *Crop J.* 7 (1), 101–112. doi: 10.1016/j.cj.2018.08.006

Lu, D., Lu, F., Pan, J., Cui, Z., Zou, C., Chen, X., et al. (2015). The effects of cultivar and nitrogen management on wheat yield and nitrogen use efficiency in the North China Plain. *Field Crops Res.* 171, 157–164. doi: 10.1016/j.fcr.2014.10.012

Lyu, T., Shen, J., Ma, J., Ma, P., Yang, Z., Dai, Z., et al. (2021). Hybrid rice yield response to potted-seedling machine transplanting and slow-release nitrogen fertilizer application combined with urea topdressing. *Crop J.* 9 (4), 915–923. doi: 10.1016/j.cj.2020.08.013

Machado, S., Bynum, E. D., Archer, T. L., Lascano, R. J., Wilson, L. T., Bordovsky, J., et al. (2002). Spatial and temporal variability of corn growth and grain yield: Implications for site-specific farming. *Crop Sci.* 42 (5), 1564–1576. doi: 10.2135/cropsci2002.1564

Peng, S., Buresh, R. J., Huang, J., Zhong, X., Zou, Y., Yang, J., et al. (2010). Improving nitrogen fertilization in rice by site specific N management. A review. *Agron. Sustain. Dev.* 30 (3), 649–656. doi: 10.1051/agro/2010002

Qu, Z. M., Qi, X. C., Wang, J., Chen, Q., and Li, C. L. (2018). Effects of nitrogen application rate and topdressing times on yield and quality of Chinese cabbage and soil nitrogen dynamics. *Environ. pollut. Bioavailab.* 31, 1–8. doi: 10.1080/09542299.2018.1546555

Ravier, C., Meynard, J. M., Cohan, J. P., Gate, P., and Jeuffroy, M. H. (2017). Early nitrogen deficiencies favor high yield, grain protein content and N use efficiency in wheat. *Eur. J. Agron.* 89, 16–24. doi: 10.1016/j.eja.2017.06.002

Shi, Z., Jing, Q., Cai, J., Jiang, D., Cao, W., and Dai, T. (2012). The fates of ^{15}N fertilizer in relation to root distributions of winter wheat under different N splits. *Eur. J. Agron.* 40, 86–93. doi: 10.1016/j.eja.2012.01.006

Shi, L., and Yan, H. (2013). *Experimental guide of plant physiology* (Beijing, China: China Higher Education Press).

Shi, Y., Yu, Z., Wang, D., Li, Y., and Wang, X. (2007). Effects of nitrogen rate and ratio of base fertilizer and topdressing on uptake, translocation of nitrogen and yield in wheat. *Front. Agric. China* 1 (2), 142–148. doi: 10.1007/s11703-007-0025-8

Sinha, S. K., Kumar, A., Tyagi, A., Venkatesh, K., Paul, D., Singh, N. K., et al. (2020). Root architecture traits variation and nitrate-influx responses in diverse wheat genotypes under different external nitrogen concentrations. *Plant Physiol. Bioch.* 148, 246–259. doi: 10.1016/j.plaphy.2020.01.018

Sui, B., Feng, X., Tian, G., Hu, X., Shen, Q., and Guo, S. (2013). Optimizing nitrogen supply increases rice yield and nitrogen use efficiency by regulating yield formation factors. *Field Crops Res.* 150, 99–107. doi: 10.1016/j.fcr.2013.06.012

Sun, Y., Yang, Y., Hou, M., Huang, X., Zhang, T., Huang, S., et al. (2020). Optimized nitrogen topdressing strategies enhance steviol glycoside productivity in stevia (Stevia rebaudiana Bertoni) plants. *J. Soil Sci. Plant Nutt.* 20 (3), 1133–1143. doi: 10.1007/s42729-020-00199-w

Tao, Z. Q., Wang, D. M., Yang, Y. S., Zhao, G. C., and Chang, X. H. (2018). Light interception and radiation use efficiency response to tridimensional uniform sowing in winter wheat. *J. Integr. Agric.* 17 (3), 566–578. doi: 10.1016/S2095-3119(17)61715-5

Tian, G., Gao, L., Kong, Y., Hu, X., Xie, K., Zhang, R., et al. (2017). Improving rice population productivity by reducing nitrogen rate and increasing plant density. *PloS One* 12 (8), e0182310. doi: 10.1371/journal.pone.0182310

Tsujimoto, Y., Pedro, J. A., Boina, G., Murracama, M. V., Tobita, S., Oya, T., et al. (2017). An application of digital imagery analysis to understand the effect of N application on light interception, radiation use efficiency, and grain yield of maize under various agro-environments in Northern Mozambique. *Plant Prod. Sci.* 20 (1), 12–23. doi: 10.1080/1343943X.2016.1240013

Viña, A., Gitelson, A. A., Nguy-Robertson, A. L., and Peng, Y. (2011). Comparison of different vegetation indices for the remote assessment of green leaf area index of crops. *Remote Sens. Environ.* 115 (12), 3468–3478. doi: 10.1016/j.rse.2011.08.010

Wu, W., Ma, B. L., Fan, J. J., Sun, M., Yi, Y., Guo, W. S., et al. (2019). Management of nitrogen fertilization to balance reducing lodging risk and increasing yield and protein content in spring wheat. *Field Crops Res.* 241, 107584. doi: 10.1016/j.fcr.2019.107584

Xu, K., Chai, Q., Hu, F., Fan, Z., and Yin, W. (2021). N-fertilizer postponing application improves dry matter translocation and increases system productivity of wheat/maize intercropping. *Sci. Rep.* 11 (1), 1–15. doi: 10.1038/s41598-021-02345-5

Xue, H., Han, Y., Li, Y., Wang, G., Feng, L., Fan, Z., et al. (2015). Spatial distribution of light interception by different plant population densities and its relationship with yield. *Field Crops Res.* 184, 17–27. doi: 10.1016/j.fcr.2015.09.004

Ye, C., Huang, X., Chu, G., Chen, S., Xu, C., Zhang, X., et al. (2019). Effects of postponing topdressing-N on the yield of different types of japonica rice and its relationship with soil fertility. *Agronomy* 9 (12), 868. doi: 10.3390/agronomy9120868

Yin, Y., Ying, H., Xue, Y., Zheng, H., Zhang, Q., and Cui, Z. (2019). Calculating socially optimal nitrogen (N) fertilization rates for sustainable N management in China. *Sci. Total Environ.* 688, 1162–1171. doi: 10.1016/j.scitotenv.2019.06.398

Zhao, B., Ata-Ul-Karim, S. T., Duan, A., Gao, Y., Lou, H., Liu, Z., et al. (2022). Estimating the impacts of plant internal nitrogen deficit at key top dressing stages on corn productivity and intercepted photosynthetic active radiation. *Front. Plant Sci.* 13. doi: 10.3389/fpls.2022.864258

Zhao, H., and Si, L. (2015). Effects of topdressing with nitrogen fertilizer on wheat yield, and nitrogen uptake and utilization efficiency on the Loess Plateau. *Acta Agr. Scand. B-S P* 65 (8), 681–687. doi: 10.1080/09064710.2015.1045933

Zörb, C., Ludewig, U., and Hawkesford, M. J. (2018). Perspective on wheat yield and quality with reduced nitrogen supply. *Trends Plant Sci.* 23 (11), 1029–1037. doi: 10.1016/j.tplants.2018.08.012

frontiers | Frontiers in Plant Science

TYPE Original Research
PUBLISHED 01 September 2023
DOI 10.3389/fpls.2023.1225895

OPEN ACCESS

EDITED BY
Houcheng Liu,
South China Agricultural University, China

REVIEWED BY
Ronghua Li,
South China Agricultural University, China
Zi-Shan Zhang,
Shandong Agricultural University, China

*CORRESPONDENCE
Yuntong Ma
mayuntong@cdutcm.edu.cn
Tao Zhou
364462907@qq.com
Binjie Xu
binjiexu@outlook.com

†These authors have contributed equally to this work

RECEIVED 20 May 2023
ACCEPTED 11 August 2023
PUBLISHED 01 September 2023

CITATION
Ke W, Li Y, Zhong F, Pen M, Dong J, Xu B, Ma Y and Zhou T (2023) Relatively high light inhibits reserves degradation in the *Coptis chinensis* rhizome during the leaf expansion by changing the source-sink relationship. *Front. Plant Sci.* 14:1225895. doi: 10.3389/fpls.2023.1225895

Relatively high light inhibits reserves degradation in the *Coptis chinensis* rhizome during the leaf expansion by changing the source-sink relationship

Wenjia Ke[1,2†], Yirou Li[1,2†], Furong Zhong[1,2], Maoyao Pen[1,2], Jijing Dong[1,2], Binjie Xu[3*], Yuntong Ma[1,2*] and Tao Zhou[1,2*]

[1]State Key Laboratory of Southwestern Chinese Medicine Resources, Chengdu University of Traditional Chinese Medicine, Chengdu, Sichuan, China, [2]College of Pharmacy, Chengdu University of Traditional Chinese Medicine, Chengdu, Sichuan, China, [3]Innovative Institute of Chinese Medicine and Pharmacy, Chengdu University of Traditional Chinese Medicine, Chengdu, Sichuan, China

The early spring is a seasonal high-light "window" for new leaf growth and photosynthetic carbon capture by the shade-tolerant evergreen understory plants. However, it remains unclear how light regulates the source–sink relationship between rhizome (RO), mature leaf (ML), and immature leaf (IL) during *Coptis chinensis* leaf expansion. Understanding this relationship is essential to reducing RO reserve degradation and ultimately promote RO biomass accumulation. The plants grew in an artificial climate chamber with low (50 μmol m^{-2} s^{-1}) and relatively high (200 μmol m^{-2} s^{-1}) light intensity treatments. Leaf fluorescence, foliar phosphorus (P) fractions, soluble sugars, starch, total P, and alkaloid concentrations in ILs, MLs, and RO were measured, and ^{13}C labeling was used to indicate the direction of photosynthetic carbon flow between organs. The plants grown under high light intensity had higher levels of starch in RO and higher RO biomass at the end of the year compared to those grown under low light intensity. The photosystem II (PSII) operating efficiency [*Y*(II)], relative electron transport rate (*r*ETR), and photochemical quenching (qP), as well as sucrose and glucose, in ILs and MLs under relatively high light, was higher than those under low light. The glucose and starch concentrations in ILs at 35 d was significantly higher than that at 15 d when plants were under 200 μmol m^{-2} s^{-1}, while they were not significantly changed and remained low at 50 μmol m^{-2} s^{-1}. The ^{13}C was detected in the RO when plants were grown at 200 μmol m^{-2} s^{-1}, regardless of ILs and MLs ^{13}C labeling, while no ^{13}C was detected in the RO when plants were under 50 μmol m^{-2} s^{-1}. Additionally, the proportion of photosynthetic transport from ILs to MLs was significantly higher than that from MLs to ILs under the 50-μmol m^{-2} s^{-1} limit. Total P concentration in ILs was lower under relatively high light, but there was no difference in nucleic acid P concentration in ILs under the two light intensity treatments. The alkaloid concentration in RO was lower under 200 μmol m^{-2} s^{-1} than that under 50 μmol m^{-2} s^{-1}. We propose that relatively high light reduces the need for carbohydrates and P stored in the RO to support IL growth by (1) accelerating the sink-to-source transition in ILs, which inhibits the use of reserves in the RO; (2) using energy from MLs to support IL growth, thereby

reducing RO reserve consumption, and (3) reducing the demand for P by investing less in the development of photosynthetic machinery. Furthermore, under low light, MLs serve as a sink and rely on other organs for support, directly or indirectly exacerbating the reserves lost in the RO.

KEYWORDS

source-sink, leaf, *Coptis chienesis*, light intensity, foliar P

Introduction

Coptis chinensis is a perennial, shade-tolerant, evergreen, understory medicinal plant. The rhizome (RO) of *C. chinensis*, which contains alkaloids, especially berberine, is the main effective component for its therapeutic effects, such as immune-enhancing, hepatoprotective, treating diabetes, Alzheimer's disease, etc. (Jiang et al., 2013; Xu et al., 2015; Li et al., 2018). *Coptis* ROs are also widely used in other East Asian countries such as Korea and Japan, with an annual demand of 3,500–4,000 tons, which continues to rise every year. China accounts for two-thirds of the global production. Owing to overharvesting, global warming, and dimming, the wild resources of *C. chinensis* have almost been depleted, and over 90% of the medicinal herb is produced by cultivation (IUCN, 2004; Li et al., 2020). Cultivation practices involve shading *C. chinensis* with shade cloth throughout the growing period (Supplementary Figure S1), which takes 6–8 years to produce a harvest, resulting in low yields and high costs. As the demand for *C. chinensis* herbs exceeds supply, improving cultivation technology is crucial.

Understory plants in deciduous forests leaf out earlier in spring than do conspecific canopy trees, although there are some exceptions, such as in *Fagus grandifolia*, *Fagus crenata*, and *Betula lenta* (Tomita and Seiwa, 2004; Richardson and O'Keefe, 2009). The earlier leaf out allows understory plants to take advantage of the relatively high light conditions before canopy closure, which is considered a mechanism that allows them to thrive in the understory despite low summer light availability (Gill et al., 1998; Seiwa, 1999; Augspurger et al., 2005; Kwit et al., 2010). Estimates show that the early-leafing species intercept 33%–98% of their growing season total irradiance before canopy closure (Augspurger et al., 2005). Indeed, the high light intensity window in the spring is critical for the growth and survival of the understory plants (Augspurger, 2008; Lopez et al., 2008; Richardson and O'Keefe, 2009; Osada and Hiura, 2019).

C. chinensis, like most understory evergreens in winter deciduous forests, experiences new leaf emergence and expansion in the early spring, before the canopy is closed by the upper canopy trees (Augspurger et al., 2005; Ida and Kudo, 2008; Liao et al., 2021; Liu et al., 2021). High light intensity promotes leaf growth and biomass accumulation in understory plants before canopy closure by mediating leaf physiological and morphological changes that have been well documented (Kwit et al., 2010; Heberling et al., 2019). The leaf development of shade-tolerant understory species, especially delayed-greening species, is divided into three stages: rapid leaf expansion, developing photosynthetic capacity, and maturing as a source organ (Czech et al., 2009). In the first stage, immature leaves (ILs) act as a sink and receive carbohydrates and nutrients from the source organ (e.g., mature leaves, rhizome, and stem) for their own growth (Turgeon, 1989; Vitoria et al., 2016). In the second stage, the transition from being a sink to becoming a source occurs, and the earlier the transition occurs or the greater the photosynthetic capacity of the ILs, the better it is for reducing reserve consumption in the source organ (Turgeon, 1989; Turgeon, 2006). Finally, the leaves act as a source of support for the growth of sink organs (Czech et al., 2009). The rate of transition and photosynthetic capacity of ILs are controlled by multiple environmental signals, especially light (Lake et al., 2001; Lim, 2003; Trouwborst et al., 2011; Fotis and Curtis, 2017). However, it remains unclear how the light intensity regulates the photosynthetic capacity and sink-to-source transition rate of ILs, thereby reducing reserve consumption in the RO of *C. chinensis*. Understanding the underlying mechanisms of the trade-off between reserve storing and supporting new leaf growth regulated by light intensity in the spring is beneficial for better understanding the survival strategies of understory plants and for exploring high-yield cultivation practices in *C. chinensis*.

Light plays a crucial role in plant growth, development, and morphology, while also serving as a signal for altering the relationship between sinks and sources (Hangarter, 1997; Valladares and Niinemets, 2008; Shafiq et al., 2021). This is because light directly influences photosynthesis and the demand for metabolites by sinks, which indirectly regulates the redistribution of reserves (Iqbal et al., 2012). Low light intensity can cause a shortage of photosynthates and nutrients, forcing plants to transport them from storage organs to shoot tissues to meet growth demands (Lynch and Brown, 2001; Myers and Kitajima, 2007; Franklin, 2008; Obendorf et al., 2009). In contrast, excess carbohydrates produced under high light are stored in leaves or transferred to sink organs, indirectly inhibiting their export from the source once reserves are full (Rossi et al., 2015; Zhou et al., 2021). For example, high light increases the photosynthetic capability of saffron seedling leaves, reducing the carbohydrate demand from leaf development in the source organ and leading to reduced carbohydrate consumption in the mother corm (Zhou et al., 2022). Furthermore, in shade-intolerant plants such as corn, soybean, wheat, rice, and *Arabidopsis*, low light intensity speeds up the senescence of mature leaves (MLs), resulting in the transfer of carbohydrates and nutrients to sink organs. On the other hand, low light does not induce senescence in the MLs of shade-tolerant plants, as they adapt by reducing their respiratory consumption to

ensure survival (Reich et al., 1998; Yao et al., 2017). These findings indicate that the role of MLs as a source for supporting new leaf growth is environmentally dependent, especially in light conditions.

The concentration of phosphorus (P) in leaves under high light conditions has been found to be lower than that under low light conditions (Cheng et al., 2014; Kuppusamy et al., 2021). However, it remains uncertain whether high light reduces the P requirement during the expansion stage of ILs. During this stage, plants require a higher proportion of P compared to nitrogen and potassium to support rapid growth. This is because organisms must allocate a disproportionately greater amount of P to rRNA to meet the protein synthesis demands of growth (Hughes et al., 2007; Lambers, 2022). Various studies have shown that plants can maintain their photosynthetic capability with lower foliar P concentrations when exposed to high light intensity compared to those in low light, including *Lupinus abnus* L., *Glycine max* (Linn.) Merr., *Zea mays* L., and Proteaceae (Cheng et al., 2014; Hayes et al., 2018; Zhou et al., 2019a; Zhou et al., 2019b; Kuppusamy et al., 2021). These results imply that, at least in part, the P needed for the development of the photosynthetic capacity of ILs under high light may be lower than that required under low light during the transition phase from sink to source, potentially leading to a reduction in P consumption in source organs.

In the main distribution region of *C. chinensis* in southwest China, the total irradiance generally ranges from 3,350 MJ m^{-2} $year^{-1}$ to 4,190 MJ m^{-2} $year^{-1}$, which falls below the annual average of 5,900 MJ m^{-2} $year^{-1}$ for China (Zhou et al., 2021). Given the low radiation levels in this area, the high light experienced during early spring is particularly valuable for promoting the growth of *C. chinensis*. Although, the influence of light intensity on leaf development and its ultimate effect on rhizome biomass, *via the* regulation of reserve flow between source and sink organs, has not been clearly understood. To fill this knowledge gap, we conducted a systematic study of *C. chinensis* under low and relatively high light intensities in a greenhouse setting. The photochemistry efficiency (F_v/F_m; Y(II); qP; rETR; NPQ) in ILs and MLs, foliar P concentration and fractions, and carbohydrate contents in leaves and RO were evaluated. To evaluate the direction and intensity of carbon movement among ILs, MLs, and RO, we employed ^{13}C isotopic labeling, a well-established method for tracking the pathway of reserves in plants (Vitoria et al., 2016; Zhang et al., 2021). Specifically, during the leaf expansion stage, we formulated the hypothesis that (1) increasing the light intensity appropriately promotes the transition from sink to source in ILs, resulting in a decrease in reserve (carbohydrates and P) consumption in RO; and (2) as the temperature rises in the spring, under low light, MLs do not function as a source and may even act as a sink organ.

Materials and methods

Plant materials

The 3-year-old *C. chinensis* used in the present study were collected from the cultivation base in Pengzhou, Sichuan, China (31° 10′ N, 103° 50′ E). The average daily sunshine duration, air temperature, and precipitation for the last 20 years (2000–2020) were obtained from the nearby meteorological station and are shown in Supplementary Figure S2. During the period of leaf expansion (early spring), which had the highest number of daily sunshine hours throughout the year, the range of sunshine hours was between 4 h and 5.5 h (Supplementary Figure S2). Before the experiment was conducted, the plants were transplanted (February 2022) from the Pengzhou to the Chinese Medicine plant garden of Chengdu University of Traditional Chinese Medicine (30° 68′ N, 103° 81′ E) for 1 month of acclimatization. The plants were grown individually in plastic pots (13 cm^3 × 15 cm^3). An ochric aquic cambosol soil was obtained from the surface layer (0–20 cm) of farmland in the plant garden. The soil was air-dried, sieved to 2 mm, and thoroughly mixed, and properties were as follows: pH (1:2.5, soil:water) was 6.31, organic matter content was 24.1 g kg^{-1}, total N was 1.6 g kg^{-1}, available N was 120 mg kg^{-1}, Olsen-P was 15.3 mg kg^{-1}, and available K was 110 mg kg^{-1}. Each pot was filled with 5 kg of air-dried soil. As the fertility of the soil was adequate for plant growth, no extra mineral fertilizers were added to the soil. All pots were watered daily until they were moved to the greenhouse.

Experimental design and plant growth conditions

The experiment was a randomized block design in an artificial climate chamber with 85% relative humidity and a day/night temperature of 20°C/10°C. According to the daily sunshine hours during the period of leaf expansion, a photoperiod of 8 h day/16 h night was employed. A light-emitting diode (LED), with wavelengths ranging from 380 nm to 800 nm, provides the irradiance, with a red-to-blue ratio of 3:1. The lamps were evenly distributed on the panel with a 4-cm row distance, a 5-cm lamp distance, and increased density around the panel to ensure uniformity and stability of light intensity under the lamp (Supplementary Figure S3). Usually, 0%–4% and 4%–12% of the open-sky light are approximately closed forest understory and tree-fall gap light environments, respectively (Canham et al., 1990; Walters and Reich, 1999). In combination with the light intensity of the growing area (canopy light intensity at noon averages about 2,000 µmol m^{-2} s^{-1}) of *C. chinensis* (Supplementary Figure S4), two light intensities were employed: 50 µmol m^{-2} s^{-1} ± 5 µmol m^{-2} s^{-1} (low light) and 200 µmol m^{-2} s^{-1} ± 5 µmol m^{-2} s^{-1} (relatively high light), which represent 2.5% and 10% of the canopy light, respectively. Our previous study using a fast light response curve also found that a light intensity of 200 µmol m^{-2} s^{-1} is typical for the cultivation of *C. chinensis in the* laboratory (Supplementary Tables S1, S2), although it is much lower than natural light intensities found in field conditions. Light intensity was measured using a quantum sensor (UPRtek, PG100N, Taiwan, China).

When the new leaves were ready to appear (March 10, 2022), the uniformly growing and healthy plants in pots were transferred from the Chinese Medicine plant garden to the artificial climate chamber. The arrangement of pots under the LED panel is shown in Supplementary Figure S3. The pots were arranged in a diamond shape, with a 20-cm distance between two pots to ensure that the plants were unobstructed from each other and received almost the

same amount of light from the LED. A distance of 50 cm was maintained between the canopy and the light to eliminate the effect of temperature produced by the lamp in the two light conditions.

Plants from both light treatments were transplanted back to the Pengzhou base after the controlled experiment, and the field management after transplanting was the same as the local cultivation practice. The plants were dug up in October to determine the dry weight of the RO.

Plant sampling

The chlorophyll fluorescence parameters of the ILs and MLs were measured at 15 d (ILs fully expanded and pale green; MLs grow normally dark green) and 35 d (ILs fully expanded and dark green; MLs with no obvious changes) after the start of the light treatment, respectively. The ILs of fresh plants were cut for the determination of pigment content. Plants were harvested 15 d and 35 d after the start of light treatment, frozen in liquid nitrogen, and stored at −80°C for subsequent index determination.

Chlorophyll *a* fluorescence

The chlorophyll fluorescence of ILs and MLs, respectively, was measured using a MINI-PAM-II Portable Fluorometer (Walz, Effeltrich, Germany) *in situ* in complete darkness in an artificial climate chamber on day 15 and day 35 of light treatment. The leaves were dark-adapted for 30 min, and then a 0.6-s saturating light pulse (1,100 μmol m^{-2} s^{-1}) and an actinic light for 60 s (261 μmol m^{-2} s^{-1}) were applied to obtain the minimal and maximal fluorescence yield (F_0 and F_m). The maximum light-adapted fluorescence (F_m') and steady-state fluorescence (F_s) were then measured with continuous actinic light. The PSII operating efficiency [Y(II)], relative electron transport rate (*r*ETR), photochemical quenching (qP), the maximum photochemical efficiency PSII (F_v/F_m), and the nonphotochemical dissipation of absorbed energy (NPQ) were calculated with the following formula (Kooten and Snel, 1990; Oquist and Chow, 1992):

$$Y(\mathrm{II}) = (F_m' - F)/F_m' \quad (1)$$

$$\mathrm{rETR} = Y(\mathrm{II}) \times \mathrm{PAR} \times 0.84 \times 0.5 \quad (2)$$

$$\mathrm{qP} = (F_m' - F_s)/(F_m' - F_0) \quad (3)$$

$$F_v/F_m = (F_m - F_0)/F_m' \quad (4)$$

$$\mathrm{NPQ} = (F_m - F_m')/F_m' \quad (5)$$

Determination of chlorophyll concentration

After 15 d and 35 d of treatment, fresh ILs were cut and crushed immediately with liquid nitrogen, and 0.1 g (fresh weight (FW)) of powder was soaked in 10 mL of 80% v/v acetone (20% ethanol) at 25°C to extract chlorophyll for 24 h in the dark (Lichtenthaler and Buschmann, 2001). Powdering the leaves speeds up the leaching of chlorophyll and shortens the steeping time. The absorbance at 645 nm and 663 nm was measured with an enzyme-labeled instrument (SpectraMax iD3, Molecular Devices, USA), and the chlorophyll concentration was calculated with the following formula (Arnon, 1949; Porra et al., 1989).

$$\text{Chlorophyll } a \text{ (Chl } a\text{)} = (12.7 \times A663 - 2.69 \times A645) \times V/(1,000 \times W) \quad (6)$$

$$\text{Chlorophyll } b \text{ (Chl } b\text{)} = (22.9 \times A645 - 4.68 \times A663) \times V/(1,000 \times W) \quad (7)$$

Where V is the total volume of extract (mL) and W is the leaf fresh weight (g).

Determination of soluble sugar and starch

Soluble sugars from lyophilized (FDU-2110, EYELA, Japan) leaves and RO (dry weight (DW)) were extracted with 80% v/v ethanol at 80°C for 10 min, and the supernatants of the two extractions were combined to prepare soluble sugar samples for analysis. Soluble sugar was measured directly in the extract by a Waters Binary HPLC System (Waters 1525-2707, Milford, USA) equipped with a refractive index detector (2414, Waters, Milford, USA). The analytical conditions were as follows: column Agilent Hi-Plea Ca (8% crosslinked) 300 mm × 7.7 mm, 8 μm in diameter (Agilent Technologies Inc., USA); column temperature 85°C; mobile phase Milli-Q water; flow rate 0.6 mL min^{-1} (Zhou et al., 2022). Data were collected and processed by the Waters Chromatography Station DataApex. Sugars were identified by comparison with retention times and coelution of authentic standard solutions.

The residue after ethanol extraction was washed several times with ultra-pure water and used for starch analysis. The precipitate was gelatinized at 100°C for 10 min, and the process was repeated once. The resulting supernatants were combined and treated with perchlorate before analysis. The starch content was determined by taking an appropriate amount of sample by the anthrone method (Setter and Ella, 1994).

Observation of chloroplast ultrastructure and starch by transmission electron microscope

Small squares of 1 mm^2 size were cut from the ILs after 35 d of growth in the light resource and immediately placed in 3% glutaraldehyde for prefixation. The tissue was then postfixed in 1% osmium tetroxide, dehydrated in series acetone, infiltrated in Epox 812 for a longer period, and embedded. The semithin sections were stained with methylene blue, and ultrathin sections (EMUC7,

Leica, Germany) were cut with a diamond knife and stained with uranyl acetate and lead citrate. Sections were examined with TEM (JEM-1400FLASH, JEOL, Japan).

Labeling of selected leaves with $^{13}CO_2$

To explore the role of ILs and MLs in plant development under different light intensities, the ILs or MLs were labeled with $^{13}CO_2$. After 20 d of light treatment, six pots (three for IL labeling and three for ML labeling) in each light treatment were subjected to $^{13}CO_2$ labeling. Leaf labeling was performed 1 h after the start of illumination. Similar sizes of the ILs or MLs were carefully covered with a homemade sealing bag (sealed with foam glue). A syringe was used to inject 40 mL of $^{13}CO_2$ gas into the bag, and 30 min later, the marking device was disassembled.

Two weeks after labeling, the plants (ILs labeled, MLs labeled, and unlabeled) were harvested and oven-dried at 70°C for 3 d for an assay of ^{13}C abundance in the ILs, MLs, and RO. The movement of ^{13}C under different light conditions was monitored; we used the labeled part as the denominator and the unlabeled part as the numerator, which reflects the amount transferred from labeled to unlabeled. A 0.2-mg plant sample was precisely weighed, and the $^{13}C/^{12}C$ ratio was measured using a stable isotope mass spectrometer (Delta V Advantage, Thermo Fisher Scientific, Germany).

Determination of foliar P fractions and rhizome total P

The four fractions of foliar P (lipid P, nucleic acid P, metabolic P (including Pi), and residual P) were extracted from 50 mg of freeze-dried ILs and MLs according to Hidaka and Kitayama (2013) with modifications. The plant samples were digested with a mixed acid solution (nitric acid: perchlorate = 3:1, v/v) to extract different P fractions. The RO of total P was extracted by sulfuric acid. P was determined by the molybdenum blue method using a spectrophotometer (UV-6100, Mapada, Shanghai, China) (AMSs, 1966).

Determination of alkaloid content using high-performance liquid chromatography

The determination of the alkaloid content of *C. chinensis* in RO was performed after 35 d of light intensity treatment according to the method of Qi Qi et al. (2018) with high-performance liquid chromatography (HPLC) (LC-20AT, Shimadzu, Japan). The lyophilized RO was weighed and ultrasonically dissolved in a hydrochloric acid–methanol solution (1:100, v/v). An Xtimate C18 chromatographic column (250 mm × 4.6 mm, 5 μm) (Welch, China) was applied to separate different alkaloid compounds, and the column temperature was 25°C. The mobile phase included acetonitrile (A) and 30 mmol/L ammonium bicarbonate solution (consisting of 0.7% ammonia and 0.25% triethylamine) (B) at a flow rate of 1 mL/min. The gradient program was set as follows: 0–15 min, 90%–75% B; 15–25 min, 75%–70% B; 25–50 min, 70%–55% B. The injection volume was set as 10 μL, and the detection wavelength was set at 270 nm.

Statistical analysis

A one-way analysis of variance was performed to compare the data between the light-intensity experiments. The data was compared between two light intensity treatments or between the two sampling times of the same light intensity treatment using Tukey's honestly significant difference test. All statistical analyses were performed using the software SPSS 25.0 (SPSS Inc., USA). The figures were drawn using Origin 2019 (Origin, USA).

Results

Chlorophyll *a* fluorescence in immature leaves and mature leaves

Light intensity affected the photochemistry of *C. chinensis* leaves during the leaf expansion stage. The *Y*(II), ETR, and qP in ILs under 200 μmol m^{-2} s^{-1} were significantly higher than those exposed to 50 μmol m^{-2} s^{-1} light intensity (Figures 1A–C). However, in MLs, the *Y*(II) showed no significant difference between the two light treatments (Figure 1F), and there was no difference between the observed ETR and qP between the two sampling times (Figures 1G, H). Compared to relatively high light, the F_v/F_m in leaves was higher when the plants were under low light, but there was no change at the two sampling times (Figures 1D, I). In ILs, light intensity had little effect on NPQ (Figure 1E), while NPQ in MLs under relatively high light was significantly higher than that under low light (Figure 1J).

Chlorophyll concentration in immature leaves

The plant phenotype observed that ILs turn green quickly under low light (Figure 2A). The chlorophyll concentration in ILs was consistent with our observations that decreasing light intensity increased the chlorophyll concentration, particularly Chl *b* concentration, and subsequently decreased the ratio of Chl *a*/Chl *b* ratio (Figures 2B, C).

Sucrose, glucose, and starch concentrations in leaves and rhizomes and starch morphology in immature leaves

Light intensity affected the sucrose, glucose, and starch concentrations in ILs, MLs, and RO at the two sampling times (Figure 3). The sucrose concentration in ILs and MLs under 200 μmol m^{-2} s^{-1} light intensity was higher than that under 50 μmol m^{-2} s^{-1} light intensity, and it was higher at 15 d compared to 35 d

10.3389/fpls.2023.1225895

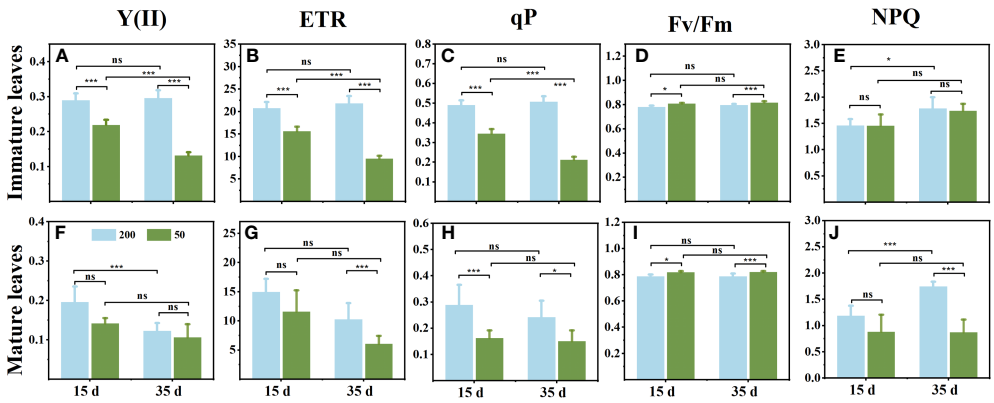

FIGURE 1
Changes of chlorophyll fluorescence parameters in immature leaves **(A–E)** and mature leaves **(F, G)** at 15 d and 35 d under 50 μmol m^{-2} s^{-1} and 200 μmol m^{-2} s^{-1} light intensity treatment. **(A, F)** The actual photochemical efficiency PSII [*Y*(II)]. **(B, G)** Relative electron transport rate (ETR). **(C, H)** Photochemical quenching (qP). **(D, I)** The maximum photochemical efficiency PSII (F_v/F_m). **(E, J)** Nonphotochemical dissipation of absorbed energy (NPQ). Each column represents the mean (± SE) of three replicates. Significant difference between the treatments: ***$p \leq 0.001$ (*t*-test); *$p \leq 0.05$ (*t*-test); ns, no difference.

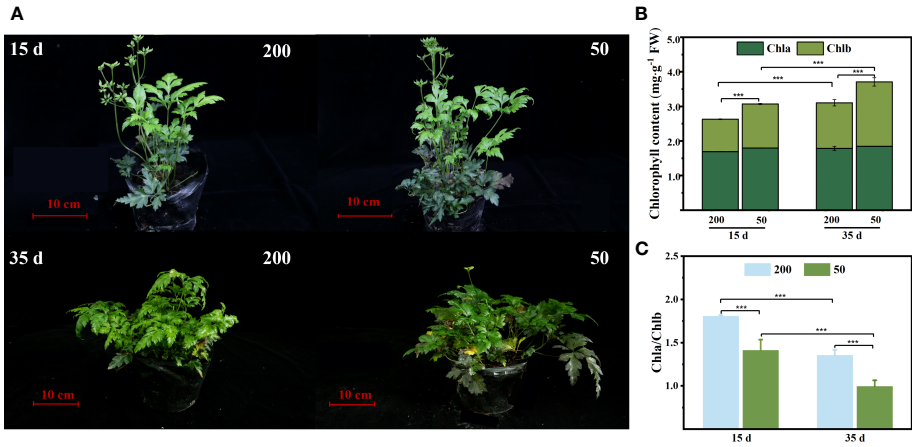

FIGURE 2
Chlorophyll concentration of immature leaves (IL) at 15 d and 35 d under 50 μmol m^{-2} s^{-1} and 200 μmol m^{-2} s^{-1} light intensity treatment. **(A)** Plant phenotypic. **(B)** Chlorophyll *a* (Chl *a*), chlorophyll *b* (Chl *b*), and total chlorophyll content (Chl *a* + Chl *b*). **(C)** The ratio of Chl *a* to Chl *b*. Each column represents the mean (± SE) of three replicates. Significant difference between the treatments: ***$p \leq 0.001$ (*t*-test). FW, fresh weight.

(Figures 3A, B). Compared with plants under low light intensity, relatively high light intensity increased the glucose concentration at both sampling times, irrespective of the age of the leaves (Figures 3C, D). In ILs, the starch concentration showed no difference between the two light treatments at 15 d, but in relatively high light, it was significantly higher than that in the low light at 35 days (Figures 3E, F). In MLs, the starch concentration showed a decrease from 15d to 35 d under both two light treatments, which was decreased further under low light (Figure 3F). After 35 d light intensity treatment, the starch and glucose in the RO under 200 μmol m^{-2} s^{-1} were higher than those under 50 μmol m^{-2} s^{-1} (Figure 3G). In addition, the results of the electron microscope photography were consistent with the results obtained above. The chloroplasts were full of starch granules under 200 μmol m^{-2} s^{-1}, but almost no starch granules were observed under 50 μmol m^{-2} s^{-1} (Figures 3H–K).

The atomic percentage of ^{13}C in different plant parts

^{13}C labeling plays an important role in monitoring carbon flow. The proportion of ^{13}C in ILs under 200 μmol m^{-2} s^{-1} was significantly higher than that under 50 μmol m^{-2} s^{-1}, regardless of whether ILs or MLs were labeled with ^{13}C. Furthermore, under 200 μmol m^{-2} s^{-1} treatment, ^{13}C atoms were detected in ILs and RO

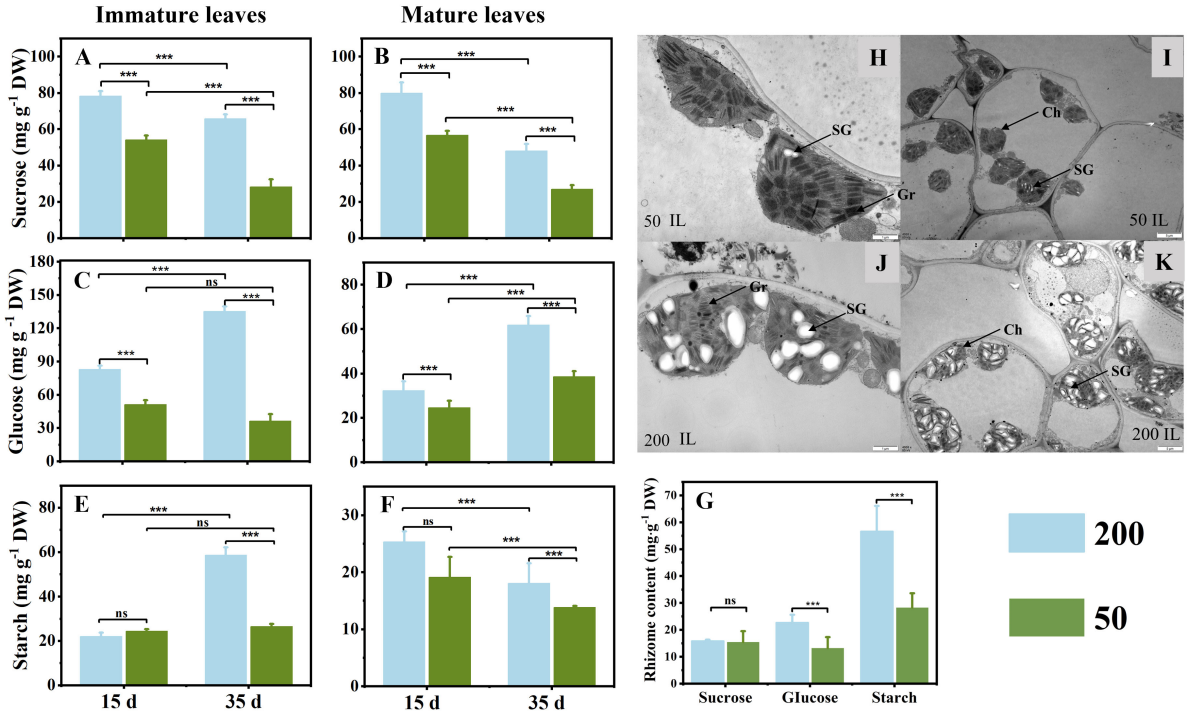

FIGURE 3
Sucrose **(A, B)**, glucose **(C, D)**, and starch **(D, E)** concentrations in immature leaves **(A, C, E)** and mature leaves **(B, D, F)** at 15 d and 35 d under 50 µmol m^{-2} s^{-1} and 200 µmol m^{-2} s^{-1} light intensity treatment. **(G)** Sucrose, glucose, and starch concentrations in rhizome at 35 d under two light intensities. **(H–K)** The ultrastructures of chloroplasts in ILs after 35 d of light treatment were observed under a transmission electron microscope (TEM); **(H, J)** ×15,000, **(I, K)** ×4,000. Ch, chloroplast; Gr, grana; SG, starch grain. Each column represents the mean (± SE) of three replicates. Significant difference between the treatments: ***$p \leq 0.001$ (*t*-test); ns, no difference between the treatments. DW, dry weight.

but not in MLs when ^{13}C was labeled in ILs. Under 50 µmol m^{-2} s^{-1} light, the ratio of mature-to-immature leaf ^{13}C concentration in the treatment of IL ^{13}C labeling (12.2%) was higher than the ratio of immature-to-mature leaf ^{13}C concentration in the treatment of ML ^{13}C labeling (7.3%), ^{13}C atoms were detected in ILs and MLs but were not in the RO (Figure 4).

Concentrations of total P in leaves and rhizomes and foliar P fractions

The total P concentration in leaves and RO under 200 µmol m^{-2} s^{-1} was lower than that under 50 µmol m^{-2} s^{-1} (Figures 5A–C). Under 50 µmol m^{-2} s^{-1} light intensity, the leaf P concentration of MLs showed no difference observed at both sampling times (Figure 5B). However, the leaf P concentration of ILs under 200 µmol m^{-2} s^{-1} light intensity was lower than that under 50 µmol m^{-2} s^{-1} light intensity at both sampling times (Figure 5A). Light not only affected the foliar total P concentration but also the foliar P fractions, especially the organic P (Figures 5D–G). In ILs, the lipid P and metabolite P under relatively high light were significantly lower than those under low light intensity at both sampling times (Figures 5D, E). At 15 d, the main sources of phosphorus in ILs were lipid P and metabolic P (Figure 5D), but metabolic P and nucleic P had a high proportion at 35 d (Figure 5E). In MLs, only nucleic P increased with decreasing light intensity at 15 d (Figure 5F). Nucleic P had a high proportion in MLs at 15 d, and the proportion of lipid P and metabolic P increased at 35 d compared to 15 d (Figures 5F, G). Furthermore, the residual P showed no difference in ILs and MLs under the two light intensity treatments at both measuring times (Figures 5D–G).

The concentration of alkaloids in the rhizome and biomass accumulation, and the correlation between alkaloids and starch in the rhizomes

The findings demonstrated that under low light conditions, the alkaloid concentrations in the RO of berberine (23.0%), coptisine (19.9%), and palmatine (17.9%) were all greater than those under relatively high light intensity (Figure 6). The light treatment at the leaf expansion stage has an effect on the biomass of RO at the mature stage. The RO dry weight of plants under relatively high light at the mature stage was significantly higher than that under low light (Supplementary Figure S6).

The relationships between the starch concentration in RO and the concentration of the three main alkaloids in RO were investigated *via* regression analyses (Figure 7). The concentrations of the three main alkaloids (Figure 7) were negatively correlated with starch concentration

10.3389/fpls.2023.1225895

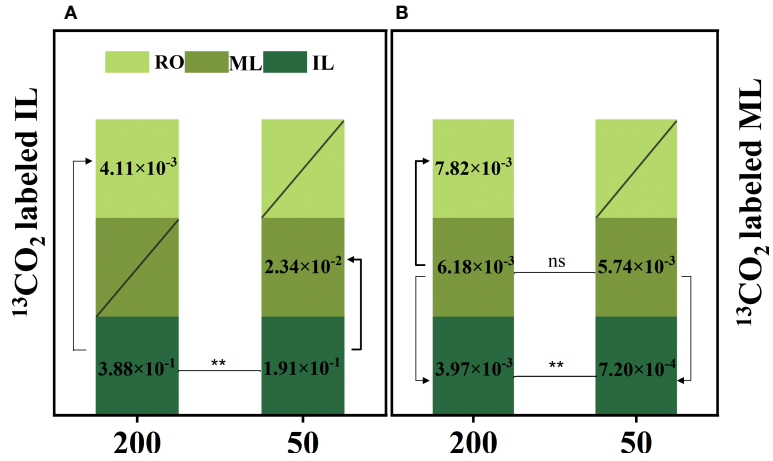

FIGURE 4
The atomic percentage of ^{13}C [AT% $=^{13}C\ /(^{13}C\ +^{12}C\ ) \times 100\%$] in immature leaves (IL), mature leaves (ML), and rhizomes (RO) after ^{13}C-labeled IL **(A)** and ML **(B)**. Data represent the atomic percent of ^{13}C, "/" indicates the ^{13}C atom was not detected. Each column represents the mean (± SE) of three replicates. Significant difference between the treatments: $^{**}p \leq 0.01$ (*t*-test); ns, no difference between the treatments. The thickness of the line represents the amount of transfer.

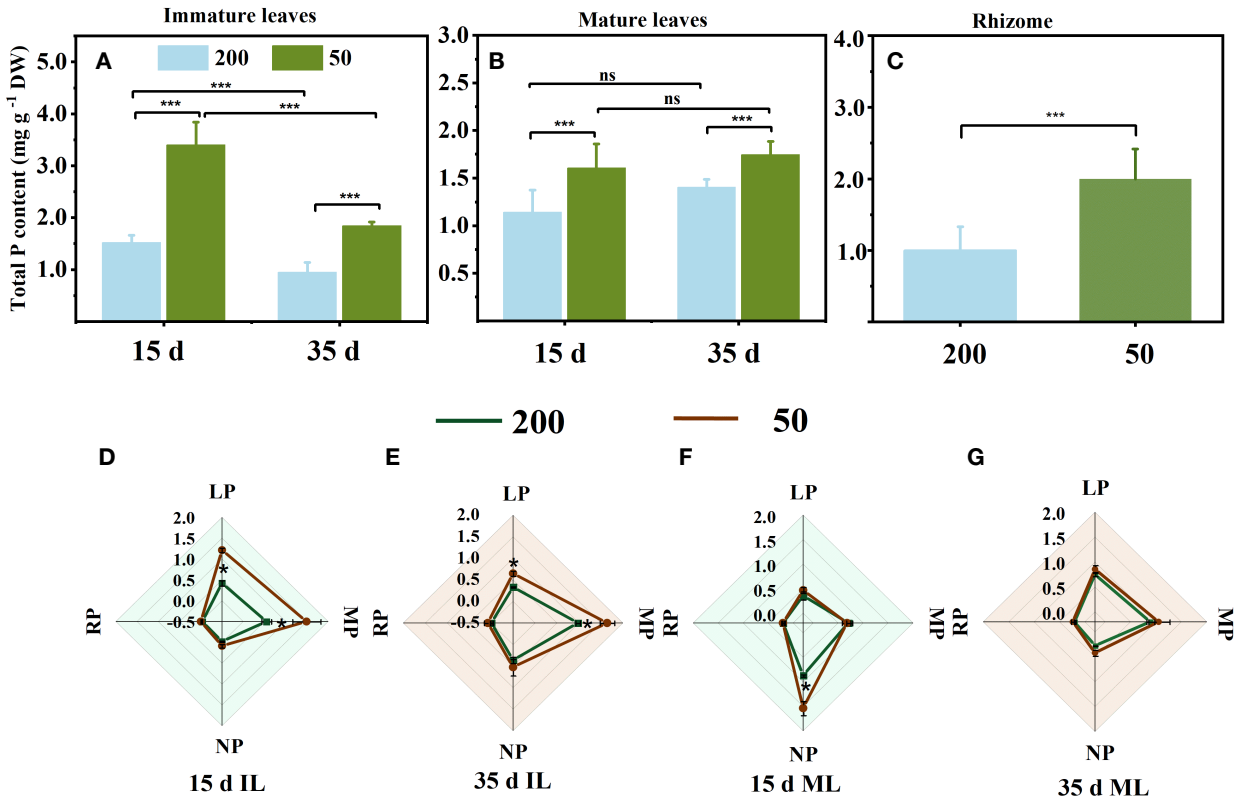

FIGURE 5
Total phosphorus concentration in immature leaves (IL) **(A)**, mature leaves (ML) **(B)**, and rhizome **(C)**, and foliar phosphorus fractions concentration **(D–G)** at 15 d and 35 d under 50 μmol m^{-2} s^{-1} and 200 μmol m^{-2} s^{-1} light intensity. Each column represents the mean (± SE) of three replicates. Significant differences between the treatments: $^{***}p \leq 0.001$ (*t*-test); $^{*}p \leq 0.05$ (*t*-test); ns, no difference between the treatments. DW, dry weight; RP, residual P; LP, lipid P; MP, metabolite P; NP, nucleic P.

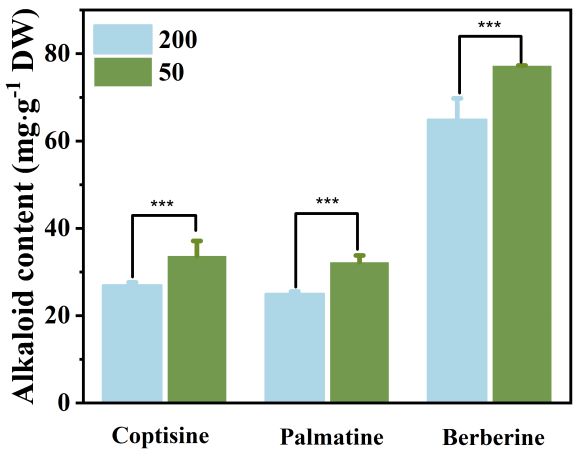

FIGURE 6
The concentration of three kinds of alkaloids in rhizomes under 50 μmol m^{-2} s^{-1} and 200 μmol m^{-2} s^{-1} light treatments after 35 d. Each column represents the mean (± SE) of three replicates. Significant difference: ***$p \leq 0.05$. DW, dry weight.

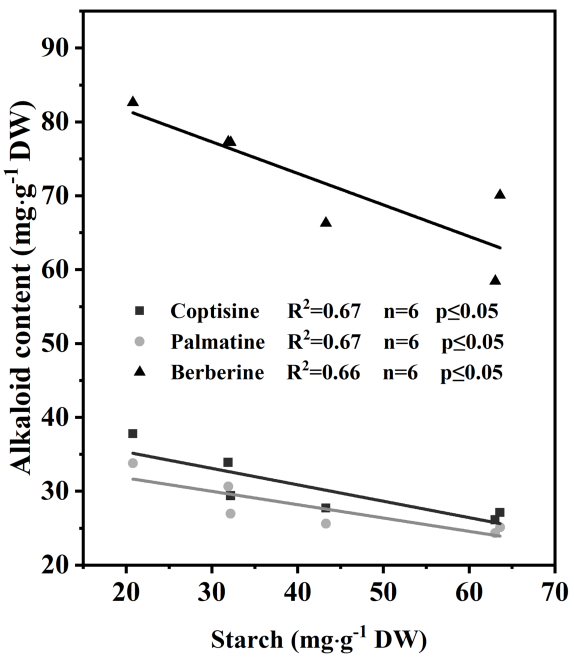

FIGURE 7
Correlation of alkaloids with starch concentration in rhizomes after 35 d of light treatment (n = 6).

in RO ($n = 6$; R^2 = 0.67, 0.67, 0.66; $p \leq 0.05$), indicating that the lower the starch concentration, the higher the alkaloid concentrations.

Discussion

Light intensity changed the sink–source relationships among ILs, MLs, and RO during the expansion of ILs

The initial growth stages of ILs primarily rely on imported reserves from source organs such as MLs, stems, and RO, but eventually become net exporters of carbon and rely on their own photosynthates (Miyazawa et al., 2003). High light intensity enhances local photosynthesis, which induces the transfer of produced carbohydrates to source organs, reducing the consumption of reserves in source organs to supply new leaf growth, making reserves more durable, and ultimately increasing their biomass (Rossi et al., 2015; Feng et al., 2019; Wimalasekera, 2019; Zhou et al., 2022). Our findings confirm that increased carbon assimilation by ILs and MLs under high light during leaf expansion reduces RO reserve consumption (Figure 4), ultimately increasing RO biomass (Supplementary Figure S6). Additionally, high light accelerates the conversion of ILs from sink to source, which reduces RO reserve consumption. However, we observed that MLs exacerbated the depletion of RO reserves as a sink under low-light conditions, which contrasts with prior studies.

In *C. chinensis*, a delayed-greening species, leaves from emergence to maturity take at least 45–60 d. In this process of leaf maturation, ILs, MLs, and RO are involved in a high intensity of reserve exchange. In most dicotyledonous plants, the leaf changes from sink to source when the leaf area reaches 10%–60% of the final area (Miyazawa et al., 2003; Pantin et al., 2012). In the present study, some ILs were not fully expanded 15 d after treatment, and all had reached the maximum area by 35 d, but the chlorophyll concentration in ILs was lower than MLs (Figure 2). Furthermore, the F_v/F_m showed no difference between the two sampling times and reached a high level above 0.8 (Figures 1D, I). The amount of glucose and starch, the major carbohydrate forms for transport and storage, increased markedly from 15 d to 35 d in ILs (Figures 3C, E). These results are consistent with the typical characteristics of the transition from the sink to the source of ILs in the studies that have been reported (Turgeon, 1989; Czech et al., 2009). Indeed, the growth of ILs in *C. chinensis* at least partially depends on its photosynthesis from 15 d to 35 d after emergence of leaves. The glucose and starch concentrations in ILs increased markedly from 15 d to 35 d when plants were grown under 200 μmol m^{-2} s^{-1} (Figures 3C, E). In contrast, under 50 μmol m^{-2} s^{-1}, the glucose and starch concentrations in ILs remained at very low levels and did not show significant changes at the two sampling times (Figures 3C, E). Interestingly, the glucose concentration in the RO was lower in plants grown under 200 μmol m^{-2} s^{-1} than those grown under 50 μmol m^{-2} s^{-1} at 35 d (Figure 3G), suggesting that starch breakdown was triggered to support shoot growth under low light conditions (Hajirezaei et al., 2003; Stitt and Zeeman, 2012). Additionally, ^{13}C was detected in the RO of the ILs ^{13}C label under 200 μmol m^{-2} s^{-1} but not under 50 μmol m^{-2} s^{-1} (Figure 4). These findings indicate that increasing light intensity before leaf maturation in *C. chinensis* can significantly enhance the autotrophic capacity of ILs by providing carbohydrates to support their own growth and transporting carbohydrates underground to accumulate RO biomass. In contrast, under low light, the RO continues to supply the growth of ILs, leading to increased consumption of reserves in the RO.

The MLs of evergreen species can resume their functions in early spring to sustain themselves and provide partial resources to support the new leaf growth as the temperature rises (Walters and Reich, 1999; Ida and Kudo, 2008). Our findings reveal that the functional performance of MLs is mainly influenced by the light intensity to which they are exposed. Under high light intensity, a higher proportion of ^{13}C was detected in the RO and ILs when MLs were labeled with ^{13}C. This observation provided evidence to support the view that MLs provide partial resource support for IL growth (Turgeon, 1989). No difference in starch concentration was observed in the MLs between the two light intensity treatments at 15 d (Figure 3F). However, at 35 d, MLs under low light exhibited a lower starch concentration compared to those under high light (Figure 3F). These suggest that under 50 μmol m^{-2} s^{-1}, MLs rely on stored starch to ensure their survival (Stitt & Zeeman, 2012). Furthermore, the ratio of ^{13}C in mature-to-immature leaf in IL ^{13}C labeling was 12.2%, and the ratio of ^{13}C in immature-to-mature leaf in ML ^{13}C labeling was 7.3% under 50 μmol m^{-2} s^{-1} light intensity (Figure 4). Moreover, under 200 μmol m^{-2} s^{-1}, the ^{13}C was not even detected in MLs in IL ^{13}C labeling (Figure 4). Therefore, under low light, MLs did not have additional carbon to sustain IL growth, but instead received energy from the ILs.

Shade-tolerant plants have evolved a trade-off between growth potential and survival in low light, such as increasing their photosynthesis efficiency and decreasing the respiration rate to decrease the consumption of energy when the plants are grown in deep shade (Loach, 1967; Reich et al., 1998; Yao et al., 2017). However, in our study, MLs maintained the same respiration rate under low light intensity as under high light and remained at a high level (data not shown), which is inconsistent with previous observations in other species (Loach, 1967; Reich et al., 1998; Yao et al., 2017). One possible explanation for this discrepancy might be that the 50-μmol m^{-2} s^{-1} light intensity harmed the carbon fixation of *C. chinensis* but did not cause severe stress (Supplementary Figure S5). For example, the F_v/F_m, a sensitive indicator of plant responses to environmental stresses (Baker, 2008), showed no difference between 15 d and 35 d in the two samples, regardless of leaf age (Figures 1D, I). Additionally, *C. chinensis* is typically found in mountainous regions at elevations of 1,000–2,000 m. During the new leaf growth period (from February to April), the average day/night temperature is around 15°C/5°C (Supplementary Figure S2D). Under low temperatures, *C. chinensis*, like other shade-tolerant plants, can survive under low light by reducing their respiration rate (Walters and Reich, 1999; Walters and Reich, 2000). However, the day/night temperatures set in this experiment were higher than those found in its natural habitat. To ensure survival, MLs may need to utilize energy from other organs. Nevertheless, the strategy of MLs of shade-tolerant perennial plants to adapt to low light stress at higher temperatures by consuming energy provided by other organs to sustain survival rather than rapid senescence needs more evidence.

The energy consumption in the source organ (especially RO) by flowering was not considered in this experiment. This may have potentially amplified the result indicating that light-mediated IL growth increases the consumption of reserves in the source organ (RO), particularly under low-light conditions. However, the amount of reserves in the RO did not change the source–sink relationship among ILs, MLs, and RO, which is mainly determined by the light-regulated carbon assimilation capacity of ILs and MLs.

Relatively high light decreased the P demand needed to maintain the photosynthesis potential of immature leaves

The expansion of new leaves in understory plants during spring is mainly supported by stored P rather than uptake by roots in the current season (Schachtman et al., 1998; Rychter and Rao, 2005). The low P concentration in the new leaves suggests a low total of P export from the source organ. Our data are consistent with this observation, as the ILs of plants grown under 200 μmol m^{-2} s^{-1} had lower P concentration than those grown under 50 μmol m^{-2} s^{-1} (Figure 5A). In addition, the *Y*(II) *of* ILs under 200 μmol m^{-2} s^{-1} was higher than those under 50 μmol m^{-2} s^{-1} (Figure 1A).

Relatively high light increased photosynthesis efficiency in ILs associated with lower P concentrations in two ways. First, the level of enzymes involved in Rubisco and other Calvin–Benson cycles is mainly connected to the amount of rRNA, which is mainly determined by the amount of nucleic P (Rychter and Rao, 2005; Hussain et al., 2021). The high light intensity did not decrease the nucleic P concentration in the ILs compared to that under low light (Figures 5D, F). Second, under high light intensity, a lower number of chloroplasts and a low chlorophyll concentration will decrease the investment of P in protein synthesis and cellular growth (Elser et al., 2010; Veneklaas et al., 2012). Light intensity rather than chlorophyll concentration is the main factor limiting photosynthesis (Rychter and Rao, 2005; Hussain et al., 2021). Our data are consistent with this observation, as the chloroplast number and chlorophyll concentration in ILs of plants grown under 200 μmol m^{-2} s^{-1} were lower than those of ILs grown under 50 μmol m^{-2} s^{-1} (Figures 2B, 3H–K). Furthermore, when the plants were grown under 50 μmol m^{-2} s^{-1} light intensity, the increased chlorophyll concentration was mostly attributed to a high proportion of Chl *b* (Figures 2B, C), which is currently believed to improve light harvesting under low light conditions and has been demonstrated in numerous earlier investigations (Escoubas et al., 1995; Sun et al., 2003; Valladares and Niinemets, 2008; Melgar et al., 2009; Feng et al., 2019).

The P concentration in the RO of *C. chinensis* grown under 200 μmol m^{-2} s^{-1} was lower than that of plants grown under 50 μmol m^{-2} s^{-1}, which may challenge the view that high light suppresses the amount of P exported from the RO. One possible explanation is due to the concentration effect (Supplementary Figure S6) (Jarrell and Beverly, 1981). Under 50 μmol m^{-2} s^{-1}, the amount of carbohydrates was much higher than P from RO to supply the growth of ILs, resulting in an increased P concentration in the RO. Indeed, relatively high light intensity reduced the demand for P to

10.3389/fpls.2023.1225895

maintain the photosynthesis potential of ILs, thus inhibiting the export of P from the RO (Figure 8).

Effects of light on the rhizome alkaloid concentration

Rather than directly mediating synthesis, low light promotes the increase in alkaloid concentration in *C. chinensis* RO in early spring by mediating substance translocation. However, low light significantly reduces RO biomass (Supplementary Figure S6). In most evergreen plants, nonstructural carbohydrate concentrations typically reach their maximum in the fall, decline during the winter, and reach minimum levels immediately after growth initiation in the spring (Wyka, 1999). The alkaloid concentration in the RO of *C. chinensis* showed two peaks in March (new leaf expansion) and September (vigorous growth period), with the concentration in September being significantly higher than that in March (Ke, unpublished; Zhao and Du, 2002). RO alkaloids and nonstructural carbohydrates were negatively correlated in March and positively correlated in September. Secondary metabolism usually uses the end products of primary metabolism as substrates (Drew and Demain, 1977), suggesting that the increase in RO alkaloids in March may not be regulated by synthesis.

In the present study, RO under low light in the early spring had lower starch and higher alkaloid concentration than that of plants under high light (Figure 6). Furthermore, there was a negative correlation between starch and alkaloid concentration (Figure 7). The increase in alkaloid concentration mainly attributed to the concentration effect (Jarrell and Beverly, 1981), as the amount of carbohydrates in the RO supplying ILs growth was higher under low light than under high light, resulting in an increased alkaloid concentration in the RO. These findings support our view, but further exploration is needed to understand the effect of light on alkaloid synthesis in *C. chinensis*.

Conclusions

Our findings have demonstrated that during leaf expansion, the RO of *C. chinensis* had lower carbohydrate and P losses under 200 μmol m^{-2} s^{-1} compared to plants under 50 μmol m^{-2} s^{-1}. After rapid leaf expansion, the high light intensity can enhance the photosynthetic capacity and sink to the source transition rate of ILs, thereby reducing reserve consumption in RO. Under high light, MLs served as a source to provide carbohydrates for IL growth, reducing the consumption of reserves in RO. Conversely, under low light, MLs have low photosynthesis efficiency but maintain relatively high metabolic activity, acting as a sink to survive and supported by other organs, which aggravates the reserves lost in the RO. Furthermore, under high light intensity, less P is required in ILs to maintain a high rate of photosynthesis, resulting in less P distributed from RO to ILs (Figure 8). Nevertheless, the regulation of light on the synthesis and accumulation of alkaloids in RO requires further investigation. This study found that light accelerates the development of photosynthetic capacity in ILs, resulting in reduced reserve consumption in the RO and ultimately leading to increased yield. Under low light and high-temperature conditions, MLs of *C. chinensis* may survive by consuming energy supplied by other organs, which may be a new mechanism for its adaptation to environmental stress, but more evidence is needed. Nevertheless, it is recommended that light intensity be appropriately increased during the development of ILs to promote leaf development and reduce the reserve consumption in the source organ. However, further research is needed to determine the optimal intensity and duration of high-light exposure.

Data availability statement

The original contributions presented in the study are included in the article/Supplementary Material. Further inquiries can be directed to the corresponding authors.

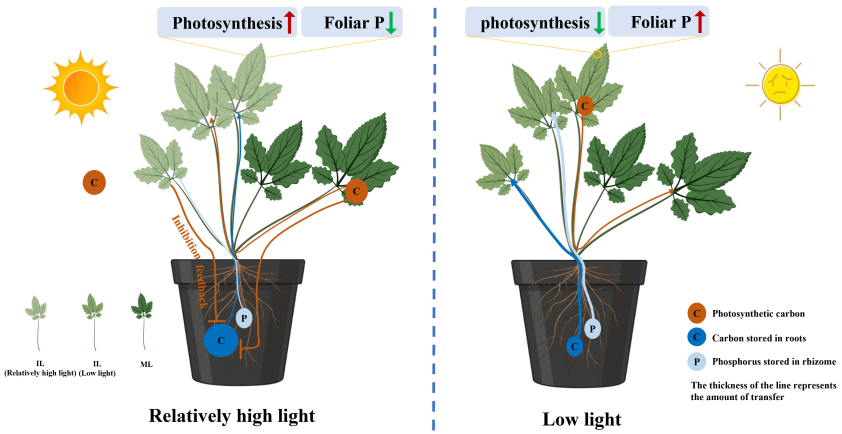

FIGURE 8
Schematic of a proposed model showing the decreased consumption of reserves in the rhizomes (RO) relating to the source–sink relationship changes regulated by light intensity. Relatively high light intensity during the period of leaf expansion increased the photosynthetic capability of immature leaves (ILs) that are associated with low P concentration. The increased carbon capture and decreased P demand in the ILs inhibited the transport of carbohydrates and P from the RO to the leaves. In addition, under low light, barely any reserves are exported from mature leaves (MLs) to feed ILs growing, which aggravates the amount of reserves lost in the RO. The thickness of the line represents the amount of transfer.

Author contributions

TZ, WK, YM, and BX carried out the design of this research work and wrote this paper. WK, YL, FZ, and JD carried out the plant cultivation, chemical analysis, and statistical analysis of this work, and MP participated in experiment management and manuscript revision.

Funding

This work was supported by the Sichuan Science and Technology Program (2022ZHCG0096), the Sichuan Development Service Center for Traditional Chinese Medicine—a major project for the development of the traditional Chinese medicine industry (510201202109711), and the Innovation Team and Talents Cultivation Program of the National Administration of Traditional Chinese Medicine (No. ZYYCXTD-D-202209).

Acknowledgments

We also thank Dr. Xing Fu (Innovative Institute of Chinese Medicine and Pharmacy) for help in sucrose and starch analysis and Li Wang (Sichuan Agricultural University) for help in foliar phosphorus analysis.

Conflict of interest

The authors declare that the research was conducted in the absence of any commercial or financial relationships that could be construed as a potential conflict of interest.

Publisher's note

Supplementary material

The Supplementary Material for this article can be found online at: https://www.frontiersin.org/articles/10.3389/fpls.2023.1225895/full#supplementary-material

References

AMSs, B. (1966). Assay of inorganic phosphate, total phosphate and phosphatase. *Methods Enzymol.* 8, 115–118. doi: 10.1016/0076-6879(66)08014-5

Arnon, D. I. (1949). Copper enzymes in isolated chloroplasts. Polyphenoloxidase in *Beta vulgaris*. *Plant Physiol.* 24 (1), 1. doi: 10.1104/pp.24.1.1

Augspurger, C. K. (2008). Early spring leaf out enhances growth and survival of saplings in a temperate deciduous forest. *Oecologia* 156, 281–286. doi: 10.1007/s00442-008-1000-7

Augspurger, C. K., Cheeseman, J., and Salk, C. (2005). Light gains and physiological capacity of understorey woody plants during phenological avoidance of canopy shade. *Funct. Ecol.* 19, 537–546. doi: 10.1111/j.1365-2435.2005.01027.x

Baker, N. R. (2008). Chlorophyll fluorescence: a probe of photosynthesis in *vivo*. *Annu. Rev. Plant Biol.* 59, 89. doi: 10.1146/annurev.arplant.59.032607.092759

Canham, C. D., Denslow, J. S., Platt, W. J., Runkle, J. R., Spies, T. A., and White, P. S. (1990). Light regimes beneath closed canopies and tree-fall gaps in temperate and tropical forests. *Can. J. For. Res.* 20 (5), 620–631. doi: 10.1139/x90-084

Cheng, L., Tang, X., Vance, C. P., White, P. J., Zhang, F., and Shen, J. (2014). Interactions between light intensity and phosphorus nutrition affect the phosphate-mining capacity of white lupin (*Lupinus albus L.*). *J. Exp. Bot.* 65 (12), 2995–3003. doi: 10.1093/jxb/eru135

Czech, A. S., Strzałka, K., Schurr, U., and Matsubara, S. (2009). Developmental stages of delayed-greening leaves inferred from measurements of chlorophyll content and leaf growth. *Funct. Plant Biol.* 36 (7), 654–664. doi: 10.1071/FP09035

Drew, S. W., and Demain, A. L. (1977). Effect of primary metabolites on secondary metabolism. *Annu. Rev. Microbiol.* 31 (1), 343–356. doi: 10.1146/annurev.mi.31.100177.002015

Elser, J. J., Fagan, W. F., Kerkhoff, A. J., Swenson, N. G., and Enquist, B. J. (2010). Biological stoichiometry of plant production: metabolism, scaling and ecological response to global change. *New Phytol.* 186, 593–608. doi: 10.1111/j.1469-8137.2010.03214.x

Escoubas, J.-M., Lomas, M., LaRoche, J., and Falkowski, P. G. (1995). Light intensity regulation of cab gene transcription is signaled by the redox state of the plastoquinone pool. *PNAS* 92, 10237–10241. doi: 10.1073/pnas.92.22.10237

Feng, L., Raza, M. A., Li, Z., Chen, Y., Khalid, M. H. B., Du, J., et al. (2019). The influence of light intensity and leaf movement on photosynthesis characteristics and carbon balance of soybean. *Front. Plant Sci.* 9, 1952. doi: 10.3389/fpls.2018.01952

Fotis, A. T., and Curtis, P. S. (2017). Effects of structural complexity on within-canopy light environments and leaf traits in a northern mixed deciduous forest. *Tree Physiol.* 37 (10), 1426–1435. doi: 10.1093/treephys/tpw124

Franklin, K. A. (2008). Shade avoidance. *New Phytol.* 179, 930–944. doi: 10.1111/j.1469-8137.2008.02507.x

Gill, D. S., Amthor, J. S., and Bormann, F. H. (1998). Leaf phenology, photosynthesis, and the persistence of saplings and shrubs in a mature northern hardwood forest. *Tree Physiol.* 18, 281–289. doi: 10.1093/treephys/18.5.281

Hajirezaei, M. R., BoĚrnke, F., Peisker, M., Takahata, Y., Lerchl, J., Kirakosyan, A., et al. (2003). Decreased sucrose content triggers starch breakdown and respiration in stored potato tubers (*Solanum tuberosum*). *J. Exp. Bot.* 54 (382), 477–488. doi: 10.1093/jxb/erg040

Hangarter, R. P. (1997). Gravity, light and plant form. *Plant Cell Environ.* 20 (6), 796–800. doi: 10.1046/j.1365-3040.1997.d01-124.x

Hayes, P. E., Clode, P. L., Oliveira, R. S., and Lambers, H. (2018). Proteaceae from phosphorus-impoverished habitats preferentially allocate phosphorus to photosynthetic cells: An adaptation improving phosphorus-use efficiency. *Plant Cell Environ.* 41, 605–619. doi: 10.1111/pce.13124

Heberling, J. M., Cassidy, S. T., Fridley, J. D., and Kalisz, S. (2019). Carbon gain phenologies of spring-flowering perennials in a deciduous forest indicate a novel niche for a widespread invader. *New Phytol.* 221 (2), 778–788. doi: 10.1111/nph.15404

Hidaka, A., and Kitayama, K. (2013). Relationship between photosynthetic phosphorus-use efficiency and foliar phosphorus fractions in tropical tree species. *Ecol. Evol.* 3, 4872–4880. doi: 10.1002/ece3.861

Hughes, N. M., Morley, C. B., and Smith, W. K. (2007). Coordination of anthocyanin decline and photosynthetic maturation in juvenile leaves of three deciduous tree species. *New Phytol.* 175, 675–685. doi: 10.1111/j.1469-8137.2007.02133.x

Hussain, S., Ulhassan, Z., Brestic, M., Zivcak, M., Weijun, Z., and Allakhverdiev, S. I. (2021). Photosynthesis research under climate change. *Photosynth Res.* 150, 5–19. doi: 10.1007/s11120-021-00861-z

Ida, T. Y., and Kudo, G. (2008). Timing of canopy closure influences carbon translocation and seed production of an understorey herb, *Trillium apetalon (Trilliaceae)*. *Ann. Bot.* 101 (3), 435–446. doi: 10.1093/aob/mcm296

Iqbal, N., Masood, A., and Khan, N. A. (2012). Analyzing the significance of defoliation in growth, photosynthetic compensation and source-sink relations. *Photosynthetica* 50, 161–170. doi: 10.1007/s11099-012-0029-3

IUCN (2004). IUCN red list of threatened species.

Jarrell, W. M., and Beverly, R. B. (1981). The dilution effect in plant nutrition studies. *Adv. Agron.* 34, 197–224. doi: 10.1016/S0065-2113(08)60887-1

Jiang, S., Du, P., An, L., Yuan, G., and Sun, Z. (2013). Anti-diabetic effect of *Coptis Chinensis* polysaccharide in high-fat diet with STZ-induced diabetic mice. *Int. J. Biol. Macromol* 55, 118–122. doi: 10.1016/j.ijbiomac.2012.12.035

Kooten, O., and Snel, J. F. (1990). The use of chlorophyll fluorescence nomenclature in plant stress physiology. *Photosynth Res.* 25, 147–150. doi: 10.1007/BF00033156

Kuppusamy, T., Hahne, D., Ranathunge, K., Lambers, H., and Finnegan, P. M. (2021). Delayed greening in phosphorus-efficient *Hakea prostrata* (*Proteaceae*) is a photoprotective and nutrient-saving strategy. *Funct. Plant Biol.* 48, 218–230. doi: 10.1071/FP19285

Kwit, M. C., Rigg, L. S., and Goldblum, D. (2010). Sugar maple seedling carbon assimilation at the northern limit of its range: the importance of seasonal light. *Can. J. For. Res.* 40, 385–393. doi: 10.1139/X09-196

Lake, J. A., Quick, W. P., Beerling, D. J., and Woodward, F. I. (2001). Signals from mature to new leaves. *Nature* 411 (6834), 154–154. doi: 10.1038/35075660

Lambers, H. (2022). Phosphorus acquisition and utilization in plants. *Annu. Rev. Plant Biol.* 73, 11–126. doi: 10.1146/annurev arplant-102720-125738

Li, J., Fan, G., and He, Y. (2020). Predicting the current and future distribution of three Coptis herbs in China under climate change conditions, using the MaxEnt model and chemical analysis. *Sci. Total Environ.* 698, 134141. doi: 10.1016/j.scitotenv.2019.134141

Li, Y., Guan, S., Liu, C., Chen, X., Zhu, Y., Xie, Y., et al. (2018). Neuroprotective effects of *Coptis chinensis* Franch polysaccharide on amyloid-beta (Aβ)-induced toxicity in a transgenic Caenorhabditis elegans model of Alzheimer's disease (AD). *Int. J. Bol Macromol* 113, 991–995. doi: 10.1016/j.ijbiomac.2018.03.035

Liao, H., Huang, L., Li, N., Ke, W., Xiang, Y., and Ma, Y. (2021). Auxiliary rapid identification of pathogenic and antagonistic microorganisms associated with *Coptis chinensis* root rot by high-throughput sequencing. *Sci. Rep.* 11, 1–15. doi: 10.1038/s41598-021-90489-9

Lichtenthaler, H. K., and Buschmann, C. (2001). Chlorophylls and carotenoids: measurementand characterization by UV–vis spectroscopy. *Curr. Protoc. Food Analytical Chem.* 1 (1), F4–F3. doi: 10.1002/0471142913.faf0403s01

Lim, P. (2003). Molecular genetics of leaf senescence in Arabidopsis. *Trends Plant Sci.* 8, 272–278. doi: 10.1016/S1360-1385(03)00103-1

Liu, Y., Wang, B., Shu, S., Li, Z., Song, C., and Liu, D. (2021). Analysis of the *Coptis chinensis* genome reveals the diversification of protoberberine-type alkaloids. *Nat. Commun.* 12, 3276. doi: 10.1038/s41467-021-23611-0

Loach, K. (1967). Shade tolerance in tree seedlings: I. leaf photosynthesis and respiration in plants raised under artificial shade. *New Phytol.* 66, 607–621. doi: 10.1111/j.1469-8137.1967.tb05432.x

Lopez, O. R., Farris-Lopez, K., Montgomery, R. A., and Givnish, T. J. (2008). Leaf phenology in relation to canopy closure in southern Appalachian trees. *Am. J. Bot.* 95 (11), 1395–1407. doi: 10.3732/ajb.0800104

Lynch, J. P., and Brown, K. M. (2001). Topsoil foraging–an architectural adaptation of plants to low phosphorus availability. *Plant Soil* 237, 225–237. doi: 10.1023/A:1013324727040

Melgar, J. C., Guidi, L., Remorini, D., Agati, G., Degl'innocenti, E., and Castelli, S. (2009). Antioxidant defenses and oxidative damage in salt-treated olive plants under contrasting sunlight irradiance. *Tree Physiol.* 29, 1187–1198. doi: 10.1093/treephys/tpp047

Miyazawa, S. I., Makino, A., and Terashima, I. (2003). Changes in mesophyll anatomy and sink–source relationships during leaf development in *Quercus glauca*, an evergreen tree showing delayed leaf greening. *Plant Cell Environ.* 26 (5), 745–755. doi: 10.1046/j.1365-3040.2003.01011.x

Myers, J. A., and Kitajima, K. (2007). Carbohydrate storage enhances seedling shade and stress tolerance in a neotropical forest. *J. Ecol.* 95, 383–395. doi: 10.1111/j.1365-2745.2006.01207.x

Obendorf, R. L., Zimmerman, A. D., Zhang, Q., Castillo, A., Kosina, S. M., and Bryant, E. G. (2009). Accumulation of soluble carbohydrates during seed development and maturation of low-raffinose, low-stachyose soybean. *Crop Sci.* 49, 329–341. doi: 10.2135/cropsci2008.06.0370

Oquist, G., and Chow, W. S. (1992). On the relationship between the quantum yield of Photosystem II electron transport, as determined by chlorophyll fluorescence and the quantum yield of CO_2-dependent O_2 evolution. *Photosynth Res.* 33, 51–62. doi: 10.1007/BF00032982

Osada, N., and Hiura, T. (2019). Intraspecific differences in spring leaf phenology in relation to tree size in temperate deciduous trees. *Tree Physiol.* 39 (5), 782–791. doi: 10.1093/treephys/tpz011

Pantin, F., Simonneau, T., and Muller, B. (2012). Coming of leaf age: control of growth by hydraulics and metabolics during leaf ontogeny. *New Phytol.* 196 (2), 349–366. doi: 10.1111/j.1469-8137.2012.04273.x

Porra, R. J., Thompson, W. A. A., and Kriedemann, P. E. (1989). Determination of accurate extinction coefficients and simultaneous equations for assaying chlorophylls a and b extracted with four different solvents: verification of the concentration of chlorophyll standards by atomic absorption spectroscopy. *BBA Bioenergetics* 975 (3), 384–394. doi: 10.1016/S0005-2728(89)80347-0

Qi, L., Ma, Y., Zhong, F., and Shen, C. (2018). Comprehensive quality assessment for Rhizoma Coptidis based on quantitative and qualitative metabolic profiles using high performance liquid chromatography, Fourier transform near-infrared and Fourier transform mid-infrared combined with multivariate statistical analysis. *J. Pharm. BioMed. Anal.* 161, 436–443. doi: 10.1016/j.jpba.2018.09.012

Reich, P. B., Walters, M. B., Tjoelker, M., Vanderklein, D., and Buschena, C. (1998). Photosynthesis and respiration rates depend on leaf and root morphology and nitrogen concentration in nine boreal tree species differing in relative growth rate. *Funct. Ecol.* 12, 395–405. doi: 10.1046/j.1365-2435.1998.00209.x

Richardson, A. D., and O'Keefe, J. (2009). "Phenological differences between understory and overstory: a case study using the long-term Harvard Forest records," in *Phenology of ecosystem processes: applications in global change research* (New York: Springer), 87–117. doi: 10.1007/978-1-4419-0026-5_4

Rossi, M., Bermudez, L., and Carrari, F. (2015). Crop yield: challenges from a metabolic perspective. *Curr. Opin. Plant Biol.* 25, 79–89. doi: 10.1016/j.pbi.2015.05.004

Rychter, A. M., and Rao, I. (2005). Role of phosphorus in photosynthetic carbon metabolism. *Handb. photosynthesis* 2, 123–148. doi: 10.1201/9781420027877.ch7

Schachtman, D. P., Reid, R. J., and Ayling, S. M. (1998). Phosphorus uptake by plants: from soil to cell. *Plant Physiol.* 116, 447–453. doi: 10.1104/pp.116.2.447

Seiwa, K. (1999). Changes in leaf phenology are dependent on tree height in *Acer mono*, a deciduous broad-leaved tree. *Ann. Bot-London* 83, 355–361. doi: 10.1006/anbo.1998.0831

Setter, T. L., and Ella, E. S. (1994). Relationship between coleoptile elongation and alcoholic fermentation in rice exposed to anoxia. I. Importance of treatment conditions and different tissues. *Ann. Bot.* 74, 265–271. doi: 10.1006/anbo.1994.1117

Shafiq, I., Hussain, S., Raza, M. A., Iqbal, N., Asghar, M. A., and Raza, A. (2021). Crop photosynthetic response to light quality and light intensity. *J. Integr. Agr* 20, 4–23. doi: 10.1016/S2095-3119(20)63227-0

Stitt, M., and Zeeman, S. C. (2012). Starch turnover: pathways, regulation and role in growth. *Curr. Opin. Plant Biol.* 15 (3), 282–292. doi: 10.1016/j.pbi.2012.03.016

Sun, B., Dilcher, D. L., Beerling, D. J., Zhang, C., Yan, D., and Kowalski, E. (2003). Variation in *Ginkgo biloba* L. leaf characters across a climatic gradient in China. *PNAS* 100, 7141–7146. doi: 10.1073/pnas.1232419100

Tomita, M., and Seiwa, K. (2004). Influence of canopy tree phenology on understorey populations of *Fagus crenata*. *J. Veg Sci.* 15, 379–388. doi: 10.1111/j.1654-1103.2004.tb02275.x

Trouwborst, G., Sander, W. H., Harbinson, J., and Van, I. W. (2011). The influence of light intensity and leaf age on the photosynthetic capacity of leaves within a tomato canopy. *J. Hortic. Sci. Biotech.* 86 (4), 403–407. doi: 10.1080/14620316.2011.11512781

Turgeon, R. (1989). The sink-source transition in leaves. *Annu. Rev. Plant Biol.* 40 (1), 119–138. doi: 10.1146/annurev.pp.40.060189.001003

Turgeon, R. (2006). Phloem loading: how leaves gain their independence. *Bioscience* 56 (1), 15–24. doi: 10.1641/0006-3568(2006)056[0015:PLHLGT]2.0.CO;2

Valladares, F., and Niinemets, Ü (2008). Shade tolerance, a key plant feature of complex nature and consequences. *Annu. Rev. Plant Biol.* 39, 237–257. doi: 10.1146/annurev.ecolsys.39.110707.173506

Veneklaas, E. J., Lambers, H., Bragg, J., Finnegan, P. M., Lovelock, C. E., and Plaxton, W. C. (2012). Opportunities for improving phosphorus-use efficiency in crop plants. *New Phytol.* 195, 306–320. doi: 10.1111/j.1469-8137.2012.04190.x

Vitoria, A. P., de Oliveira Vieira, T., de Barbosa Camargo, P., and Santiago, L. S. (2016). Using leaf δ13C and photosynthetic parameters to understand acclimation to irradiance and leaf age effects during tropical forest regeneration. *For. Ecol. Manag* 379, 50–60. doi: 10.1016/j.foreco.2016.07.048

Walters, M. B., and Reich, P. B. (1999). Low-light carbon balance and shade tolerance in the seedlings of woody plants: do winter deciduous and broad-leaved evergreen species differ? *New Phytol.* 143 (1), 143–154. doi: 10.1046/j.1469-8137.1999.00425.x

Walters, M. B., and Reich, P. B. (2000). Trade-offs in low-light CO2 exchange: a component of variation in shade tolerance among cold temperate tree seedlings. *Funct. Ecol.* 14 (2), 155–165. doi: 10.1046/j.1365-2435.2000.00415.x

Wimalasekera, R. (2019). "Effect of light intensity on photosynthesis," in *Photosynthesis, productivity and environmental stress* (Chichester, UK: John Wiley & Sons), 65–73. doi: 10.1002/9781119501800.ch4

Wyka, T. (1999). Carbohydrate storage and use in an alpine population of the perennial herb, *Oxytropis sericea*. *Oecologia* 120, 198–208. doi: 10.1007/s004420050849

Xu, X., Wang, J., Wen, F., and Chen, G. (2015). Determination of alkaloids in Rhizoma coptidis by capillary electrophoresis with acidic potassium permanganate chemiluminescene detection. *Anal. Methods* 7 (3), 976–981. doi: 10.1039/C4AY02248C

Yao, X., Li, C., Li, S., Zhu, Q., Zhang, H., and Wang, H. (2017). Effect of shade on leaf photosynthetic capacity, light-intercepting, electron transfer and energy distribution of soybeans. *Plant Growth Regul.* 83, 409–416. doi: 10.1007/s10725-017-0307-y

Zhang, Z., Sun, D., Cheng, K. W., and Chen, F. (2021). Investigation of carbon and energy metabolic mechanism of mixotrophy in *Chromochloris zofingiensis*. *Biotechnol. Biofuels* 14, 1–16. doi: 10.1186/s13068-021-01890-5

Zhao, G., and Du, Z. (2002). Effect on quality and yield of *Coptis chinensis* with its differernt age and mouth at different altitude. *Chin. Tradition Herbal Drugs*, 66–68.

Zhou, T., Qiu, X., Zhao, L., Yang, W., Wen, F., and Wu, Q. (2022). Optimal light intensity and quality increased the saffron daughter corm yield by inhibiting the degradation of reserves in mother corms during the reproductive stage. *Ind. Crop Prod* 176(114396). doi: 10.1016/j.indcrop.2021.114396

Zhou, T., Wang, L., Sun, X., Wang, X., Chen, Y., Rengel, Z., et al. (2019a). Light intensity influence maize adaptation to low P stress by altering root morphology. *Plant Soil* 447, 183–197. doi: 10.1007/s11104-019-04259-8

Zhou, T., Wang, L., Sun, X., Wang, X., Pu, T., Yang, H., et al. (2021). Improved post-silking light interception increases yield and P-use efficiency of maize in maize/soybean relay strip intercropping. *Field Crop Res.* 262, 108054. doi: 10.1016/j.fcr.2020.108054

Zhou, T., Wang, L., Yang, H., Gao, Y., Liu, W., and Yang, W. (2019b). Ameliorated light conditions increase the P uptake capability of soybean in a relay-strip intercropping system by altering root morphology and physiology in the areas with low solar radiation. *Sci. Total Environ.* 688, 1069–1080. doi: 10.1016/j.scitotenv.2019.06.344

frontiers | Frontiers in Plant Science

TYPE Original Research
PUBLISHED 24 October 2023
DOI 10.3389/fpls.2023.1221163

OPEN ACCESS

EDITED BY
Jung Eek Son,
Seoul National University,
Republic of Korea

REVIEWED BY
Dongpil Kim,
Rural Development Administration,
Republic of Korea
Qingming Li,
Chinese Academy of Agricultural Sciences,
China

*CORRESPONDENCE
Martina Paponov
martina.paponov@outlook.com
Ivan A. Paponov
ivpa@food.au.dk

RECEIVED 11 May 2023
ACCEPTED 09 October 2023
PUBLISHED 24 October 2023

CITATION
Paponov M, Verheul MJ, Dobrev PI and Paponov IA (2023) Additive effects of light and branching on fruit size and chemical fruit quality of greenhouse tomatoes. *Front. Plant Sci.* 14:1221163. doi: 10.3389/fpls.2023.1221163

Additive effects of light and branching on fruit size and chemical fruit quality of greenhouse tomatoes

Martina Paponov[1]*, Michel J. Verheul[1], Petre I. Dobrev[2] and Ivan A. Paponov[1,3]*

[1]Division of Food Production and Society, Norwegian Institute of Bioeconomy Research (NIBIO), Ås, Norway, [2]Institute of Experimental Botany, Czech Academy of Sciences, Prague, Czechia, [3]Department of Food Science, Aarhus University, Aarhus, Denmark

Introduction: Greenhouse tomato growers face the challenge of balancing fruit size and chemical quality traits. This study focused on elucidating the interplay between plant branching and light management on these traits, while maintaining consistent shoot density.

Methods: We evaluated one- and two-shoot plants under varying top light intensities using high-pressure sodium lamps and light-emitting diode (LED) inter-lighting.

Results: The reduced yield in the two-shoot plants was mainly due to smaller fruit size, but not due to source strength limitations, as evaluated through leaf weight ratio (LWR), chlorophyll index, specific leaf area (SLA), leaf dry matter percentage, and stem soluble carbohydrate accumulation. Enhanced lighting improved fruit weight and various fruit traits, such as dry matter content, total soluble carbohydrate content, and phenolic content, for both one- and two-shoot plant types. Despite lower mean fruit weight, two-shoot plants exhibited higher values for chemical fruit quality traits, indicating that the fruit growth of two-shoot plants is not limited by the available carbohydrates (source strength), but by the fruit sink strength. Diurnal analysis of fruit growth showed that two-shoot plants had reduced expansion during light transitions. This drop in fruit expansion was not related to changes in root pressure (measured as xylem sap exudation from decapitated plants), but might be related to diminished xylem area in the stem joint of the two-shoot plants. The concentration of several hormones, including cytokinins, was lower in two-shoot plants, suggesting a reduced fruit sink capacity.

Discussion: The predominant impact of branching to two-shoot plants on sink capacity suggests that the fruit growth is not limited by available carbohydrates (source strength). Alongside the observation that light supplementation and branching exert independent additive effects on fruit size and chemical traits, this illuminates the potential to independently regulate these aspects in greenhouse tomato production.

KEYWORDS

tomato, light-emitting diode, fruit growth, fruit quality, plant hormones, sink-source relationship, branching

Introduction

Tomato is the most economically important horticultural crop and is widely used as a model plant, particularly for investigations of fruit development and fruit quality. The high market value and challenges imposed in transporting tender tomato fruits have made tomato the main income crop for local greenhouse production. The optimization of climate control, crop management, and tomato breeding for greenhouse production has doubled the yield during the last decades [reviewed in (Bertin and Genard, 2018)]; however, this high yield is often associated with poor fruit quality, which lowers the customers' interest in greenhouse-cultivated tomatoes (Rana et al., 2014). Thus, understanding the physiological processes that can improve yield and fruit quality is a key element for future success in greenhouse tomato production.

One of the main reasons for the reduction in yield and fruit quality of greenhouse-grown tomatoes is low light intensity (Gruda, 2005), especially in northern latitudes or during the winter season. To overcome low light conditions, supplemental lighting is widely applied in greenhouses (Marcelis et al., 2006). Traditionally, the light is supplied from the top of the greenhouse, mostly from high-pressure sodium (HPS) lamps. The introduction of cost-efficient LED lamps with low heat emission provided the possibility of using LED inter-lighting with a more uniform light distribution along the canopy (Gomez et al., 2013). The implementation of uniform lighting has a dual purpose: firstly, it prevents the top canopy leaves from receiving excessive illumination, and secondly, it promotes an increase in photosynthetic activity in the lower leaves (Evans et al., 1993). Inter-lighting also provides sufficient light to the otherwise shaded lower leaves to maintain a good photosynthetic rate and prevent leaf senescence (Davis and Burns, 2016; Bantis et al., 2018). The combination of supplemental top-lighting and LED inter-lighting increases the yield of tomato plants, with increased fruit weight being a commercially important component of this yield enhancement (Cockshull et al., 1992; Li et al., 2015; Paponov et al., 2020).

The simplest mechanism that explains the positive effect of additional light on fruit weight is related to a direct effect of light on source activity (i.e., plant photosynthesis), as increased photosynthetic activity can increase carbohydrate transport to the fruits (Lemoine et al., 2013). The enhanced supply of carbohydrates can affect fruit size through increased cell division, which is typically completed within 10 days after anthesis (Ho and Hewitt, 1986), and by cell enlargement during the subsequent fruit developing stage (Ho, 1996). During the cell division stage, sugar can act as a signal that stimulates cell division, thereby defining a greater sink capacity of the fruit (Palmer et al., 2015). During the cell enlargement phase, an enhanced supply of carbohydrates generates a higher turgor pressure, which stimulates cell elongation and results in a heavier fruit weight (Kanayama, 2017). Thus, the ultimate fruit weight depends on the dynamic availability of carbohydrates to individual fruits at different stages of fruit development.

Apart from the supply from source activity, the carbohydrates available to individual fruits depend on the competition for resources among the plant's trusses (inflorescences) and between fruits within one truss (Bertin, 1995). Tomato plants have a complex bicollateral phloem system that allows for an unusual transport in both directions, where basal leaves export photosynthate to the upper stem and shoot apex, while upper leaves export to the lower stem and roots (Khan and Sagar, 1966; Hocking and Steer, 1994). This pattern of assimilate movement is considered "inefficient" (Ryle et al., 1981), because it goes against the principle of using the shortest translocation pathway between a source and sink. However, this movement pattern can help buffer the strong light gradient along the canopy and provide sufficient assimilates for key organs (e.g., roots and fruits during the loading stage) that are localized far from the upper leaves exposed to the highest light intensity. Thus, for tomato plants, inter-lighting might have a positive effect due to enhanced total photosynthesis, rather than from a better assimilate supply for organs located distantly from the upper leaves.

Fruits within a truss compete for resources, leading to smaller distal fruits compared to proximal ones. Under conditions of unlimited carbohydrate supply, the size differences between distal and proximal fruits are mainly defined during the cell division stage. At the end of that stage, the ultimate cell number is related to the sink strength (Bangerth and Ho, 1984). However, source limitation causes a competition among fruits during both the cell division and fruit loading stages and creates a greater weight deviation between distal and proximal fruits (Paponov et al., 2020). Thus, the relative difference observed between distal and proximal fruit weights can be used to characterize a source limitation and/or an imbalance between source and sink activities and should be increased when the source activity of plants is decreased.

Supplemental lighting increases the fruit size while also promoting the accumulation of primary metabolites, such as sugars and secondary compounds, in the fruits, thereby improving several fruit quality traits. For example, supplemental light increases the content of soluble sugars (Davies and Hobson, 1981), ascorbic acid (Dumas et al., 2003), and phenolics (Hernandez et al., 2019) but does not appear to change organic acid concentrations (Dorais et al., 2001). The main mechanism involved in the enhanced accumulation of secondary compounds might be related to the increased amount of C-skeletons available for the biosynthesis of secondary compounds (Løvdal et al., 2010). In addition, LED inter-lighting can have different effects than top lighting on fruit quality, given that direct exposure of the fruits themselves to light can have a strong effect on the accumulation of several secondary compounds (Gautier et al., 2009; Pek et al., 2011) and that the accumulation of primary and secondary compounds shows specific responses to the light spectrum (Ntagkas et al., 2020). Nevertheless, despite numerous investigations on the effect of light on fruit quality, the interplay between light intensity, distribution, and cultivation techniques on yield and quality remains underexplored.

One widely used cultivation technique, which can increase fruit quality (e.g., enhancing soluble solids content) is to grow tomato plants with two shoots connected to a single root system. However, although this cultivation technique improves quality, it also reduces fruit size (Max et al., 2016; Vargas et al., 2017). This trade-off between fruit size and fruit quality is commonly observed (Hanson et al., 2004), but its underlying mechanism remains elusive.

Tomato plant cultivation as one- or two-shoot plants has been widely used as a tool to study long-distance interactions between

plant roots and shoots and the involvement of plant hormones, such as auxin and cytokinins (Li and Bangerth, 1999; Li and Bangerth, 2003; Kotov and Kotova, 2018). These studies showed that auxin is predominantly synthesized in the shoot (mostly in young tissues, such as shoot apical meristems) and transported to the roots, suppressing cytokinin production. This results in decreased cytokinin concentrations in the xylem sap (Bangerth, 1994; Li et al., 1995; Kotov and Kotova, 2018). While the two-shoot model has been explored in young plants of various species, its applicability to older plants during the generative stage, and its influence on yield and fruit quality, warrants further investigation.

In two-shoot plants, each shoot shares the root's capacity, necessitating double the root activity or transport efficiency to sustain the same solute flux per shoot as in one-shoot plants. The xylem water supply is an important component of fruit growth, whereas treatments that decrease root activity (root pressure), such as drought and salt, usually enhance fruit quality traits such as total soluble solids and soluble sugars (Araki et al., 2001;Van de Wal et al., 2017; Cui et al., 2020). The beneficial impact of light on these traits is linked to an increased phloem transport relative to xylem transport (Hanssens et al., 2015), further supporting that the balance between these transports contributes substantially to fruit quality traits. As two-shoot plants have only one root system for both shoots, we hypothesize that the effect of two-shoot plants on fruit quality traits may occur through modulation of the balance between xylem and phloem transport into the fruits.

The aim of the present work was to understand the mechanisms underlying the effects of plant branching and their interplay with different light distributions on fruit weight and fruit quality. We assumed that if the mechanisms of action between branching and modified light supply are independent, no significant interactions would be noted between the branching and light levels (i.e., top light or LED inter-lighting). In addition, we asked whether two-shoot plants show decreased xylem transport per shoot and a consequent change in the phloem/xylem balance that could contribute to better fruit quality. Ultimately, we tested the hypothesis that the number of shoots on the plants, in combination with different light conditions, modulates the xylem sap plant hormone composition, and especially the concentration of cytokinins, as these are key players in the sink activity of tomato plants during the generative period.

Materials and methods

The investigations were conducted simultaneously in two identical, structurally modern, and adjacent greenhouse compartments at the NIBIO Særheim research station, located in southwestern Norway (lat. 58.47 long. 5.41, alt. about 90 m a.s.l.) from 29 July 2018 until 15 February 2019. We used the indeterminate variety Dometica (*Solanum lycopersicum*, DOMETICA RZ F1, Rijk Zwaan), a long-cropping type with upright foliage and high production output. The tomato fruits are loosely arranged within the truss. These tomatoes are red, round, and firm and have an average fruit weight of 80 g with good flavor due to their high sugar and acidity content.

Experimental setup

The experimental setup included two top light treatments, each in a separate compartment: a low top HPS light at 290 μmol m^{-2} s^{-1} (161 W m^{-2}) and a high top HPS light at 436 μmol m^{-2} s^{-1} (242 W m^{-2}). HPS top light was combined with three levels of supplemental LED inter-lighting: no LED, supplemental 60 W m^{-2} LED inter-lighting, or 120 W m^{-2} LED inter-lighting (only with the low top light treatment) (Figure 1). LED lamps from Union Power Star (160 W, Munich, Germany) were positioned in the middle of the V-row system, emitting light horizontally in two directions. They operate with wavelength bands of 450 and 660 nm at a diode energy ration of 20/80. The detailed light environment was described in our previous publication (Verheul et al., 2022).

For each of these light treatments, we investigated their effects on one-shoot and two-shoot plants. In total, we investigated 10 treatments, 8 of which formed a complete 3-factorial experiment, including the treatments of top light at 161 W m^{-2}, top light at 161 W m^{-2} + LED 60 W m^{-2}, top light at 242 W m^{-2}, and top light at 242 W m^{-2} + LED 60 W m^{-2}; each light treatment was applied to one-shoot and two-shoot plants. The additional two treatments with top light at 161 W m^{-2} + LED 120 W m^{-2} for one- and two-shoot plants corresponded to the total light intensities of the high-top light compartment, but the light was provided strongly from the side. To account for potential variation between LED lamps, plants within these treatments were exposed to different LED lamps.

It is important to note that these treatments were deliberately chosen. The environment with 161 W m^{-2} HPS + 60 W m^{-2} LED has approximately the same photosynthetic photon flux density (PPFD) as the environment with 242 W m^{-2} HPS. Similarly, the environment with 161 W m^{-2} HPS + 120 W m^{-2} LED has approximately the same PPFD as the environment with 242 W m^{-2} HPS + 60 W m^{-2} LED.

Growing conditions

Each compartment was 224 m^2 (17.5 m × 12.8 m) in size, with 6 gutters with double rows and 2 gutters with simple border rows in each compartment. The distance between the rows was 90 cm, and the distance between gutters was 180 cm. High pressure sodium (HPS) lamps (Philips GP Plus 600 W and 750 W, Gavita Nordic AS, Norway) were positioned ca. 1.5 m above the top of the canopy, at a height of 6 m. One double row was used for each light treatment. Each row included 60 one-shoot plants and 18 two-shoot plants, for a total of 36 shoots. For the purpose of growth and yield analysis, we collected data from 5 replications. Each replication comprised two plants from the one-shoot treatment (equating to two shoots) and one plant from the two-shoot treatment (equating to two shoots). The ambient climate was monitored every 5 min by a Priva Connext horticultural computer, which coordinated all climate, light, irrigation, water, and energy processes after adjustments. Detailed climatic conditions were described in our previous publication (Verheul et al., 2022).

The plants were first raised in a neighboring greenhouse in 0.5 L rockwool cubes (sown 29 July 2018). By 45 days after sowing, when

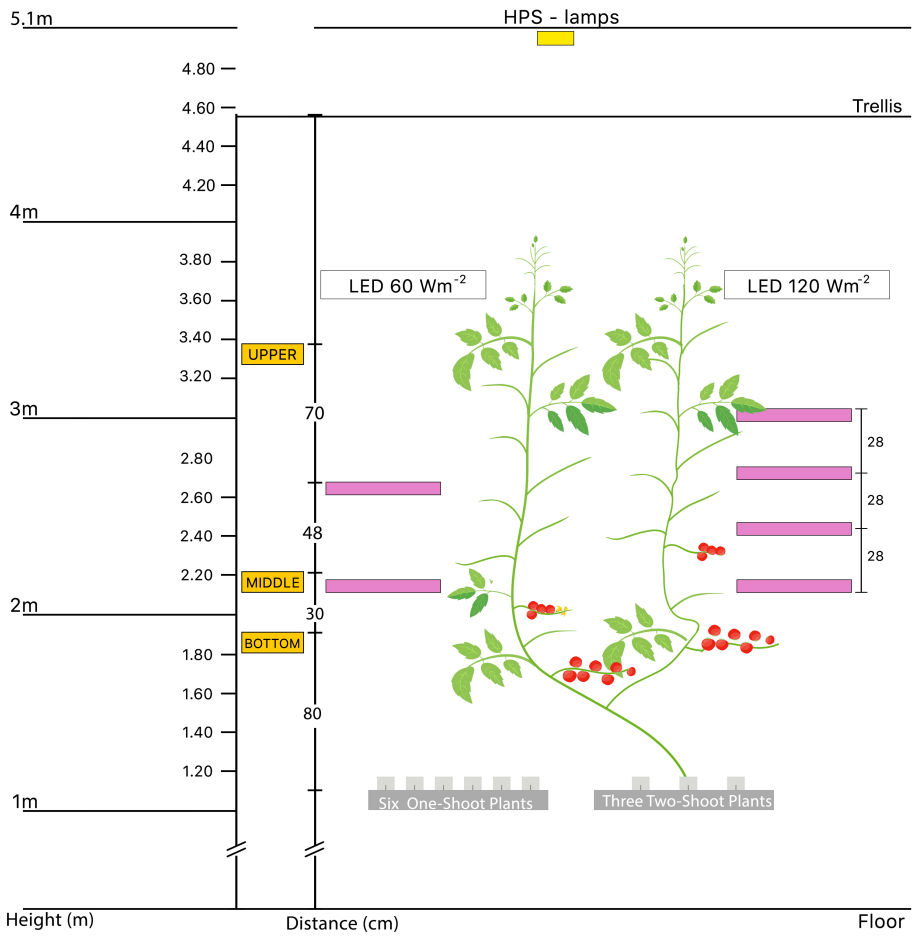

FIGURE 1
Schematic diagram of the experimental setup used to investigate the effects of different lighting treatments on one-shoot and two-shoot plants. The diagram shows an aggregated representation of all treatments, emphasizing the two-shoot plant and the positions of the top light and LED lamps. Notably, each stem of the two-shoot plants received identical lighting conditions to ensure uniform treatment exposure. The experimental setup consisted of two separate compartments: a low top light at 161 W m^{-2} and a high top light at 242 W m^{-2}. Three levels of supplemental LED inter-lighting were used in combination with the top light treatments: without LED, with supplemental 60 W m^{-2} LED inter-lighting, or with 120 W m^{-2} LED inter-lighting (only with the low top light treatment).

the first flower truss appeared, the plants were transported with the cube to the greenhouse compartments (12 September 2018). The plants were left for 5 days under mild drought stress besides the plant hole to promote better rooting in the cube and to adapt the plants to the new environment. The tomato plants were then transplanted together with the cube onto holes in standard rockwool slabs (90 cm × 10 cm × 15 cm) placed with a distance of one slab per 100 cm on gutters at 110 cm height from the ground. The plants were kept under drought (given 133 mL nutrient solution 3–4 times per day per shoot at 8:00, 11:30, and 17:00). Excess apical and basal leaves and suckers were removed regularly to promote generative growth. The tomato plants were trained to one-shoot plants by removing all suckers or to two-shoot plants by saving the side shoot in the leaf axis just below the first flower truss. Six one-shoot plants or 3 two-shoot plants were planted on each rockwool slab. Each shoot was supported by a twine strand wrapped around the plant at the base and fixed on the overhead trellis system. Of the six one-shoot plants on a slab, half were secured to one side and the other half to the opposite side of the row, arranged in an alternating sequence. Meanwhile, each shoot of the two-shoot plants was attached to one side to form a high wire culture in a V-row system (Peeters and Welles, 2005). The final plant density was 3 plants/m^2 and 3 shoots/m^2 for the one-shoot and two-shoot plants, respectively. The plants were regularly maintained by removing all excess suckers and leaves and all leaves beneath the latest harvested tomato truss. The fruit trusses were pruned to seven fruits per truss just after the fruit set of each truss.

During the establishing phase of six weeks after transplanting, plants were grown under sunlight and at a maximum of 12 h of HPS lamp light to avoid excessive assimilate production. The CO_2 concentration was kept at 600 ppm for the first 13 weeks of the experiment, until week 50 (for 2018).

Once the plant tops reached approximately 150 cm above the rockwool cubes, we installed the LED lamps. For the 60 W m^{-2} LED treatments, lamps were installed between the shoots at heights of 110 cm and 158 cm above the rockwool cubes. For 120 W m^{-2} LED inter-lighting, lamps were set at 110, 138, 166, and 194 cm heights above the rockwool blocks (Figure 1).

Regulation of climatic conditions and irrigation when plants reached steady state

From week 44–45 (starting 29 October 2018–03 December 2018), 6 weeks after final transplanting, the tomato plants reached a size of about 250 cm. The plant reached a 'steady state condition', when the first tomato turned red and a stable balance was established between developing plant parts and ripening of the tomatoes.

Good plant vigor in each compartment with different top light preconditions was maintained by adjusting the temperature according to the stem diameter approximately 25 cm below the tomato shoot apex. The stem diameter is a sensitive indicator of plant resource distribution, as it indicates investments in vegetative or generative growth. Based on our own in-house experiences and others (Mireille et al., 1997), the best tomato yield is obtained when the diameter of the stem is between 10 and 12 mm. The stem diameter was measured once per week for the control treatments, which consisted of plants that did not receive supplemental LED lighting.

When plants reached the steady state, the climate settings became stable. The artificial lighting (HPS lamps and LED lamps) were switched on for 18 h from 06:15–00:15, as natural incoming light had no impact in the wintertime. The temperature set points were slightly adjusted on a weekly basis based on plant vigor measurements. The detail temperature conditions are presented in the previous publication (Verheul et al., 2022). Humidity was maintained between at about 63% and 75% for the low and high top light compartment.

From mid-December, the setpoint for CO_2 concentration was 1000 ppm, which resulted in about 900 ppm CO_2 in the greenhouse. When the windows were opened for humidity release and temperature control, the CO_2 concentration was kept at 600 ppm. In the winter, during our investigations, the windows were mostly closed. The plants were drip irrigated with a complete nutrient solution based on standardized recommendations and containing the following: 26.43 mM NO_3^-, 1.68 mM NH_4^+, 2.23 mM P, 8.72 mM K, 10.63 mM Ca, 2.71 mM Mg, 2.67 mM S, 0.3 mM Na, 0.1 mM Cl, and micronutrients with the following concentrations: 63 µmol Fe, 27 µmol Mn, 10 µmol Zn, 68 µmol B, 6 µmol Cu and 1.6 µmol Mo. The electrical conductivity of the nutrient solution was 3.6 mS cm^{-1}, the pH was 5.9, and the daily drainage percentage was 30%. Irrigation and drainage were registered continuously using a weighing scale (Priva GroScale) combined with a drainage sensor. Plants were irrigated for 3-4 min (33 mL/min) at 8:00, 9:00, 12:00, 14:00, and 15:30. If the drainage percentage was below 30%, an additional irrigation was performed, but not later than 17:00. Conventional heating pipes provided heating in the compartments.

Tomato plants were grown under HPS top light with an installed capacity of 161 W m^{-2} and 242 W m^{-2}. The photosynthetically active radiation (PAR) 30 cm above the apex of the plants in each light treatment was 180, 214, 202 and 435, 458 µmol m^{-2} s^{-1} for low top light with no LED, + LED 60 W m^{-2},+ LED 120 W m^{-2}, high top light with no LED, and high top light +LED 60 W m^{-2}, respectively. The results are based on 10 measurements with a zenith direction of PAR sensor under complete exclusion of sunlight.

Plant care and tomato harvest

The tomato flowers were pollinated by bumblebees, and pollination success was checked two times per week. On a weekly basis, the plants were lowered by about 30 cm, all side shoots and three leaves below the truss on which fruits were reaching the turning stage (Grierson and Kader, 1986) were removed, and trusses were pruned to seven fruits per truss just after fruit set. Tomato fruits were harvested two times per week for all treatments. The harvested fruits were weighed individually, and the fruit position in the truss and number of trusses were recorded for 10 plants per treatment during the growing period. The first day of harvest was 6 November 2018. The tomato fruit next to the stem was designated as position one and the distal tomato position was designated as position 7.

Determination of specific leaf area

The fresh weights of 10 proximal leaflets were taken at three height levels for all treatments. The "upper position" represented a leaflet sample from a fully developed leaf about 40-55 cm below the apex, the "middle position" was a leaflet sampled at the height of the lower LED lamp (110 cm above the rockwool cube), and the "bottom position" was a leaflet sampled from the oldest leaf of the plant. The leaf area was determined using an LI-3100 Area Meter (LI-COR, inc. Lincoln, Nebraska, USA). The leaves were dried at 65°C for 48 h and weighed.

The final harvest

The plant yield was measured by including a destructive harvesting over a period of 5 days (11–15 February 2019), where 2 plants per treatment were removed from the canopy in a random order. The final length of the plant (cm), fresh weight of the stem, number of nodes and remaining leaves, fresh weight of leaves, and the total number of trusses with ripe tomatoes were recorded. Dry matter % (DM) of the fruits at different developmental stages was determined by measuring the fresh weight (FW) of the tomato fruits at position 3 from the basal end of a truss containing 7 fruits. This was carried out separately for the 5 lowest trusses, while the green tomatoes of the younger trusses (6–12) were collected together and measured as a group. All samples, including tomatoes, stem(s), and all leaves per plant of all treatments (n=10), were dried at 70°C until complete dryness. Since the branches of two-shoot plants have different length, we calculated average length of the entire plant as the mean of the lengths of both branches. Even though we trained the side branch below the first truss of two-shoot plants, the side shoot appeared to develop fewer trusses. To allow comparison of the data for one- and two-shoot treatments, we calculated number of red fruits/shoot.

Fruit quality analysis

For quality assessment, fruit samples were collected on 6 days (05 December 2018, 17 December 2018, and 07 January 2019) for

one-shoot plants and (06 December 2018, 18 December 2018, and 11 January 2019) for two-shoot plants. In total, 9 replications per treatment were investigated; each replication consisted of six fruits of equal size and with a ripeness of grade 8, determined visually based on a color scale from Bama AS, Norway ranging from 1 (green) to 12 (deep red). Each tomato was measured for firmness at three locations on the pericarp on a scale from 1 to 100, where 100 means full firmness and 1 a complete lack of firmness (Durofel firmness tester, Agro Technologies, France). One-quarter of each of the six tomatoes was immediately homogenized with a handheld blender on the harvesting day. The resulting homogenate was used to determine the soluble solid content (SSC) measured with a digital PR-101α refractometer (ATAGO, Japan), and the total titratable acidity (TTA), expressed as a percentage of citric acid equivalents (CAE) per 100 g FW measured with the 794 Basic Titrino (Metrohm, Switzerland) with potentiometric detection and a final pH of 8.2. An aliquot of the tomato fruit homogenate was immediately frozen in liquid nitrogen and lyophilized in a freeze drier for 24–48 h.

Assay of total phenolic content

The total phenolic content was estimated in the tomato homogenates using the Folin–Ciocalteu assay (Ainsworth and Gillespie, 2007). A 20 mg sample of freeze-dried tomato homogenate was extracted with 1.8 mL 0.5% acetic acid in 80% methanol in darkness for 6 h at 25°C with shaking at 400 rpm. The homogenate was then centrifuged for 5 min at 13,000×g (Micro Star 17R, VWR, Radnor, PA, USA) and 100 µL of the supernatant was combined with 200 µL of 10% Folin–Ciocalteu (F–C) reagent (F9252, Merck, Darmstadt, Germany) and vortexed. An 800 µL volume of 700 mM Na_2CO_3 solution (S7795, Merck, Darmstadt, Germany) was added, thoroughly mixed, and incubated at room temperature for 2 h in darkness. The samples were centrifuged again to pellet any leftover tomato fragments. Triplicate 200 µL volumes of the supernatant solution were then transferred to a spectrophotometric plate reader (Multiscan GO, Thermo Fisher Scientific, Waltham, MA, USA), and the absorbance was measured for each well at 765 nm at room temperature. Measurements were standardized against gallic acid (48630, Merck, Darmstadt, Germany) (40 µM–1.2 mM in 0.5% acetic acid in 80% MeOH).

Quantification of glucose, fructose, and sucrose contents in one-shoot and two-shoot stems

The complete dried stem of one-shoot plants and the complete initial and longer shoot for two-shoot plants were chopped up and an aliquot was ground to fine dust in a grinding mill (Star-Beater, VWR, USA). For soluble carbohydrate extraction, 75 mg of stem material was transferred into 5 mL Eppendorf tubes and extracted 3 times with 1.6 mL 80% ethanol for 15 mins at 80°C, followed by centrifugation at 3000 × g for 10 mins after each extraction. The collected supernatants were combined in a 5 mL Eppendorf tube, brought to a 5 mL volume with 80% ethanol, and 60 mg of finely ground activated charcoal was added to each tube. The tubes were closed, shaken briefly by hand, left to stand for 5 min, and then centrifuged at 3000 × g for 15 min to obtain a clear extract.

The glucose, fructose, and sucrose contents were quantified using sequential enzymatic assays with photometric detection in a spectrophotometric plate reader (Multiscan GO, Thermo Scientific) according to (Zhao et al., 2010). Glucose concentrations were determined by transferring three 20 µL aliquots of each extracted sample into separate wells of a 96-well UV-Star microplate (Greiner). The microplate, without standards added, was placed into an oven at 50°C to dry for 60 min. The dried material was then resuspended by the addition of 20 µL of deionized water. For the calibration curve, 20 µL of a standard glucose solution (0, 0.005, 0.0125, 0.025, 0.050, 0.125, 0.25, to 0.5 mg mL^{-1} in DI water, prepared weekly) was added in triplicate to each microplate into the remaining wells. The glucose hexokinase (HK) assay reagent (G3293, Supelco) was added into each well (100 µL per well) according to the manufacturer's instructions. The 96-well plate (UV-STAR, Greiner Bio-One) was covered with a lid and incubated inside the plate reader for 15 min at 30°C. The absorbance of samples, blanks, and standards was measured at 340 nm at 30°C and precision mode. The amount of fructose was determined with the phosphoglucose isomerase (PGI) assay by adding 10 µL of PGI assay reagent (0.2 M HEPES with pH 7.8) to each well previously used for glucose quantification. The absorption was measured at 340 nm after incubation inside the spectrophotometer for 15 min at 30°C. The sucrose amount was determined by adding 10 µL of invertase assay reagent (10 mg mL^{-1}, I4504, 300 units/mg, Sigma) in 0.1 M Na-citrate buffer pH 6.0 to each well. The absorption was measured at 340 nm after incubation inside the spectrophotometer for 60 min at 30°C. Glucose, fructose, and sucrose absorption values were calculated based on triplicate replications and used in statistical analysis, as suggested by (Zhao et al., 2010).

Chlorophyll index

The chlorophyll index was measured (Hansatech Instruments Chlorophyll Content System CL-01, Norfolk, United Kingdom) on each of the registered plants at three different heights (upper, middle, and bottom) at 2 different days (20 November 2018 and 9 January 2019). The second distal leaflet pair was measured 3 times and the average values were used for statistical analysis The "upper" position included the first fully developed leaf (which is still expanding) approximately 6 or 7 leaves counted from the top of the plant, the "middle" position was at the level of height of the lower LED lamp, and the "bottom" position was the lowest leaf.

Daily fruit growth

The diurnal changes in fruit diameter were measured over 2–4 days on the third tomato fruits in a truss with fruits with diameters of 2.6–3.4 cm; these fruits were typically located about 40–50 cm below the tops of the plants. The change in fruit diameter was

monitored using the fruit and vegetable dendrometer from Ecomatik and the Dendrometer Data Logger from Ecomatik (DL18, Dachau/Munich, Germany) interfaced to a 4-channel analog Dendrometer Data Logger from HOBO (Onset Computer Corporation, Bourne, USA). The experiment was replicated at least twice so that at least 9 and 5 fruits were investigated for control plants (161 W m^{-2} HPS lighting) for one-shoot and two-shoot plants, respectively. The values show the relative increase in fruit diameter every 30 min after min–max normalization (Han et al., 2012) with the assumption that the fruit diameter would increase by 1 U over a 24 h period.

Xylem sap collection and hormone analysis

The xylem sap was sampled by the root pressure method (Alexou and Peuke, 2013) on 5 sequential days on 1 replication per treatment chosen randomly. The plants were cut with a clean garden scissor 5 cm above the root–shoot interface. The cut surface was cleaned with deionized water and a silicon tube was fixed over the stump and sealed with silicone grease. The xylem exudate collection was initiated 30 min later. The sap was collected with a pipette for 30 min, transferred to plastic vials on ice, and subsequently frozen in liquid nitrogen and stored at -80°C. To minimize the potential effect of diurnal variation, we spred the harvesting process over 5 days. This approach ensured that xylem sap collections were consistently performed during a relatively short and uniform period each day, specifically between 10:00 and 11:30. The hormones in the xylem sap were analyzed with an HPLC system (Ultimate 3000, Dionex, Sunnyvale, CA, USA) coupled to a 3200 Q TRAP hybrid triple quadrupole/linear ion trap mass spectrometer (Applied Biosystems, Waltham, MA, USA). The sample preparation and analysis procedures were as described by Paponov et al. (Paponov et al., 2021).

Results

Yield

We carried out a three-factorial ANOVA to estimate the effects and interactions between branching (one- or two-shoot plants), level of top light intensity, and the use of supplemental LED inter-lighting. All factors significantly affected yield. Under low top light, 60 W m^{-2} LED inter-lighting led to yield increases of 32.8% for one-shoot and 26.8% for two-shoot plants. However, under high top light, the increases were more modest at 10.0% and 5.9%, respectively. For one-shoot plants, increasing LED inter-lighting to 120 W m^{-2} resulted in a yield increase of 31.6%, which was almost the same as the increase observed with 60 W m^{-2}, suggesting to advantage in further increasing inter-lighting. In contrast, two-shoot plants showed a yield increase of 38.3% with the highest LED inter-lighting (120 W m^{-2}) combined with low top light compared to the control (Figure 2A).

Biomass and dry matter allocation

The effects of light treatments and branching on total plant biomass were similar to their effects on fruit yield, indicating that total photosynthesis during plant growth is the main determinant of plant yield (Figure 2B). High top light or 60 W m^{-2} inter-lighting at low top light led to more efficient dry matter allocation to generative organs, boosting yield. However, the highest LED inter-lighting (120 W m^{-2}) tended to decrease the dry matter allocation to the fruits, indicating that an excessive amount of inter-lighting may negatively affect harvest index (HI) in comparison with the high top lighting (compare 161 W + 120 W vs. 242 W + 60 W m^{-2}). No difference was found in dry-matter allocation to generative organs between one- and two-shoot plants (Figure 2C; Table S1).

Likewise, no significant difference was found between one- and two-shoot plants for dry matter allocation to leaves (LWR) (Figure 2D; Table S1). Both high top light and supplemental LED inter-lighting (60 W m^{-2}) reduced LWR. Interestingly, the highest LED inter-lighting level (120 W m^{-2}) tended to increase rather than decrease dry matter allocation to leaves (Figure 2D). This might be because carbohydrate utilization from leaves was limited due to a more uniform light distribution along the canopy. Dry matter allocation to the stems remained unchanged across light treatment (Figure 2E; Table S1). Under high top light intensity, two-shoot plants allocated less dry matter to the stem than one-shoot plants. This difference is attributable to the two-shoot plants' structure, where a single stem from roots to the first inflorescence connects both shoots. However, extremely high LED-inter-lighting (120 W m^{-2}) tended to increase dry matter allocation to the stems of two-shoot plants, indicating better DM allocation from leaves in two-shoot plants than in one-shoot plants under this condition.

Stem dry matter content

Dry matter content (DMC, %) in the stem can indicate the accumulation of non-structural carbohydrates. Both top light and 60 W m^{-2} LED inter-lighting increased stem DMC, with a more noticeable effect under lower top light (Figure 2F). No significant difference in stem DMC was observed between one- and two-shoot plants. However, their responses to the highest LED inter-lighting level varied: Stem DMC decreased for one-shoot plants at 120 W m^{-2} compared to 60 W m^{-2}, while it increased for two-shoot plants. The elevated stem DMC in two-shoot plants (Figure 2F) aligns with their higher dry matter allocation to the stems under the highest LED inter-lighting level (120 W m^{-2}) (Figure 2E).

Stem soluble carbohydrates

Consistent with the observed effects on DMC, both top and inter-mediate lighting enhanced the levels of total soluble carbohydrates (Figure 2G). The interaction among top lighting, inter-lighting, and branching was significant for the Sucrose/TSC

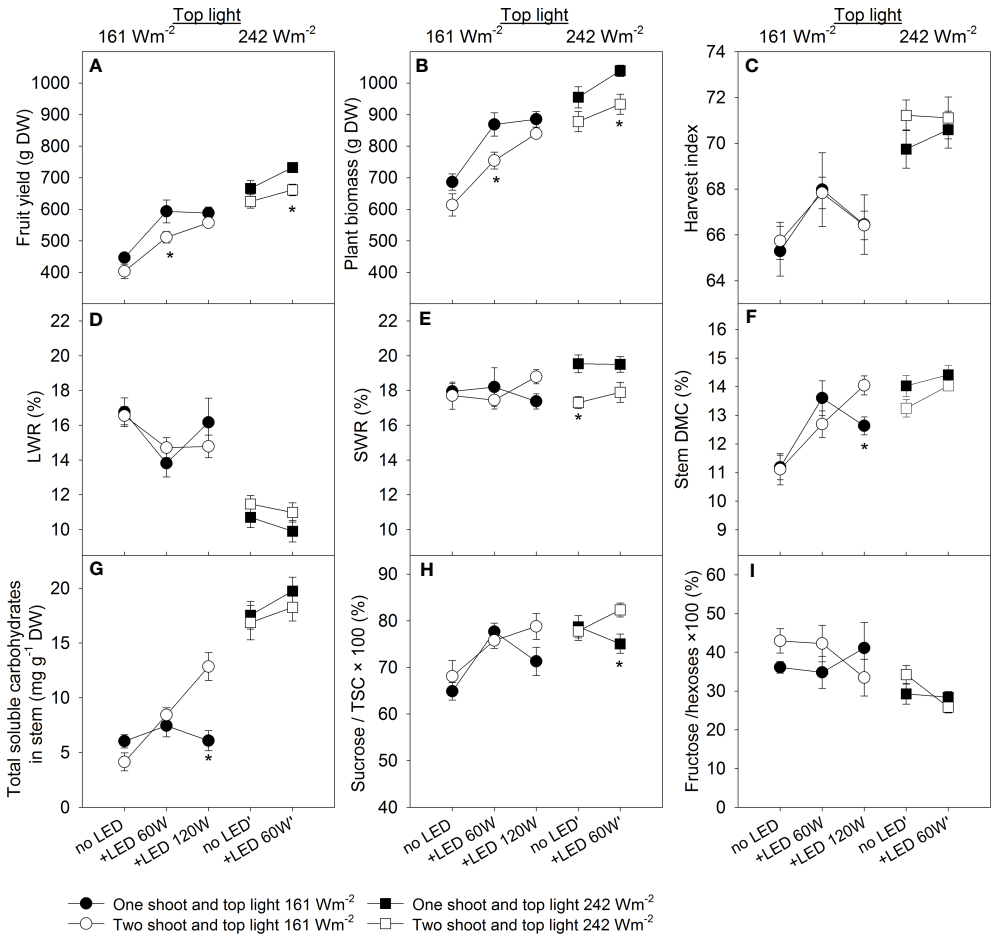

FIGURE 2
The effects of HPS top light (161 W or 242 W m^{-2}) and LED inter-lighting on tomato yield, biomass, and other physiological traits. In the compartment with low top light supplemental LED inter-lighting was added at the levels 0, 60, and 120 W m^{-2} and in the compartment with high top light, the LED inter-lighting was added at the levels 0 and 60 W m^{-2}. Each treatment is represented with 5 replications with 2 shoots. **(A)** Tomato fruit yield in g DW per shoot. **(B)** Plant biomass in g DW per shoot (leaves, stem, and total fruit yield). **(C)** Harvest index, defined as total DW fruit yield/total DW plant biomass × 100%. **(D)** Leaf weight ratio, leaf dry matter/total plant biomass × 100% (LWR (%)). **(E)** Stem weight ratio, stem dry matter/total plant biomass × 100 (SWR (%)). **(F)** Stem dry matter content, DW of stem (g DW)/fresh weight (DW) of stem × 100 (DMC (%)). **(G)** Total soluble carbohydrates (TSC) (mg g^{-1} DW) in the stem (n=4-12). **(H)** Sucrose/total soluble carbohydrates (%) in the stem (n=4-12). **(I)** Fructose/hexoses × 100 (%) in the stem (n=4-12). The data were presented as mean values ± se. The error bars show ± standard error. A star represents a statistically significant difference between one- and two-shoot plants within one light treatment (LSD test significant difference comparison, $p < 0.05$).

value (Figure 2H; Table S1), indicating that branching responses vary based on lighting combination. Specifically, our data showed that both plant types exhibited an increased Sucrose/TSC ratio in the stem with inter-lighting under low top light. However, their responses diverged under high top light: One-shoot plants tended to exhibit a decrease in Sucrose/TSC value, while two-shoot plants tended to exhibit an increase. The ratio of fructose to total hexoses was predominantly influenced by top lighting, with a decrease observed at the high lighting level (Figure 2I).

Leaf physiological traits in relation to canopy position

To assess the differences in source activity among treatments, we estimated the related physiological traits of leaves, such as specific leaf area (SLA), leaf dry matter content (LDM), and chlorophyll index. As the plants were cultivated in a high-wire system, the leaves were analyzed separately at three different positions along the canopy (upper, middle, and bottom). The SLA reflects a strategy of resource allocation within an individual leaf and is negatively related to the leaf thickness and dry matter percentage in leaves. Two-shoot plants showed higher SLA in the top leaves compared to one-shoot plants for almost all treatments (Figure 3A). However, no significant differences were observed for the middle and bottom leaves between plant types (Figures 3B, C). The treatment with the lowest light intensity (only 161 W m^{-2} top light) generally accounted for the highest SLA, which was associated with low leaf dry matter (LDM) (Figure 3D); thus, the higher SLA was not due to thinner leaves but instead to low LDM. The higher SLA for two- than for one-shoot plants under maximum light intensity (242 W top + 60 W m^{-2}, Figure 3A) can also be explained by a lower LDM (Figure 3D).

Impact of lighting and branching on SLA and LDM

The significant triple interaction was found between top lighting, inter-lighting and branching in relation to SLA and LDM in leaves (Table S2). Under low top lighting, inter-lighting similarly reduced SLA for both plant types, a response that can be attributed to both the increased light intensity and the modified light spectrum introduced by the supplemental LED. However, under high top lighting, inter-lighting had a stronger effect on decreasing SLA in one-shoot plants compared to two-shoot plants.

While differences in SLA were noted between the two plant types under conditions of low top light and LED inter-lighting (60 W vs. 120 W m^{-2}), LDM remained consistent. This suggests that two-shoot plant leaves were thinner. As expected, the increased light intensity (applied as top or inter-lighting) decreased the SLA. The supplemental LED inter-lighting (60 W m^{-2}) reduced SLA more strongly in the bottom leaves than in the top and middle leaves, which may reflect the longer exposure of these leaves to direct supplemental LED lighting.

The middle and the bottom leaves had similar or higher dry matter content (LDM, %) in two-shoot plants than in one-shoot plants (Figures 3E, F), indicating that source activity of these two-shoot plants was not the limiting factor leading to reduced plant growth. However, under the 120 W m^{-2} LED inter-lighting condition, a pronounced accumulation of dry matter in middle leaves suggests an imbalance in two-shoot plants: their sink activity was lower than source capacity, leading to increased dry matter storage in these leaves (Figure 3E).

Chlorophyll index responses to lighting and plant type

Both elevated top lighting intensity and supplemental LED inter-lighting increased the chlorophyll index in the leaves. No

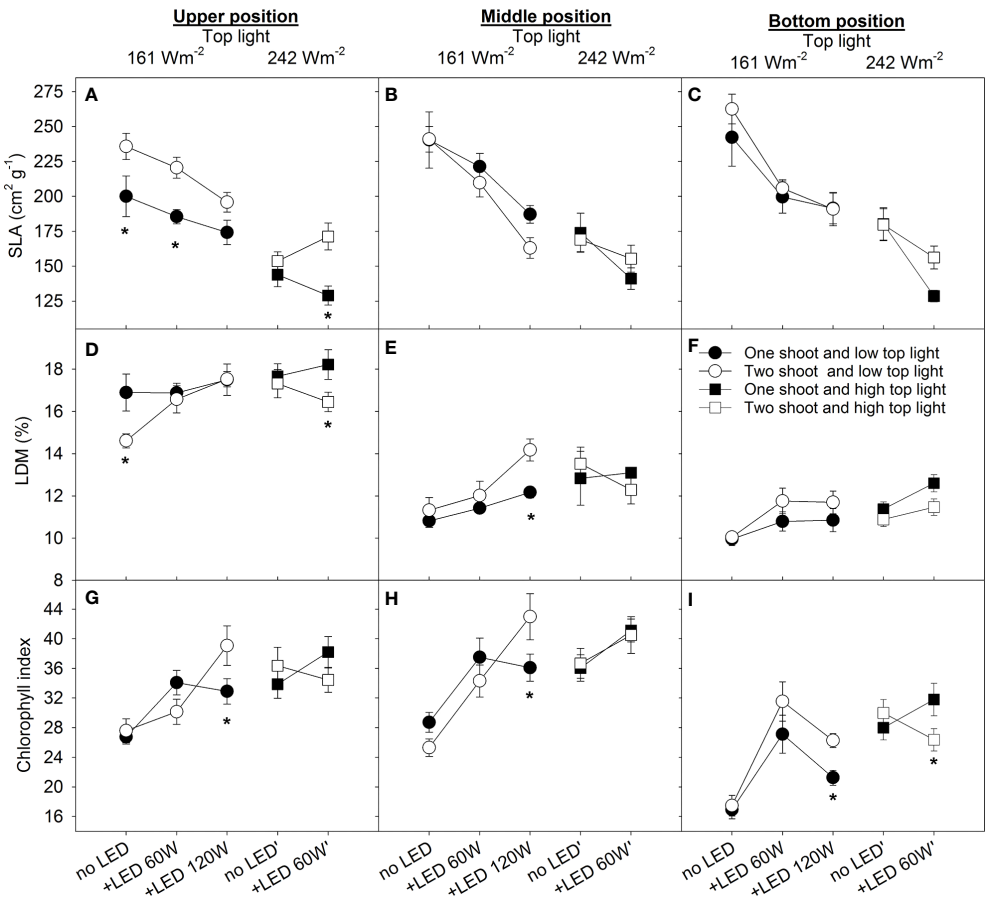

FIGURE 3
The effect of top lighting, the supplemental LED inter-lighting, and shoot branching (one- or two-shoot plants) on specific leaf area, leaf dry matter content, and chlorophyll index at 3 different 2leaf positions in a tomato canopy.The light conditions were top light at 161 W m^{-2} and 242 W m^{-2} combined with 2–3 levels of supplemental LED inter-lighting (without, 60 W m^{-2}, and 120 W m^{-2}). The investigated leaves were growing at three different levels of height being representative for 3 different stages of leaf development and different light conditions. The positions were upper (7 developed leaves from apex), middle (height at the level of the lower LED lamp) and bottom (oldest existing leaf) of the plant. Specific leaf area (SLA) (cm^2 g^{-1}), n=10 for each position **(A–C)**, Leaf dry matter (LDM) content in percentage, n=10 for each position **(D–F)**, Chlorophyll index (CL-01 units, n=20 for each position **(G–I)**, bars represent SE. The star represents a statistically significant difference at $p<0.05$ between one- and two-shoot plants within one light-treatment and calculated with the LSD test.

statistically significant differences were observed between one- and two-shoot plants (Figures 3G–I; Table S2), suggesting that two-shoot cultivation does not directly affect plant source activity. However, under extremely high inter-lighting, two-shoot plants displayed a higher chlorophyll index compared to one-shoot plants. This suggests that two-shoot plants might be better equipped to adjust to a more uniform light distribution along the canopy.

Stem elongation response to plant type and lighting

Under low top lighting, two-shoot plants typically exhibited greater length than one-shoot plants. In contrast, with high top lighting, two-shoot plants were, or tended to be, shorter (Figure 4A). A significant portion of these length differences can be attributed to the distance between trusses (Figure 4B), indicating that stem elongation is a primary factor contributing to these differences.

Fruit count and truss formation

Tomato plant yield is a product of both the number of fruits and the individual weight of each fruit. Our findings indicate that the number of fruits increased with higher top light, supplemental 60 W m^{-2} LED inter-lighting, and during one-shoot plant cultivation (Figure 4C). Generally, the fruit count corresponds to the truss count per shoot (Figure 4D), as all tomato trusses were standardized to seven fruits per truss each during their formative phase. The reduced number of trusses in two-shoot plants can be explained by their structure, where the second shoot is preserved in the leaf axis just below the first flower truss. This structure delays truss formation on the second shoot. However, when comparing the main stems, truss numbers remained consistent between one-shoot and two-shoot plants (Table S3). The differences in number of trusses bearing at least one ripe tomato were also maintained across the two shoots of two-shoot plants (Table S4). The increase of number of trusses with at least one ripe fruit under 120 W m^{-2} inter-lighting appears related to faster ripening, as the total count remained consistent.

Plant type and lighting affect fruit weight

High top lighting reduced the weight differences between fruits of one- and two-shoot plants. The fruit weight of two-shoot plants was 2.3% and 4.2% less than the fruit weight of one-shoot plants under 0 and 60 W m^{-2} LED, respectively. Under low top lighting, this difference was 9.0% and 7.7% for 0 and 60 W m^{-2} LED inter-lighting, respectively (Figure 4E). While 120 W m^{-2} inter-lighting did not further increase one-shoot plant fruit weight, it did enhance the weight of two-shoot plant fruits.

Fruit weight distribution along the truss

Analysis of fruit weight at positions 1—7 in the truss showed that two-shoot cultivation led to reductions in both proximal and

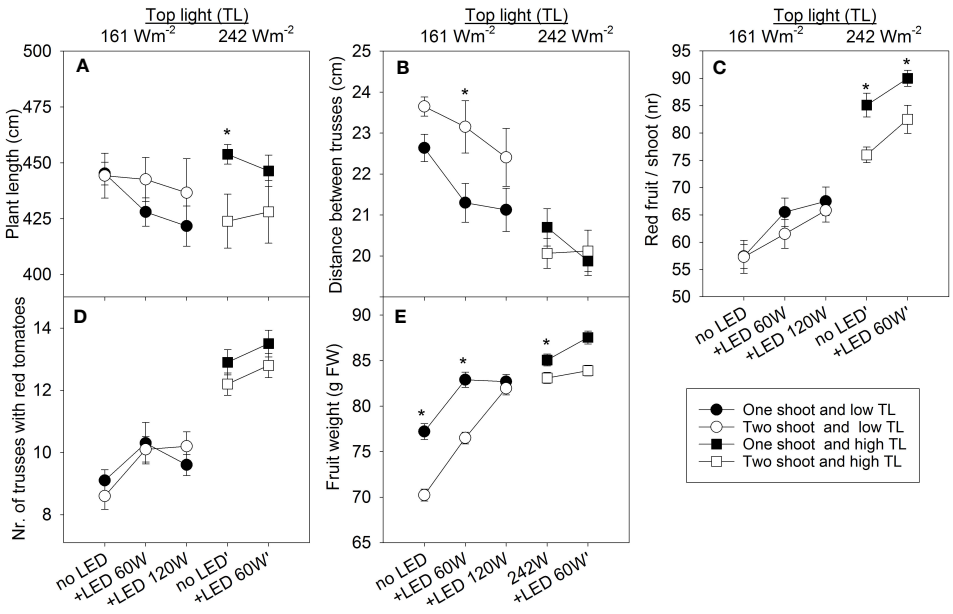

FIGURE 4
The effect of top light intensities (161 W m^{-2} and 242 W m^{-2}) and supplemental LED inter-lighting on plant growth and yield components of greenhouse tomato plants grown as one- and two-shoot plants. The top light intensities were combined with 2 or 3 levels of supplemental LED inter-lighting (no LED, 60 W m^{-2}, or LED 60 W m^{-2} with low 120 W m^{-2} top light). **(A)** Plant length (cm) at final harvest (n=10). **(B)** Distance between trusses (plant length/total number of fruit trusses) (n=10 for each treatment). **(C)** Number of red fruit/shoot (n=10/treatment). **(D)** Sum of all fruit trusses that carried at least one red tomato during the entire growth period. **(E)** Average fruit weight (g FW) of all red tomatoes (n=573–900). The data are presented as mean values ± SE. The star represents a statistically significant difference at $p < 0.05$ between one- and two-shoot plants within one light-treatment and calculated with the LSD test.

distal fruit weights under low top light conditions (Figures 5A, B). However, this trend was not observed under the highest LED inter-lighting (120 W m^{-2}). Despite weight reduction, the ratio between the distal and proximal fruit weights remained consistent in both one- and two-shoot plants (Figure 5C). This consistency suggest there was no heightened competition among fruits for assimilates. Consequently, the decline in fruit weight in two-shoot plants was not due to altered source activity. Conversely, both top light and LED inter-lighting under low top light increased or tended to increase the ratio between distal to proximal fruit weights, supporting our suggestion that increased source activity due to increased light intensity mitigated the competition between apical and proximal fruits.

Diurnal growth rate of fruits: one-shoot vs. two-shoot plants

To better understand the physiological factors affecting fruit size, we analyzed the diurnal growth rate of fruits of one- and two-shoot plants under conditions of low top light without LED, where the most significant differences in average fruit size were observed due to shoot branching (Figures 5A, B). We found that two-shoot cultivation decreased the relative fruit growth shortly after a change in the light conditions: during the first 2 h of the dark period and the first hour of the light period. This decrease in relative fruit growth rate was largely offset by accelerated growth in the latter half of the light period (Figure 6).

Fruit quality assessment

Assessment of quality is made via a set of recognized parameters, and fruit dry matter (DM) is a valuable indicator of quality that is linked to many aspects of fruit cultivation. Two-shoot plants tend to have a higher DM% in fruits at all fruit development stages (Figures 7A–C). As expected, both top light and LED inter-light increased the DM% in the fruits, supporting the positive contribution of source activity to dry matter accumulation in the fruits. Other crucial attributes determining fruit quality include firmness, soluble solids content (SSC), total titratable acidity (TTA), and total phenolic content (TPC). Two-shoot plant cultivation affected not only the fruit size and DM% of fruits but also the quality traits. Specifically, the fruits of two-shoot plants showed decreased fruit firmness. Cultivation under high top light also decreased fruit firmness, whereas supplemental LED inter-lighting

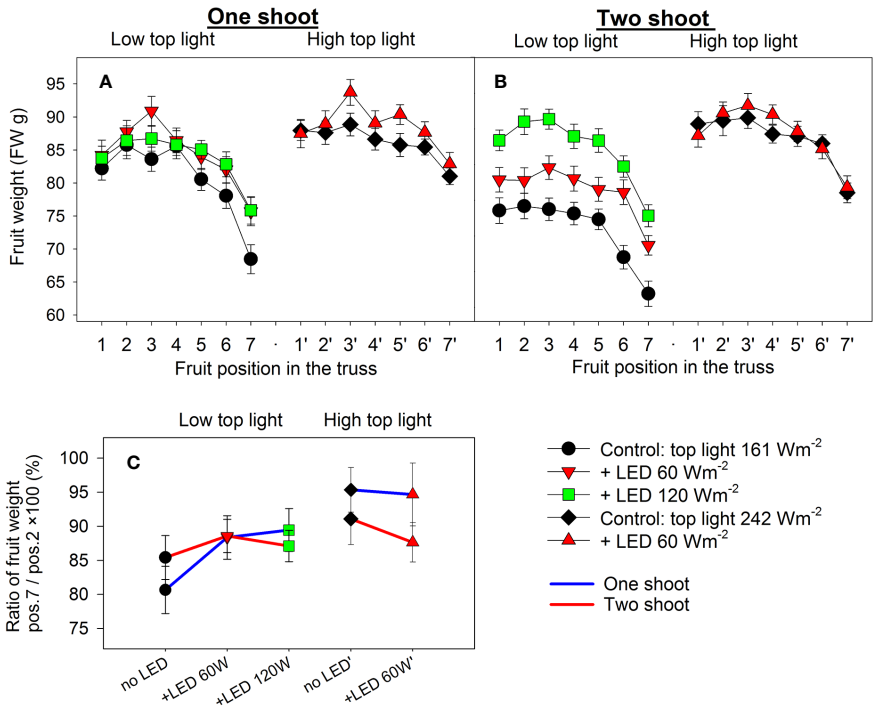

FIGURE 5
The effect of top lighting, supplemental LED inter-lighting, shoot branching, and fruit position in the truss on the mean fresh fruit weight of a greenhouse tomato. The investigated factors were light source top light at two levels (161 W m^{-2} and 242 W m^{-2}) combined with 2 or 3 levels of supplemental LED inter-lighting (no LED, +60 W m^{-2} and +120 W m^{-2} with 161 W m^{-2} top light), shoot branching at 2 levels for one-shoot **(A)** and two-shoot **(B)** plants and fruit position (1–7) in the truss. The mean shown for every treatment is based on 56–119 measurements **(A, B)**. Fruit weight distribution in the truss is represented by the ratio of the mean weight of fruits at position 7 divided by the mean fruit weight at position 2 × 100 (%) **(C)**. Every mean shown is based on the calculated ratio of the averaged fruit weight values (n=10) for 13 trusses. Letters indicate significant differences at $p < 0.05$. Analysis of the source of variation (3-way ANOVA for factors top light, LED, and shoot) showed significant differences for the factor top light ($p<0.013$). Analysis of the source of variation (2-way ANOVA for factor LED and shoot) for low top light treatments showed no significant differences. Bars represent standard error (SE). Trusses were pruned to have 7 tomato fruits; trusses with fewer than 7 tomatoes were excluded from analysis.

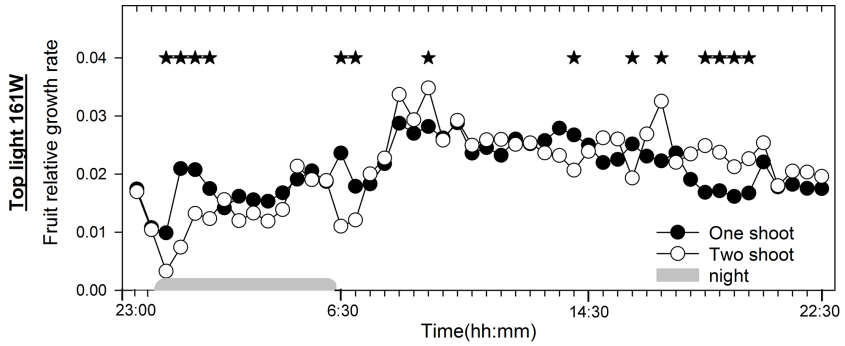

FIGURE 6
Diurnal fruit growth in one-shoot and two-shoot tomato plants. Relative changes in fruit diameter during the day for one- and two-shoot plants receiving 161 W m^{-2} top light. Every mean is based on 15 and 13 measurement for one- and two-shoot plants, respectively. The experiment was analyzed using two-factor analysis of variance (ANOVA). The first factor was shoot (S) and the second factor was time (T) (30 min intervals). Analysis of the source of variation (ANOVA) showed a significant interaction between S and T at $p < 0.001$. Stars indicate significant differences at $p < 0.05$. The night period was from 00:15 to 06:15.

had no significant effect (Figure 8; Table S6). Two-shoot plant cultivation did not change fruit SSC, while high top light strongly increased SSC. Extremely high LED-inter-lighting increased SSC in fruits of two-shoot plants but had only a weak effect on one-shoot plants (Figure 8B).

Two-shoot plants' fruit increased total acidity (TAA) irrespective of light treatments (Figure 8C). Phenolic accumulation varied with shoot branching and light intensity. Under low-top light, two-shoot plants showed significantly enhanced accumulation of phenolic compounds in fruits; however, this effect was absent at extremely high inter-lighting (120 W m^{-2}) or with the combination of high-top light and supplemental LED inter-lighting.

The phenolic concentration in the fruits was positively correlated with DM%, SSC, and TTA (Table S7), indicating that the higher accumulation of phenolics was not due to increased competition between primary and secondary metabolism but due to excess C-skeletons that were used in both primary and secondary metabolic activities. The correlation between fruit weight and fruit quality traits revealed that the responses of one- and two-shoot plants to varying light conditions were similar; however, the sensitivity was different. At the same fruit weight, two-shoot fruits had lower firmness, but higher SSC, TTA, and total phenolic content (Figures 8E–H).

Plant hormone composition in xylem sap

To address the question of whether the modulation of fruit size and quality composition of the fruits occurred through the modification of a root-driven signal induced by one of two shoot cultivation, we analyzed the plant hormone composition in the xylem sap (Figure 9). Two-shoot plants managed to double the xylem sap flow rate for each root, leading an equivalent xylem sap rate when computed per shoot (Figure S1; Table S9). A significant reduction in concentration was found for ABA, jasmonate, and cytokinins. Evidently, the hormone flow in the xylem can influence plant development, leaf activity, and fruit sink capacity. Notably, the diminished concentrations of several

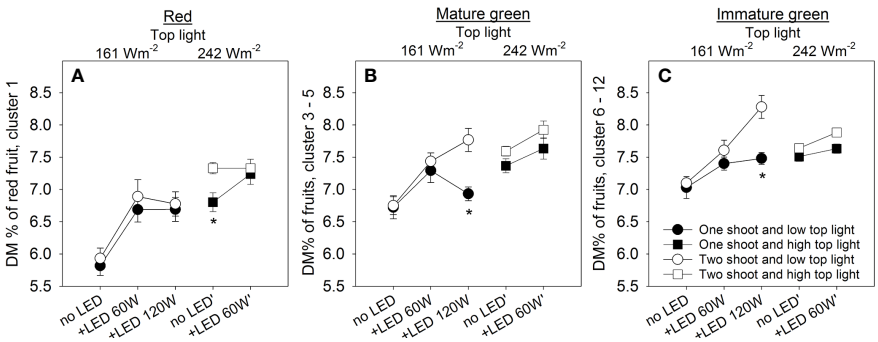

FIGURE 7
The effect of top light intensities, supplemental LED inter-lighting, shoot branching, and fruit development stage on dry matter percentage (DM%) of tomato fruits. The investigated factors were light source top light at two levels (161 W m^{-2} and 242 W m^{-2}) combined with 2 or 3 levels of supplemental LED inter-lighting (no LED, +60 W m^{-2}, and +120 W m^{-2} with 161 W m^{-2} top light), shoot branching at 2 levels (one- and two-shoot plants) and 3 fruit developmental stages. Mean dry matter percentage of red mature fruits for lowest truss (n=10) **(A)**. Mean dry matter percentage (DM%) of green tomatoes from trusses 3–5 (n=30) at the height of the lower LED lamp **(B)**. Mean dry matter percentage of all green tomatoes from trusses 6–12 (n=10), which were above the lowest LED lamp **(C)**. The data are presented as mean values ± SE. Stars indicate significant differences at $p < 0.05$ (LSD test) for one- and two-shoot plants within the same light treatment.

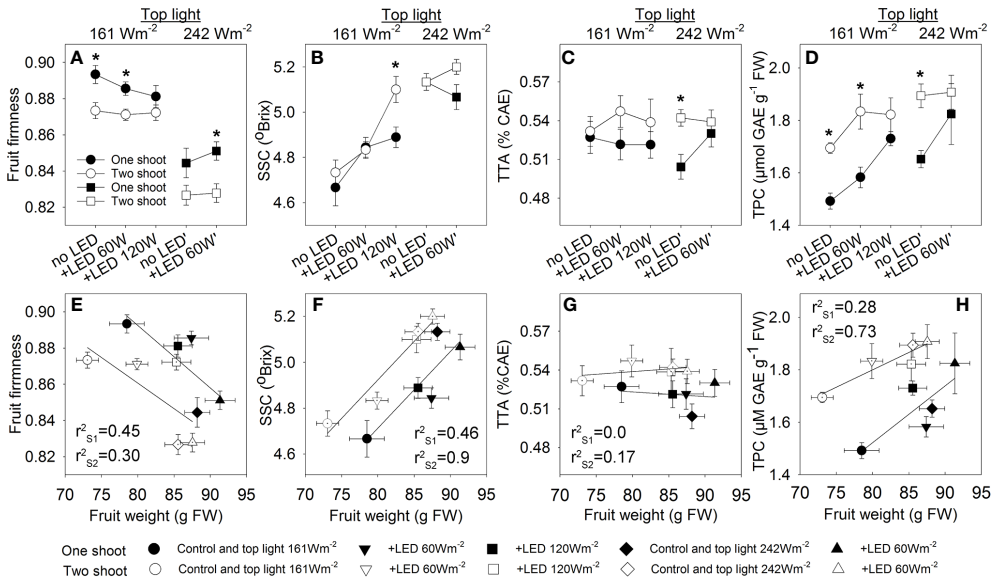

FIGURE 8
The effect of top light intensities, supplemental LED inter-lighting, and shoot branching on tomato fruit quality. The investigated factors were top lighting at two levels (161 W m^{-2} and 242 W m^{-2}) combined with 3 or 2 levels of supplemental LED inter-lighting (no LED, +60 W m^{-2}, and +120 W m^{-2} with 161 W m^{-2} top light) and shoot branching at 2 levels (one-shoot [black] and two-shoot [white] plants). For the quality analysis, tomato fruits at position 3 in a truss were collected on 3 harvesting days during the growth period. The data are presented as mean values ± SE. The stars represent statistically significant differences at $p < 0.05$ between one- and two-shoot plants within the same light treatment (based on the LSD test) **(A–D)**. Relationships between tomato weight and tomato fruit quality traits presented. The r^2 values of the regression line were calculated for all 5 treatments of the one-shoot (SL) and two-shoot (DL) plants **(E–H)**. Fruit firmness was based on a scale from 0 to 1, where "0" means lack of firmness and "1" is full firmness, determined with a Durofel firmness tester (n=9) **(A, E)**. Soluble solid content (SSC) (expressed as °Brix) was measured with a digital refractometer (PR-101α 293; ATAGO, Japan) (n=9) **(B, F)**. Total titratable acidity (TTA) was determined using an automatic titrator (794 Basic Titrino 294; Metrohm, Switzerland) and expressed as percentage of citric acid equivalents (CAE) g^{-1} FW. (n=6) **(C, G)**. Total phenolic compounds (TPC) in tomato fruits (mg GAE 100 g^{-1} FW; n=3-6) **(D, H)**.

cytokinins in xylem sap of decapitated two-shoot plants hint at a role for these cytokinins in the observed reduction in sink capacity in fruits of two-shoot plants. The effect of top light on fruit development seems to act independently of the regulation of hormone composition in xylem sap, as top light intensity did not affect hormone concentrations. On the other hand, LED-inter-lighting was able to increase JA-Ileu and cZR, though the increase in JA-Ileu was only noticeable in one-shoot plants.

A significant three-way interaction among top lighting, inter-lighting, and plant branching (one- or two-shoot plants) on ABA and PA concentration was determined by the varying responses of ABA and PA accumulation in xylem sap (Figure 9; Table S8). Under low top lighting conditions, inter-lighting markedly enhanced ABA accumulation in two-shoot plants compared to one-shoot plants. However, when top lighting was high, the inter-lighting effect on ABA accumulation reversed, favoring one-shoot plants. In contrast, PA concentration exhibited an opposing response: at low top lighting, inter-lighting increased PA concentration in one-shoot plants, while at high top lighting, a positive inter-lighting effect was only observed for two-shoot plants.

Discussion

The primary challenge faced by tomato growers is that achieving high yields in greenhouse cultivation often coincides with reduced fruit quality, characterized by lower sugar content and altered phytochemical composition. Therefore, an understanding of the mechanisms guiding both fruit size and quality is crucial for the optimization of tomato production in greenhouses, as this knowledge will identify practices that allow both high yield and high quality of greenhouse tomatoes. Factors known to affect fruit weight, yield, and quality include top light intensities, LED inter-lighting, and shoot branching in one- and two-shoot plants, leading to the question of whether synergetic or antagonistic interactions occur between these factors.

Our study reveals distinct effects of lighting and two-shoot branching on fruit size and other quality traits. Specifically, enhanced lighting increased fruit size, while two-shoot cultivation decreased it. However, both enhanced lighting and two-shoot cultivation positively influenced fruit quality traits. The present study did not identify a significant interaction between light conditions and shoot branching concerning fruit size and fruit quality traits (Tables S5, S6). This suggests that these treatments affect different physiological processes that guide fruit development. While light primarily boosts source activity by directly increasing leaf photosynthesis per leaf area, the effects of two-shoot cultivation on plant growth and development remain underexplored. Our findings indicate that two-shoot cultivation reduces fruit size and modulates fruit quality, primarily through a decrease in the sink capacity of the fruits, rather than by any effect on source activity.

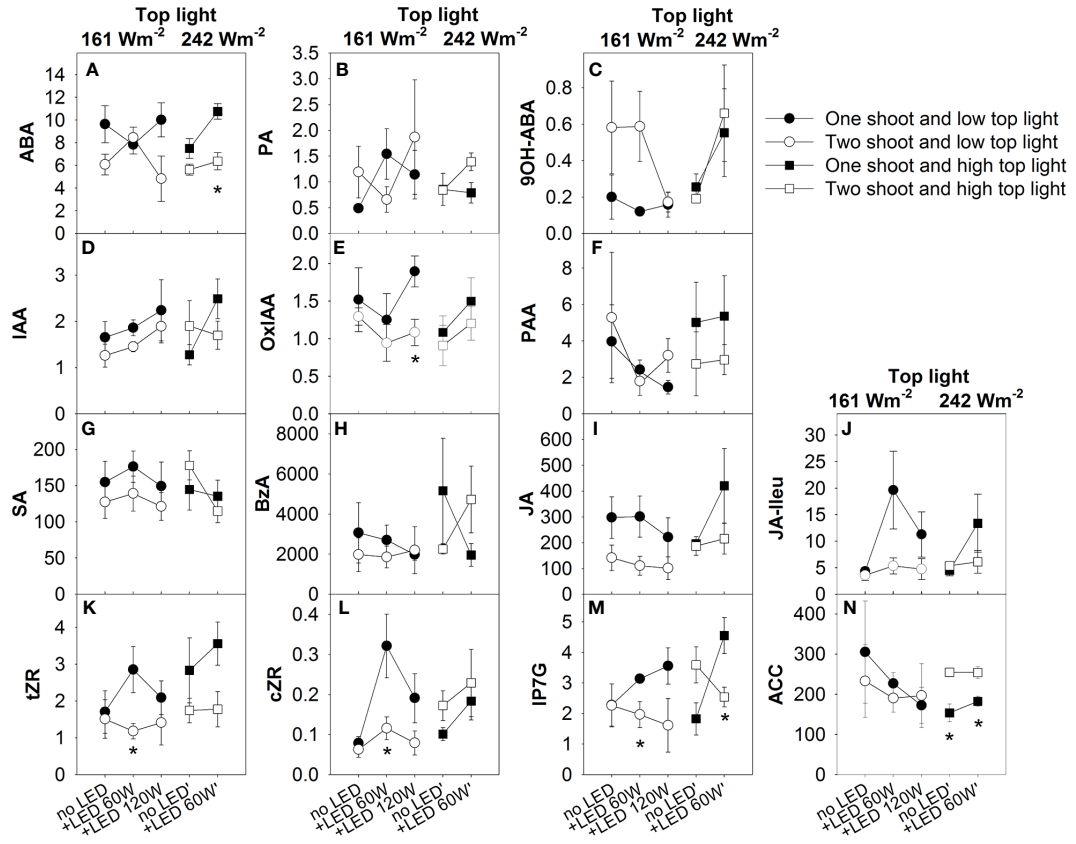

FIGURE 9
The effect of top light intensities, supplemental LED inter-lighting distribution, and shoot branching on the plant hormone composition of the xylem sap at final harvest. The studied factors were top lighting at two levels (161 W m^{-2} and 242 W m^{-2}) combined with 3 or 2 levels of supplemental LED inter-lighting (no LED, +60 W m^{-2}, and +120 W m^{-2} with 161 W m^{-2} top light), and 2 levels of shoot branching (one- and two-shoot plants). Variables are plant hormone concentration in xylem sap (pmol/mL): abscisic acid (ABA) **(A)**, phaseic acid (PA) **(B)**, 9-hydroxy-ABA (9OH-ABA) **(C)** indole-3-acetic acid (IAA) **(D)**,oxo-IAA (OxIAA) **(E)**, phenylacetic acid (PAA) **(F)**, salicylic acid (SA) **(G)**, benzoic acid (BzA) **(H)**, jasmonic acid (JA) **(I)**, and JA-isoleucine (JA-Ileu) **(J)** (n=4–5), trans-zeatin riboside (tZR) **(K)**, cis-zeatin-riboside (cZR) **(L)**, isopentenyl adenine-7-glucoside (iP7G) **(M)**, 1-aminocyclopropane-1-carboxylic acid (ACC) **(N)**. The data are presented as mean values ± SE. The stars represent statistically significant differences at $p < 0.05$ between one- and two-shoot plants within the same light treatment (LSD test) (n = 5).

Two-shoot plants reduce the sink capacity of fruits

The evidence that source activity did not limit fruit size was based on the comparison of the major leaf-related traits that characterize plant source activity. Specifically, the dry matter allocation to the leaves, leaf chlorophyll content, SLA, and accumulation of dry matter in the leaves were all found to be the same or higher in two-shoot plants when compared to one-shoot plants. Furthermore, analysis of soluble sugars in the stem indicated that two-shoot plants accumulated similar amounts of soluble sugars, which can be used as carbohydrate resources for fruit growth, compared to one-shoot plants. These findings further support the suggestion that the modulation of source activity was not responsible for the changes in fruit size observed in two-shoot plant cultivation.

Another indication that sink capacity, rather than source activity, was the main determinant of fruit size came indirectly from the comparison of the individual fruit weights located at proximal and distal positions in the truss. Usually, larger fruits develop at the proximal positions (closer to the stem and the first develop) than at the distal position (Bangerth and Ho, 1984). The consistent distal/proximal fruit weight ratios between one- and two-shoot plants suggest that two-shoot cultivation does not alter fruit competition during development. However, both top light and inter-lighting decreased the relative difference between distal and proximal fruits (Figure 5), supporting the assumption that this trait is sensitive to the amount of available carbohydrates, and thus to source activity. A positive effect of inter-lighting in reducing the difference between distal and proximal fruits was also demonstrated in our previous study (Paponov et al., 2020).

More evidence that the sink capacity limits fruit size is based on the observation that the fruits of two-shoot plants at all developmental stages have equal or higher dry matter content. The dry matter content in growing fruits consists of non-structural carbohydrate (Serio et al., 2004); therefore, the dry matter content in fruits can also reflect the balance between source activity and sink capacity in the plants. Under source-limiting conditions (low light intensity), both fruit size and dry matter content in the fruits decreased (Figures 4E, 7). These decreases are in agreement with

the fact that cell expansion in the fruits is sensitive to the level of assimilates supplied to the fruits during the fruit loading phase (Bertin and Genard, 2018), whereby the dynamics of dry matter accumulation in the fruits reflect the balance of water and carbohydrate fluxes to the fruits (Guichard et al., 2001). However, the ability of two-shoot plants to generate fruits with higher dry matter content at a specific fruit weight indicates alternative regulation of solute fluxes into the fruits when the fruit size is not limited by the availability of assimilates, but by sink capacity. The higher dry matter accumulation in the fruits of two-shoot plants can reflect a higher contribution of phloem flux than xylem flux for fruit formation (Hanssens et al., 2015).

The capacity of two-shoot plants to build fruits with higher dry matter content at a specific fruit size might be related to the fact that the final fruit size is defined shortly before the beginning of the fruit loading stage, when the ultimate number of cells in a fruit is determined (Bertin et al., 2003). This number of cells can limit the ultimate size of the fruit, even if carbohydrate availability during fruit loading is not limited. Thus, the smaller fruit size of two-shoot plants at maturity might reflect a reduced sink size due to the formation of a smaller number of cells during the cell division stage. Restriction of fruit size due to less cell division before fruit loading, together with maintenance of carbohydrate fluxes to the fruits during the loading phase, will generate a fruit with a smaller size but higher accumulation of dry matter and other modifications of fruit quality traits.

Potential hormonal regulation of sink capacity in two-shoot plants

In two-shoot plants, plant hormones, particularly cytokinins, appear to play a role in modulating sink capacity. Our data reveals a notable reduction in cytokinin levels in the xylem sap of these plants, especially under conditions of low top light with LED inter-lighting. This reduction might be associated with the diminished sink capacity observed in their fruits. Parallel findings from studies on two- branched beans and peas also reported a decline in xylem sap cytokinin concentration in two-shoot plants (Bangerth, 1994; Li et al., 1995; Kotov and Kotova, 2018). The trend has been attributed to an increased auxin transport to the roots due to the additional shoot, which subsequently suppresses cytokinin synthesis, leading to its reduced presence in the xylem sap.

Hormonal pathways, especially involving cytokinins, are also integral in modulating fruit size and quality under stress conditions. For instance, drought and osmotic stress have been shown to reduce cytokinin levels (Kudoyarova et al., 2006; Gujjar and Supaibulwatana, 2019). Given the central role of cytokinins in regulating fruit cell division (Zhang and Whiting, 2011; Matsuo et al., 2012), a systemic decrease in their levels might impact fruit sink capacity and strength.

However, cytokinins alone can' t explain all fruit weight variation. For instance, under low top lighting without LED, fruit weight differences persisted despite similar cytokinin concentration in both plant types. This suggests other hormonal influences at play. Observations indicate that two-shoot plants under low top lighting display variations in hormone concentrations particularly a rise in 9OH'-ABA, known for its ABA-like activities (Zhou et al., 2004). The role of this hormone in sink activity warrants further exploration.

Phloem and xylem flux modulation in two-shoot plants

In addition to the regulation of fruit size through hormone pathways, the intricate balance between xylem and phloem solute transport is crucial in shaping fruit size and quality. One possible mechanism that could contribute to the accumulation of dry matter content in fruits (and the improvement of other fruit quality traits) is the reduction in xylem flux relative to phloem flux directed to fruits. This phenomenon has been observed under environmental stresses like drought and salt stress. Here, heightened nutrient concentrations due to these stresses result in a decreased solute flux from roots, attributed to reduced root pressure (Ehret and Ho, 1986; Araki et al., 2001; Van de Wal et al., 2017; Cui et al., 2020).

In the context of two-shoot plants, the enhanced fruit quality is not easily attributed to reduced root pressure, as the two-shoot plants were able to duplicate the xylem sap flow rate per root, resulting in the same xylem sap rate calculated per shoot (Figure S1; Table S9). This maintained pressure cannot be explained by an increased amount of carbohydrates transported to the roots because increased carbohydrate biosynthesis due to increased light intensity did not enhance root exudation rate in either one- or two-shoot plants. Intriguingly, a previous study showed increased xylem sap flow rate with supplemental LED inter-lighting (Paponov et al., 2020). Such discrepancies might arise from the use of different genotypes or varied experimental setups. Moreover, xylem sap flux regulation might exhibit a circadian rhythm, as observed in young maize plants (Lopez et al., 2003).

The nighttime reduction in fruit growth could be indicative of a dip in xylem sap pressure, given that root pressure is the primary solute supply source during this period (Hanssens et al., 2015). The consistent xylem sap rate per shoot (Figure S1; Table S9) suggests that the transient reduction in fruit growth during the initial 2 h of the night, and shortly after lights are turned on, cannot be explained by a reduced xylem sap flow rate. Instead, the distinct architecture of two-shoot plants might increase resistance to xylem flow, particularly during pivotal water supply periods, such as during light transitions. This restricted solute supply from the xylem to fruits for two-shoot plants might be due to increased hydraulic resistance associated with the reduced xylem area, vessel numbers, and vessel size (Lang and Ryan, 1994; Choat et al., 2009).

Abrupt changes in greenhouse lighting like turning lights on or off, can initiate these trigger critical periods. Turning light on promotes morning water movement via transpiration, with leaves drawing from the root-extended water column. Conversely, turning lights off decreases transpiration, positioning root pressure as the main force pushing the water flux into the plant's aboveground parts. The observed decline in fruit growth after abrupt light changes suggests that the two-shoot architecture's adjusted hydraulic resistance might influence the final fruit quality by reducing xylem flux to fruits.

The interplay of shoot branching and light on fruit quality

Fruit size and metabolite accumulation are largely determined by sink capacity and solute transport via phloem and xylem. Both of these processes can be modulated by plant architecture and light conditions. Understanding their combined effects can guide adjustments for appropriate fruit quality traits. One key aspect for fruit quality is the balance between sugars and organic acids, which plays a pivotal role in determining tomato flavor (Agius et al., 2018). Our observations show that while two-shoot plants maintain a consistent SSC, they exhibit an increase in total acidity (Figures 8B, C, Table S6). In contrast, increasing light intensity boosts SSC without affecting total acidity, highlighting significance of source activity in the accumulation of soluble compounds in fruits.

Delving deeper into the metabolic dynamics, the elevated organic acid content in fruits from two-shoot plants might reflect the dynamics of sugars and organic acid use for respiration during fruit maturation. As fruit develop, the roles of sugars and organic acids in respiration evolve. Notably, as fruits approach maturity, sugars become predominantly stored in vacuoles, rendering them less accessible for respiration (Coombe, 1976). This dynamic could lead to a shift in respiratory substrates from sugars to organic acids, particularly citrate. Given the smaller fruits size typical of two-shoot plants, it is plausible that these fruits exhibit reduced respiratory activity as they near maturity. This would result in a decreased consumption of organic acids for respiration, leading to their heightened content at full maturity (Figure 8C; Table S6).

Fruit firmness is another complex quality trait and can be influenced by cellular turgor pressure. A strong positive correlation exists between fruit firmness and the content of dry matter or total soluble solids, as observed in tomatoes (Saha et al., 2009; Aurand et al., 2012) and kiwis (Nardozza et al., 2011). However, the diminished firmness of fruits from two-shoot plants (Figure 8A), despite their greater accumulation of dry matter (Figure 7), suggests other underlying factors affecting firmness. One such factor could be the number of cells in the fruits. Fruits with smaller cells and more cell structures tend to exhibit higher mechanical resistance. Indeed, comparisons across various tomato genotypes have indicated that fruits with smaller cells and more cell structures are typically firmer (Aurand et al., 2012). While we did not quantify cell numbers in our tomato fruits, our findings underscore that a limited sink capacity was the main factor restricting fruit growth, leading to the assumption that the number of cells was reduced in the fruits of two-shoot plants. The excess carbohydrates available during fruit loading might contribute to a stronger elongation of fruit cells of two-shoot plants, and this would ultimately reduce firmness. Interestingly, plants given high top lighting also showed decreased fruit firmness despite the higher accumulation of dry matter content or SSC in the fruits. This phenomenon could be attributed to elevated temperatures in the high top light compartment, as previous studies have linked high temperature to reduced fruit firmness (Hertog et al., 2004).

Greenhouse-grown tomato plants frequently experience sub-optimal lighting, which can lead to reduced accumulation of both primary and secondary metabolites. Given the health benefits associated with many secondary metabolites, the observed increase in phenolic compounds in two-shoot cultivated tomatoes underscores the potential advantages of this cultivation approach in greenhouses. The interplay between primary and secondary metabolism might favor the accumulation of secondary metabolites at the cost of primary ones (Herms and Mattson, 1992).

The elevated accumulation of phenolic compounds in fruits from two-shoot plants can be partly attributed to their smaller size and the varied distribution of these compounds within the fruit. Tomato phenolic concentrations differ across fruit sections, with the highest levels found in epidermal and placental tissues. For example, an analysis of flavonol distribution in Spanish cherry tomatoes showed that 98% of the total flavonols occurred in the skin (Stewart et al., 2000). This localized accumulation aligns with other research, highlighting that a majority of certain flavonols and quercetin derivatives are predominantly found in the epidermis (Moco et al., 2007; Slimestad and Verheul, 2009). Due to their reduced size, fruits from two-shoot plants have an enhanced surface-to-volume ratio. Given the skin's rich phenolic compound content, its increased proportion in these smaller fruits likely contributes to a higher overall phenolic content. Additionally, our findings indicate that enhanced light intensity increased both SSC and total phenolics (Figures 8B, D), suggesting a redirection of excess carbohydrates towards the synthesis of secondary metabolites.

Conclusion

The balance between source strength, which comes from plant photosynthesis, and sink capacity, mainly determined by the number and potential size of fruits, is crucial for plant growth and performance (Lemoine et al., 2013). Understanding the relationships between source and sink, especially the transport and partitioning of assimilates to different organs, can help improve fruit yield and quality (Ho, 1996). Our study indicates that greenhouse practices, such as creating two-shoot plants through shoot branching and using supplemental lighting, can independently regulate the size and quality of the produced fruits. Overall, two-shoot branching primarily modified sink capacity, while lighting primarily affected source activity. Two-shoot cultivation reduced the xylem sap concentration of cytokinins that can inhibit the sink capacity of young fruits. Additionally, the increased hydraulic resistance associated with two-shoot plant architecture appears to improve fruit quality due to the higher solute flux from the phloem at the expense of the xylem. The stronger inhibition of sink than source activity, together with the increased hydraulic resistance in the stem, resulted in fruits that were smaller but showed higher accumulation of dry matter content and improved fruit quality traits. Notably, fruits from two-shoot plants had enhanced accumulations of dry matter and phenolic contents. Further investigation of the interactions between shoot branching practices and environmental factors is required to establish the optimal combinations that maximize both yield and fruit quality traits in tomatoes.

Data availability statement

The original contributions presented in the study are included in the article/Supplementary Material. Further inquiries can be directed to the corresponding authors.

Author contributions

IP, MV and MP designed the experiment. MP performing the majority of the experimental work. MP conducted all data analysis and collaborated with IP on the writing of the paper. PD carried out hormone analysis. All authors provided critical feedback and corrections on the final version of the paper.

Funding

The present study is supported by the Bionær program of the Research Council of Norway ('Biofresh' project no 255613/E50).

Acknowledgments

We would like to thank to Kristoffer Hodnebrog, Henk Maessen, and Anne Kvitvær for the technical support. We also thank to Anush Panosyan, Zaruhi Hoveyan, Dmitry Kechasov, Sonja Ginnard and Lea Zalar Pettersen, Mariam Poghosyam, and Hayk Manukyan for data collection.

Conflict of interest

The authors declare that the research was conducted in the absence of any commercial or financial relationships that could be construed as a potential conflict of interest.

Publisher's note

Supplementary material

The Supplementary Material for this article can be found online at: https://www.frontiersin.org/articles/10.3389/fpls.2023.1221163/full#supplementary-material

References

Agius, C., Von Tucher, S., Poppenberger, B., and Rozhon, W. (2018). Quantification of sugars and organic acids in tomato fruits. *MethodsX* 5, 537–550. doi: 10.1016/j.mex.2018.05.014

Ainsworth, E. A., and Gillespie, K. M. (2007). Estimation of total phenolic content and other oxidation substrates in plant tissues using Folin-Ciocalteu reagent. *Nat. Protoc.* 2, 875–877. doi: 10.1038/nprot.2007.102

Alexou, M., and Peuke, A. D. (2001). "Methods for xylem sap collection," in *Plant Mineral Nutrients: Methods and Protocols*. Ed. F. J. M. Maathuis (Totowa, NJ: Humana Press), 195–207. doi: 10.1007/978-1-62703-152-3_13

Araki, T., Kitano, M., Okano, K., Yoshida, S., and Eguchi, T. (2001). Environmental effects on dynamics of fruit growth and photoassimilate translocation in tomato plants. (3) Effect of salt stress. *Environ. Control Biol.* 39, 53–58. doi: 10.2525/ecb1963.39.53

Aurand, R., Faurobert, M., Page, D., Maingonnat, J.-F., Brunel, B., Causse, M., et al. (2012). Anatomical and biochemical trait network underlying genetic variations in tomato fruit texture. *Euphytica* 187, 99-116. doi: 10.1007/s10681-012-0760-7

Bangerth, F. (1994). Response of cytokinin concentration in the xylem exudate of bean (*Phaseolus vulgaris* L.) plants to decapitation and auxin treatment, and relationship to apical dominance. *Planta* 194, 439–442. doi: 10.1007/BF00197546

Bangerth, F., and Ho, L. C. (1984). Fruit position and fruit-set sequence in a truss as factors determining final size of tomato fruits. *Ann. Bot.* 53, 315–319. doi: 10.1093/oxfordjournals.aob.a086695

Bantis, F., Smirnakou, S., Ouzounis, T., Koukounaras, A., Ntagkas, N., and Radoglou, K. (2018). Current status and recent achievements in the field of horticulture with the use of light-emitting diodes (LEDs). *Sci. Hortic.* 235, 437–451. doi: 10.1016/j.scienta.2018.02.058

Bertin, N. (1995). Competition for assimilates and fruit position affect fruit set in indeterminate greenhouse tomato. *Ann. Bot.* 75, 55–65. doi: 10.1016/S0305-7364(05)80009-5

Bertin, N., Borel, C., Brunel, B., Cheniclet, C., and Causse, M. (2003). Do genetic make-up and growth manipulation affect tomato fruit size by cell number, or cell size and DNA endoreduplication? *Ann. Bot.* 92, 415–424. doi: 10.1093/aob/mcg146

Bertin, N., and Genard, M. (2018). Tomato quality as influenced by preharvest factors. *Sci. Hortic.* 233, 264–276. doi: 10.1016/j.scienta.2018.01.056

Choat, B., Gambetta, G. A., Shackel, K. A., and Matthews, M. A. (2009). Vascular function in grape berries across development and its relevance to apparent hydraulic isolation. *Plant Physiol.* 151, 1677–1687. doi: 10.1104/pp.109.143172

Cockshull, K. E., Graves, C. J., and Cave, C. R. J. (1992). The influence of shading on yield of greenhouse tomatoes. *J. Hort Sci.* 67, 11–24. doi: 10.1080/00221589.1992.11516215

Coombe, B. G. (1976). The development of fleshy fruits. *Annu. Rev. Plant Physiol.* 27, 207–228. doi: 10.1146/annurev.pp.27.060176.001231

Cui, J., shao, G., lu, J., and Keabetswe, L. (2020). Yield, quality and drought sensitivity of tomato to water deficit during different growth stages. *Sci. Agric.* 77. doi: 10.1590/1678-992x-2018-0390

Davies, J. N., and Hobson, G. E. (1981). The constituents of tomato fruit - the influence of environment, nutrition, and genotype. *Crit. Rev. Food Sci. Nutr.* 15, 205–280. doi: 10.1080/10408398109527317

Davis, P. A., and Burns, C. (2016). Photobiology in protected horticulture. *Food Energy Secur* 5, 223–238. doi: 10.1002/fes3.97

Dorais, M., Papadopoulos, A., and Gosselin, A. (2001). "Greenhouse tomato fruit quality," in *Horticultural Reviews*. Ed. J. Janick (New York, NY: John Wiley & Sons), 239–319.

Dumas, Y., Dadomo, M., Di Lucca, G., and Grolier, P. (2003). Effects of environmental factors and agricultural techniques on antioxidant content of tomatoes. *J. Sci. Food Agr* 83, 369–382. doi: 10.1002/jsfa.1370

Ehret, D. L., and Ho, L. C. (1986). Translocation of calcium in relation to tomato fruit growth. *Ann. Bot.* 58, 679–688. doi: 10.1093/oxfordjournals.aob.a087230

Evans, J., Jakobsen, I., and Ögren, E. (1993). Photosynthetic light-response curves. *Planta* 189, 191–200. doi: 10.1007/BF00195076

Gautier, H., Massot, C., Stevens, R., Sérino, S., and Génard, M. (2009). Regulation of tomato fruit ascorbate content is more highly dependent on fruit irradiance than leaf irradiance. *Ann. Bot.* 103, 495–504. doi: 10.1093/aob/mcn233

Gomez, C., Morrow, R. C., Bourget, C. M., Massa, G. D., and Mitchell, C. A. (2013). Comparison of intracanopy light-emitting diode towers and overhead high-pressure sodium lamps for supplemental lighting of greenhouse-grown tomatoes. *HortTechnology* 23, 93–98. doi: 10.21273/HORTTECH.23.1.93

Grierson, D., and Kader, D. D. (1986). "Fruit ripening and quality," in *The tomato Crop (A Scientific Basis for Improvement)*. Eds. J. G. Atherton and J. Rudich (Dordrecht: Springer), 1389–1393.

Gruda, N. (2005). Impact of environmental factors on product quality of greenhouse vegetables for fresh consumption. *Crit. Rev. Plant Sci.* 24, 227–247. doi: 10.1080/07352680591008628

Guichard, S., Bertin, N., Leonardi, C., and Gary, C. (2001). Tomato fruit quality in relation to water and carbon fluxes. *Agronomie* 21, 385–392. doi: 10.1051/agro:2001131

Gujjar, R. S., and Supaibulwatana, K. (2019). The mode of cytokinin functions assisting plant adaptations to osmotic stresses. *Plants* 8, 542. doi: 10.3390/plants8120542

Han, J., Kamber, M., and Pei, J. (2012). *Data mining: Concepts and techniques* (Waltham, MA: Morgan Kaufmann).

Hanson, P., Yang, R.-Y., Wu, J., Chen, J.-T., Ledesma, D., Tsou, S., et al. (2004). Variation for antioxidant activity and antioxidants in tomato. *J. Am. Soc. Hort Sci.* 129, 704–711. doi: 10.21273/JASHS.129.5.0704

Hanssens, J., De Swaef, T., and Steppe, K. (2015). High light decreases xylem contribution to fruit growth in tomato. *Plant Cell Environ.* 38, 487–498. doi: 10.1111/pce.12411

Herms, D. A., and Mattson, W. J. (1992). The dilemma of plants - to grow or defend. *Q Rev. Biol.* 67, 283–335. doi: 10.1086/417659

Hernandez, V., Hellin, P., Fenoll, J., and Flores, P. (2019). Interaction of nitrogen and shading on tomato yield and quality. *Sci. Hortic.* 255, 255-259. doi: 10.1016/j.scienta.2019.05.040

Hertog, M., Ben-Arie, R., Róth, E., and Nicolaï, B. M. (2004). Humidity and temperature effects on invasive and non-invasive firmness measures. *Postharvest Biol. Technol.* 33, 79–91. doi: 10.1016/j.postharvbio.2004.01.005

Ho, L. C. (1996). The mechanism of assimilate partitioning and carbohydrate compartmentation in fruit in relation Ito the quality and yield of tomato. *J. Exp. Bot.* 47, 1239–1243. doi: 10.1093/jxb/47.Special_Issue.1239

Ho, L. C., and Hewitt, J. D. (1986). "Fruit development," in *The tomato crop*. Eds. J. G. Atherton and J. Rudich (London: Chapman and Hall), 201–240.

Hocking, P. J., and Steer, B. T. (1994). The distribution and identity of assimilates in tomato with special reference to stem reserves. *Ann. Bot.* 73, 315–325. doi: 10.1006/anbo.1994.1037

Kanayama, Y. (2017). Sugar metabolism and fruit development in the tomato. *Hort J.* 86, 417–425. doi: 10.2503/hortj.OKD-IR01

Khan, A. A., and Sagar, G. R. (1966). Distribution of 14C-labelled products of photosynthesis during the commercial life of the tomato crop. *Ann. Bot.* 30, 727–743. doi: 10.1093/oxfordjournals.aob.a084109

Kotov, A. A., and Kotova, L. M. (2018). Auxin cytokinin interactions in the regulation of correlative inhibition in two-branched pea seedlings. *J. Exp. Bot.* 69, 2967–2978. doi: 10.1093/jxb/ery117

Kudoyarova, G. R., Vysotskaya, L. B., Cherkozyanova, A., and Dodd, I. C. (2006). Effect of partial rootzone drying on the concentration of zeatin-type cytokinins in tomato (Solanum lycopersicum L.) xylem sap and leaves. *J. Exp. Bot.* 58, 161–168. doi: 10.1093/jxb/erl116

Lang, A., and Ryan, K. G. (1994). Vascular development and sap flow in apple pedicels. *Ann. Bot.* 74, 381–388. doi: 10.1006/anbo.1994.1131

Lemoine, R., La Camera, S., Atanassova, R., Dedaldechamp, F., Allario, T., Pourtau, N., et al. (2013). Source-to-sink transport of sugar and regulation by environmental factors. *Front. Plant Sci.* 4. doi: 10.3389/fpls.2013.00272

Li, C., and Bangerth, F. K. (1999). Autoinhibition of indoleacetic acid transport in the shoots of two branched pea (*Pisum sativum*) plants and its relationship to correlative dominance. *Physiol. Plant* 106, 415–420. doi: 10.1034/j.1399-3054.1999.106409.x

Li, C., and Bangerth, F. (2003). Stimulatory effect of cytokinins and interaction with IAA on the release of lateral buds of pea plants from apical dominance. *J. Plant Physiol.* 160, 1059–1063. doi: 10.1078/0176-1617-01042

Li, C. J., Guevara, E., Herrera, J., and Bangerth, F. (1995). Effect of apex excision and replacement by 1-naphthylacetic acid on cytokinin concentration and apical dominance in pea plant. *Physiol. Plant* 94, 465–469. doi: 10.1034/j.1399-3054.1995.940314.x

Li, T., Heuvelink, E., and Marcelis, L. F. M. (2015). Quantifying the source-sink balance and carbohydrate content in three tomato cultivars. *Front. Plant Sci.* 6. doi: 10.3389/fpls.2015.00416

Lopez, M., Bousser, A. S., Sissoeff, I., Gaspar, M., Lachaise, B., Hoarau, J., et al. (2003). Diurnal regulation of water transport and aquaporin gene expression in maize roots: Contribution of PIP2 proteins. *Plant Cell Physiol.* 44, 1384–1395. doi: 10.1093/pcp/pcg168

Løvdal, T., Olsen, K. M., Slimestad, R., Verheul, M., and Lillo, C. (2010). Synergetic effects of nitrogen depletion, temperature, and light on the content of phenolic compounds and gene expression in leaves of tomato. *Phytochemistry* 71, 605–613. doi: 10.1016/j.phytochem.2009.12.014

Marcelis, L. F. M., Broekhuijsen, A. G. M., Meinen, E., Nijs, E., and Raaphorst, M. G. M. (2006). Quantification of the growth response to light quantity of greenhouse grown crops. *Acta Hortic.* 711, 97–103. doi: 10.17660/ActaHortic.2006.711.9

Matsuo, S., Kikuchi, K., Fukuda, M., Honda, I., and Imanishi, S. (2012). Roles and regulation of cytokinins in tomato fruit development. *J. Exp. Bot.* 63, 5569–5579. doi: 10.1093/jxb/ers207

Max, J., Schmidt, L., Mutwiwa, U., and Kahlen, K. (2016). Effects of shoot pruning and inflorescence thinning on plant growth, yield and fruit quality of greenhouse tomatoes in a tropical climate. *J. Agric. Rural Dev. Trop. Subtrop* 117, 45–56. doi: 10.15488/589

Mireille, N., Jeannequin, B., and Sebillotte, M. (1997). Vigour of greenhouse tomato plants (*Lycopersicon esculentum* Mill.): Analysis of the criteria used by growers and search for objective criteria. *J. Hort Sci.* 72, 821–829. doi: 10.1080/14620316.1997.11515576

Moco, S., Capanoglu, E., Tikunov, Y., Bino, R. J., Boyacioglu, D., Hall, R. D., et al. (2007). Tissue specialization at the metabolite level is perceived during the development of tomato fruit. *J. Exp. Bot.* 58, 4131–4146. doi: 10.1093/jxb/erm271

Nardozza, S., Gamble, J., Axten, L. G., Wohlers, M. W., Clearwater, M. J., Feng, J., et al. (2011). Dry matter content and fruit size affect flavour and texture of novel *Actinidia deliciosa* genotypes. *J. Sci. Food Agric.* 91, 742–748. doi: 10.1002/jsfa.4245

Ntagkas, N., De Vos, R. C. H., Woltering, E. J., Nicole, C. C. S., Labrie, C., and Marcelis, L. F. M. (2020). Modulation of the tomato fruit metabolome by LED light. *Metabolites* 10, 266. doi: 10.3390/metabo10060266

Palmer, W. M., Ru, L., Jin, Y., Patrick, J. W., and Ruan, Y. L. (2015). Tomato ovary-to-fruit transition is characterized by a spatial shift of mRNAs for cell wall invertase and its inhibitor with the encoded proteins localized to sieve elements. *Mol. Plant* 8, 315–328. doi: 10.1016/j.molp.2014.12.019

Paponov, M., Arakelyan, A., Dobrev, P. I., Verheul, M. J., and Paponov, I. A. (2021). Nitrogen deficiency and synergism between continuous light and root ammonium supply modulate distinct but overlapping patterns of phytohormone composition in xylem sap of tomato plants. *Plants* 10, 573. doi: 10.3390/plants10030573

Paponov, M., Kechasov, D., Lacek, J., Verheul, M. J., and Paponov, I. A. (2020). Supplemental light-emitting diode inter-lighting increases tomato fruit growth through enhanced photosynthetic light use efficiency and modulated root activity. *Front. Plant Sci.* 10. doi: 10.3389/fpls.2019.01656

Peeters, A. J. M., and Welles, G. W. H. (2005). "Greenhouse tomato production," in *Tomatoes*. Ed. E. Heuvelink (UK: CABI Publishing), 257–304.

Pek, Z., Szuvandzsiev, P., Nemenyi, A., Helyes, L., and Lugasi, A. (2011). The effect of natural light on changes in antioxidant content and color parameters of vine-ripened tomato (*Solanum lycopersicum* L.) fruits. *Hortscience* 46, 583–585. doi: 10.21273/hortsci.46.4.583

Rana, N., Kumar, M., Walia, A., and Sharma, S. (2014). Tomato fruit quality under protected environment and open field conditions. *Int. J. Bio-Resour Stress Manag* 5, 422. doi: 10.5958/0976-4038.2014.00592.2

Ryle, G. J. A., Powell, C. E., and Gorddon, A. J. (1981). Patterns of 14C-labelled assimilate partitioning in red and white clover during vegetative growth. *Ann. Bot.* 47, 505–514. doi: 10.1093/oxfordjournals.aob.a086046

Saha, P., Das, N. R., Deb, P., and Suresh, C. P. (2009). Effect of NAA and GA3 on yield and quality of tomato (*Lycopersicon esculentum* Mill.). *Environ. Ecol.* 27, 1048–1050. doi: 10.1016/j.jafr.2022.100450

Serio, F., Gara, L. D., Caretto, S., Leo, L., and Santamaria, P. (2004). Influence of an increased NaCl concentration on yield and quality of cherry tomato grown in posidonia (*Posidonia oceanica* (L) Delile). *J. Sci. Food Agric.* 84, 1885–1890. doi: 10.1002/jsfa.1883

Slimestad, R., and Verheul, M. (2009). Review of flavonoids and other phenolics from fruits of different tomato (*Lycopersicon esculentum* Mill.) cultivars. *J. Sci. Food Agric.* 89, 1255–1270. doi: 10.1002/jsfa.3605

Stewart, A. J., Bozonnet, S., Mullen, W., Jenkins, G. I., Lean, M. E. J., and Crozier, A. (2000). Occurrence of flavonols in tomatoes and tomato-based products. *J. Agric. Food Chem.* 48, 2663–2669. doi: 10.1021/jf000070p

Van De Wal, B., Van De Put, H., Hanssens, J., and Steppe, K. (2017). Modelling the effects of osmotic stress on tomato fruit development. *Acta Hortic.* 1154, 201–206. doi: 10.17660/ActaHortic.2017.1154.26

Vargas, P., Duarte, L., Silva, E., Zecchini, A., Soares, R., and Grava De Godoy, L. (2017). Performance of mini-tomato hybrids in different training systems with different number of stems. *Hortic. Bras.* 35, 428–433. doi: 10.1590/s0102-053620170319

Verheul, M. J., Maessen, H. F. R., Paponov, M., Panosyan, A., Kechasov, D., Naseer, M., et al. (2022). Artificial top-light is more efficient for tomato production than inter-light. *Sci. Hortic.* 291, 110537. doi: 10.1016/j.scienta.2021.110537

Zhang, C. X., and Whiting, M. D. (2011). Improving 'Bing' sweet cherry fruit quality with plant growth regulators. *Sci. Hortic.* 127, 341–346. doi: 10.1016/j.scienta.2010.11.006

Zhao, D., Mackown, C. T., Starks, P. J., and Kindiger, B. K. (2010). Rapid analysis of nonstructural carbohydrate components in grass forage using microplate enzymatic assays. *Crop Sci.* 50, 1537–1545. doi: 10.2135/cropsci2009.09.0521

Zhou, R., Cutler, A. J., Ambrose, S. J., Galka, M. M., Nelson, K. M., Squires, T. M., et al. (2004). A new abscisic acid catabolic pathway. *Plant Physiol.* 134, 361–369. doi: 10.1104/pp.103.030734

frontiers | Frontiers in Plant Science

TYPE Original Research
PUBLISHED 26 October 2023
DOI 10.3389/fpls.2023.1289120

OPEN ACCESS

EDITED BY
Qingming Li,
Chinese Academy of Agricultural Sciences, China

REVIEWED BY
Chang Liu,
Mississippi State University, United States
Tao Li,
Chinese Academy of Agricultural Sciences, China
Feng Wang,
Shenyang Agricultural University, China

*CORRESPONDENCE
Yan Li
edmonlee@hotmail.com

RECEIVED 05 September 2023
ACCEPTED 09 October 2023
PUBLISHED 26 October 2023

CITATION
Gao J, Dou Y, Wang X, Zhang D, Wei M and Li Y (2023) Transcriptome analysis reveals the mechanism for blue-light–induced biosynthesis of delphinidin derivatives in harvested purple pepper fruit. *Front. Plant Sci.* 14:1289120. doi: 10.3389/fpls.2023.1289120

Transcriptome analysis reveals the mechanism for blue-light–induced biosynthesis of delphinidin derivatives in harvested purple pepper fruit

Jinhui Gao[1], Yuwei Dou[1], Xiaotong Wang[1], Dalong Zhang[1,2], Min Wei[1,2] and Yan Li[1,2]*

[1]College of Horticultural Science and Engineering, Shandong Agricultural University, Tai'an, Shandong, China, [2]Scientific Observing and Experimental Station of Environment Controlled Agricultural Engineering in Huang-Huai-Hai Region, Ministry of Agriculture, Tai'an, Shandong, China

Anthocyanins are the main pigments that affect the color and quality of purple-fruited sweet pepper (*Capsicum annuum*). Our previous study indicated that blue light can induce anthocyanin accumulation in purple pepper. In view of its underlying mechanism that is unclear, here, anthocyanin content was determined, and transcriptome analysis was performed on pepper fruits harvested from different light treatments. As a result, among the identified anthocyanin metabolites, the levels of delphinidin (Dp) glycosides, including Dp-3-*O*-rhamnoside, Dp-3-*O*-rutinoside, and Dp-3-*O*-glucoside, were highly accumulated in blue-light–treated fruit, which are mainly responsible for the appearance color of purple pepper. Correlation between anthocyanin content and transcriptomic analysis indicated a total of 1,619 upregulated genes were found, of which six structural and 12 transcription factor (TF) genes were involved in the anthocyanin biosynthetic pathway. Structural gene, for instance, *CaUFGT* as well as TFs such as *CaMYC2-like* and *CaERF113*, which were highly expressed under blue light and presented similar expression patterns consistent with Dp glycoside accumulation, may be candidate genes for anthocyanin synthesis in response to blue-light signal.

KEYWORDS

light spectrum, blue light, purple pepper, delphinidin derivatives, transcriptomic

1 Introduction

Peppers (*Capsicum annuum* L.) are one of the world's most important vegetables and are favored by consumers for their vibrant color and nutritional benefits. The color of pepper fruit is influenced by the pigment content of chlorophylls, carotenoids, anthocyanins, etc., (Liu et al., 2022b). Among them, anthocyanins not only are an important factor in promoting fruit coloration but also have a rich nutritional and

medicinal value (Liu et al., 2018b; Colanero et al., 2020; Sun et al., 2023). The different color-fruited genotypes of pepper have shown variation in kinds and content of anthocyanins (Lightbourn et al., 2007; Tang et al., 2020; Guo et al., 2021), among which delphinidin (Dp) derivatives were found to make a major contribution to the purple color formation of unripe pepper fruit in our previous study (Wang et al., 2022b).

Anthocyanin is the final product of flavonoids pathway, the biosynthesis of this metabolite has been clarified in many crops, and it was also well studied in pepper (Aguilar-Barragán and Ochoa-Alejo, 2014; Liu et al., 2018b; Meng et al., 2022; Xie et al., 2022). The structural genes associated with the anthocyanin biosynthetic pathway are usually divided into early (EBGs) and late biosynthetic genes (LBGs). Of the latter cluster, flavonoid 3′,5′ hydroxylase (*F3′5′H*), dihydroflavonol 4-reductase (*DFR*), anthocyanidin synthase (*ANS*), and uridine 5′-diphosphate (UDP)-glucose: flavonoid 3-O-glucosyltransferase (*UFGT*) are essential for producing Dp glycosides, which determines the purple color (Tanaka and Brugliera, 2013; Naing and Kim, 2018). In addition, previous studies indicated that the transcription of LBGs is activated by several transcription factors (TFs), including NAM-ATAF1/2-CUC2 (NAC), basic leucine zipper (bZIP), and ethylene-responsive factor (ERF) families, along with MYB-bHLH (basic helix-loop-helix)-WD40 (WD40-repeat proteins) (MBW) complex, within which the activation or repression is mainly determined by v-myb avian myeloblastosis viral oncogene homolog (MYB) (Liu et al., 2016; Liu et al., 2018b).

Light is one of the most critical environmental factors regulating anthocyanin biosynthetic pathway (Guo et al., 2022; Li et al., 2023). In addition to light intensity, light spectrum, especially blue light, has been demonstrated to regulate anthocyanin accumulation (Liu et al., 2022b; Lee and Kim, 2023). For instance, the elevated anthocyanin accumulation was found concurrently when exposed to blue light and overexpressed *CRY1a* in tomato fruit (Liu et al., 2018a), and the anthocyanin levels from postharvest purple pepper fruit were enhanced with a higher fraction of blue light (Liu et al., 2022b). Moreover, blue light could induce the expression of downstream anthocyanin synthesis structural genes through cryptochrome (CRY)-constitutive photomorphogenesis protein 1 (COP1)-MYB and/or -elongated hypocotyl 5 (HY5), which, in turn, accelerating anthocyanin accumulation in eggplant (Jiang et al., 2016), red pear (Tao et al., 2018), and petunia petals (Fu et al., 2020).

Anthocyanin accumulation is essential for the fruit quality of purple pepper, and our previous study showed that blue light could promote anthocyanin synthesis more than white light in purple pepper (Wang et al., 2022b). Although multiple TF and structural genes involved in anthocyanin biosynthesis have been well studied, the molecular mechanism of blue light regulating anthocyanin synthesis in purple pepper remains unclear. In the present study, we thus performed transcriptome analysis to characterize the potential transcripts involved in the anthocyanin accumulation in postharvest pepper fruit irradiated under blue light. These findings may expand our understanding of the molecular mechanism of blue light in regulating pepper anthocyanin biosynthesis.

2 Materials and methods

2.1 Plant materials and experimental conditions

The experiment was performed from April to September 2021, and the purple-fruited pepper cultivar (*Capsicum annuum* cv. Amethyst) was planted in a growth chamber, where the average air temperature, relative humidity, photoperiod, and CO_2 concentration is 400 mmol mol-1 were 26°C/18°C (day/night), 70%, 14 h/10 h, respectively. The pepper plants were irradiated with white light LED at the photosynthetic photon flux density (PPFD) of 200 µmol m^{-2} s^{-1} (Figure 1A). In our previous study, the total content of anthocyanins and expression levels of key structure genes involved in the anthocyanin biosynthesis were determined in

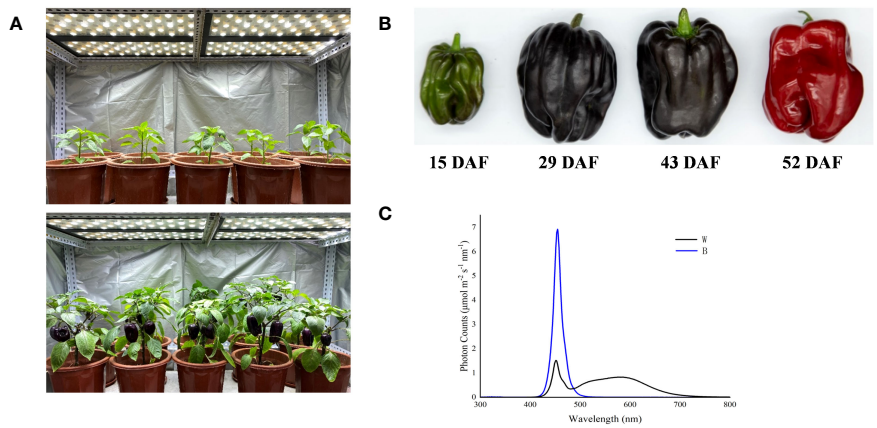

FIGURE 1
Spectral light treatments of purple pepper plants and fruits. **(A)** Purple pepper plants grown under white light before treatment. **(B)** Developmental stages of pepper fruit: 15 DAF, small unripe green fruit; 29 DAF, large unripe purple fruit; 43 DAF, ripening purple fruit; 52 DAF, fully ripening red fruit. **(C)** Spectral distribution of light treatments irradiated on purple pepper fruits. DAF, day after flowering; W, white light; B, blue light.

pepper fruits, which harvested at different ripening stages of 15, 29, 43, and 52 days after flowering (DAF; Figure 1B) and then irradiated under white and blue light for 4 h. These parameters were found to be enhanced significantly at 29 DAF (Wang et al., 2022b). Therefore, in this study, the defect-free fruits with similar size and setting position were harvested at 29 DAF and randomly divided into two groups. Subsequently, all fruits were transferred and irradiated under blue (457.2 nm) and white (control) LED light sources (Figure 1C) with a PPFD of 200 μmol m^{-2} s^{-1}, and the peel was subsequently collected at different treatment duration of 0 h, 2 h, 4 h, 8 h, 12 h, and 24 h with three replicates (at least three fruits for each replicate per sampling stage). Fruit peels were manually separated by using surgical scalpel blades, avoiding as much as possible to collect flesh material. Each peel sample was constituted of 2-cm-wide and 1-mm-thick skin taken from the equatorial part, then immediately frozen in liquid nitrogen, and stored at −80°C.

2.2 Determination of anthocyanin content

In our previous study, the metabolite profiling of pepper fruits at different ripening stages of 15, 29, 43, and 52 DAF irradiated by white and blue spectrum for 4 h was performed using a targeted metabolome method by Wuhan Metware Biotechnology Co., Ltd. (Wuhan, China), and most anthocyanins were found to be enriched at 29 DAF. In the present study, pepper peels were thus sampled from fruit at 29 DAF with different treatment duration of 0 h, 2 h, 4 h, 8 h, 12 h, and 24 h as well as with 4 h of white and blue-light treatment for determination of total anthocyanin content and quantification of anthocyanins, respectively. To measure total anthocyanins according to Liu et al. (2022b) with some modifications, each 0.5-g peel tissue sample was combined with 0.5% hydrochloric acid methanol reagent, vortexed, and incubated at 40°C for 40 min. Then, the samples were centrifuged at 10,000 g for 5 min at 4°C, and the supernatants were collected. The absorbance of samples was measured at 530 nm, 620 nm, and 650 nm, respectively, using an ultraviolet-visible spectrophotometer (UV-5500, Bilon Instrument Co., Ltd., Shanghai, China). Total anthocyanin content was calculated according to the following formula: (1) $\triangle OD = (OD_{530} - OD_{620}) - 0.1 \times (OD_{650} - OD_{620})$ and (2) anthocyanin content = $(\triangle OD \times V \times 10^6) / (\xi \times m)$, where V is the dilution volume, ξ is the molar absorption coefficient, and m is the fresh weight of sample.

To quantify the most abundant anthocyanin, the freeze-dried samples were crushed, and 50 mg of powdered tissue was extracted overnight at 4°C in 500 μL of 50% aqueous methanol. Following centrifugation at 12,000 g under 4°C for 3 min. Then, these extracts were absorbed, filtrated, and analyzed by an ultra-performance liquid chromatography with tandem mass spectrometry (UPLC-MS/MS. UPLC, Shim-pack UFLC SHIMADZU CBM30A, Shimadzu Scientific Instruments, Inc., Kyoto, Japan; MS, Applied Biosystems 6500 Triple Quadrupole, AB SCIEX, Framingham, USA) system. Analytical conditions were as follows: HPLC column, Waters ACQUITY BEH C18 (1.7 μm, 2.1 mm × 100 mm, Milford, USA). The mobile phase comprised solvent A (ultrapure water, 0.1% formic acid) and solvent B (methanol, 0.1% formic acid). Gradient programs were as follows: solvent A:solvent B (v:v), 95:5 at 0 min, 50:50 at 6 min, 5:95 at 12 min, maintained at 2 min, 95:5 at 14 min, and maintained at 2 min. The flow rate, column temperature, and injection volume were set as 0.35 mL/min, 40°C, and 2 μL, respectively. The effluent was alternatively connected to the Q-Trap 6500 equipped with an electrospray ionization (ESI) according to Liu et al. (2020). The MS parameters mainly including 550°C of ESI source temperature, 5,500 V for ion spray voltage floating, and 35 psi of curtain gas. In Q-Trap 6500, each ion pair was scanned on the basis of the optimized declustering potential and collision energy.

2.3 Expression of anthocyanin biosynthetic genes

Total RNA was extracted from fruit harvested at 29 DAF with treatment duration of 0 h, 2 h, 4 h, 8 h, 12 h, and 24 h under white and blue light by the Quick RNA Isolation Kit (Huayueyang Biological Technology Co., Ltd., Beijing, China). Reverse transcription was performed with the ReverTra Ace qPCR RT-Kit (Toyobo Bio-Tech, Co., Ltd., Toyobo, Japan). Expression of structural genes involved in the anthocyanin biosynthesis was conducted by employing quantitative real-time PCR (qRT-PCR) under the following programs: 95°C for 30 s, followed by 40 cycles of 95°C for 15 s, 60°C for 30 s, and 95°C for 15 s. The relative expression levels of the genes were analyzed by the $2^{-\Delta\Delta Ct}$ method (Livak and Schmittgen, 2001). The information of the primers used for the qRT-PCR is given in Table 1.

2.4 Transcriptome sequencing and data analysis

Transcriptome sequencing and Library preparation were conducted by Wuhan Metware Biotechnology Co., Ltd. (Wuhan, China). Total RNA was extracted from the same peel powder, which collected from fruits at 29 DAF irradiated by 0 h, 2 h, and 4 h of white and blue light, to construct an mRNA library, and sequenced on the Illumina HiSeq 4000 platform. After raw data filtering, sequencing error rate checking, and guanine-cytosine (GC) content distribution detection, clean reads for subsequent analysis were obtained, and, then, the clean reads were mapped to the pepper reference genome (Zunlal v1.0) using HISAT2 (Kim et al., 2015). On the basis of the raw data, screening for differentially expressed genes (DEGs) was performed using DESeq2 software. Gene expression levels were assessed on the basis of the fragments per kilobase of transcript per million fragments mapped reads (FPKM) method. Genes meeting the threshold of $|\log_2 \text{fold change}| \geq 1$ and false discovery rate < 0.05 were defined as the DEGs and were subjected to Gene Ontology (GO) and Kyoto Encyclopedia of Genes and Genomes (KEGG) enrichment analysis.

2.5 Validation of DEGs by qRT-PCR

To validate the results obtained from transcriptome sequencing, qRT-PCR analysis was performed. Samples were collected from

TABLE 1 Sequences of primers for RT-qPCR.

Gene	Forward primer sequence (5′-3′)	Reverse primer sequence (5′-3′)	Gene ID
CaCHI	CCTTGCTGGTGCAGGGATTA	GGAACGGCACTCTCTTCCAT	LOC107871144
CaF3H	AGGCAGTAATGGATGAGCCC	CTCAATGGGCATGGATTCCAAC	LOC107859880
CaF3′5′H	GGCCTACAATGCCCAAGACA	ATATCCGCCACCACAACGC	LOC107848667
CaDFR	CGGCTGGATTTATCGGCTCT	CTTCCACGGTCAAGTCTGCT	LOC107860031
CaANS	TTCTCCTCCCAGACACCGAT	AATCACTCTGTGCTCCACGC	LOC107843451
CaUFGT	AAACAAGGCAATGACACCCC	TTCCTCCTCTGCCTCTTTCA	LOC107867844
CaMYB1R1	ATGGACGGAGGTGGAGC	GGCGACGATTGAGGTTAGT	LOC107862462
CabHLH13	AATGTGAAGCCAGTGAA	ACAACAGCTCGTAATGC	LOC107854119
CaERF113	AGGGAGCGGGAGAAGAC	TGGGCATACTGGAGAAGGT	LOC107858557
CaMYC2-like	AGAAAGGCAAAAGCAGCAGG	TGGTTCAAAGGCGTTTCACG	LOC107845814
Actin	GTCCTCTTCCAACCATCCAT	TACTTTCTCTCTGGTGGTGC	LOC107850541

fruits at 29 DAF irradiated by 0 h, 2 h, and 4 h of white and blue light, and seven genes involved in light response and anthocyanin synthesis were selected. Actin was used as an internal reference gene for gene expression correction, and the sequences of primers are listed in Table 1. qRT-PCR was performed in triplicate using a Roche LightCycler 480 fluorescent PCR system (Roche, Basel, Switzerland) and a MagicSYBR Mixture fluorescent dye kit (Kangwei Century Biotechnology Co., Ltd., Beijing, China) using the same programs and method as those used for structural gene expression.

2.6 Statistical analysis

The experimental data were processed using SPSS 22.0 (SPSS Inc, Chicago, USA), and Duncan's test was performed by employing one-way ANOVA. The significance level was set at $p < 0.05$.

3 Results

3.1 Anthocyanin accumulation and expression of anthocyanin biosynthetic genes in purple pepper under blue light

In our previous study, the most abundant anthocyanin in pepper fruit at different ripening stages under white and blue light was identified as Dp glycosides, which accounted for 94.70% of the total anthocyanin content, followed by glycosides of petunidin (Pt), cyanidin (Cy), pelargonidin (Pg), peonidin, and malvidin (Figure 2). Moreover, these metabolites were found to be highly accumulated in fruit at 29 DAF. In this study, we determined the total anthocyanin content and structural genes involved in anthocyanin biosynthesis in pepper fruit at this ripening stage with treatment duration of 0 h, 2 h, 4 h, 8 h, 12 h, and 24 h. It was indicated that the total anthocyanin content increased over time under both spectrum treatment (Figure 3), and the level was significantly higher in fruit under blue light than that of fruit under white at 4 h, 12 h, and 24 h ($P < 0.05$). The transcript abundance of anthocyanin biosynthetic genes was also hardly affected (Figure 4). Compared with white light, the structural genes, especially *CaF3′5′H* and *CaUFGT*, were significantly upregulated at 4 h of blue-light treatment. This indicates that the genes related to anthocyanin synthesis in purple pepper are regulated by blue light, and a short period of blue-light irradiation can affect their expression levels.

We thus investigated the levels of primary anthocyanins, including Dp, Pt, Cy, and Pg derivatives in pepper fruit at 29 DAF treated with 4 h of blue light in the present study (Figure 5). The Dp glycosides mainly consisted of Dp-3-*O*-rhamnoside, Dp-3-*O*-rutinoside, and Dp-3-*O*-glucoside, which were specifically accumulated in both blue- and white-light–irradiated pepper fruit than those of Dp-3-*O*-(6"-*O*-malonyl)-beta-D-glucoside and Dp-3,5-*O*-diglucoside. The concentration of Pt-3-*O*-rutinoside, Cy-3-*O*-glucoside, and Pg-3-*O*-rutinoside was significantly lower relative to the Dp glycosides from fruit irradiated by both spectrum. Moreover, all these metabolites were evidently enhanced by blue light in comparison with white light ($P < 0.05$).

3.2 Summary of mRNA sequencing

To investigate the mechanism of anthocyanin synthesis regulated by blue light in postharvest purple peppers, mRNA sequencing was used to analyze the DEGs. Among the total nine sequencing samples, each sample produced 4.51-Gb clean reads on average. Q30 values were distributed between 93.23% and 94.14%. GC content was distributed between 41.17% and 42.11%. Mapping clean reads to the specified pepper reference genome (Pepper_Zunla_1_Ref_v1.0 version), the average mapping ratios of these sequencing samples were 94.12% (Table 2). This indicated that the selected reference genome was adequate for subsequent analysis. A total of 2,052 and 3,276 DEGs were screened, of which 1,279 and 1,619 upregulated genes as well as 773 and 1,657 downregulated genes were screened at 2 h and 4 h, respectively (Figures 6A, C). We obtained 3,276 DEGs

10.3389/fpls.2023.1289120

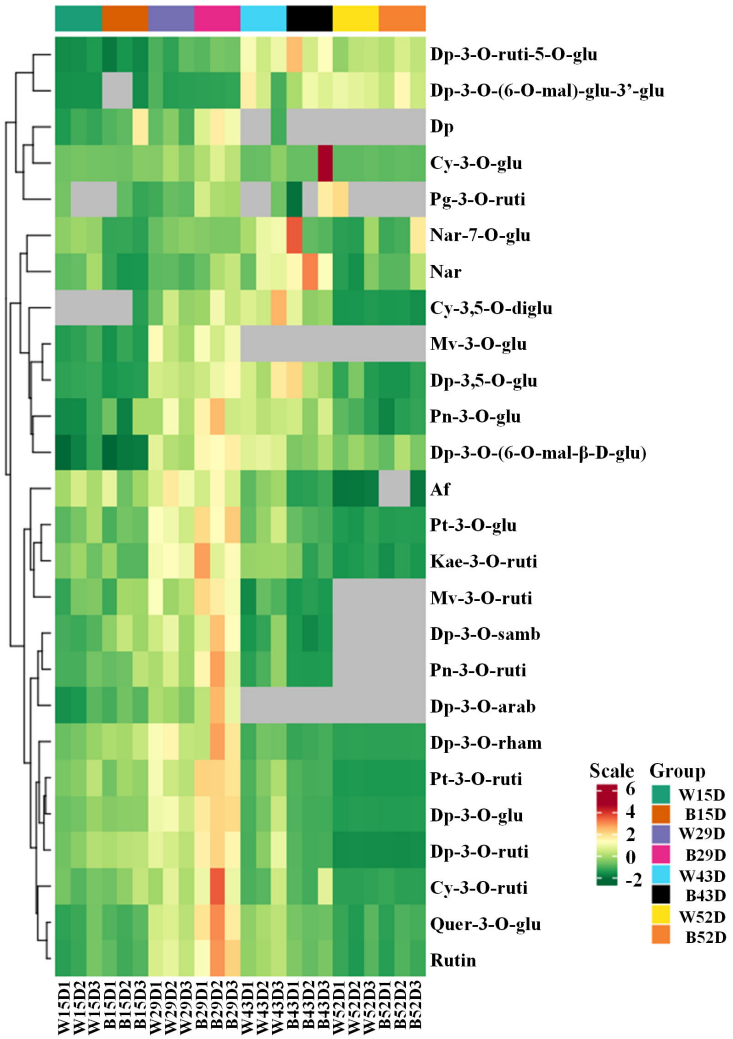

FIGURE 2
Cluster analysis of anthocyanins in the peel of purple pepper fruit at 15, 29, 43, and 52 DAF under white and blue light for 4 h. DAF, day after flowering; W, white light; B, blue light; Dp, delphinidin; Cy, cyanidin; Pg, pelargonidin; Nar, naringenin; Mv, malvidin; Pn, peonidin; Af, afzelin; Pt, petunidin; Kae, kaempferol; Quer, quercetin; Rutin, rutin; ruti, rutinoside; glu, glucoside; mal, malonyl; diglu, diglucoside; samb, sambubioside; arab, arabinoside; rham, rhamnoside.

from the samples and screened 1,479 genes (Figure 6B). Furthermore, the correlation was above 84% for all nine sequenced samples (Supplementary Figure 1).

3.3 GO and KEGG functional enrichment analysis

Functional annotation of DEGs through the GO database identified 51 important functional categories, including biological process, molecular function, and cellular component. Compared with 0 h, the GO entries annotated for 2 h and 4 h of blue-light treatment were mainly for processes such as biosynthesis of secondary metabolites, stress response, transmembrane transport, and transcriptional regulatory activity (Figure 6D). As anthocyanins are secondary metabolites, they are important parts of the metabolic pathway. The anthocyanins were unstable and need to be transferred to the vesicles for storage. Therefore, anthocyanin accumulation is related to transporter protein activity. Second, in this study, we focused on blue-light–induced anthocyanin accumulation. The previous study indicated that the effect of light on anthocyanin synthesis involves light signal transduction and transcriptional regulation processes. In conclusion, we focused on the functional groups of metabolic processes (GO:0008152), signal transduction (GO:0023052), transcriptional regulatory activity (GO:0140110), transporter protein activity (GO:0005215), and stress response (GO:0050896).

The DEGs were used to make KEGG pathway enrichment analysis and were found to be significantly enriched in metabolic pathway (ko01100), secondary metabolite biosynthesis (ko01110), plant circadian movements (ko04712), and plant mitogen-activated protein kinase (MAPK) signaling pathways (ko04016) as well as phytohormone signaling (ko04075) (Supplementary Figure 2). Furthermore, 20 significantly different pathways were selected

10.3389/fpls.2023.1289120

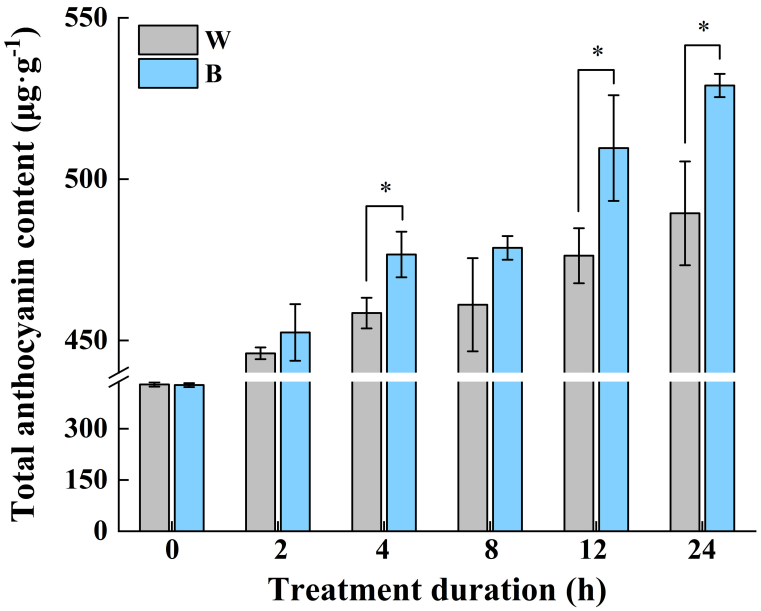

FIGURE 3
Changes of total anthocyanin content in purple pepper fruit at 29 DAF with treatment duration of 0 h, 2 h, 4 h, 8 h, 12 h, and 24 h under white and blue light. Anthocyanin levels are indicated as the mean ± SD of three biological replicates. DAF, day after flowering; W, white light; B, blue light. *$p < 0.05$.

(Figure 6E). As important parts of environmental adaptation and biosynthesis of secondary metabolites, circadian rhythm pathway (ko04712), flavonoid biosynthesis pathway (ko00941), and anthocyanin biosynthesis pathway (ko00942) were selected, which were associated with light response and anthocyanin synthesis, respectively. Genes associated with light response and anthocyanin biosynthesis were screened against selected DEGs enriched for the KEGG pathway and combined with GO functional annotation. Twenty-four genes showed expressional differences in pathways of circadian rhythm, flavonoid biosynthesis, and anthocyanin biosynthesis, which contained three genes involved in light response and six structural genes associated with anthocyanin biosynthesis, such as *CaLHY*, *CaCHI*, *CaDFR*, *CaLDOX*, and *CaUFGT* (Table 3).

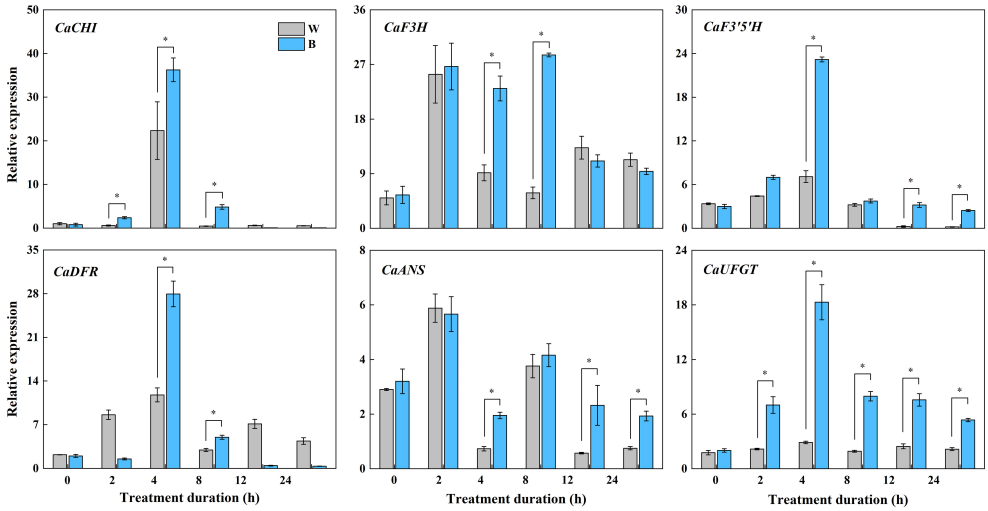

FIGURE 4
Expression variations of structural genes involved in anthocyanin synthesis in purple pepper fruit at 29 DAF with treatment duration of 0 h, 2 h, 4 h, 8 h, 12 h, and 24 h under white and blue light. Relative expression is indicated as the mean ± SD of three biological replicates. DAF, day after flowering; W, white light; B, blue light; CHI, chalconeisomerase; F3H, flavanone-3-hydroxylase; F3′5′H, flavonoid 3′,5′ hydroxylase; DFR, dihydroflavonol 4-reductase; ANS, anthocyanidin synthase; UFGT, UDP-glucose: flavonoid 3-O-glucosyltransferase. *$p < 0.05$.

10.3389/fpls.2023.1289120

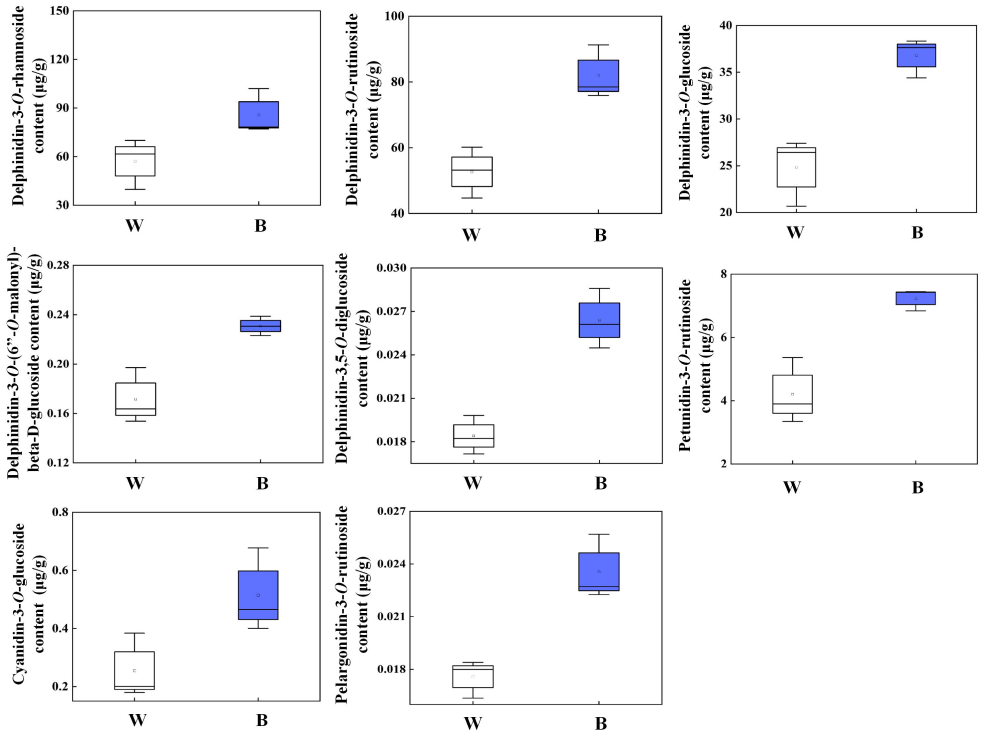

FIGURE 5
Different kinds of anthocyanin accumulation in purple pepper fruit at 29 DAF with 4 h of white and blue-light irradiation. Anthocyanin levels are indicated as the mean ± SD of three biological replicates. DAF, day after flowering; W, white light; B, blue light.

3.4 The selection of TFs and validation of transcriptome sequencing by qRT-PCR

The expression of structural genes involved in anthocyanin biosynthesis is regulated by upstream TFs. Thus, TF associated with light signaling and anthocyanin synthesis must be existed. In our study, a total of 50 and 103 genes were defined as TFs for the 2 h and 4 h of treatments, respectively, which classified into 13 and 19 TF families, among which ERF family was the largest, followed by bHLHs and MYBs (Figure 7).

The gene functions derived from ERFs mainly in ethylene response and take participate in plant secondary metabolites biosynthesis. We found that eight and five genes were upregulated, and three and fifteen genes were downregulated from ERFs in purple pepper peel after 2 h and 4 h of exposure of blue light relative to 0 h, respectively. Comparison of FPKM values for upregulated genes revealed

TABLE 2 Quality evaluation of sample sequencing output data.

Sample	Reads Sum	≥ Q30 (%)	GC Content (%)	Mapped Ratio (%)
0h1	43,839,658	94.12	41.45	94.46
0h2	45,492,834	94.14	41.89	94.75
0h3	43,250,106	93.67	41.30	94.16
2h1	44,594,684	93.23	42.11	94.48
2h2	43,014,342	93.34	41.43	93.90
2h3	42,465,108	93.89	41.49	94.21
4h1	55,414,632	93.87	41.58	94.10
4h2	43,301,086	93.68	41.17	93.08
4h3	44,140,764	93.52	41.71	93.94
Average	45,057,023.78	93.72	41.57	94.12

Note reads sum, total number of paired-end reads in clean data; ≥ Q30, the percentage of bases with a clean data quality score of 30 or higher; GC content, the percentage of G and C bases in clean data with respect to the total bases; mapped ratio, the mapped to the reference genome reads as a percentage of total reads.

10.3389/fpls.2023.1289120

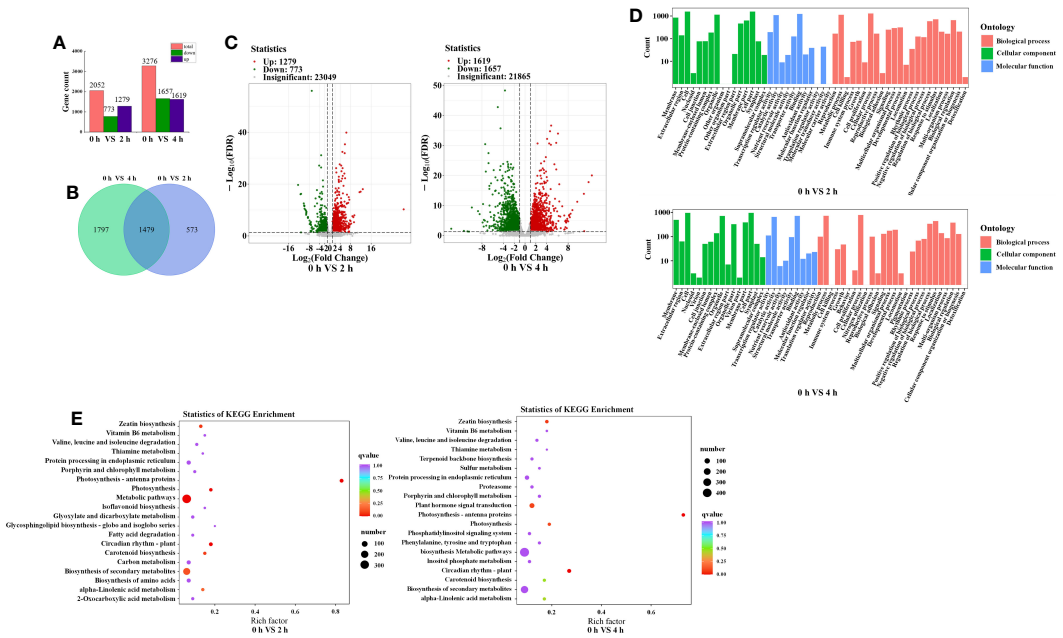

FIGURE 6
Comprehensive analysis of transcriptome data. **(A)** Number of DEGs identified by transcriptome sequencing analysis in purple pepper fruit with 2 h and 4 h of blue-light irradiation. **(B)** Venn diagram depicting numbers of DEGs. **(C)** Volcano plots of the DEGs between 0 h versus 2 h and 0 h versus 4 h. **(D)** GO enrichment analysis of the DEGs between 0 h versus 2 h and 0 h versus 4 h. **(E)** 20 tops of KEGG enrichment analysis of the DEGs between 0 h versus 2 h and 0 h versus 4 h. The ordinate represents KEGG pathway, and the abscissa represents rich factor. The larger the rich factor, the greater the degree of enrichment. The larger the point, the greater the number of differentially enriched genes in the pathway. The redder the dot, the more significant the enrichment. DEGs, differentially expressed genes; GO, Gene Ontology; KEGG, Kyoto Encyclopedia of Genes and Genomes.

significant differences in *ERF113-like* (LOC107858557), *ABR1-like* (LOC107867626), *ERF54* (LOC107855040), and *ERF5-like* (LOC107871072) at both 2 h and 4 h of treatments (Figure 8A). However, *RAV1* (LOC107847951), *ERF27-like* (LOC107851517), *ERF16-like* (LOC107874934), and *ERF1-like* (LOC107872603) were significantly highly expressed only at the treatment of 2 h.

Many previous studies have been reported on the involvement of the MYB family in plant anthocyanin biosynthesis. In the present study, we found four upregulated genes and three downregulated genes from MYBs in purple pepper peel after 2 h and 4 h of irradiation under blue light relative to 0 h. Then, four upregulated MYB genes, including *MYB1R1-1* (LOC107862462), *MYB1R1-2* (LOC107868015), *MYB44-like* (LOC107869439), and *DIVARICATA* (LOC107862150) were further screened for analysis (Figure 8B). Among them, *MYB1R1-1* (LOC107862462) accumulated specifically under 2 h and 4 h of blue spectrum irradiation and was defined as *CaMYB1R1*. The expression level of *MYB44-like* (LOC107869439) was significantly upregulated under 2 h irradiation of blue light compared with 0 h, but there was almost no expression under 4 h of treatment.

TABLE 3 The detailed information of DEGs related to anthocyanin biosynthesis.

Gene name	Gene ID	log_2 FC	p-value	q-value
CaCHI	LOC107871144	−2.1375	$2.66828E^{-05}$	0.00084
CaDFR	LOC107860031	−2.5558	0.00027	0.00549
CaLDOX4	LOC107845999	4.8146	$9.35842E^{-06}$	0.00035
CaLDOX3	LOC107844833	4.2115	0.00055	0.00956
CaFLS	LOC107861925	1.489	0.00013	0.00311
CaUFGT	LOC107867844	2.5983	$7.06399E^{-05}$	0.00188
CaLHY	LOC107845265	−3.3882	$1.78769E^{-35}$	$7.43917E^{-32}$
CaAPRR5	LOC107862999	2.527	$5.00799E^{-10}$	$6.01151E^{-08}$
CaPRR37	LOC107850219	1.498	$1.5002E^{-12}$	$3.09562E^{-10}$

DEGs, differentially expressed genes; FC, fold change.

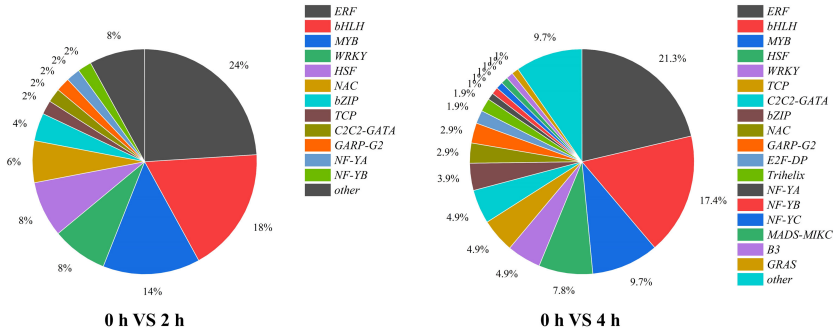

FIGURE 7
The proportion and types of transcription factors in purple pepper fruit with 2 h and 4 h of white and blue-light irradiation.

bHLH family TFs are also involved in anthocyanin biosynthesis. We found that eight DEGs in purple peppers under both 2 and 4 h of blue-light irradiation compared with white light. Among them, five genes were upregulated and three genes were downregulated. Further screening analysis of significant differences in expression levels of *UNE10* (LOC107845481), *MYC2-like* (LOC107845814), and *bHLH13-like* (LOC107854119) suggested that they were all significantly elevated under 2 h and 4 h of treatment (Figure 8C).

To confirm the reliability of RNA-seq data, three structural genes and four TFs were chosen, and their relative expression profiles were quantified using qRT-PCR (Figure 8D). The expression of the selected genes in transcriptome sequencing

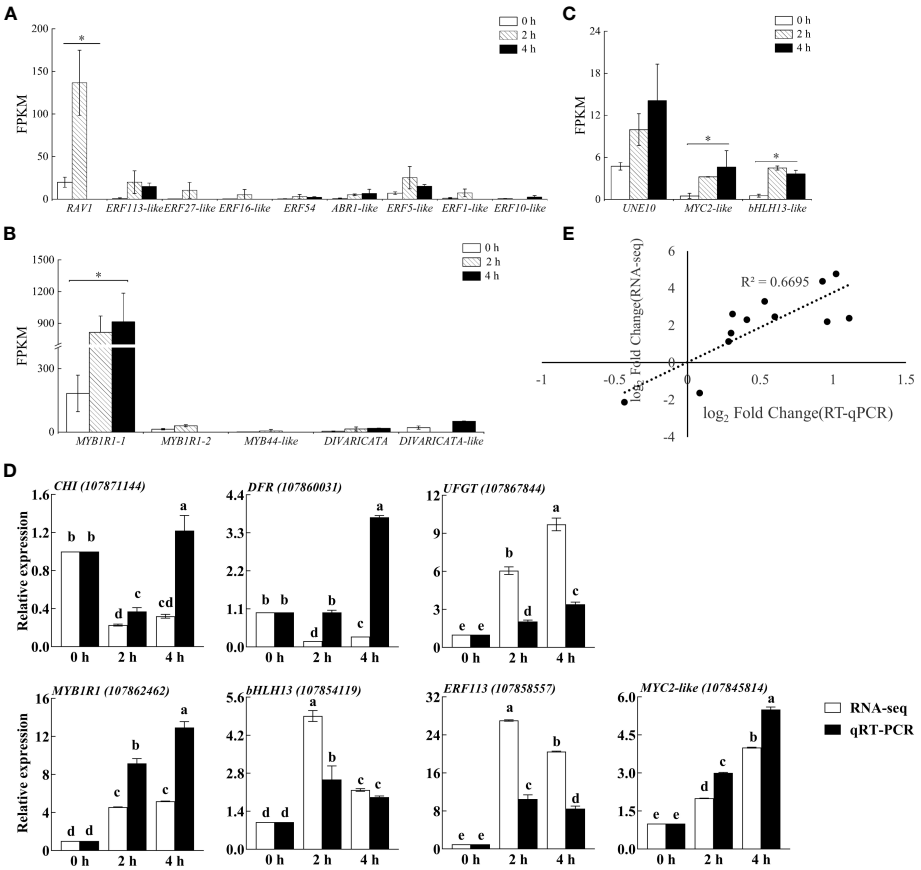

FIGURE 8
The FPKM verification of all transcription factors identified by transcriptome sequencing analysis in purple pepper fruit with 2 h and 4 h of white and blue-light irradiation, including families of **(A)** ERF, **(B)** MYB, and **(C)** bHLH. **(D)** Verification of relative expression levels of structural genes and transcription factors associated with the anthocyanin synthesis pathway in purple pepper fruit under 2 h and 4 h of white and blue-light irradiation. **(E)** Correlation analysis between transcript levels of qRT-PCR and transcriptome sequencing data. Relative expression is indicated as the mean ± SD of three biological replicates. FPKM, fragments per kilobase of transcript per million fragments mapped reads. Bars with different lowercase letters indicate significant differences at $p < 0.05$.

FPKM (log_2fold change) was correlated with the relative gene expression level log_2 ($2^{-\Delta\Delta Ct}$) values in qRT-PCR. The expression patterns of these genes obtained from qRT-PCR were highly consistent with those in the RNA-seq data (Figure 8E), suggesting that the results of RNA-seq were reliable.

4 Discussion

Anthocyanins are usually considered as a cause of purple pepper's color (Tang et al., 2020; Meng et al., 2022). It was reported that six common anthocyanins have been found and Dp derivatives are the predominant anthocyanins in purple *Solanaceous* vegetables (Liu et al., 2018b), specifically accumulated in purple pepper fruit (Meng et al., 2022; Wang et al., 2022b). In this study, the accumulation levels of these Dp glycosides particularly Dp-3-*O*-rhamnoside, Dp-3-*O*-rutinoside, and Dp-3-*O*-glucoside were positively correlated with the purple peel coloration, implying that these Dp derivatives mainly contribute to the purple color of pepper fruit (Liu et al., 2020). Furthermore, these compounds were most responsive to the blue-light irradiation relative to other Dp derivatives as well as the Pt, Cy, and Pg derivatives in comparison with white light, indicating that blue light mainly accelerates the postharvest fruit of purple pepper to appear purple-black color by promoting the accumulation of Dp-3-*O*-rhamnoside, Dp-3-*O*-rutinoside, and Dp-3-*O*-glucoside.

Existing findings reported that the transcript level of LBGs, such as *F3'5'H* and *UFGT*, coincides well with anthocyanin content and is significantly higher in pigmented compared with non-pigmented tissues, suggesting that variations in LBG expression determine the quantitative variation of anthocyanins in *Solanaceous* vegetables (Liu et al., 2018b). This was confirmed in our present study. Moreover, our validation results suggested that, compared with white light, the anthocyanin biosynthetic LBG, such as *CaUFGT* (Figure 8D), which is a key link in the formation of anthocyanin diversity, was separately regulated and highly responsive to blue light at both 2 h and 4 h of treatment. This led to the higher accumulation of anthocyanin exposed to blue spectrum compared with control fruits. Furthermore, the expression level of *CaF3'5'H*, the gene directing dihydroflavonol precursors to Dp compounds biosynthesis, was found to be highly upregulated under this wavelength (Figure 4). These changed the anthocyanin profile toward Dp derivatives in purple peppers under blue light (Samkumar et al., 2021).

In addition to structural genes, TFs, such as MYB, bHLH, and ERF families, are also the key factors in the regulation of anthocyanin metabolism in plants (Meng et al., 2022; Sun et al., 2023). A high number of DEGs representing ERF, MYB, and bHLH genes were found from our RNA-seq libraries, among which the expression levels of *CaMYC2-like* and *CaERF113* under both 2 h and 4 h of blue-light irradiation were validated through qRT-PCR, indicating that their regulation is strongly influenced by this light spectral quality. As a jasmonic acid (JA) signaling hub, MYC2 participates in anthocyanin synthesis in many crops (Li et al., 2018; Liu et al., 2022a). However, unlike the previous study in which MYC2 is a negative regulator of blue-light–induced photomorphogenesis (Yadav et al., 2005). *CaMYC2-like* was positively expressed correlated with variation tendency of key anthocyanin biosynthetic genes under 2 h and 4 h of blue-light spectrum treatment compared with white light in our present study, and this indicated its important role in anthocyanin biosynthetic pathway regulated by blue light (Liu et al., 2019).

It has been previously reported that *ERF* genes functioned as a transcriptional activator in promoting anthocyanin biosynthesis by interacting with related *MYB* genes to form the ERF-MYB protein complex or activating the transcription of anthocyanin biosynthetic genes, including *UFGT* (An et al., 2018; Chang et al., 2023). Furthermore, previous studies reported that the expression of *MYC2* was induced by JA in apple and activates the expression of *ACS1*, by upregulating the transcription of *ERF*, thereby promoting ethylene synthesis and fruit ripening (Li et al., 2017; Wang et al., 2022a). Thus, we speculated that CaMYC2-like was capable of combining directly with the *CaERF113* promoter to promote *CaACS1* transcription and facilitate pepper fruit ripening and coloring. On the other hand, CaERF113 could activate the promoters of downstream genes in the anthocyanin biosynthetic pathway of *CaUFGT*, ultimately accelerating anthocyanin accumulation in purple pepper fruit.

MYBs commonly combine with bHLHs to form a protein complex that participates in the regulation of anthocyanin biosynthesis. Previous study found that MYB can interact with bHLH to promote the activity of the *UFGT* promoter and anthocyanin biosynthesis (Starkevic et al., 2020). In this research, *CaMYB1R1* was differentially expressed under blue light from RNA-seq analysis. However, the qRT-PCR results of this gene were inconsistent with the RNA-seq analysis. Whether it acts as a major TF, which is influenced by blue light and subsequently contributing to the anthocyanin biosynthesis, needs further investigation. CRY is an important photoreceptor and can induce anthocyanin synthesis under blue light (Sun et al., 2020). Previous studies have reported the involvement of an indirect action module CRY-COP1-HY5 in photomorphogenesis (Tao et al., 2018; Wang et al., 2020). Therefore, we inferred that blue-light–CRY system plays important roles in regulation of anthocyanin synthesis in purple pepper. On the basis of our results, we conclude that CaMYC2-like facilitates the promotion of Dp glycosides accumulation by interacting with CaERF113 and increasing *CaUFGT* expression under blue light (Figure 9).

5 Conclusion

Transcriptome data were applied to illustrate the regulation metabolism of blue light on anthocyanin biosynthesis metabolic pathway in purple pepper fruit. Changes in anthocyanin metabolites, especially Dp glycosides, comprising Dp-3-*O*-rhamnoside, Dp-3-*O*-rutinoside, and Dp-3-*O*-glucoside, could be mainly responsible for the purple color. In addition, 12 TFs were also found to be potential contributors to anthocyanin metabolite biosynthesis regulated by blue light in pepper fruit. Correlation analysis of the changes in gene expression and transcriptome data suggested that blue-light spectrum could induce *CaMYC2-like* and

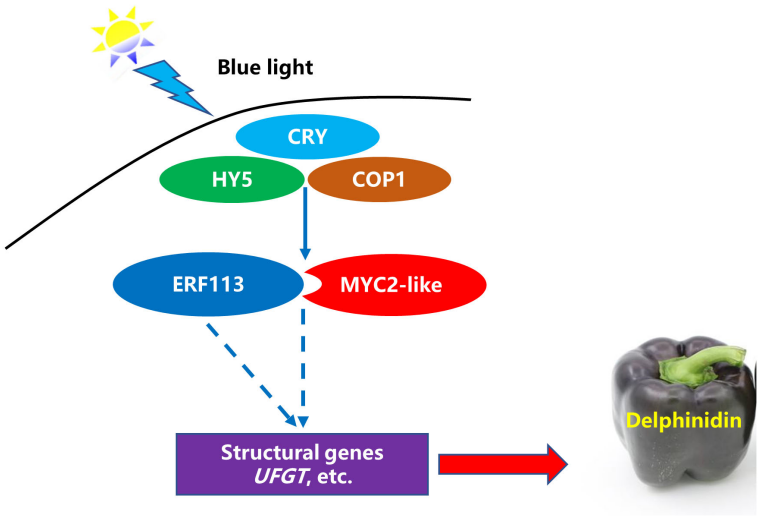

FIGURE 9
A possible model for blue-light–induced delphinidin derivatives biosynthesis in purple pepper fruit. The solid line indicates that the functional mechanism is clear, and the dotted line refers to the functional mechanism needs to be further studied.

CaERF113 expression to promote the accumulation of Dp glycosides. These results provided valuable information on the anthocyanin metabolites and the candidate genes involved in the anthocyanin biosynthesis pathways in pepper.

Data availability statement

The datasets presented in this study can be found in online repositories. The original data is publicly available at NCBI, PRJNA1014603.

Author contributions

JG: Conceptualization, Data curation, Investigation, Visualization, Writing – original draft. YD: Investigation, Methodology, Project administration, Software, Writing – original draft. XW: Investigation, Methodology, Project administration, Software, Writing – original draft. DZ: Validation, Writing – review & editing. MW: Validation, Writing – review & editing. YL: Conceptualization, Formal Analysis, Funding acquisition, Methodology, Resources, Supervision, Writing – original draft, Writing – review & editing.

Funding

The author(s) declare financial support was received for the research, authorship, and/or publication of this article. This work was supported by the Natural Science Foundation of Shandong Province (ZR2020MC148), National Natural Science Foundation of China (32272796), and China Agriculture Research System (CARS-23-C04).

Conflict of interest

The authors declare that the research was conducted in the absence of any commercial or financial relationships that could be construed as a potential conflict of interest.

Publisher's note

Supplementary material

The Supplementary Material for this article can be found online at: https://www.frontiersin.org/articles/10.3389/fpls.2023.1289120/full#supplementary-material

SUPPLEMENTARY FIGURE 1
Correlation chart of DEGs identified by transcriptome sequencing analysis in purple pepper fruit with 2 h and 4 h of white and blue-light irradiation. DEGs, differentially expressed genes.

SUPPLEMENTARY FIGURE 2
KEGG enrichment analysis of the DEGs between 0 h versus 2 h and 0 h versus 4 h. KEGG, Kyoto Encyclopedia of Genes and Genomes; DEGs, differentially expressed genes.

References

Aguilar-Barragán, A., and Ochoa-Alejo, N. (2014). Virus-induced silencing of MYB and WD40 transcription factor genes affects the accumulation of anthocyanins in chilli pepper fruit. *Biol. Plant* 58, 567–574. doi: 10.1007/s10535-014-0427-4

An, J. P., An, X. H., Yao, J. F., Wang, X. N., You, C. X., Wang, X. F., et al. (2018). BTB protein MdBT2 inhibits anthocyanin and proanthocyanidin biosynthesis by triggering MdMYB9 degradation in apple. *Tree Physiol.* 38, 1578–1587. doi: 10.1093/treephys/tpy063

Chang, Y., Chen, G., Yang, G., Sun, C., Wei, W., Korban, S. S., et al. (2023). The *PcERF5* promotes anthocyanin biosynthesis in red-fleshed pear (*Pyrus communis*) through both activating and interacting with PcMYB transcription factors. *J. Integr. Agr.* 22, 2687–2704. doi: 10.1016/j.jia.2023.07.007

Colanero, S., Perata, P., and Gonzali, S. (2020). What's behind purple tomatoes? Insight into the mechanisms of anthocyanin synthesis in tomato fruits. *Plant Physiol.* 182, 1841–1853. doi: 10.1104/pp.19.01530

Fu, Z., Shang, H., Jiang, H., Gao, J., Dong, X., Wang, H., et al. (2020). Systematic identification of the light-quality responding anthocyanin synthesis-related transcripts in *Petunia* petals. *Hortic. Plant J.* 6, 428–438. doi: 10.1016/j.hpj.2020.11.006

Guo, Y., Bai, J., Duan, X., and Wang, J. (2021). Accumulation characteristics of carotenoids and adaptive fruit color variation in ornamental pepper. *Sci. Hortic.* 275, 109699. doi: 10.1016/j.scienta.2020.109699

Guo, X., Shakeel, M., Wang, D., Qu, C., Yang, S., Ahmad, S., et al. (2022). Metabolome and transcriptome profiling unveil the mechanisms of light-induced anthocyanin synthesis in rabbiteye blueberry (*vaccinium ashei*: Reade). *BMC Plant Biol.* 22, 223. doi: 10.1186/s12870-022-03585-x

Jiang, M., Ren, L., Lian, H., Liu, Y., and Chen, H. (2016). Novel insight into the mechanism underlying light-controlled anthocyanin accumulation in eggplant (*Solanum melongena* L.). *Plant Sci.* 249, 46–58. doi: 10.1016/j.plantsci.2016.04.001

Kim, D., Langmead, B., and Salzberg, S. L. (2015). HISAT: A fast spliced aligner with low memory requirements. *Nat. Methods* 12, 357–360. doi: 10.1038/nmeth.3317

Lee, H. Y., and Kim, J. S. (2023). Cherry fruit anthocyanins cyanidin-3-*O*-glucoside and cyanidin-3-*O*-rutinoside protect against blue light-induced cytotoxicity in HaCaT cells. *Appl. Biol. Chem.* 66, 3. doi: 10.1186/s13765-023-00767-5

Li, H., Bai, Y., Yang, Y., Zheng, H., Xu, X., Li, H., et al. (2023). Transcriptomic analyses reveal light-regulated anthocyanin accumulation in 'ZhongShan-HongYu' grape berries. *Sci. Hortic.* 309, 111669. doi: 10.1016/j.scienta.2022.111669

Li, X., Qian, X., Lǚ, X., Wang, X., Ji, N., and Zhang, M. (2018). Upregulated structural and regulatory genes involved in anthocyanin biosynthesis for coloration of purple grains during the middle and late grainfilling stages. *Plant Physiol. Bioch.* 130, 235–247. doi: 10.1016/j.plaphy.2018.07.011

Li, T., Xu, Y., Zhang, L., Ji, Y., Tian, D., Yuan, H., et al. (2017). The jasmonate-activated transcription factor MdMYC2 regulates *ETHYLENE RESPONSE FACTOR* and ethylene biosynthetic genes to promote ethylene biosynthesis during apple fruit ripening. *Plant Cell* 29, 1316–1334. doi: 10.1105/tpc.17.00349

Lightbourn, G. J., Stommel, J. R., and Griesbach, R. J. (2007). Epistatic interactions influencing anthocyanin gene expression in *Capsicum annuum*. *J. Am. Soc Hortic. Sci.* 132, 824–829. doi: 10.21273/JASHS.132.6.824

Liu, C. C., Chi, C., Jin, L. J., Zhu, J., Yu, J. Q., and Zhou, Y. H. (2018a). The bZip transcription factor HY5 mediates *CRY1a*-induced anthocyanin biosynthesis in tomato. *Plant Cell Environ.* 41, 1762–1775. doi: 10.1111/pce.13171

Liu, Y., Lin-Wang, K., Espley, R. V., Wang, L., Yang, H., Yu, B., et al. (2016). Functional diversification of the potato R2R3 MYB anthocyanin activators AN1, MYBA1, and MYB113 and their interaction with basic helix-loop-helix cofactors. *J. Exp. Bot.* 67, 2159–2176. doi: 10.1093/jxb/erw014

Liu, Y., Lv, J., Liu, Z., Wang, J., Yang, B., Chen, W., et al. (2020). Integrative analysis of metabolome and transcriptome reveals the mechanism of color formation in pepper fruit (*Capsicum annuum* L.). *Food Chem.* 306, 125629. doi: 10.1016/j.foodchem.2019.125629

Liu, Y., Schouten, R. E., Tikunov, Y., Liu, X., Visser, R. G. F., Tan, F., et al. (2022b). Blue light increases anthocyanin content and delays fruit ripening in purple pepper fruit. *Postharvest Biol. Tec.* 192, 112024. doi: 10.1016/j.postharvbio.2022.112024

Liu, Y., Tikunov, Y., Schouten, R. E., Marcelis, L. F. M., Visser, R. G. F., and Bovy, A. (2018b). Anthocyanin biosynthesis and degradation mechanisms in solanaceous vegetables: a review. *Front. Chem.* 6. doi: 10.3389/fchem.2018.00052

Liu, S., Wang, Y., Shi, M., Maoz, I., Gao, X., Sun, M., et al. (2022a). SmbHLH60 and SmMYC2 antagonistically regulate phenolic acids and anthocyanins biosynthesis in *Salvia miltiorrhiza*. *J. Adv. Res.* 42, 205–219. doi: 10.1016/j.jare.2022.02.005

Liu, B., Wang, L., Wang, S., Li, W., Liu, D., Guo, X., et al. (2019). Transcriptomic analysis of bagging-treated 'Pingguo' pear shows that MYB4-like1, MYB4-like2, MYB1R1 and WDR involved in anthocyanin biosynthesis are up-regulated in fruit peels in response to light. *Sci. Hortic.* 244, 428–434. doi: 10.1016/j.scienta.2018.09.040

Livak, K. J., and Schmittgen, T. D. (2001). Analysis of relative gene expression data using realtime quantitative PCR and the 2(-Delta DeltaC(T)) method. *Methods* 25, 402–408. doi: 10.1006/meth.2001.1262

Meng, Y., Zhang, H., Fan, Y., and Yan, L. (2022). Anthocyanins accumulation analysis of correlated genes by metabolome and transcriptome in green and purple peppers (*Capsicum annuum*). *BMC Plant Biol.* 22, 358. doi: 10.1186/s12870-022-03746-y

Naing, A. H., and Kim, C. K. (2018). Roles of R2R3-MYB transcription factors in transcriptional regulation of anthocyanin biosynthesis in horticultural plants. *Plant Mol. Biol.* 98, 1–18. doi: 10.1007/s11103-018-0771-4

Samkumar, A., Jones, D., Karppinen, K., Dare, A. P., Sipari, N., Espley, R. V., et al. (2021). Red and blue light treatments of ripening bilberry fruits reveal differences in signalling through abscisic acid-regulated anthocyanin biosynthesis. *Plant Cell Environ.* 44, 3227–3245. doi: 10.1111/pce.14158

Starkevic, P., Razanskiene, A., Starkevic, U., Kazanaviciute, V., Denkovskiene, E., Bendokas, V., et al. (2020). Isolation and analysis of anthocyanin pathway genes from *ribes* genus reveals MYB gene with potent anthocyanin-inducing capabilities. *Plants* 9, 1078. doi: 10.3390/plants9091078

Sun, L., Huo, J., Liu, J., Yu, J., Zhou, J., Sun, C., et al. (2023). Anthocyanins distribution, transcriptional regulation, epigenetic and post-translational modification in fruits. *Food Chem.* 411, 135540. doi: 10.1016/j.foodchem.2023.135540

Sun, L., Li, S., Tang, X., Fan, X., Zhang, Y., Jiang, J., et al. (2020). Transcriptome analysis reveal the putative genes involved in light-induced anthocyanin accumulation in grape 'Red Globe' (*V. vinifera* L.). *Gene* 728, 144284. doi: 10.1016/j.gene.2019.144284

Tanaka, Y., and Brugliera, F. (2013). Flower colour and cytochromes P450. *Philos. Trans. R. Soc B Biol. Sci.* 368, 1–15. doi: 10.1098/rstb.2012.0432

Tang, B., Li, L., Hu, Z., Chen, Y., Tan, T., Jia, Y., et al. (2020). Anthocyanin accumulation and transcriptional regulation of anthocyanin biosynthesis in purple pepper. *J. Agric. Food Chem.* 68, 12152–12163. doi: 10.1021/jf503453e

Tao, R., Bai, S., Ni, J., Yang, Q., Zhao, Y., and Teng, Y. (2018). The blue light signal transduction pathway is involved in anthocyanin accumulation in 'Red Zaosu' pear. *Planta* 248, 37–48. doi: 10.1007/s00425-018-2877-y

Wang, X., Dou, Y., Chen, X., Li, Y., Luan, H., and Li, Y. (2022b). Effects of blue light on anthocyanin biosynthesis in postharvest fruit of purple sweet pepper at different ripening stages. *Plant Physiol. J.* 58, 1507–1518. doi: 10.13592/j.cnki.ppj.100130

Wang, S., Li, L. X., Fang, Y., Li, D., Mao, Z., Zhu, Z. H., et al. (2022a). MdERF1B–MdMYC2 module integrates ethylene and jasmonic acid to regulate the biosynthesis of anthocyanin in apple. *Hortic. Res.* 9, uhac142. doi: 10.1093/hr/uhac142

Wang, Y., Zhang, X., Zhao, Y., Yang, J., He, Y., Li, G., et al. (2020). Transcription factor PyHY5 binds to the promoters of *PyWD40* and *PyMYB10* and regulates its expression in red pear 'Yunhongli No. 1'. *Plant Physiol. Biochem.* 154, 665–674. doi: 10.1016/j.plaphy.2020.07.008

Xie, G., Zhou, X., Liang, Z., Xu, D., He, J., Xie, K., et al. (2022). Integrated metabolomic and transcriptomic analyses reveal molecular response of anthocyanins biosynthesis in perilla to light intensity. *Front. Plant Sci.* 13. doi: 10.3389/fpls.2022.976449

Yadav, V., Mallappa, C., Gangappa, S. N., Bhatia, S., and Chattopadhyay, S. (2005). A basic helix-loop-helix transcription factor in Arabidopsis, MYC2, acts as a repressor of blue light-mediated photomorphogenic growth. *Plant Cell* 17, 1953–1966. doi: 10.1105/tpc.105.032060

frontiers | Frontiers in Plant Science

TYPE Original Research
PUBLISHED 24 January 2024
DOI 10.3389/fpls.2023.1305182

OPEN ACCESS

EDITED BY
Jung Eek Son,
Seoul National University, Republic of Korea

REVIEWED BY
Ki-Ho Son,
Gyeongsang National University, Republic of Korea
Athanasios Koukounaras,
Aristotle University of Thessaloniki, Greece

*CORRESPONDENCE
Tomohiro Jishi
jishi@criepi.denken.or.jp

RECEIVED 30 September 2023
ACCEPTED 07 December 2023
PUBLISHED 24 January 2024

CITATION
Jishi T (2024) Estimation of time course in phytochrome photostationary state under artificial light for controlling plant growth. *Front. Plant Sci.* 14:1305182. doi: 10.3389/fpls.2023.1305182

Estimation of time course in phytochrome photostationary state under artificial light for controlling plant growth

Tomohiro Jishi*

Grid Innovation Research Laboratory, Central Research Institute of Electric Power Industry, Chiba, Japan

A model to estimate the time course of a phytochrome photostationary state (PSS) under an arbitrary light environment was developed. It is the solution of differential equations that use conversion rates between active and inactive forms of previously reported phytochromes. The model estimated that 90% of the PSS changes were completed using approximately 3.4 mmol m^{-2} of integrated end-of-day far-red light irradiation, and 99% of the changes were completed with approximately 6.9 mmol m^{-2} irradiation. Although these values were affected by the spectral photon flux density of the far-red light. They were consistent with previous results that examined dose requirements of far-red irradiation. The rate at which the PSS changes approached equilibrium was maximized under a red light, followed by far-red, green, and blue light. This estimation method could be used to control phytochrome responses for horticulture via artificial lighting.

KEYWORDS

artificial lighting, dose response, end-of-day far-red light, low fluence response, model

1 Introduction

Phytochromes are photoreceptors that have major effects on plant development and morphogenesis, including germination (Borthwick et al., 1952; Mancinelli et al., 1966), bud formation for flowers (Halliday et al., 1994), and stem elongation (Smith and Whitelam, 1997). In particular, phytochrome B changes reversibly between inactive (P_r) and active (P_{fr}) states. The P_r state has an absorption maximum at red wavelengths, which change it to $P_{fr,}$. Whereas, P_{fr} has an absorption maximum at far-red wavelengths, which converts it to P_r. The ratio of P_r to P_{fr} varies with the relative spectral photon flux density distribution (RSPFD), thereby serving as a sensor for the RSPFD. Promoted stem elongation, suppressed leaf development, and promoted flower bud formation under a high proportion of far-red (FR) light are characteristics of a shade-avoidance response (Folta and Carvalho, 2015).

There have been attempts to control plant growth, development, and morphology by regulating phytochrome B (hereinafter, simply referred to as phytochrome) reaction via artificial lighting. Blom et al. (1995) induced stem elongation in greenhouse-grown lilies via end-of-day far-red light (EODFR). Mata and Botto (2009) reported that poinsettia flowering was delayed by using a high percentage of red light produced with a film that absorbed far-red light. The widespread use of light-emitting diodes (LEDs) has facilitated narrow-band lighting, resulting in more reports on plant responses mediated by phytochromes (e.g., Chia and Kubota, 2010).

In these reports, the R/FR ratio of red light to far-red light in the photon flux density (PFD) and the phytochrome photostationary state (PSS) have been used as indicators of environmental light effects on the phytochrome status. Red and far-red light have been defined as having wavelengths over 600–700 nm and 700–800 nm, respectively (Yang et al., 2012; Shibuya et al., 2023), but sometimes the wavelengths were defined as 655–665 nm and 725–735 nm (Smith, 1986), or 660–670 nm and 725–735 nm (Franklin, 2008).

The PSS, sometimes called the phytochrome photo-equilibrium, is the ratio of active phytochrome to the total phytochrome (P_{fr}/P_{all}), and can be calculated from absorptivity data of isolated phytochromes (Sager et al., 1988). P_r and P_{fr} can also change their state by absorbing blue and green light. Some reports have suggested that monochromatic blue light affects plant morphology by reducing the PSS (Hernández and Kubota, 2016; Jishi et al., 2021a; Jishi et al., 2021b). When using blue or green light, the R/FR ratio is not a suitable indicator of the phytochrome reaction and PSS should be used instead.

When the light environment changes over a short timescale, phenomena occur that cannot be explained solely by calculating the steady-state PSS. Even though the calculated steady-state PSS is independent of the photon flux density (PFD), and is determined solely by the RSPFD, higher doses (=integrated PFD) of EODFR, produced longer hypocotyl lengths in tomato seedlings (Chia and Kubota, 2010). The hypocotyl elongation was saturated at 4 mmol m^{-2} s^{-1} EODFR doses, which could have been attributed to temporal changes in the PSS. Because PSS changes can take several minutes to complete (Quail, 1983), it has been suggested that a higher PFD produces faster PSS changes *in vivo* (Spruit and Kendrick, 1972). Therefore, if the dose, which is the product of PFD and the irradiation time, was not sufficient for the PSS to reach a steady state, the PSS change could stop midway.

If the PSS temporal changes could be estimated, then the effects of artificial lighting on plants via the action of the phytochrome could be estimated in more detail, and plant morphology and development could be controlled more efficiently and accurately. For example, there have been few effects on the PSS if the irradiation was continued after the steady state was reached, and energy consumption could be reduced by providing sufficient irradiation as needed (Chia and Kubota, 2010; Zou et al., 2021). In addition, one could attempt to stop the PSS change midway by adjusting the light irradiation time.

Here, a method for estimating temporal changes in the PSS is discussed. By using previously reported spectral data for phytochrome photochemical cross-sections, reaction rate constants for each change between P_r and P_{fr} were calculated, and the differential equations were solved. In addition, examples of model estimation results are discussed and compared with previously reported measurements.

2 Calculation method

2.1 Definition of phytochrome photochemical cross-section and PSS calculation

The phytochrome photochemical cross-section was defined as the conversion rate constant (m^2 mol^{-1}) for the PFD at each wavelength. Therefore, the rate of decrease in the PSS per unit time because of the inactivation conversion of P_{fr} to P_r is defined in Equation 1, and the rate of increase in the PSS per unit time because of the activation conversion of P_r to P_{fr} is defined in Equation 2:

$$\frac{dP}{dt} = -P \times \sum_{\lambda=300}^{800} E_\lambda \sigma_{fr\lambda} \tag{1}$$

$$\frac{dP}{dt} = (1-P) \times \sum_{\lambda=300}^{800} E_\lambda \sigma_{r\lambda} \tag{2}$$

In Equations 1, 2, P is PSS, λ is the wavelength (nm), E_λ is the spectral photon flux density at λ (mol m^{-2} s^{-1} nm^{-1}), and $\sigma_{r\lambda}$ and $\sigma_{fr\lambda}$ are the phytochrome photochemical cross-sections (m^2 mol^{-1}) of P_r and P_{fr}, respectively, at λ.

After a sufficient time and a constant RSPFD, these reaction rates were balanced, and Equation 3 could be assumed:

$$P \times \sum_{\lambda=300}^{800} E_\lambda \sigma_{fr\lambda} = (1-P) \times \sum_{\lambda=300}^{800} E_\lambda \sigma_{r\lambda} \tag{3}$$

By solving Equation 3, the steady-state PSS could be formulated as Equation 4 (Sager et al., 1988):

$$P = \frac{\sum_{\lambda=300}^{800} E_\lambda \sigma_{fr\lambda}}{\sum_{\lambda=300}^{800} E_\lambda \sigma_{r\lambda} + \sum_{\lambda=300}^{800} E_\lambda \sigma_{fr\lambda}} \tag{4}$$

2.2 Method for estimating temporal changes in the PSS

Based on the above, temporal changes in PSS could be expressed as:

$$\frac{dP}{dt} = -P \times \sum_{\lambda=300}^{800} E_\lambda \sigma_{fr\lambda} + (1-P) \times \sum_{\lambda=300}^{800} E_\lambda \sigma_{r\lambda} \tag{5}$$

To simplify Equation 5, the sums were replaced by a and b:

$$a = \sum_{\lambda=300}^{800} E_\lambda \sigma_{fr\lambda} \quad (6)$$

$$b = \sum_{\lambda=300}^{800} E_\lambda \sigma_{r\lambda} \quad (7)$$

Then, by solving Equation 5, the following was obtained:

$$P = \frac{b}{a+b} - C\ e^{-(a+b)t} \quad (8)$$

where C is the constant of integration and e is the base of the natural logarithm. Defining P_0 as P at $t = 0$, Equation 9 was obtained:

$$C = \frac{b}{a+b} - P_0 \quad (9)$$

Therefore, Equation 8 could be expressed as:

$$P = \frac{b}{a+b} - \left(\frac{b}{a+b} - P_0\right)e^{-(a+b)t} \quad (10)$$

After substituting data for the spectral light and the phytochrome photochemical cross-sections into Equations 6, 7, and substituting a, b, and the initial PSS into Equation 10, the temporal change in PSS could be estimated.

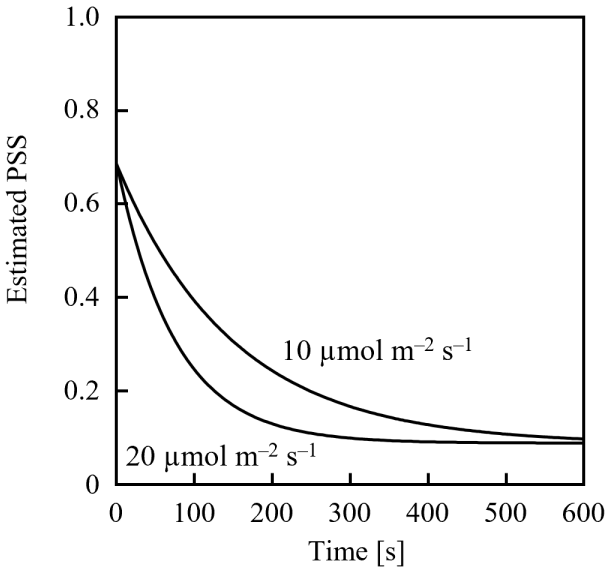

FIGURE 1
Estimated temporal changes in the phytochrome steady state (PSS) when 10- or 20-µmol m^{-2} s^{-1} end-of-day far-red lighting was applied. A spectral photon flux density distribution of a far-red LED with a 745-nm peak wavelength was used, as well as spectral data of the phytochrome photochemical cross-section (Sager et al., 1988).

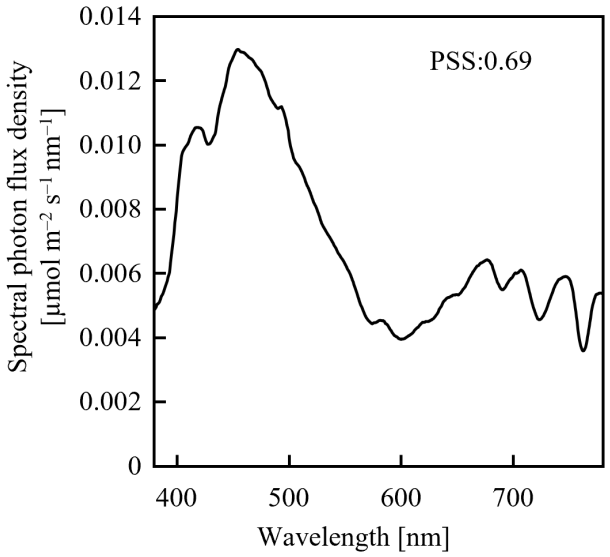

FIGURE 2
Spectral photon flux density distribution of sunlight measured on a clear June day in Chiba, Japan at 18:50 (sunset at 18:50).

3 Calculation examples

3.1 End-of-day far-red light

Assuming an initial PSS of 0.69, its temporal change was estimated, as shown in Figure 1, after irradiation with far-red LED light having a PFD of 10 µmol m^{-2} s^{-1} or 20 µmol m^{-2} s^{-1}. 0.69 was the PSS under a sunlight spectrum (Figure 2) in Chiba, Japan (35.8°N, 140.0°E) measured with a photometric sensor (LA-105; Nippon Medical & Chemical Instruments Co., Ltd) at 18:50 on a clear day in June 2020 (sunset at 18:50). A far-red LED (IR749JQ-5AJ2-F1; Toricon, Shimane, Japan), with a 745-nm peak wavelength and a 32-nm full-width at half-maximum (FWHM) was used for the spectral data. The rate of PSS change was estimated to be twice as fast for the far-red LED light irradiation having a PFD of 20 µmol m^{-2} s^{-1}, relative to that with 10 µmol m^{-2}-s^{-1} (Figure 1). Because the rate constant for the PSS change was assumed to be proportional to the PFD (Equation 5), it was estimated that equal integrated light doses with the same RSPD resulted in equal PSS changes. Under the above conditions, 90% of the PSS change was calculated to be complete at a 10 µmol m^{-2} s^{-1} × 345 s = 3.45 mmol m^{-2} EODFR dose and 99% complete at a 6.90 mmol m^{-2} EODFR dose.

If the sunlight was continued after the EODFR completion, the effect on PSS regulation was small because the PSS was expected to increase after EODFR, according to Equation 5. Sunlight at Chiba, including red light, was still present after sunset with a PPFD greater than 2 mmol m^{-2} (data not shown), and its effect on the phytochrome could not be ignored. Therefore, to reduce the PSS, the EODFR should be started after sunset, when sunlight PFD is sufficiently small.

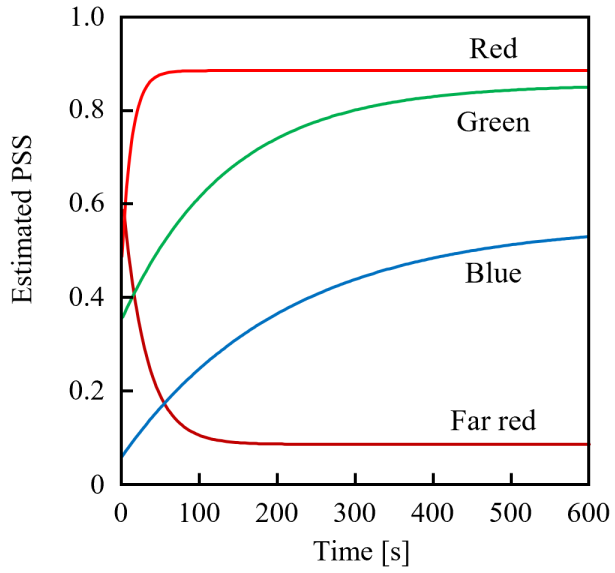

FIGURE 3
Estimated temporal changes in the phytochrome steady state (PSS) from initial PSS values 0.5 away from the equilibrium value when exposed to blue, green, red, or far-red light-emitting diodes.

3.2 Monochromatic LED light irradiation

Figure 3 shows the estimated temporal changes in the PSS under various monochromatic LED sources with PFDs of 10 μmol m^{-2} s^{-1}. The blue LED (OSUB5161P; Optosupply Limited, Hong Kong) had a 471-nm peak wavelength and a 25-nm FWHM; the green LED (OSPG5161P; Optosupply Limited, Hong Kong) had a 531-nm peak wavelength and a 36-nm FWHM; the red LED (OS5RKA5B61P) had a 632-nm peak wavelength and a 20-nm FWHM; and the far-red LED was as described above. The initial PSS value was 0.5 different from the steady-state value. The rate constants of PSS changes were approximately 2:3:33:14 when irradiated with blue, green, red, and far-red light, respectively. The estimated rate of PSS change was the product of the difference between the current and steady-state values and the rate constant, and was not affected by whether the PSS increased or decreased. If the P_{fr} dark reversion was ignored (detailed in Sec. 3.3 below), the time required to complete x% of the PSS change could be expressed in Equation 11 and was only affected by the value of Equation 12.

$$t = -\frac{\log\left(1-\frac{x}{100}\right)}{a+b} \tag{11}$$

$$a + b = \sum_{\lambda=300}^{800} E_\lambda(\sigma_{r\lambda} + \sigma_{fr\lambda}) \tag{12}$$

Because the values of $\sigma_{r\lambda} + \sigma_{fr\lambda}$ were comparable in the 700–740 nm range (Figure 4), it was estimated that the dose of far-red LED light required for sufficient PSS changes did not differ significantly depending on the selected LED. Conversely, for red light, the rate of PSS change was estimated to be approximately half that at 600 nm and 700 nm, relative to red light containing more intensity at 660 nm.

3.3 Dark reversion

The conversion of P_{fr} to P_r in the dark is referred to as P_{fr} dark or thermal reversion (see review of Klose et al., 2020). Kasperbauer et al. (1964) estimated the rate of P_{fr} dark reversion to be 0.8% min^{-1} from the flowering response in Chenopodium rubrum L. This value was comparable to that reported by Klose et al. (2015) for a 60-min half-life of the PSS. These values were comparable to the effect of 0.3-μmol m^{-2} s^{-1} far-red LED light irradiation.

4 Discussion

It was calculated that 90–99% of the PSS change was completed with a 3.45–6.90-mmol m^{-2} EODFR dose, although the values were slightly affected by the RSPFD of the light. This was comparable to the results of Chia and Kubota (2010), who reported that EODFR effects on tomato morphology were almost saturated at 2–4 mmol m^{-2} doses, and the results of Yang et al. (2012) who reported that the EODFR effect on hypocotyl elongation of pedunculate squash was saturated at 4 mmol m^{-2}.

Zou et al. (2021) reported that the EODFR effects on the leaf areas and dry weights of lettuce saturated at approximately 10 mmol m^{-2}; but those effects slightly increased with increased EODFR doses up to 180 mmol m^{-2}. Based on the present model, the PSS slightly approached a steady-state value as the FR dose increased. However, the calculated difference in the PSS after 10-mmol m^{-2} and 180-mmol m^{-2} EODFR was less than 0.1%, and it was unlikely

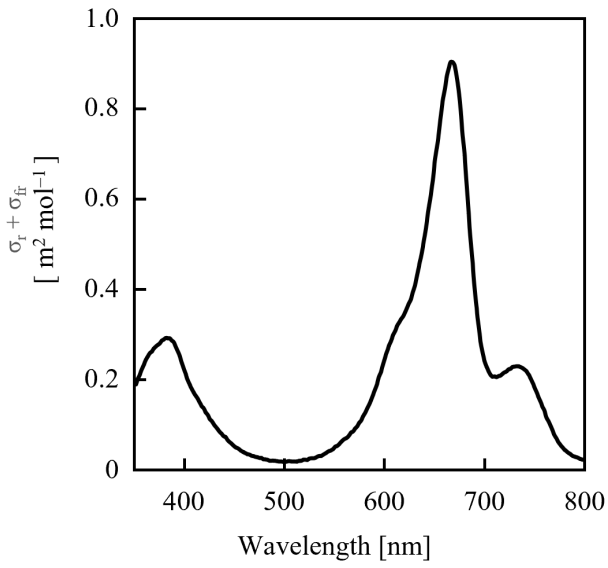

FIGURE 4
Sum of phytochrome photochemical cross-sections of P_r ($\sigma_{r\lambda}$) and P_{fr} ($\sigma_{fr\lambda}$) calculated from the data of Sager et al. (1988).

that this small difference had any effect. These results could be attributed to overlapping leaves. Zou et al. (2021) conducted cultivation for about 29 days after sowing, which is a longer period than other reports. Thus, the canopy should have grown great, and the lower leaves should have been exposed to lower-PFD light penetrating the upper leaves. More EODFR doses outside the canopy may have been needed to saturate the response of the lower leaves. It is difficult to estimate the phytochrome response of the entire canopy. The PSS in each leaf of the canopy would be estimated by using the light-environment distribution model of the canopy, in addition to the present PSS estimation model. This may lead to advances in future environmental light-control techniques that take into account differences in SPFD attributed to locations within the canopy.

Changes in the total phytochrome amount were not considered in the model here. The important physical quantity as a signal to plants was not the PSS but the absolute amount of active P_{fr} (Schmict and Mohr, 1982). Schäfer and Mohr (1974) estimated that under greater far-red light intensity, the total amount of phytochrome was reduced. Consideration of changes in the total phytochrome amount may lead to more precise estimates of phytochrome-mediated responses. Also, the PSS here was calculated using the phytochrome data of Sager et al. (1988) derived from oats (Mancinelli, 1986). Because light is also absorbed by plant pigments other than phytochromes, the model equation could be improved, especially with regard to the estimation of absolute PSS values.

When attempting to control the phytochrome reaction in plants via artificial lighting, the plant response is not always linear with the PSS value. The response may occur when the PSS exceeds a threshold value and may be saturated at a certain PSS. Furthermore, plants are affected by other photoreceptors, and those reactions may interact with phytochrome reactions. Hence, artificial lighting in horticulture should be designed with those considerations as well as the cost of light sources.

5 Conclusions

Based on previously reported data on isolated phytochromes, a model equation was developed to estimate temporal change in the PSS with respect to initial PSS values and the SPFD of the light. The calculated estimations were consistent with previous studies that examined dose requirements of end-of-day far-red light irradiation. The model also enabled estimates of the time required for progress in PSS changes up to x %. This model could be used to control plant responses via phytochrome reactions induced by artificial lighting.

Data availability statement

The original contributions presented in the study are included in the article/Supplementary Material. Further inquiries can be directed to the corresponding author.

Author contributions

TJ: Conceptualization, Data curation, Methodology, Writing – original draft.

Funding

The author(s) declare that no financial support was received for the research, authorship, and/or publication of this article.

Acknowledgments

We thank Edanz (https://jp.edanz.com/ac) for editing a draft of this manuscript.

Conflict of interest

The author declares that the research was conducted in the absence of any commercial or financial relationships that could be construed as a potential conflict of interest.

Publisher's note

Supplementary material

The Supplementary Material for this article can be found online at: https://www.frontiersin.org/articles/10.3389/fpls.2023.1305182/full#supplementary-material

SUPPLEMENTARY TABLE 1
A calculator that outputs the estimated time course in PSS.

References

Blom, T. J., Tsujita, M. J., and Roberts, G. L. (1995). Far-red at end of day and reduced irradiance affect plant height of easter and asiatic hybrid lilies. *HortSci.* 30, 1009–1012. doi: 10.21273/HORTSCI.30.5.1009

Borthwick, H. A., Hendricks, S. B., Parker, M. W., Toole, E. H., and Toole, V. K. (1952). A reversible photoreaction controlling seed germination. *Proc. Natl. Acad. Sci.* 38, 662–666. doi: 10.1073/pnas.38.8.662

Chia, P. L., and Kubota, C. (2010). End-of-day far-red light quality and dose requirements for tomato rootstock hypocotyl elongation. *Hortsci.* 45 (10), 1501–1506. doi: 10.1590/S0102-05362010000400020

Folta, K. M., and Carvalho, S. D. (2015). Photoreceptors and control of horticultural plant traits. *HortSci.* 50, 1274–1280. doi: 10.21273/hortsci.50.9.1274

Franklin, K. A. (2008). Shade avoidance. *New Phytol.* 179, 930–944. doi: 10.1111/j.1469-8137.2008.02507.x

Halliday, K. J., Koornneef, M., and Whitelam, G. C. (1994). Phytochrome B and at least one other phytochrome mediate the accelerated flowering response of Arabidopsis thaliana L. @ to low red/far-red ratio. *Plant Physiol.* 104, 1311–1315. doi: 10.1104/pp.104.4.1311

Hernández, R., and Kubota, C. (2016). Physiological responses of cucumber seedlings under different blue and red photon flux ratios using LEDs. *Environ. Exp. Bot.* 121, 66–74. doi: 10.1016/j.envexpbot.2015.04.001

Jishi, T., Matsuda, R., and Fujiwara, K. (2021a). Blue light monochromatic irradiation for 12 hours in lighting pattern with combinations of blue and red light elongates young cos lettuce leaves and promotes growth under high daily light integral. *HortScience* 56, 940–945. doi: 10.21273/HORTSCI15959-21

Jishi, T., Matsuda, R., and Fujiwara, K. (2021b). Manipulation of intraday durations of blue- and red-light irradiation to improve cos lettuce growth. *Front. Plant Sci.* 12. doi: 10.3389/fpls.2021.778205

Kasperbauer, M. J., Borthwick, H. A., and Hendricks, S. B.. (1964). Reversion of phytochrome 730 (Pfr) to P660 (Pr) assayed by flowering in Chenopodium rubrum. *Botan. Gaz.* 125, 75–80.

Klose, C., Venezia, F., Hussong, A., Kircher, S., Schäfer, E., and Fleck, C. (2015). Systematic analysis of how phytochrome B dimerization determines its specificity. *Nat. Plants* 1, 15090. doi: 10.1038/nplants.2015.90

Klose, D., Nagy, F., and Schäfer, F. (2020). Thermal reversion of plant phytochromes. *Mol. Plant* 13 (2), 386–397. doi: 10.1016/j.molp.2019.12.004

Mancinelli, A. L. (1986). Comparison of spectral properties of phytochromes from different preparations. *Plant Physiol.* 82, 956–961. doi: 10.1104/pp.82.4.956

Mancinelli, A. L., Borthwick, H. A., and Hendricks, S. B. (1966). Phytochrome action in tomato-seed germination Bor. *Gaz.* 127 (1), 1–5. doi: 10.1104/pp.82.4.956

Mata, D. A., and Botto, J. F. (2009). Manipulation of light environment to produce high-quality poinsettia plants. *HortScience* 44, 702–706. doi: 10.21273/hortsci.44.3.702

Quail, P. H. (1983). "Rapid action of phytochrome in photomorphogenesis," in *Photomorphogenesis*. Eds. W. Shropshire and H. Mohr (Berlin: Springer Nature), 178–212.

Sager, J. C., Smith, W. O., Edwards, J. L., and Cyr, K. L. (1988). Photosynthetic efficiency and phytochrome photoequilibria determination using spectral data. *Trans. ASAE* 31, 1882–1889. doi: 10.13031/2013.30952

Schäfer, E., and Mohr, H. (1974). Irradiance dependency of the phytochrome system in cotyledons of mustard (Sinapis alba L.). *J. Math. Biol.* 1, 9–15. doi: 10.1007/BF02339485

Schmict, R., and Mohr, H. (1982). Evidence that a mustard seedling responds to the amount of P_{fr} and not to the P_{fr}/P_{tot} ratio. *Plant Cell Environ.* 5 (6), 495–499. doi: 10.1111/1365-3040.ep11611856

Shibuya, T., Kataoka, C., Nishio, K., Endo, R., Kitaya, Y., Shinto, Y., et al. (2023). Cucumber leaf necrosis caused by radiation with abrupt increase of far-red component. *Biol. plantarum* 67, 28–35. doi: 10.32615/bp.2022.039

Smith, H. (1986). "The perception of light quality," in *Photomorphogenesis in Plants*. Eds. R. E. Kendrick and G. H. M. Kronenberg (Berlin: Springer Nature), 187–217.

Smith, H., and Whitelam, G. C. (1997). The shade avoidance syndrome: Multiple responses mediated by multiple phytochromes. *Plant Cell Environ.* 20, 840–844. doi: 10.1046/j.1365-3040.1997.d01-104.x

Spruit, C. J. P., and Kendrick, R. E. (1972). On the kinetics of phytochrome photoconversion in *vivo*. *Planta* 103 (4), 319–332. doi: 10.1007/BF00386703

Yang, Z. C., Kubota, C., Chia, P. L., and Kacira, M. (2012). Effect of end-of-day far-red light from a movable LED fixture on squash rootstock hypocotyl elongation. *Sci. Hortic.* 136, 81–86. doi: 10.1016/j.scienta.2011.12.023

Zou, J., Fanourakis, D., Tsaniklidis, G., Cheng, R., Yang, Q., and Li, T. (2021). Lettuce growth, morphology and critical leaf trait responses to far-red light during cultivation are low fluence and obey the reciprocity law. *Sci. Hortic.* 289, 110455. doi: 10.1016/j.scienta.2021.110455

Frontiers in Plant Science

Cultivates the science of plant biology and its applications

The most cited plant science journal, which advances our understanding of plant biology for sustainable food security, functional ecosystems and human health.

Discover the latest Research Topics

See more →

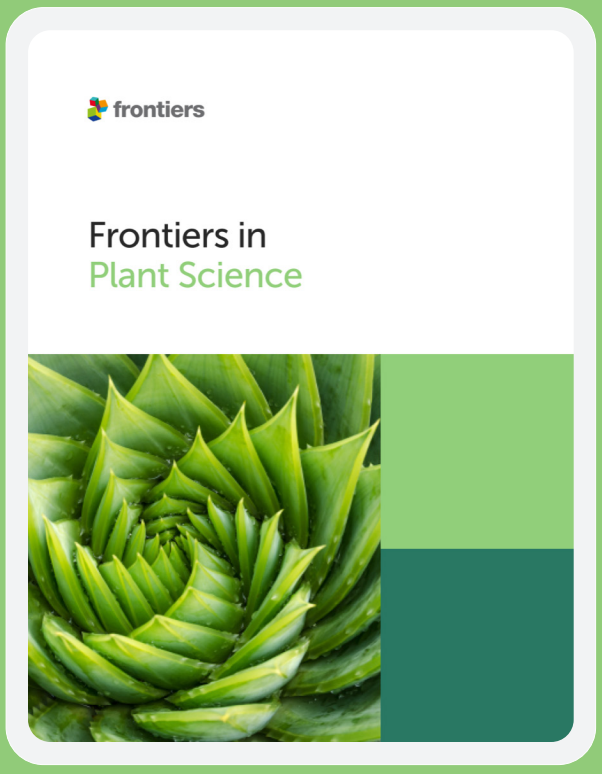

Frontiers

Avenue du Tribunal-Fédéral 34
1005 Lausanne, Switzerland
frontiersin.org

Contact us

+41 (0)21 510 17 00
frontiersin.org/about/contact